Post Processing for Nylon 12 Laser Sintered Components

Ahmad Kamil
079039969

School of Mechanical and Systems Engineering
Newcastle University
Newcastle upon Tyne, United Kingdom

Thesis submitted for partial fulfilment for
the degree of Doctor of Philosophy

November 2016

Declaration

This is to certify that I am responsible for the work submitted in this thesis, that the original work is my own except in acknowledgement or within the text, and that neither the thesis nor the original work contained herein has been submitted to this or any other institution for a higher degree.

Signed .....

Date: 1st November 2016

ACKNOWLEDGEMENTS

I would like to express my appreciation and gratitude to my supervisor, Prof. Kenny Dalgarno, for his guidance and support during the research work.

I gratefully acknowledge the Government of the Republic of Indonesia, through the Ministry of Research, Technology and High Education for financial support during my PhD programme.

I would also like to thank my colleagues in Rapid Manufacturing Group at Newcastle University, for their friendship, helpful discussions, suggestions and advice. Thanks also to the laboratory operators and technicians for their assistances.

Special acknowledgements go to my lovely wife, Rina Wahyuni, and my daughters Farah Nabilah and Raisa Kamila, for their understanding and patience during my study, as well as to Naila Ulfa Safitri (latest).

I deeply express my thanks to my beloved mother, who has always prayed for me. Without her prayers, I would not have been able to complete this research.

Finally, thanks to all my relatives for their overwhelming support for me and my family when we have faced difficult situations.

Newcastle upon Tyne, November 2016

DEDICATED TO

MY WONDERFUL FAMILY

ABSTRACT

This research investigates the effect of post-processing on the mechanical characteristics and behaviour of laser sintered components produced by selective laser sintering (SLS). It aims to understand the material's behaviour and to develop post-processing methods that can be used to improve and maintain consistency in the mechanical properties of the layer manufactured material.

Duraform Polyamide (Nylon 12) and a Sinterstation Vanguard™ SLS machine were used to produce test specimens. The behaviour of the layer material characteristics was established using different fabrication orientations and tensile, compression, shear and flexure tests as benchmarking investigations. The results show that there are significant variations in mechanical properties, as well as divergences from previous results.

In addition, section thickness in closed and open hollow structures was investigated in order to establish its effect on mechanical properties. The larger a sintered area, the greater the tensile properties gained when there is an increase of section thickness and when solid specimens are used. Moreover, when fill and outline scanning strategies were implemented in producing the specimens, the improvements were obtained in the tensile properties of nylon 12 laser-sintered material with no impact on geometry.

To further improve the mechanical properties, a new post processing method that included heat treatment in air and vacuum environments was investigated. Experiments were conducted in air from room temperature to 140^{o}C with a treatment time of 120 minutes and vacuum heat treatment was conducted from room temperature to 180^{o}C with 16 hours and 100 hours treatment time. The material properties in both conditions were then analysed in terms of tensile properties, thermal characterisations, microstructure and geometrical changes.

Heat treatment in air showed no significant improvement in mechanical properties. However, Nylon 12 SLS material heat-treated in a vacuum showed considerable improvement in crystallinity and peak melting point. Heat treatment for a longer period to approach the melting point, especially on material with the different section thicknesses and solid specimens and particularly in a vacuum, has a greater impact on mechanical properties, but this may not be sufficient to justify the cost and time involved.

TABLE OF CONTENTS

LIST OF FIGURES

LIST OF TABLES

ABBREVIATIONS AND NOTATIONS

ABBREVIATIONS

3DP : Three dimensional printing

AM : Additive manufacturing

CAD : Computer aided design

DMLS : Direct metal laser sintering

EBM : Electron beam melting

DLF : Direct laser formin

DSC : Differential scanning calorimetry

FDM : Fused deposition modeling

LC : Laser Cusing

MJM : Multi Jet Modelling

OLM : Optical light microscopy

PA : Polyamide

RM : Rapid manufacturing

RP : Rapid prototyping

RT : Rapid tooling

SLA : Stereolithography

SLM : Selective laser melting

SLS : Selective laser sintering

SPLS : Solid phase laser sintering

NOTATIONS

σ : the surface tension (mN/m)

α : thermal absortivity ratio

ω : the characteristic of beam radius (mm)

ρ : the apparent density (kg/m^3)

μ : the solid fraction $\mu = \frac{\rho}{\rho_s}$

η_o : the melting viscosity (Pa.S)

ρ_S : theoretical solid density (kg/m^3)

BS : beam speed (mm/sec)

C_p : specific heat (J/kg K)

d : laser beam diameter (mm)

E_μ : the activation energy for viscous flow (J)

E/R : ratio of sintering activation energy to the gas constant (K^{-1})

ED : energy density (J/mm^2)

h : slice/layer thickness (mm)

I : the intensity of the beam (W/mm^2)

k : thermal conductivity (W/m K)

M_w : molecular weight (mg)

m : mass of material (kg)

P : laser power (W)

R : Scan radius (mm)

r : the radius of a sphere (mm)

s : laser scan spacing (mm)

SP : scan spacing (mm)

T : absolute temperature (^oC or K)

T_{cc} : crystallization temperature (^oC)

T_m : melting temperature (^oC)

T_b : powder bed temperature (^oC)

T_g : glass transition temperature (^oC)

t : time (s)

w : laser scan vector length or part width (mm)

x : sintering neck radius (mm)

CHAPTER 1. INTRODUCTION

1.1 Background

Manufacturing industry is seeking innovative methods to accelerate new product development and to manufacture products more rapidly, due to global competition among companies striving to improve their business processes. In this situation, rapid manufacturing has become an attractive option.

Rapid manufacturing has developed as an advanced technology used to shorten the time to market. Such technologies are based on an additive approach, where a component is built gradually by adding material layer by layer so as to create a geometry of components in two-dimensional profiles, controlled directly from 3D computer-aided design (CAD) solid model systems. This additive manufacturing approach has several advantages. The technologies are able to fabricate parts rapidly without the use of any additional tooling or moulds for any level of geometrical complexity [Kruth et al, 1998; Pham, 2001; Levy, 2002]. In addition, it allows reduced design and production lead-times and cost.

Many different commercial additive manufacturing technologies are available, such as stereolithography (SLA), selective laser sintering (SLS), fused deposition modelling (FDM), solid ground curing (SGC), and three-dimensional printing (3DP). All these technologies have limitations concerning the types and properties of materials that can be used [Gibson and Shi, 1997; Dutta et al, 2001; Pham, 2001].

Selective laser sintering (SLS) was developed in the late 1980s as a technique for rapid prototyping (RP) using a wide range of materials, including metals (steel, titanium, alloy mixtures and composites), polymers (nylon, glass-filled or other fillers, and polystyrene), and foundry sand [Kruth et al, 2003; Levy et al, 2003]. Hence, SLS is frequently used for prototyping, tooling and manufacturing purposes.

In order to manufacture products, acceptable material characteristics must be available. The properties of materials, and mainly the mechanical properties of products such as strength and stiffness, are critical issues regarding service loading and operation [Caufield et al, 2007].

1.2 Research Gaps and Problems

In conventional manufacturing processes, the repeatability of mechanical properties is known. However, in layer manufacture material properties are less well understood and depend on the orientation of fabrication [Gibson and Shi, 1997], where the tensile strength and density of specimens produced in different orientations with different fabrication parameters may vary. In addition, Hague et al [2004] and Hou [2005] concluded that SLS material can be considered as anisotropic, showing different levels of strength and modulus in different orientations.

Another issue in the rapid manufacturing field concerns mechanical properties and improvements. Zarringhalam, et al [2006] investigated the effects of various processing factors on the microstructure and properties of SLS Nylon 12, analysing different specimens of SLS Nylon 12 powder and parts produced using different thermal histories and various machines configured with contrasting parameters. Significant increases in elongation at break were found for refreshed and used powder compared with virgin powder for parts made on different machines. Small variations were also demonstrated in ultimate strength between virgin and refreshed material, with increases in tensile strength for used powder. The values of Young's modulus also varied, even though the same machine and material were used to fabricate specimens.

Used powder is the powder left from every run of the machine during the SLS process. Some may have overflown from bins, some powder remains from the part cake after its removal from the machine, and also powder is removed from the part build and feed cylinders when the machine is emptied. However, in reusing this powder, there are concern involving how many times the powder has been used and where it was extracted from in the machine, since a certain amount of degradation occurs due to increases in molecular weight which hinder the sintering process. Part quality and indeed the ability to build is reduced when used powder is reused in repeated builds (Gornet, T.J., et al, 2002).

Virgin powder is as supplied from the manufacturer. However, virgin powder is currently expensive and it is more practical in industry to use a refreshed powder, in which used powder is mixed predefined proportions of virgin powder. However, this does not solve the problem of variations in properties.

It has been recognised that material properties are influenced by microstructure, the formation of which depends on temperature and process duration. In addition, the properties of a structure can be affected by different temperatures, times and heating/cooling rates in heat treatment processes.

Several studies have investigated the heat treatment of polymer materials. Zarringhalam and Hopkinson [2003] reported that using heat treatment in a conventional heating chamber as post-processing can increase the tensile and impact strength of SLS parts made from Nylon 12. In addition, Scobbo and Hwang [1994] showed that after annealing PolyPhenyleneSulfide material, its modulus increased as a result of an increase in crystallinity.

The effect of annealing on the thermal properties and crystalline structure of Nylon 11 (polyundecaneamide) and Nylon 12 (polylaurolactam) was investigated by Gogolewski [1979] and Gogolewski, et al [1980], who found that crystal size, melting temperature and the heat of melting rose with increased annealing temperature.

Ramazani and Mousavi [2005] investigated vacuum annealing effects on the mechanical properties of thermoplastic materials, polystyrene and Nylon 6. They studied the heat treatment process at different vacuum levels and for different time-temperature settings. They showed that heat treatment in a vacuum has a positive impact on the mechanical properties of polymeric parts.

From the brief summary above of other research, it can be concluded that the mechanical properties of laser-sintered material depend on the process parameters, materials and orientation and position of design products in the envelope of the machine when it is manufactured. Furthermore, some research has utilised the technology of heat treatment to improve the characteristics of polymer material.

Questions arise therefore concerning techniques that could be applied after a product is finished to improve its properties and characteristics. Can a heat treatment approach serve this purpose?

For example, the mechanical properties of laser-sintered material might be improved if the product is designed with closed and open hollow structures with different wall thicknesses using a default setting for a filling and outline scanning strategy. Then, if the heat treatment approach is applied, it may show significant and consistent changes in properties.

Furthermore, if the filling and outline scanning strategy changed for product designs with closed hollow structures but with different wall thickness, this might lead to significant changes in mechanical properties and their consistency?

Therefore, in this study the mechanical properties of Nylon SLS parts are investigated and methods for improving and making more consistent its mechanical properties using heat treatment are evaluated.

1.3 Research Aim and Objectives

The main purpose of this study is to investigate post-processing methods that can be used to improve and ensure the consistency of mechanical properties in layer manufacture materials.

To achieve the aim of this study, the following objectives were determined:

1. To determine the mechanical performance of one SLS material (Duraform PA), over a range of stress states.
2. To develop post-processing methods for the material.
3. To determine and understand the impact that the post-processing methods have on the consistency of mechanical properties.

1.4 Research Scope and Limitation

In order to focus the investigation, further steps were determined to achieve the aim and objectives of this research. The research map consists of the following steps below:

1) Identifying a basic technology of additive manufacturing (AM).
    a) Benchmarking on mechanical properties obtained by other researchers from different SLS machines.
    b) Identification of research gap and opportunity
2) Identifying current research into the heat treatment of polymer material.
    a) Reviewing previous relevant studies in improving the tensile properties of SLS fabricated parts.
    b) Identifying a heat treatment approach to improve the tensile properties of laser-sintered material.

3) Identifying current research on the tensile properties of laser-sintered products with different wall thicknesses and possible processes to improve them with a heat treatment approach.
4) Identifying current research on filling and outline scanning strategy and possible processes to gain better tensile properties of laser-sintered material with the aforementioned strategy.

In this research, was initially performed benchmarking for mechanical properties obtained by others researchers from different SLS machines, and the tests involved tensile, compression, flexural and shear tests without a heat treatment process. However, further investigation of closed and open hollow structures with different wall thicknesses, are limited to the tensile test only to determine the tensile properties of heat-treated and non-heat-treated laser-sintered material. Moreover, the same test is conducted to compare samples of closed hollow structures with different filling and scanning outline strategies.

In this study, six samples are measured in each individual test for all experimental work, whether for heat-treated or non-heat treated samples. Refreshed powder is used for all samples manufactured, as this is applied in practice in industry using SLS machines.

In initial heat treatment, a regular furnace is used. However, for further heat treatment study, a vacuum furnace is used to avoid contaminated environments.

1.5 Structure of the Thesis

This thesis consists of seven chapters. The second chapter is a literature review that considers the fundamentals of additive manufacturing technology and its applications, and gives definitions of rapid manufacturing, selective laser sintering (SLS), materials, and post processing.

Chapter three details the experimental studies and procedures used, including the standards, test methods and analysis, and the mechanical testing equipment employed in this study. The subsequent chapter then presents the experimental results and a discussion of the benchmarking of the characterisation of mechanical properties.

Chapter five describes the heat treatment studies, showing details of the heat treatment regimes applied with selective laser-sintered Nylon 12 and their effect on

mechanical properties. In addition, heat-treated and non-heat-treated specimens are compared and the results of the characterisation are discussed.

Chapter six describes the heat treatment and mechanical properties of closed and open hollow structures, with different wall thicknesses of samples with a default filling and outline scanning strategy. Specimens with and without heat treatment are compared and the results of the characterisation are discussed.

Moreover, the mechanical properties of closed hollow specimens with different wall thicknesses that using different filling and outline scanning strategies are explained. Then, these closed hollow specimens with different filling and outline scanning strategies are compared and the results of the characterisation are discussed for specimens without heat treatment.

Chapter seven consists of a general discussion of the work, considering the implications of the results and outlining the conclusions of the study, before making recommendations for future work.

CHAPTER 2. LITERATURE REVIEW

2.1 Introduction

This chapter describes the fundamentals of additive manufacturing technologies and their systems development and application, and outlines a definition of rapid manufacturing and its technology. In addition, it also describes selective laser sintering (SLS) as the rapid manufacturing technology considered in this research study, and the characteristics of Nylon 12 as the material studied. Moreover, heat treatment as a post-processing method is also reviewed.

2.2 Additive Manufacturing (AM) and Applications

Additive manufacturing (AM) was introduced commercially in the late 1980s [Kruth et al, 2005a] by 3D-Systems, as a stereolithography process. The first application of this technology was to build solid products for prototyping purposes, hence the name rapid prototyping (RP). The technology was the developed for tool making, known as rapid tooling (RT), and to manufacture final (functional) parts rapid manufacturing (RM).

AM is a set of techniques that have the ability to generate physical models of free/form or complex-geometry parts directly from 3D CAD data by adding material on a layer-by-layer basis until the final geometry is obtained, without the use of tooling [Kruth et al, 1998; Dalgarno and Wright, 2003]. Some of the commercial advantages gained from AM technology are: decreased cycle time and cost in design; earlier detection and reduction in the potential for expensive design errors; decreased tooling costs on short-run parts; reduced time in production and marketing; the part geometry can be visualised in advance of production due to its physical existence [Pham et al, 2004; Noorani, 2006]. AM technologies have been applied to produce components or final parts using a wide range of different materials and methods. The basic principles of additive manufacturing and its system development and application are outlined in subsequent sections.

2.2.1 Basic principles

Since AM technologies were introduced, many different processes using different materials have become available. However, although these processes vary, their basic

operating principles are very similar [Pham, 2001; Cee Kai, 2003; Noorani, 2006], as illustrated in figure 2-1.

All AM technologies require a solid 3D-model file to begin with, so that the first step is to create a 3D CAD solid model of the design as input data. Then, by using any solid modelling CAD software, this model is converted to a stereolithography (STL) file, which is the "de facto" standard industry format [Pham, 2001; Gibson, 2002; Cee Kai, 2003; Noorani, 2006]. Basically, the STL file format represents a set of triangular facets to indicate the geometric model of the part's surface [Gibson, 2002]. The more triangles are used, the more accurate a representation is given of the original part the STL file is for. This STL file is then transferred to the AM system.

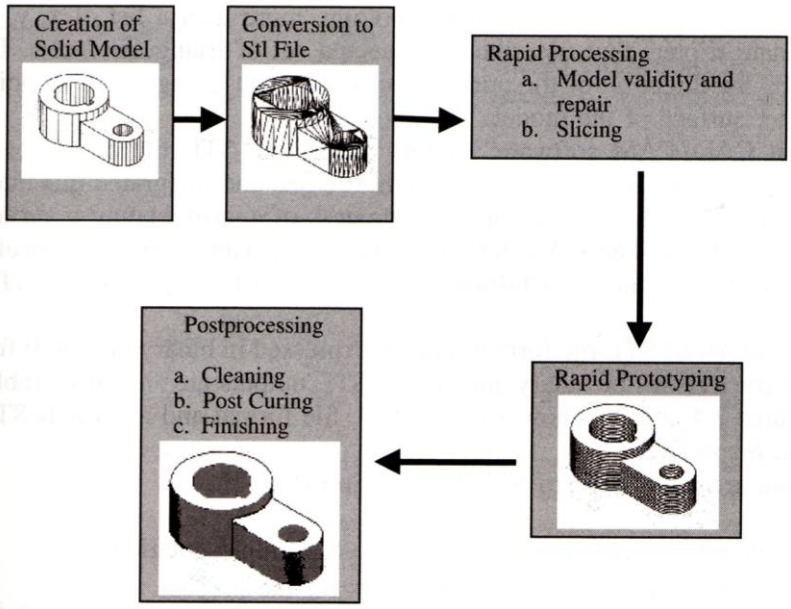

Figure 2-1 Principle processes of AM [Noorani, 2006]

In the following step, the STL format of the 3D model is reviewed by the AM system software. It is then "split" into a stack of 2D cross-sections which are the layers. In the final step, each layer is then processed and bonded to form a physical 3D solid part. The build platform descends in the Z direction after one layer thickness, and layers are then added consecutively to build the part [Pham et al, 2004]. The 3D solid part is then removed from the machine after being totally built for any post-processing to be applied.

2.2.2 Development of AM processes

Additive manufacturing has been developed for a wide range of different applications and materials. Additive manufacturing systems can be categorised in a variety of ways depending on the physics of the process, the source of energy, type of material, or size of parts [Kruth et al, 1998; Pham, 2001; Noorani, 2006]. According to the raw material used, additive manufacturing systems can be divided into: liquid-based, powder-based or solid-based processes, as shown in Figure 2-2 [Kruth et al, 1998; Pham, 2001; Noorani, 2006]. The basic processes and operation of the most common commercial AM systems based on this classification is reviewed in the following section.

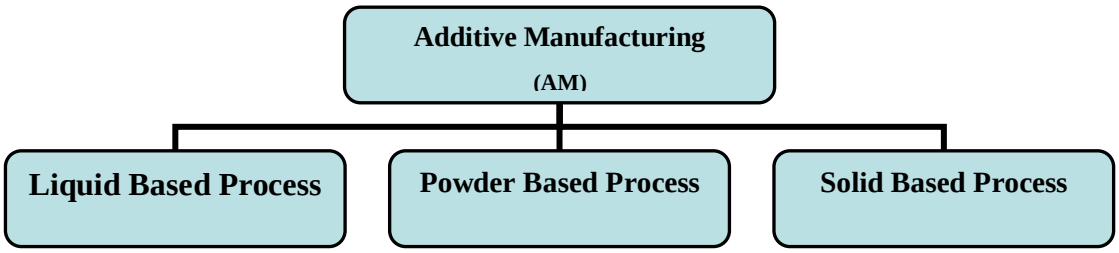

Figure 2-2 AM process classification [Kruth et al, 1998; Pham, 2001; Noorani, 2006]

2.2.2.1 Liquid-based process

The stereolithography apparatus (SLA) is the most common liquid-based process, and was the first commercial implementation of the AM system introduced by 3D Systems in 1988 [Cee Kai, 2003; Noorani, 2006].

The process of a liquid-based system begins with the raw material, a photosensitive polymer in the liquid state which is then converted into a solid state through a curing process. A schematic view of the SLA process is illustrated in figure 2-3 [Upcraft and Fletcher, 2003], where the three-dimensional part's model is built in a vat. Based on the predefined path in slicing the model, the surface layer of resin is cured or solidified selectively by a UV (ultraviolet) laser beam to form a solid layer. When one layer of the part is formed, the elevation systems control causes the elevator table to lower the part, and then a new layer of liquid resin is swept over it and the process repeated until the complete part is built [Cee Kai, 2003; Noorani, 2006]. The part is then removed from the vat and cleaned of uncured material.

SLA technology can produce parts with a good surface finish, high degree of detail and thin walls. Drawbacks include a limited range of materials (photopolymer); and the needs for a support structure during processing and postcuring [Noorani, 2006].

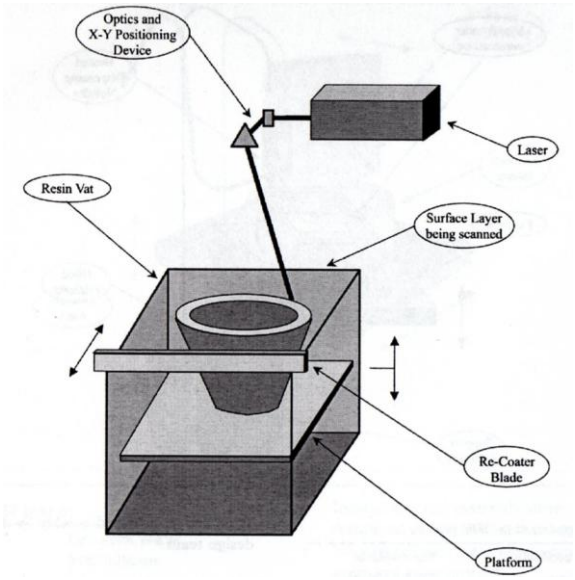

Figure 2-3 Schematic view of stereolithography apparatus (SLA) [Upcraft and Fletcher, 2003]

2.2.2.2 Powder-based process

Powder-based processes are a special category of solid-based processes that use powder as raw material. A wide range of polymers, metals and ceramics may be used [Kruth et al, 2005b]. Three-dimensional printing (3DP) and selective laser sintering (SLS) processes are the most popular type in this category.

2.2.2.2.1 Three-dimensional printing (3DP) systems

This layer manufacturing technology was invented and patented by the Massachusetts Institute of Technology (MIT). It utilises ink-jet printing technology directly for the rapid and flexible production of prototypes, parts and tooling [Noorani, 2006]. Firstly, a thin layer of powder material is spread over the surface of the powder bed. Next, by using ink-jet printing technology, a binder material is "printed" into the powder where the part model is to be formed and the powder particles are selectively bonded to form the solid part layer. Then the platform is lowered, a fresh powder layer is spread and deposited over the previous solid layer, and the binder prints again. This process is

continued until the part is completely developed [Noorani, 2006]. Figure 2-4 shows a basic schematic of three-dimensional printing (3DP) systems. For a metal part, the 3DP process is used firstly to build a green-part, which is then post-processed with debinding, sintering and infiltrating in a furnace.

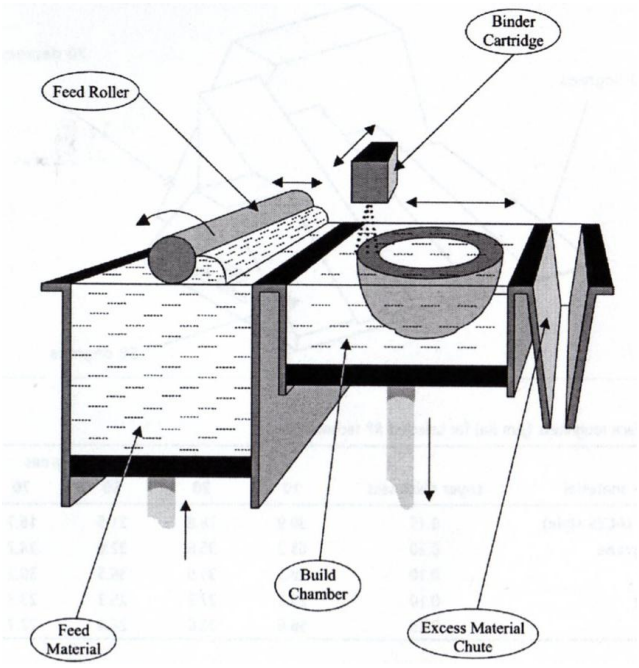

Figure 2-4 Schematic view of 3DP systems [Upcraft and Fletcher, 2003]

2.2.2.2.2 Selective laser sintering (SLS)

Selective laser sintering (SLS) was developed and patented by the University of Texas at Austin and was commercialised by the DTM Corporation (later bought by 3D Systems) [Noorani, 2006].

Selective laser sintering (SLS) builds a 3D solid part model by laser-fusing or sintering a layer of powdered raw material. Firstly, the powder is transferred to the build cylinder platform from the feed powder container through a counter-rolling cylinder or blade. When a thin layer of the heat-fusible powder is spread and deposited over the build platform, a concentrated heating laser beam selectively sinters the powder, fusing the powder particles and forming a solid part. The powder is spread again for the next layer and the process is repeated, so that layers of powder are deposited and sintered until the part building is complete. Unsintered material remains loose and can act as a support for the next powder layer and object under fabrication. When the object is completely formed, the piston is raised to elevate the

object. Excess powder is brushed away and final hand finishing may be carried out. Figure 2-5 illustrates a schematic of the SLS process.

Selective laser sintering is described in greater detail in section 2.3 below.

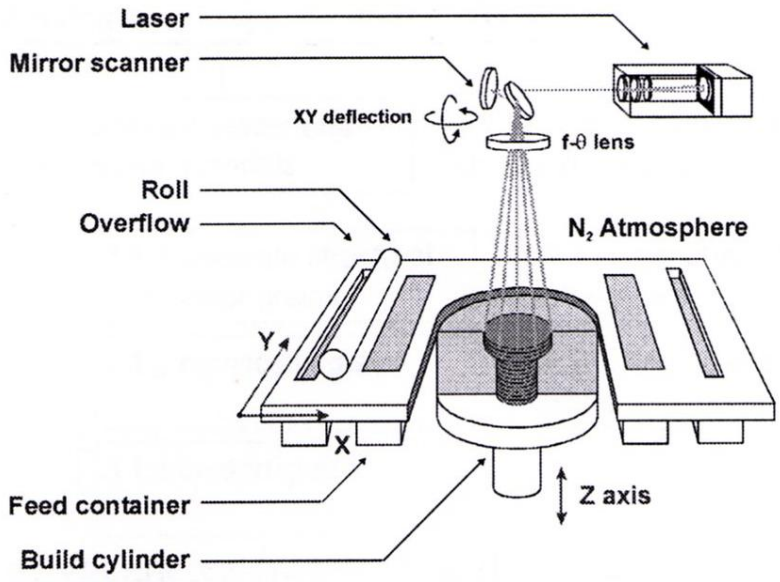

Figure 2-5 Schematic view of selective laser sintering (SLS) [Kruth et al, 2005a]

2.2.2.3 Solid-based process

Solid-based systems begin with the build material in a solid (non-powder) state, which may include material in the form of wire, a roll, laminates or pellets. The most common systems are fused deposition modelling (FDM) and multi-jet modelling (MJM) systems.

2.2.2.3.1 Fused deposition modelling (FDM)

Fused deposition modelling (FDM) technology was developed by the Stratasys company and a patent was issued in 1992 [Noorani, 2006]. FDM generates three-dimensional parts using an extrusion process. A schematic process is shown in figure 2-6. To develop a 3D solid part, a filament of thermoplastic is extruded from a heated dispensing nozzle and deposited onto a platform. The nozzle is laid across the X-Y plane to form a thin 2D layer. To build each layer, the dispensing nozzle deposits the outline of the layer first and then the next slice of the part is deposited. As each layer is built up with hot filament, it bonds to the material in the previous slice to develop a 3D solid part. To build up the support structure, when needed, another nozzle is used with different material [Pham, 2001; Noorani, 2006].

There are certain advantages to FDM, such as the variety of materials which can be used its ease of material changeover and fast build speed on small/hollow geometries; but requiring no postcuring. However, the surface finish is not as good as in conventional parts there may/be weak properties in the Z axis and for large/dense parts building speed is slow [Noorani, 2006].

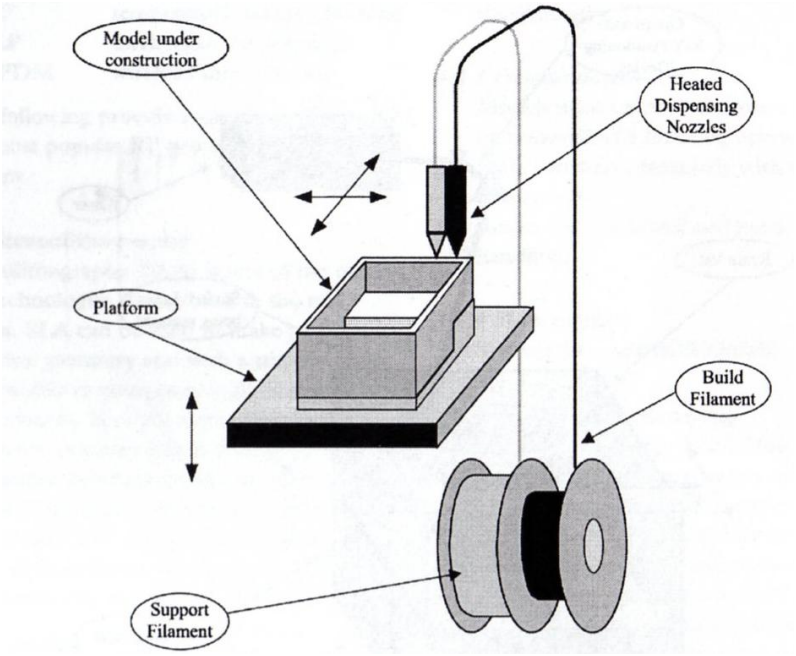

Figure 2-6 Schematic view of fused deposition modelling (FDM) [Upcraft and Fletcher, 2003]

2.2.2.3.2 Multi-jet modelling (MJM) systems

As shown in figure 2-7, the principle process of the multi-jet modelling (MJM) system is similar to the technology used in an ink-jet printer, but applied in three dimensions. To start the process, a small droplet of thermoplastic polymer material is sprayed through the print head of a linear array jets or spray nozzle. To build 3D solid parts layer-by-layer, the print head is moved in a similar fashion as a line printer. A moveable platform is used to build the part. This lowers after each layer is developed, where the hot droplet of material bonds to the previous layer of the part [Upcraft and Fletcher, 2003].

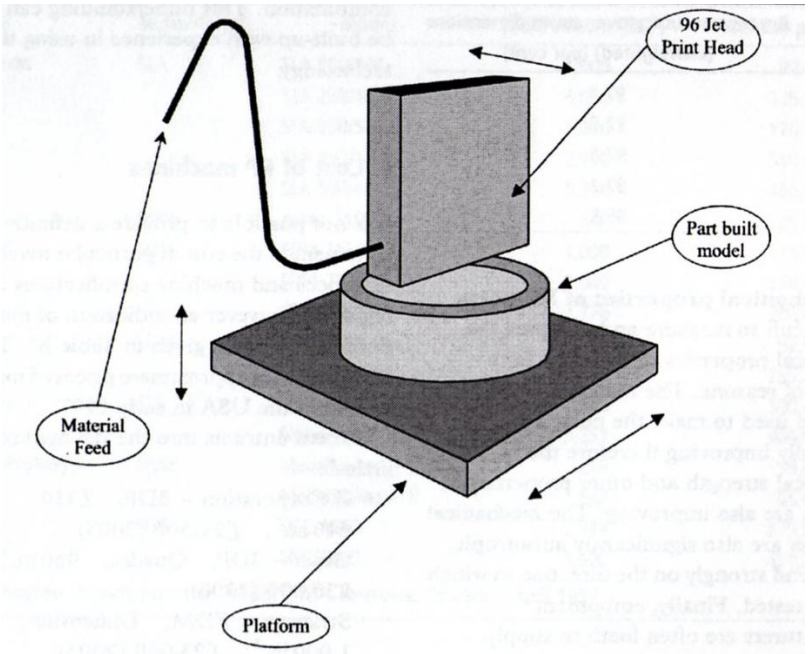

Figure 2-7 Schematic view of multi jet modelling (MJM) [Upcraft and Fletcher, 2003]

2.2.3 Advantages and disadvantages of AM technology

Compared to subtractive methods, one of the critical advantages of all additive manufacturing (AM) technologies is the ability to create parts or components with significant unrestrained geometries. AM allows a geometric freedom not possible with conventional methods, such as for variable wall thickness, zero draft angles and no split line [Hague et al, 2003a; Hague et al, 2003b; Hopkinson and Dickens, 2003]. However, it is not yet possible to have total freedom, and there are still limitations of feasibility and resolution in terms of geometry in AM systems. For instance, in SLS systems, small features such as holes, cylinders and thin walls less than 0.5mm cannot be built properly, because the enclosed loose powder is melted by surrounding heat. Also, scanned features may/be insufficient in strength to resist the forces applied during powder deposition, and wall thickness is limited by the laser beam spot size [Kruth et al, 2005b]

There are other disadvantages too, such as the speed of production not being comparable to conventional methods, and the surface finish and accuracy of the parts not always being as good as in conventional technology [Dalgarno and Wright, 2003; Castle Island's, 2010]. Post-processing, such as support removal and finishing [Dalgarno and Wright, 2003; Kruth et al, 2005b; Castle Island's, 2010] is then required. This can significantly increase costs and may be time-consuming, especially

when numerous parts are produced. Furthermore, due to the constraint of the building envelope dimensions of AM machines, the size of products is limited.

Additive manufacturing produces parts or components directly from CAD-driven data, which means that the product can theoretically be manufactured without tooling. However, due to the restrictions of current processes and materials this is still difficult or impossible to achieve. The possibility of the elimination of tooling could shorten the time to market and reduce costs [Hague et al, 2003b; Hopkinson and Dickens, 2003; Castle Island's, 2010]. In addition, the removal of tooling in the early phases of the product development process saves time and money. Another possibility is that parts and products could be produced using materials and design parameters not feasible in the past [Hague et al, 2003b; Hopkinson and Dickens, 2003; Castle Island's, 2010].

The material used is another disadvantage of each additive manufacturing (AM) process [Kruth et al, 1998]. The availability of materials for rapid manufacturing is limited compared to conventional manufacturing technologies. In addition, it may be difficult or impossible to recycle complex materials.

Using additive manufacturing makes it possible to manufacture parts with optimal material properties based on mechanical, thermal, optical and other characteristics. Material can be selected for its variability, and then, by depositing the material physically, its original properties can be optimised or changed. Using data acquired from finite element analysis (FEA), additive technology offers the possibility to use multiple materials, as well as to control the local geometric meso-structure (the fine-scale geometric features and associated visual effects in fabrication, for instance contour / profile / sketch) and micro-structure of a part. This means that the functionality of a part can be optimised in ways that are not possible with other common manufacturing methods [Kruth et al, 1998; Castle Island's, 2010].

In addition, using additive manufacturing technology decreases lead times, it has the ability to produce parts on demand, saves transportation or shipping costs when parts can be produced in or near to the place where they are needed or at the point of use, in the quantity required [Hopkinson and Dickens, 2001; Castle Island's, 2010].

2.2.4 The application of AM Systems

Rapid prototyping (RP), rapid tooling (RT) and rapid manufacturing (RM) are three categories of AM application which have been introduced in manufacturing processes [Pham, 2001, Kruth et al, 2005b].

2.2.4.1 Rapid prototyping (RP)

Additive manufacturing (AM) was first used for developing prototypes of functional products. Functional prototypes are usually used for the visualisation of the concept to verify and justify design details; the verification and optimisation of the design of the proposed part and/or assemblies in order to meet the requirements of the form/fit/function; for design review and assessment; for marketing, promotion and advertising; and for communication with customers. By using rapid prototyping, these purposes can be fulfilled relatively rapidly, since no tooling is required.

2.2.4.2 Rapid tooling (RT)

In the product development cycle, tooling is a critical issue that must be considered. Mould-making for prototypes and production is a time-consuming, high-risk and expensive task due to requirements of geometrical complexity, high accuracy and tolerance [Dalgarno and Stewart, 2001]. As a result, tooling preparation may be the slowest and most costly phase in the product development cycle. The tool must be durable, wear-resistant, and produce a quality surface finish. As reported by Pham [2001], the introduction of rapid tooling has significantly reduced the manufacturing time of prototypes, pre-production and, in some cases, full production tooling.

Rapid tooling is categorised into direct and indirect methods. Indirect rapid tooling uses rapid prototype master patterns to produce a moulding before making a tool, whereas direct rapid tooling uses the rapid prototyping machine directly to manufacture the actual core and cavity mould inserts [Noorani, 2006]. Indirect methods are more commonly used than direct methods, but direct tooling offers more opportunities in time and cost savings. There are several problems with rapid tooling, for instance, accuracy, durability, mould finishing and hardness [Pham, 2001].

2.2.4.3 Rapid manufacturing (RM)

Recently, additive manufacturing has begun to be applied to the manufacture of structural or functional end-use parts or components directly. This technology is continuously developing for a wide area of materials, including metals, polymers, and ceramics for many applications, such as in medical applications and other customised functional applications. This trend, known as rapid manufacturing (RM), is likely to be an attractive technological approach in the future, and is considered in detail in the next section.

2.2.5 Rapid manufacturing (RM)

2.2.5.1 Definition and basic process

Rapid manufacturing has been defined as "the manufacture of end-use products using additive manufacturing techniques (solid imaging)" [Levy et al, 2003]. Other sources describe rapid manufacturing as producing useable products or components directly by using additive fabrication technology [Castle Island's, 2010], or "a technique for manufacturing solid objects by the sequential delivery of energy and/or material to specified points in space to produce that solid. Current practice is to control the manufacturing process by computer using a mathematical model created with the aid of a computer" [Wikipedia, 2009a]. According to Hopkinson et al [2006], rapid manufacturing is defined as "the use of a computer-aided design (CAD)-based automated additive manufacturing process to construct parts that are used directly as finished products or components".

2.2.5.2 Process chain of rapid manufacturing

Even though the basic process of rapid manufacturing (RM) is similar to that mentioned in section 2.2.1, in this section the process is described in more detail as a rapid manufacturing chain. Figure 2-8 illustrates the process chain of rapid manufacturing, showing the relationships between phases and which parts or steps of rapid manufacturing can be used to aid engineering design, in the design phase of product realisation.

Moreover, the final step of the process chain, the post-processing phase, also shows that there is an opportunity to heat-treat the component to improve its material characteristics. This is one of the objectives developed in this research study.

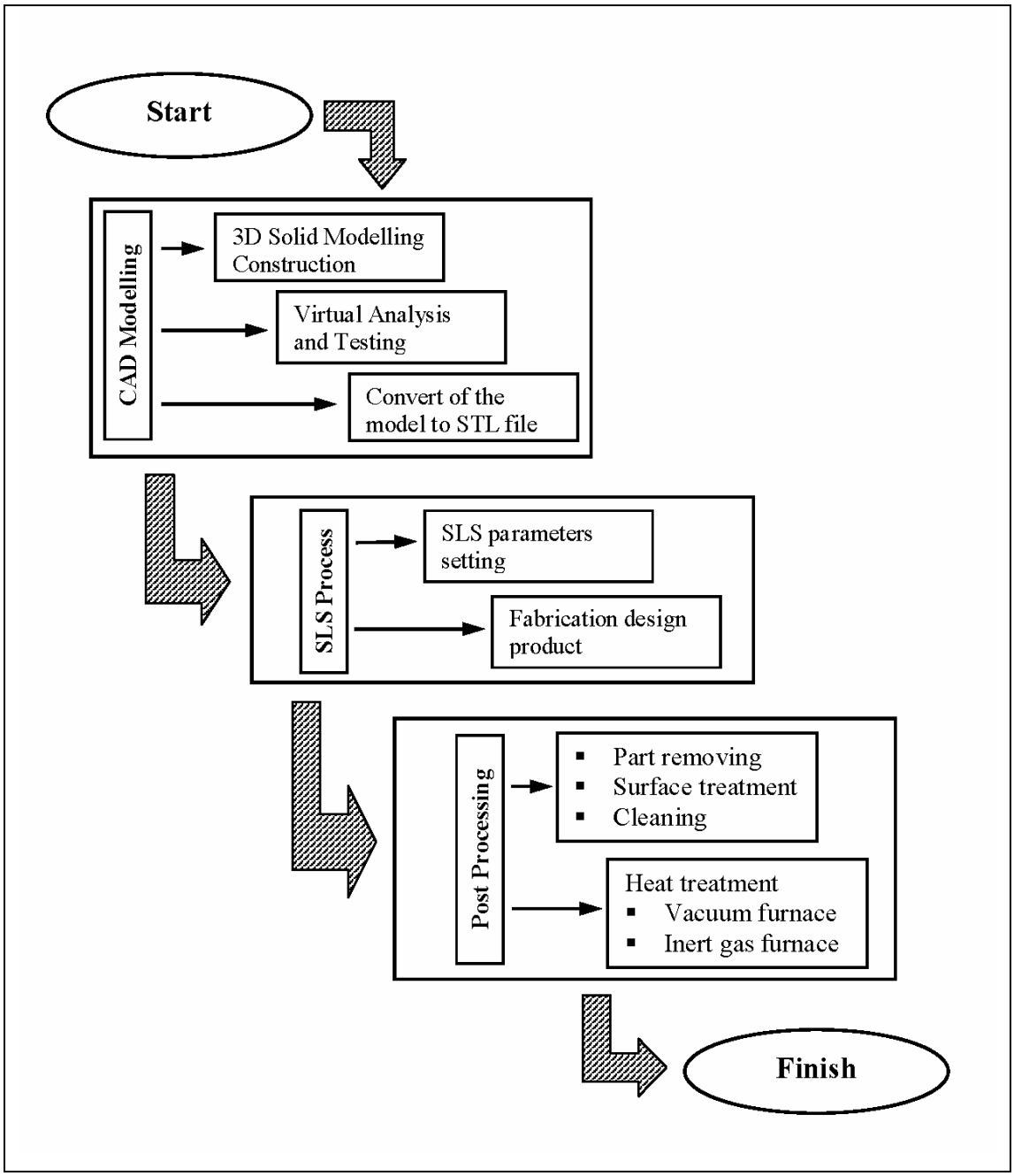

Figure 2-8 Process chain of rapid manufacturing

The basic process chain of rapid manufacturing consists of the following steps [Cee Kai, 2003; Venuvinod, 2004; Noorani, 2006]:

1. Created of CAD model of the design:

   First of all, a CAD solid model is created. Solid modelling software is commercially available, such as IDEAS, ProEngineer, SolidWorks,

Unigraphics, CATIA, or many others, which can be used to create the 3D model part. In this phase, model design can be analysed and tested virtually, for instance regarding the failure analysis of the design prototype of the product.

2. Conversion of the design model to the stereolithography (STL) file format:
   CAD software uses various algorithms to represent solid objects, so that this conversion must be conducted since the STL format has been adopted as the standard for rapid manufacturing technology. The STL format represents a 3D surface as an assembly of planar triangles.
3. Slicing of the STL file into two-dimensional (2D) cross-sectional layers:
   In this phase, the STL file is made ready for construction. By using a pre-processing program, the user adjusts the orientation, location and size of the model. The pre-processing program is normally associated with a particular type of layer manufacture machine.
4. Manufacture of the part:
   The machine constructs the part layer by layer automatically. Generally, the thickness of each layer, depending on the build technique, is in the range between 0.01 mm to 0.5 mm [Gibson and Shi, 1997].
5. Post-processing (clean and finish the model):
   Post processing is the last phase. This work involves removing the part from the machine and detaching any supports that were applied. The component may need surface treatment and minor cleaning, depending on the process and application used. Furthermore, as a post-processing action, heat treatment to modify and characterise the material can also be used to improve its properties.

2.2.5.3 Issues in RM systems

As mentioned in the previous section, there are several reasons for the use of rapid manufacturing. However, one of the most interesting reasons for adopting this technology arises from its advantages in the area of design, rather than the manufacturing approach used [Hague, 2006].

During the last few decades it has been recognised that geometry is a critical factor in design analysis and the development of products, mainly due to cost factors.

Within rapid manufacturing (RM), geometry is not a limiting factor, and freedom of design can be applied. It is claimed that this will reduce lead times and overall manufacturing costs [Hague, 2006].

The range of material, used in RM systems is still limited compared to conventional manufacturing. Since this technology has developed, the choice of possible materials and processes has grown, but not widely enough to support all materials-driven product design.

2.3 Selective Laser Sintering (SLS)

At the present time, SLS is a commonly used technique in rapid manufacturing for prototyping, tooling and manufacturing purposes [Levy et al, 2003] using a wide range of polymer, metal and ceramic materials [Kruth et al, 2003]. It was developed in the late 1980s as a technique for rapid prototyping (RP). In this section, SLS is described in more detail.

2.3.1 Definition and classification

Selective laser sintering (SLS) is an additive manufacturing process that it used to fuse small particles of powdered materials (polymer, metal or ceramic) into a solid mass of desired complex 3D shape, using thermal energy supplied by a focused high power laser beam. Then, by scanning cross-sections generated from a CAD file of the component, the laser selectively fuses and sinters powdered material on the surface of a powder bed, for the first slice of the desired pattern of the object. After each cross-section is scanned, the powder bed is lowered by one layer thickness. Then, using a roller mechanism, a new layer of material is applied on top, and the building process is repeated until the building part is complete **[**Kruth et al, 2005a**;** Wikipedia, 2009b]. A schematic of the SLS process is shown in figure 2-5.

From the definition and schematic process described above, the SLS process is based on two principles, as follows [Cee Kai, 2003; Noorani, 2006]:

a. Consolidation occurs by sintering when the laser beam hits the powder material. The interaction between the laser beam and powder material used increases the temperature toward its softening and melting point, resulting in particle bonding, fusing the particles and forming a solid.

b. The build of components is completed layer by layer, in which each layer of the building process contains the cross-sections of one or many components. Using a roller mechanism, the next layer is then deposited on top of the layers built previously. Again, that powder layer is then sintered by laser to the previous layer.

In SLS systems, the density of parts is affected by the packing density of the powder. Therefore, mechanical properties are usually better when the packing density is higher. However, this also is influenced by the machine parameters and scan pattern used [Gibson and Shi, 1997; Cee Kai, 2003; Noorani, 2006].

2.3.2 Important processing parameters

As shown in Figure 2-9, process variables which have an effect on SLS processing can be categorised into four types: controlled, machine specific and geometry-specific parameters, and material properties. Each of these factors has a different effect on sintering during the process of SLS component formation [Nelson, 1993; Agarwala et al, 1995].

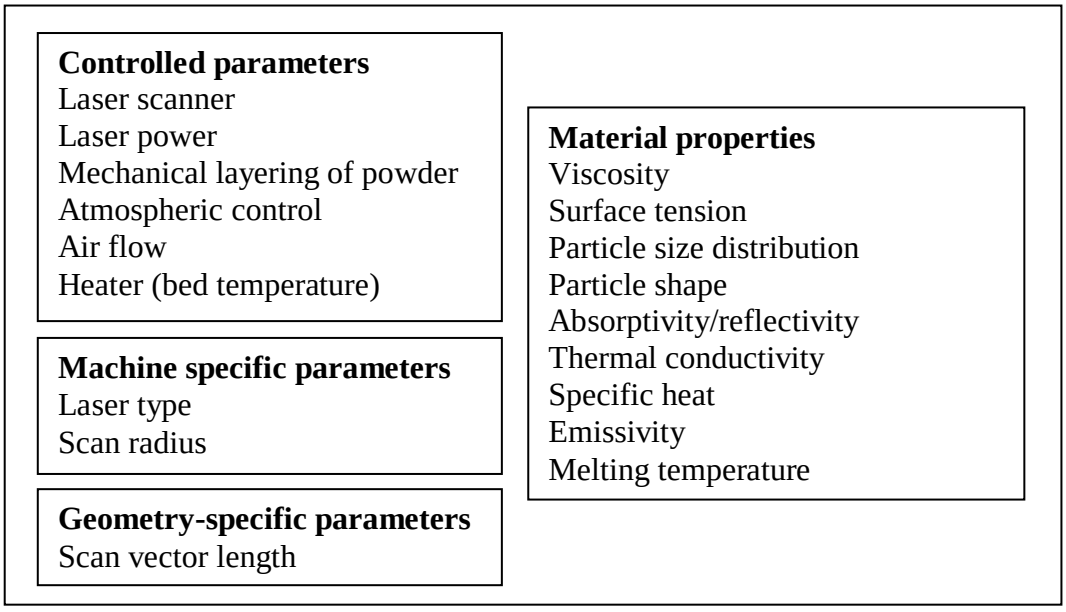

Figure 2-9 Process variables which affect sintering in the SLS process [Nelson, 1993; Agarwala et al, 1995]

This section describes fabrication parameters directly related to the properties of SLS material. These are: part bed temperature, fill laser power, laser beam speed, scan

spacing and slice thickness [Gibson and Shi, 1997; Cee Kai, 2003; Venuvinod, 2004; Noorani, 2006] as illustrated in Figure 2-10.

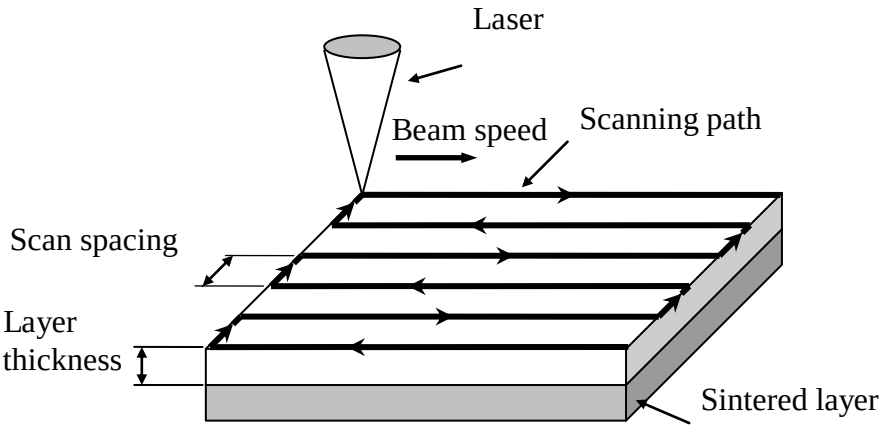

Figure 2-10 Processing parameters in SLS process

a. Part bed temperature (T_b)

The part bed temperature (T_b) is the temperature at which the powder material sits in the part cylinder. In the part cylinder, powder material is heated to the part bed temperature before the laser scanners move, in order that laser power and distortion in the sintering process can be reduced. In other words, the need for laser power is reduced when the part bed temperature is higher, and the difference in temperature between pre- and post-sintering is reduced. Part bed temperature varies depending on the material. For an amorphous polymer, the temperature is normally set near the glass transition temperature (T_g), and for a perfectly crystalline polymer it should be set 3-4^{0}C below its melting temperature (T_m), due to it having no glass transition temperature [Gibson and Shi, 1997].

b. Fill laser power (P)

The fill laser power (P) is the power used to heat the powder material during scanning. The maximum laser power of machines is different based on the type and manufacturer.

Fill laser power is influenced by laser beam speed, the diameter of the laser beam, the density, specific heat, and latent melting heat of the powder [Gibson and Shi, 1997].

In SLS technology, different kinds of lasers are used. CO_2 and Nd-YAG lasers are commonly used in SLS machines. These operate at different wavelengths of 10.6μm for CO_2 lasers and 1.06μm for Nd-YAG lasers. The absorption of laser light depends on material absorptivity, transmissivity and particle size [Nelson, 1993]. The laser wavelength should be adapted to the powder material to be sintered, due to the fact that laser absorption changes greatly according to the material and the laser light wavelength [Tolochko et al, 2000]. Normally laser absorption depends on laser wavelength, the condition of the sintered materials, surface geometry, ambient gas, and temperature [Tolochko et al, 2000]. Powder material can usually absorb laser energy better than solid material, due to multiple reflection and laser beam absorption trapped in the powder pores [Kruth et al, 2003].

CO_2 lasers with a wavelength of 10.6μm are suitable for polymer powders. On the other hand, Nd-YAG lasers with 1.06μm wavelength are better for metals [Kruth et al, 2003].

c. Laser beam speed (*BS*)

Laser beam speed is defined as the linear velocity of the laser beam across the powder surface of the material [Nelson, 1993]. This machine-specific parameter can be adjusted to suit the material being processed.

d. Scan spacing (*SP*)

The distance between the two nearest parallel scan vectors is called the scan spacing (*SP*). Scan spacing influences laser beam size and energy density. The scan spacing must be smaller than the diameter of the laser beam on the part bed, in order that a cross-section of the sintered area can be built completely. Figure 2-11 illustrates scan spacing in the SLS process [Venuvinod, 2004].

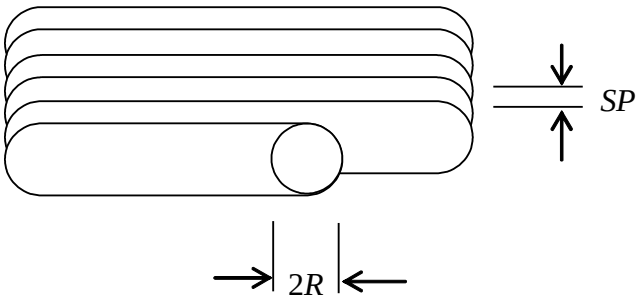

Figure 2-11 Scan spacing in the SLS process [Venuvinod, 2004]

e. Slice/layer thickness (*h)*

Slice thickness (*h)* is another important parameter that must be considered, because it can cause a stair-step effect. Slice thickness is used to determine the powder material thickness of each layer in the part. The range of slice thickness is normally set from 0.01–0.5mm, depending on the type of SLS machine [Gibson and Shi, 1997]. Slice thickness will influence building time and surface roughness. Surface roughness can be reduced by using smaller slice thickness, but the building time of the part will then be longer. The penetration depth of the powder material limits the largest slice thickness. The penetration depth of powder material is influenced by laser power, energy density, particle size, powder density, specific heat and thermal conductivity [Venuvinod, 2004]. Therefore, a suitable slice thickness can be set depending on the material and the laser power available.

f. The energy density (*ED*)

One of the most important factors that influences the quality of laser sintering process is energy density. This indicates how the amount of energy per uniform volume delivered to the powders changes with process parameters.

The energy density is a function of fill laser power (*P*), beam speed (*BS*) and scan spacing (*SP*). Therefore, the important relationship between processing parameters can be defined as in equation 2.1 [Gibson and Shi, 1997]:

$$\text{Energy density } (ED) = \frac{P}{BS * SP} \text{ (Joule/cm}^2\text{)} \quad \text{..... (2.1)}$$

where: *P* is fill laser power (watt)

BS is laser beam speed (cm/s)

SP is scan spacing (cm)

From the energy density equation, two parameters are most commonly altered to gain greater energy density. These are fill laser power (*P*) and laser beam speed (*BS*) as they are the two most influential parameters. For Scan spacing (*SS*), as mentioned in section 2.3.2 (d) must be smaller than the diameter of the laser beam, or as an alternative, it is advised that scan spacing should be 3-6 times smaller. This is in order for each point on the powder bed to receive multiple laser exposures and thus the sintered area can be built completely.

Alterating the settings of these parameters will affect the ability of the material to be built successfully and the quality and properties of the parts manufactured.

For example, the density and tensile strength of an SLS fabricated part increase as a result of increasing fill laser power, decreasing laser beam speed and decreasing scan spacing. Beside of this, the viscosity of the material also decreases, which in turn lowers the porosity and this then increases density [Williams and Deckard, 1998; Caulfield et al, 2007]. On the other hand, due to increased liquid flow if the fill laser power is too high, shear stresses between layers are created and the parts may bend or become distorted [Beaman et al, 1997; Caulfield et al, 2007].

There is an optimum energy density that is needed to achieve the maximum density and strength, which is different for each different material. If the optimum energy density is exceeded, this results in the degradation of mechanical properties and an increase in porosity and the surface degradation of the resulting laser-sintered material [Ho et al, 1999; Caulfield et al, 2007].

Research has shown that varying the energy density can cause variations in the density and tensile strength of polyamide sintered material [Gibson and Shi, 1997; Tontowi and Childs, 2001]. This is supported by research conducted by Ho et al [1999], who investigated the effect of energy density on the mechanical properties of polycarbonate powder. Further discussion regarding the relationship between energy density and mechanical properties is given in section 2.3.3 below.

2.3.3 Melting viscosity, surface tension and particle size

The other important parameters in the SLS process are melting viscosity, surface tension and particle size. The relationships among these parameters for viscous sintering was firstly established by Frenkel in 1945 [Ajoku et al, 2006b], whose formula states that the energy generated during viscous flow is equal to the energy

gained by the reduction in the surface area. Frenkel then used an equation to explain the neck formed in a combination of two adjacent particles, n, as shown in equation 2.2 and Figure 2-12.

$$\left(\frac{x}{r}\right)^2 = \frac{3\sigma t}{2r\eta_o} \quad \text{..... (2.2)}$$

where: x = half the thickness of the neck, r = radius of a sphere, σ = surface tension of the material, t = time needed for sintering and η_0 = melting viscosity.

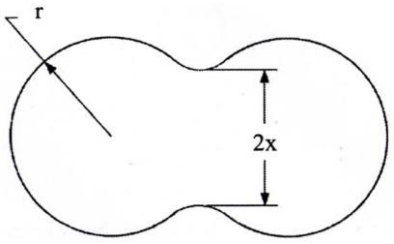

Figure 2-12 Frenkel's sintering model [Ajoku et al, 2006b]

Frenkel analysed the initial stages of the sintering process in crystalline particles and stated that, when high temperature is applied this could serve as a catalyst which will change the crystal form of the structures. Increasing the temperature of the particle resulted in an increase in surface contact area between adjacent particles, and the volume of viscous flow between the particles can cause or eliminate pores. It can be assumed that the sintering that occurs between two particles is formed completely when x/r = 0.5 [Rosenzweig and Narkis, 1981].

From this theory, using equation 2.2, Frenkel illustrated the role of temperature during the sintering process and confirmed that using higher temperatures cause an increase in necking radius between sintered particles. Greater bonding between the particles occurs and pores are reduced when the necking radius increases.

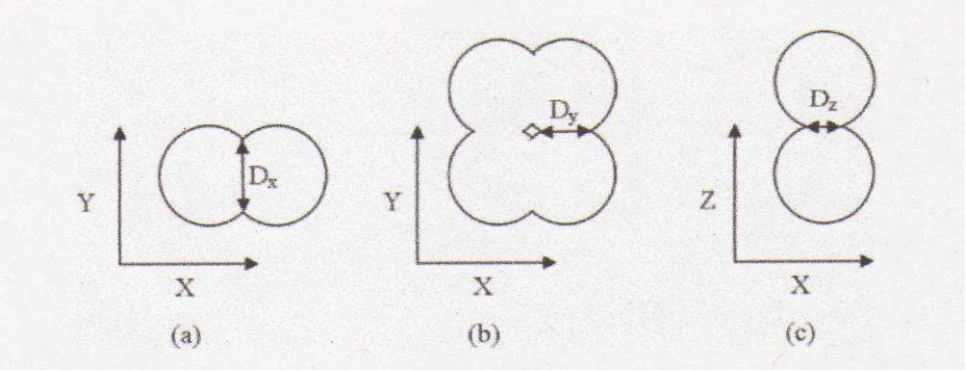

Figure 2-13 Cross-section of particle-particle bonding in x, y and z axes ($D_x > D_y > D_z$) [Ajoku et al, 2006b]

In addition, Ajoku et al [2006b] investigated the bonding between particles in each different fabrication orientation. This phenomenon was observed when they investigated the effect of build orientation and end-of-vector (EOV) effect on the mechanical properties of laser-sintered components. A 3D Systems Vanguard SI laser sintering machine was used and a laser scanning strategy in the x scan vector only was applied.

They illustrated the cross-section of particle-particle bonding in the *x, y and z* axes fabrication orientations, and the findings showed that the diameter of the neck in the*x* axis (D_x) is greater than the diameter of the neck in the *y* axis (D_y), and then (D_x) and (D_y) are greater than the diameter of the neck in the *z* axis (D_z), as illustrated in Figure 2-13.

Polymer powder melts when an infrared laser sinters the component, where the particles bond together. The laser scans as a vector on a layer to build up the first layer of component in the *x* direction and forms a neck with diameter *Dx*, as shown in Figure 2-13(a). After finishing the first vector in this direction, the laser switches off automatically and an increment occurs in the *y* direction that allows the laser to scan the next vector. The bonding in the previous vector is shown in Figure 2-13(a), and the bonding between particles in the *x* direction is quite similar. But particles in the previous vector in the *y* direction will have cooled and, therefore the bonding between these particles will be less than between those in the *x* direction, with a smaller necking diameter *Dy* (Figure 2-13(b)). After this layer is completely sintered, then a new layer of powder is applied. The particle bond in the previous layer will have cooled to the point where the bonding between particles in different layers is less than the bonding between particles in different vectors with an even smaller neck diameter, *Dz* (Figure 2-13 (c)).

From their work, Ajoku et al [2006b] summarised that the mechanical properties from different fabrication orientations are different (anisotropy). The highest tensile and compression strength results from an x axis-fabricated part and the lowest results from the z axis fabrication orientation. This agrees with the results of previous work by Gibson and Shi [1997], in which the best tensile strength of a laser-sintered part results from the test component built in the x axis orientation and the lowest value is obtained from the z axis. However, for flexural strength, the highest value is obtained

from the y axis-fabricated component, followed by that in the x axis and the lowest value for the z axis.

These findings also showed that the degrees of bonding between particles and the subsequent bonding between layers are different in each direction of fabrication. Bonding is also affected by the scanning strategy applied in each layer for different fabrication orientations.

In selective laser sintering, the laser scans across the whole two-dimensional area, which consists of parts being built. Greater time is taken for the laser to restart scanning on a subsequent layer if the two-dimensional scan area is larger.

a. Melting viscosity (η_0)

The melt flow ratio or melt flow index (MFI) can be used to determine the melt viscosity of a material. For polymer materials, the standard test of melt flow ratio can be applied to measure its melt flow properties [ASTM D1238, 2004].

The MFI has units of gram/10min, determined from the mass of polymer extruded during 10 minute of steady flow.

For instance, Kim and Creasy (2004) investigated the melt flow characteristics of PA6 and PA6/clay nanocomposite, as shown in Figure 2.14. They found that the melt flow of PA6 was 1.68 times greater than that of the PA6 nanocomposite.

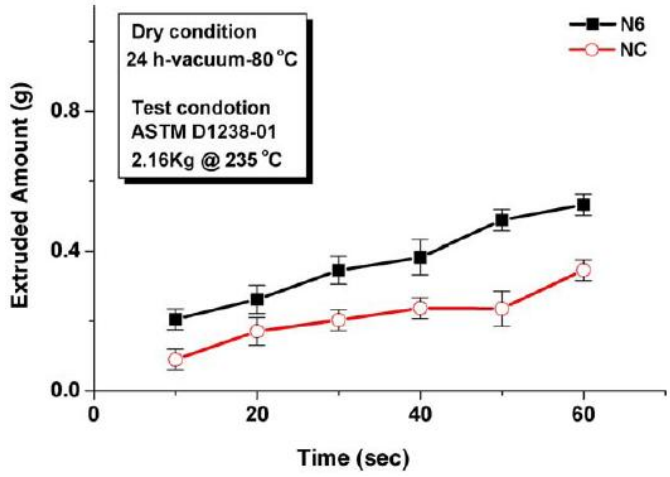

Figure 2-14 Melt flow response of polyamide with and without nanoclay reinforcement (Kim and Creasy, 2004)

For most polymers, the temperature dependence of viscosity is modeled with an Arrhenius relationship as follows (Nelson et al., 1993):

$$\mu_m = A_\mu \exp\left(\frac{E_\mu}{RT}\right) \quad \text{(2.3)}$$

where E_μ is the activation energy for viscous flow and A_μ is the frequency factor, R is the gas constant and T is the absolute temperature (K).

The melt viscosity, μ_m, of polymers follows an Arrhenius relationship with temperature (T), typically decreasing by a factor of 2 for every 25^{o}C increase in temperature at low shear rates (Nelson et al., 1993).

Equation 2.3 also suggests that, to consistently produce parts with uniform quality, the size of powder particles and their distribution must be uniform to ensure a uniformity of polymer molecule weight since melting viscosity is influenced by average molecular weight (M_w).

The melting viscosity and molecular weight of polymer material follow the relationship given by Shi et al [2004] as shown in equation 2.4:

$$\eta_0 = k(M_w)^n \quad \text{(2.4)}$$

where η_0 is the melting viscosity, M_w is molecular weight, k is a constant, and n is another constant value that depends on the critical molecular weight value M_C. When the molecular weight is less than M_C, n = 1, if it is or greater than M_C, n = 3.4.

Equation 2.4 indicates that melting viscosity varies with change in molecular weight. So the quality of the SLS product is affected by the molecular weight via the melting viscosity [Shi et al, 2004]. More discussion of this relationship is given in section 2.3.4

b. Surface tension (σ)

"Surface tension is the driving force for sintering, where the viscous forces must be overcome in order to allow powder sintering" [Ajoku et al, 2006b]. An interaction between molten and non-molten particles occurs during the sintering process, where the molten particle flow freely to attract non-molten powder particles. The powder melts as large amounts of energy go through the surface of the powder bed. The molten particles flow freely to minimise surface energy within the powder particles. As necks form between particles, surface tension causes the material from the two particles to flow together [Nelson, 1993]. The surface tension of polymer powder is about 0.02-0.03 N/m [Shi et al, 2004].

c. Particle size

The particle size of the powder material is a factor that must be considered in achieving the required surface smoothness and feature definition of the product. The precision and density of SLS parts is also affected by particle size, which may be different when different methods are used in producing the powder. For polymer material, particle sizes between 75-100μm are suitable, where a larger size of particle can cause a bigger step/layer thickness effect but a smaller size is difficult to spread [Shi et al, 2004].

2.3.4 Process parameters and material characteristics

Various research studies have been conducted regarding the relationship between process parameters and the characteristics of sintered material. Some of the most important of these are discussed in this section.

Zarringhalam and his colleague investigated the effects of various processing factors on the microstructure and properties of SLS Nylon 12 [Zarringhalam et al, 2006]. They analysed different specimens of SLS Nylon 12 powder and parts produced from different thermal histories, using different machines which were configured with contrasting parameters. Significant increases in elongation at break were shown for refreshed and used powder compared with virgin powder on parts made from different machines. Small variations between virgin and refreshed material were also demonstrated in ultimate strength, with a considerable increase in tensile strength for used powder. The values of Young's modulus also varied, even though the same machine and material was used to fabricate the specimen.

Hague and Gibson assessed the influence of process parameters on the tensile strength of thermoplastic material with different fabrication orientations [Gibson and Shi, 1997; Hague et al, 2004]. These authors showed how the material properties from the laser sintering process were influenced by build orientation, indicating fluctuations in tensile strength and density of specimens produced in different orientations with different fabrication parameters. Furthermore, Hague et al [2004] and Hou [2005] concluded that SLS parts can be considered as anisotropic material, having achieved different results for strength and modulus from different build orientation.

In addition, it has been recognised that, in the SLS process, both material properties and fabrication parameters have a great influence on mechanical properties

[Gibson and Shi, 1997; Caulfield et al, 2007]. The most important characteristics that determine the potential suitability of a material are its glass transition temperature (T_g) and melting temperature (T_m). Characteristics involving specific heat, thermal conductivity, particle size and density are also important.

Gibson and Shi [1997] studied the influence of fabrication parameters on tensile strength and part density for different variations of scan size, scan spacing and fill laser power. The results illustrated that tensile strength and part density increase with decreasing scan size and scan spacing and increasing laser power.

Tontowi and Childs [2001] showed that the powder bed temperature (the temperature of ambient build powder) affects the density of sintered parts which can then have an effect on their mechanical properties. It was reported that the density of sintered components increased when the part bed temperature increased. This relationship is illustrated in Figure 2-15.

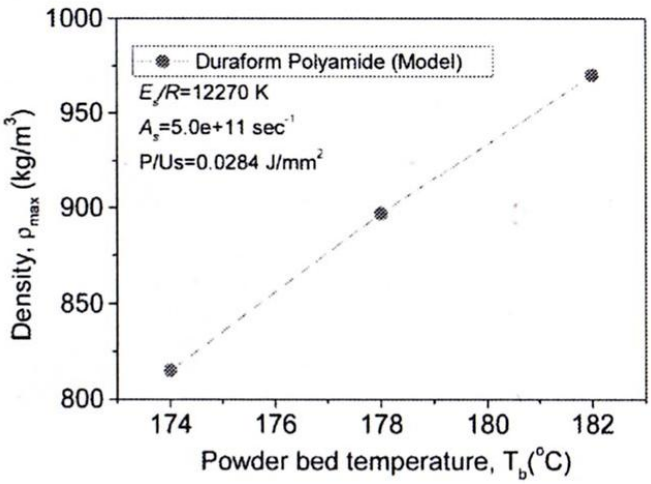

Figure 2-15 Powder bed temperature-density relationship of Duraform Polyamide [Tontowi and Childs, 2001]

In their investigation, Tontowi and Childs [2001] used Nylon 12 (Duraform Polyamide) sample material to study the effect of powder bed temperature on the density of sintered parts. They used powder bed temperatures of 174, 178 and 182^{o}C and at 182^{o}C a fully (100%) solid density resulted where 970kg/m^3 resulted from a default energy density of 0.0284J/mm^2. Meanwhile, the density of SLS fabricated parts was around 96% when the powder bed temperature was reduced to 178^{o}C at the same energy density. This confirms that higher bed temperature also affects the strength of SLS fabricated parts. It also confirms that the control of bed temperature can be used to control part density.

The effect of the properties of polymer materials on the quality of SLS parts was investigated by Shi et al [2004] and molecular weight, molten viscosity, crystallisation rate and the particle size of powder all had an impact. The work initially focused on the relationship of melt viscosity and molecular weight, aiming to increase density and improve mechanical properties. One possibility for increasing density is to maintain a steady temperature flow inside the chamber during the SLS building process. Moreover, the precision of SLS products is greatly influenced by the crystallisation rate, which is itself strongly related to crystallinity. The precision and density of SLS products are also affected by particle size, and sizes of polymer material between 75-100μm are suitable for the SLS process, whereas larger particles cause a bigger step effect and lower density, while smaller ones are difficult to spread. Figure 2-16 shows the relationship between melting viscosity and molecular weight as found by Shi et al [2004].

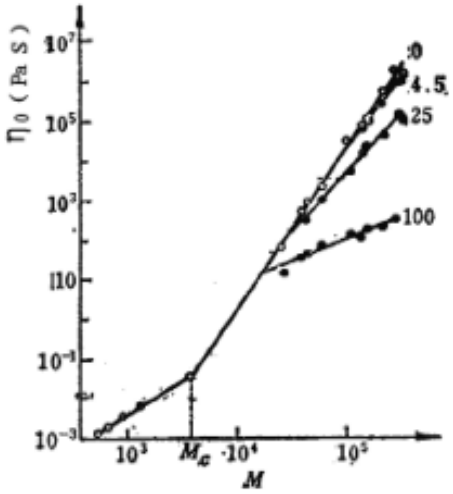

Figure 2-16 Relationship between the molecular weight and melting viscosity of polystyrene [Shi et al, 2004]

Figure 2-16 shows that there is a significant increase in molecular weight with increasing melting viscosity which confirms to Frenkel's model. Frenkel's equation suggests that the radius of the neck between two adjacent particles is closer to the particle size, this leads to a smaller cavity in the sintering part which means that *x/r* increases as η_0 decreases [Shi et al, 2004].

In research into the effects of energy density on the morphology and properties of selective laser-sintered polycarbonate, Ho et al [1999] reported that the structure can be built more densely when a high energy density of laser beam is applied. On the

other hand, when an excessively high energy density is applied, degradation of the polymer will occur and decrease its density. In addition, density directly affects the tensile strength of the specimen.

The tensile strength of sintered components can be improved by increasing laser energy density, as shown in Figure 2-17. The maximum density of 1056 kg/m^3 was obtained at an energy density of about 0.09 J/mm^2, while slight reductions in density occurred with further increases in energy density (Figure 2-17a). The same trend was shown in the relationship between energy density and tensile strength (Figure 2-17b).

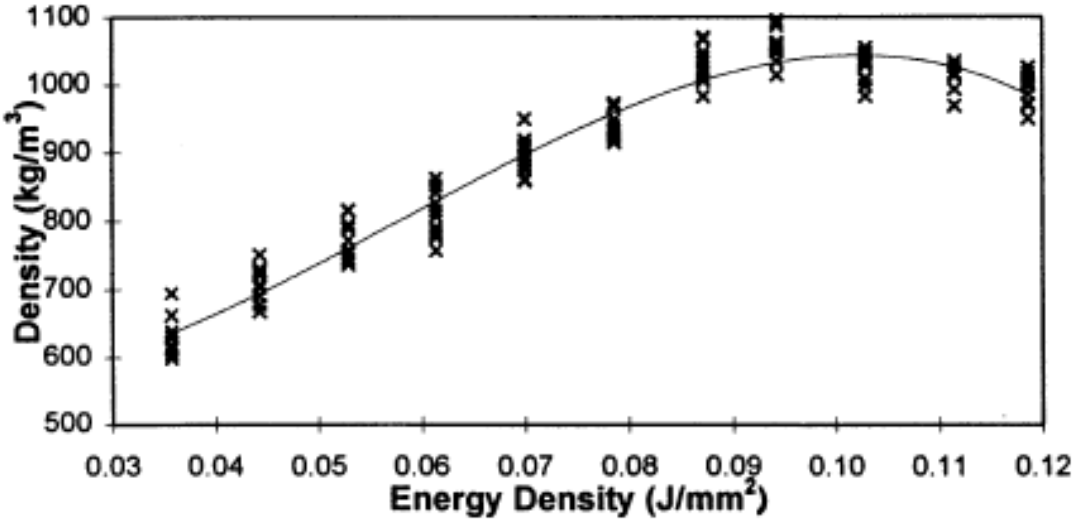

(a)

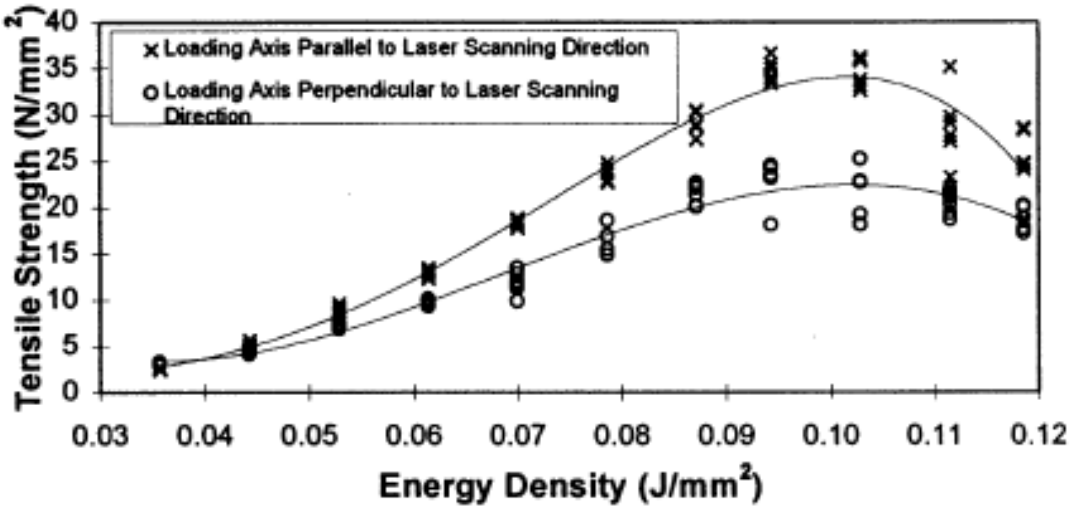

(b)

Figure 2-17 Variation in density (a) and tensile strength (b) with energy density [Ho et al, 1999]

The effect of bed temperature on the sintering process of polycarbonates has been reported by Shi et al [2007], who stated that a sintered specimen warps when the temperature is too low. When the warp is larger, the sintering cannot work normally, due to specimen movement caused by the powder spreading roller. On the other hand, the powder in the area around the specimen will agglomerate and become difficult to remove when the bed temperature is too high.

It has been recognised that the processing used to fabricate components by layer manufacture creates a structure different from normal components. This is because in layer manufacturing, and especially SLS, the material properties depend on the orientation of fabrication [Gibson and Shi, 1997; Caulfield et al, 2007].

2.3.5 Advantages and disadvantages of SLS

Compared to other AM technologies, SLS has several advantages as well as disadvantages. The key advantage of the SLS process is that it can make functional parts in actual final materials. However, the surface finish and accuracy of the parts are not quite as good as those of other technologies, even though the material properties can be quite close to those of the intrinsic materials.

Furthermore, the initial cost of the systems is high; they require various peripherals and facilities, such as hard wire power, and large amounts of floor space. Maintenance and operation costs are another disadvantage of SLS technology, since the powder must be stored appropriately and recycled for further use.

2.4 Polymer characteristics

2.4.1 Introduction

This section describes the basic structure and classification of polymers and their properties. Since SLS machines were introduced, polymers have been the most popular materials for processing. This is principally because of the low energy that is required for processing this type of material. In addition, polymeric materials have low surface energies and high melt viscosities relative to metals and other high surface energy inorganic crystalline materials. This eliminates the trend seen in metals for the molten material to have lower energy due to the formation of spherical droplets that can cause poor surface quality [Beaman, 1997].

2.4.2 Polymer classification

Polymers can be divided into two categories, namely crystalline and non-crystalline (amorphous) structures [Noorani, 2006]. As illustrated in figure 2-18, in crystalline structures, the atoms and molecules form in a repeated and regular form, while in non-crystalline (amorphous) structures the atoms and molecules are arranged locally and randomly without any overall to order or structure.

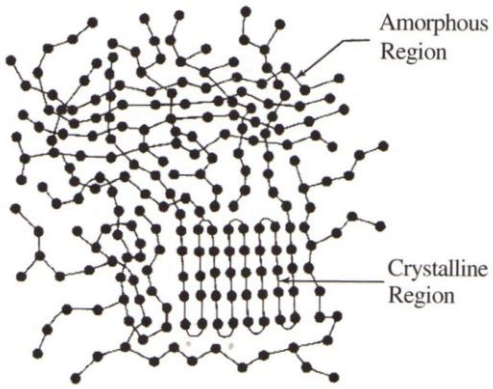

Figure 2-18 Amorphous and crystalline structure of a polymer [Noorani, 2006]

Crystalline and amorphous polymer structures respond differently to changes in temperature, particularly in their phase change from the liquid to solid states. As shown in figure 2-19, when a crystalline material is heated, thermal expansion occurs uniformly until the material changes into a liquid phase when it reaches its melting temperature (T_m), at which point the rate of increase in volume increases [Gibson and Shi ,1997].

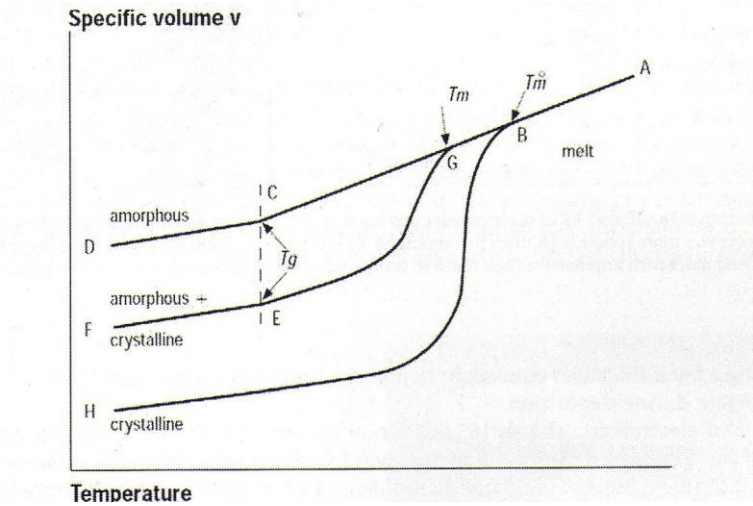

Figure 2-19 Variation of volume with temperature for amorphous and crystalline polymers [Gibson and Shi ,1997]

Conversely, in an amorphous structure, thermal expansion does not change suddenly between the solid and liquid states at the melting point. The material expands at a constant rate until reaching the glass transition temperature point (T_g), at which the solid begins to expand at a higher rate. Between T_g *and* T_m , the material is in a transition/non-equilibrium phase [Kridli, 2006]. This condition is specified by T_g in polymers, which depends on the cooling rate.

Glass and polymers are normally amorphous materials, even though some plastics also have a semi-crystalline structure as an arrangement of crystalline and amorphous structure. A plastic has a T_g above room temperature, while a rubber has a T_g below room temperature [Baker and Mead, 2002].

Compared to crystalline materials, the density of amorphous materials is lower [Kridli, 2006]. Crystallinity also affects the mechanical and physical properties of materials [Kohan, 1995; Baker and Mead, 2002; Noorani, 2006].

All polymers are produced by chemical linkages between monomers (relatively small molecules) to make polymers (very large molecules) that are packed in many monomers as a multiple repeating molecular ('mer') structure [Noorani, 2006 and Kridli, 2006].

Polymer molecular chains can be subdivided into four chain structural groups: linear, branched, cross-linked and networked, as illustrated in figure 2-20 [Griskey, 1995; Kohan, 1995; Kridli, 2006; Noorani, 2006]. The properties of polymers are influenced by the molecular chain structure along with the type of monomer they are made of.

A linear polymer is a long chain that is not straight; it is made up of several backbone atoms and many mers are joined together to form a linear polymer. Some examples of linear polymers include acrylics (polymethylmethacrylate), nylon (polyamide), and polyethylene.

Branched polymers are similar to linear polymers; however, they have side chains growing out of the main molecule. These branches can vary in number and length. Each 'block' varies in packing efficiency and the crystallinity. Compared to linear polymers, branched polymers have lower densities but higher strength. The ABS copolymer is an example of this category.

The third type of molecular chain is a cross-linked structure, whose chain has a 3D-like structure in which two or more chains acting as macromolecules are joined together by side chains/branches that are bonded covalently to the bordering chain

structure. Generally with this chain structure, the strength, stiffness, brittleness and hardness of polymers are higher. Examples of this structure are epoxies and phenolics.

The final polymer structure is the networked chain. Networked chain structures have more covalent bonds compared to cross-linked chains and are usually more rigid and stronger. Epoxies, acrylates, amorphous silica (glass) and phenolics are some examples this type of chain structure.

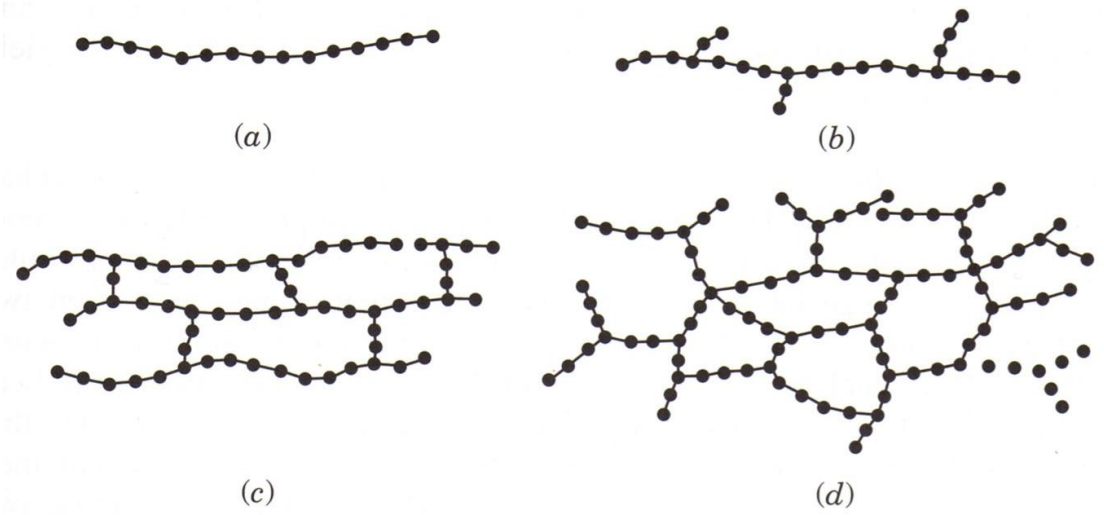

Figure 2-20 Polymer chain structure (a) linear, (b) branched, (c) cross-linked, (d) networked [Noorani, 2006]. • represents a mer

2.4.3 Nylon 12 (Duraform Polyamide)

Among the polymers used in rapid manufacturing and selective laser sintering, nylon is the one of the most popular. Known commercially as polyamides, there are several types of nylon that are commercially available, such as: Nylon 6; Nylon 6,6; Nylon 6,10; Nylon 6,12; Nylon 11; and Nylon 12. If only one monomer is involved (such as lactam or an amino acid), the nylon is identified with only one number, such as nylon 6 or nylon 12. If two monomers are used, the nylon will be identified using two numbers, for example nylon 6,6 or nylon 6,12 [Baker and Mead, 2002]. Nylon 12 is a material commonly used in selective laser sintering (SLS).

Since its early development by Carothers, nylon has recently become an important thermoplastic material [Baker and Mead, 2002]. It is a crystalline polymer that has high modulus, strength, and impact properties a low coefficient of friction and resistance to abrasion. In their backbones, all nylon materials contain the amide (-

CONH-) linkage chain structure, even though they have a variety of properties. Figure 2-21 shows their general structure.

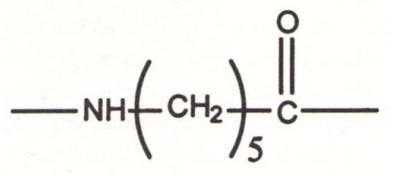

Figure 2-21 Structure of nylon [Baker and Mead, 2002]

Nylon 12 has twelve carbon atoms combined with amide groups (-CONH-). This nylon 12 molecule chain structure is shown in figure 2-22 [Kohan, 1995; Pham, 2008a]. The chain flexibility of semi-crystalline polymers is increased by the presence of the amide group (-CONH-) [Kohan, 1995; Pham, 2008a]. Therefore, the nylon 12 backbone is relatively flexible and the long irregular linear molecule chains could easily transform into a regular order of a folded chain structure during the crystallisation process.

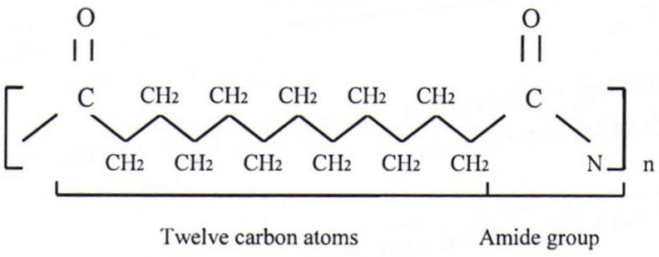

Figure 2-22 Nylon12 molecule chain structure [Kohan, 1995; Pham, 2008a]

2.4.3.1 Mechanical and physical properties

Table 2-1 shows the mechanical properties of polymers produced by the two main manufacturers, 3D systems and EOS GmbH, including Duraform PA, while table 2-2 shows the physical properties of some polymers produced by the 3D Systems manufacturer. These materials are available in powder form and are specifically designed for laser sintering, tending to fuse or sinter when heat is applied. These are predominantly polyamide-based thermoplastics, with a more recently released thermoplastic elastomer. Therefore, the properties of these powdered materials are similar to those of basic materials. However, the tensile test results in table 2-1 mostly

depend on the process parameters for each material and SLS machine used, and the standard applied.

Table 2-1. Mechanical properties of polymers

Manufacturer	Material	Type of Material	Mechanical Properties (Tensile)	
			Strength (MPa)	Modulus (MPa)
3D Systems [2010b]	- DuraForm PA	Polyamide powder (Nylon 12)	44	1600
	- DuraForm GF	Glass-filled polyamide powder	26	4068
	- DuraForm AF	Polyamide aluminium powder	35	3960
	- DuraForm Flex	Elastomeric plastic powder	1.8	7.4
	- DuraForm EX		48	1517
	- CastForm PS	Polystyrene powder	2.84	1604
	- Duraform FR100	Plastic	32	1880
EOS GmbH [2010]	- PA 2200	Polyamide powder (Nylon 12)	45	1700
	- PA 3200 CF	Glass-filled polyamide powder	48	3200
	- PrimeCast100	Polystyrene powder	1.2	1600
	- Somos 201	Flexible TPE	-	15.5

Table 2-2. Physical Properties of SLS Powder of 3D Systems [3D systems, 2006b, 2010b; Wohler, 2006]

Material	DuraForm PA	DuraForm AF	DuraForm Flex	DuraForm GF	CastForm
Type of material	Polyamide powder	Polyamide aluminium powder	Elastomeric plastic powder	Glass-filled polyamide powder	Polystyrene powder
Density-Tap (g/cm^3)	0.59	0.89	0.44	0.84	0.46
Average particle size (μm)	58	Not available	85	48	62
Specific gravity at 20^oC	0.97	Not available	Not available	1.4	0.86
Melting Temp. (^0C)	184	Not available	192	185	Not available
Benefit	Excellent heat and chemical resistance; high surface quality	Cast aluminium appearance; high stiffness; excellent surface finish detail and wear resistance	Rubber-like flexibility and functionality; create coloured components by standard infiltrants	Good heat resistance; increased stiffness	Compatible with standard foundry practices; low ash content

2.4.3.2 Melting, crystallisation and density

Polymer crystallisation takes place in two different stages, nucleation and growth [Wunderlich, 1980; Young, 1983]. Nucleation describes the process of the formation of crystal nuclei through molecular twisting at low temperatures, and this is followed by crystal growth, normally through the addition of further lengths of chain.

The change in linear dimensions of the growing entities of crystallisation at a given temperature is normally linear with time. This relationship can be shown as equation 2.4 [Young, 1983]:

$$r = vt \quad \text{.....} \quad (2.4)$$

where: ***r*** = spherulite radius, ***v*** = growth rate and ***t*** = time

Equation (2.4) is usually valid until the spherulites become so large that they contact each other. As the linear dimensions of the lamellae changes, an equation of similar form for solution crystallisation tends to be observed. Figure 2-23 demonstrates the relationship between crystal growth rate and crystallisation temperature for different fractions of poly(tetramethyl-p-phenylene) siloxane, showing that growth rate is influenced by crystallisation temperature until it reaches a certain peak.

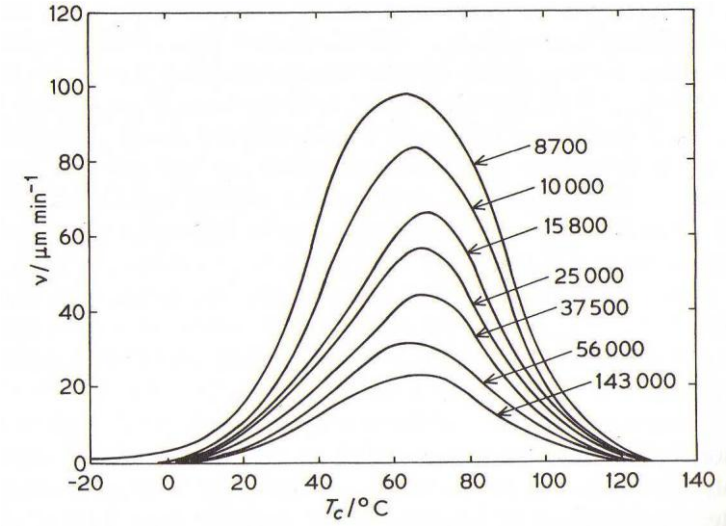

Figure 2-23 Relationship of crystal growth rate and crystallisation temperature T_c for different fractions of poly(tetramethyl-p-phenylene) siloxane (molar mass given in $gmol^{-1}$) [Young, 1983]

From this study, it was also shown that for, the polymer material, the growth rate at the crystallisation temperature near the melting temperature is relatively low. However, this will rise when the cooling rate is greater than before. Along with this, it was also found that, for a given polymer, the growth rate is influenced by the molecular mass, where the growth rate (v) increases as the molecular mass (M) is reduced. This is possible due to two factors that affect the peak of the growth rate. The first is that when the crystallisation temperature is lower, the thermodynamic driving force for crystallisation will increase. However, the viscosity will increase when the crystallisation temperature is reduced. As a result, the transfer of material to the growth point will be troubled and, at this point, the growth rate reaches a peak and then decreases even though the driving force continues to increase, as the crystallisation temperature is reduced.

Furthermore, by making some assumptions about the crystallisation process, the nucleation and growth of spherulites in a polymer liquid can be analysed, as described by Young [1983]. Nucleation will start when a polymer melt of mass W_o is cooled below the crystallisation temperature and when spherulites have been given a period of time to grow. Assuming that homogeneneous nucleation occurs, then the number of nuclei formed (per unit time per unit volume, i.e. the rate of nucleation) at a given temperature is constant, N. As a results, the total number of nuclei formed in time interval dt will then be $N\ W_o$dt/ρ_L ,where ρ_L is the density of the liquid polymer. After a period of time t, these nuclei will have grown into spherulites of radius r. The volume of each spherulite will be be $4\pi r^3/3$, or using Equation 2.4, $4\pi v^{\ 3}t^3/3$. If the density of the spherulite material is ρ_s then the mass of each spherulite will be $4\pi v^{\ 3}t^3$ ρ_s /3. A time t, and when grown from the nuclei formed in the interval dt, then the total mass of spherulite material, dW_s , will be given by:

$$dW_s = \tfrac{4}{3}\pi v^3 t^3 \rho_s N W_o \frac{dt}{\rho_L} \quad \ldots\ldots\ldots\ldots\ldots\ldots\ldots\ldots\ldots\ldots\ldots\ldots\ldots\ldots\ldots\ldots\ldots\ldots \quad (2.5)$$

Then, after a period of time t, the total massa of spherulitic material formed from all nuclei is given by:

$$W_s = \int_0^t \frac{4\pi v^3 \rho_s N W_o t^3}{3\rho_L} dt \quad \ldots\ldots\ldots\ldots\ldots\ldots\ldots\ldots\ldots\ldots\ldots\ldots\ldots\ldots\ldots\ldots\ldots\ldots \quad (2.6)$$

after integration, equation 2.6 becomes:

$$\frac{W_s}{W_o} = \frac{\pi N v^3 \rho_s t^4}{3\rho_L} \quad \ldots\ldots\ldots\ldots\ldots\ldots\ldots\ldots\ldots\ldots\ldots\ldots\ldots\ldots\ldots\ldots\ldots\ldots \quad (2.7)$$

Alternatively, the equation 2.7 can be expressed in terms of the mass of liquid, W_L , remaining after time t, since $W_s + W_L = W_o$

$$\text{i.e. } \frac{W_L}{W_o} = 1 - \frac{\pi N v^3 \rho_s t^4}{3\rho_L} \quad \ldots\ldots\ldots\ldots\ldots\ldots\ldots\ldots\ldots\ldots\ldots\ldots\ldots\ldots\ldots\ldots\ldots\ldots \quad (2.8)$$

For the overall crystallisation process, Equation 2.8 could be modified to account for the impingement of the spherulites, because it is only valid in the initial stages of crystallisation. The overall volume of the system is reduced during crystallisation due to the occurrences of the centres of spherulites moving closer to each other. However, it can be shown that, when impingement is taken into account, W_L / W_o is related to t through an equation of the form:

$$W_L / W_o = \exp\left(-zt^4\right) \quad \text{..... (2.9)}$$

Equation 2.9 is generally known as an Avrami equation. When *t* is small, equations 2.8 and 2.9 have the same form. For types of nucleation and growth other than those considered here, the Avrami equation can be expressed as:

$$W_L / W_o = \exp\left(-zt^n\right) \quad \text{..... (2.10)}$$

where *n* is called the Avrami exponent.

According to Young [1983], the history of specimen process affects the characteristics of polymer melting, especially rystallisation temperature. Besides that, the heating rate at which it is heated is also influential. So the characterisation of a single melting temperature for a polymer sample is unachievable, since melting commonly takes place over a range of temperatures.

A function of the mass per unit volume, density is a function of the weight of individual molecules and the way that they pack [Brydson, 1999]. Higher density can result when the polymer crystallises more efficiently due to molecular packing.

2.4.3.3 Degree of crystallinity

The degree of crystallinity is influenced by many factors during the crystallisation process [Anderson et al, 2003] such as thermal history. It can be calculated using the following equation [Mateva et al, 1997]:

$$X_C = \left[\frac{\Delta H_m}{\Delta H_{PA-12}}\right] \times 100\% \quad \text{..... (2.11)}$$

where ΔH_m is an experimentally determined enthalphy of melting, and $\Delta H_{PA\text{-}12}$ is the melting enthalpy per gram of 100% crystalline material. The value of $\Delta H_{PA\text{-}12}$ used for Nylon 12 is 209.3J/g based on the measurement of Gogolewski [1980].

2.4.3.4 Effect of crystallinity on mechanical properties

Crystallinity affects the mechanical and physical properties of materials [Kohan, 1995; Baker and Mead, 2002; Noorani, 2006]. Bessel et al [1975] investigated the effect of the crystallinity of polymerised Nylon 6 on its mechanical properties. As shown in figure 2-24, the modulus and failure stress increased when the crystallinity

rose, while strain to failure decreased. The fracture behaviour of the Nylon 6 changes from brittle to a ductile material with variations in percentage crystallinity. The material was relatively brittle with an elongation at break (EaB) around 16%, when crystallinity was 44%. However, at lower crystallinity around 37-42% the material became ductile with an EaB from 50-80%. Moreover, at 32% crystallinity the material became highly ductile with the EaB reaching 240%.

Zarringhalam [2007] investigated the relationship between crystallinity and degree of particle melt on the mechanical and thermal properties of SLS Nylon 12 using different settings for building parameters. The results showed that crystallinity and degree of particle melt have a definite relationship with mechanical and thermal characteristics. The values of crystallinity and degree of particle melt varied depending on the build parameters, and it was concluded that tensile strength, tensile modulus and elongation at break fluctuated with the different parameters. The processing and core peak height of heat flow and melt temperature differed as a result of different settings of the build parameters.

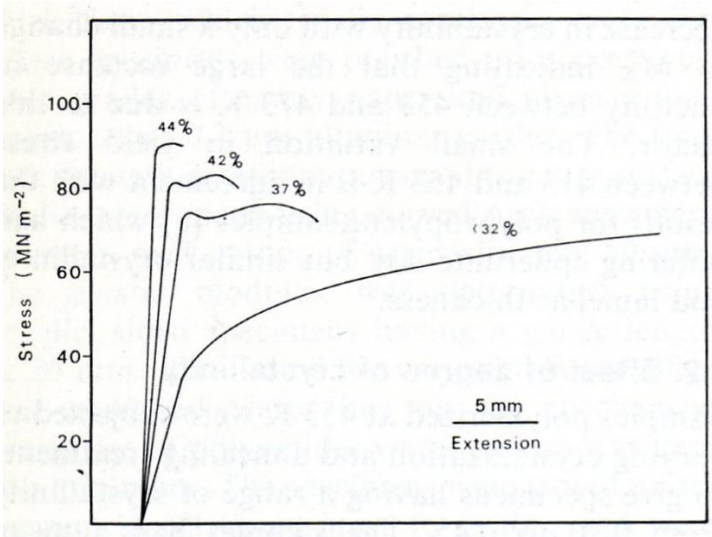

Figure 2-24 Stress-strain behaviour as a function of crystallinity for Nylon 6 polymerised at 453 K [Bessel et al, 1975]

For the degree of particle melting, a high core peak indicates a large amount of un-melted material, and a lower core peak represents more completely melted material [Hopkinson et al, 2009; Zarringhalam et al, 2009].

2.5 Heat Treatment of Polymers

To alter the characteristics of a material, such as its mechanical properties, heat treatment is an option in manufacturing process solutions. Heat treatment can be applied not only in metallurgical processes, such as to steel, but also with polymers.

The heat treatment processes for polymers and non-polymers seem similar. However, the main difference is the temperature used. Depending on the purpose of the heat treatment, polymer materials are usually heat-treated at a lower temperature than for non-polymer materials and so for the latter a furnace with higher temperature is needed.

The heat treatment of polymer material can reduce porosity and increase density and crystallinity, resulting in improved mechanical properties. Meanwhile for non-polymer material such as metal it can also be used to reduce residual stress and improve surface hardness.

Other points that distinguish heat treatment for polymer and non-polymer materials are based on the cooling media and soaking time.

2.5.1 Basic process

Heat treatment is a technique in which the material is heated to below its melting temperature in order to improve its properties. Heat treatment in polymer science can be applied to improved and more stable crystal structure, normally the aiming to improve impact strength [Wunderlich, 1976]. Figure 2-25 illustrates the heat treatment cycle during the process.

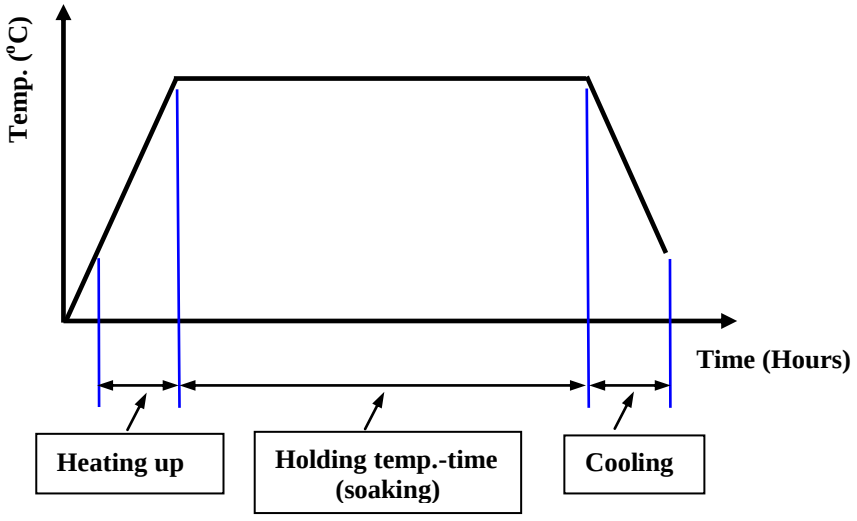

Figure 2-25 Heat treatment cycle

The process is started by increasing the temperature of the oven or furnace at a certain rate, then heating the workpiece up to a selected point, normally below the melting temperature of the material. When this temperature is reached, it is held for a certain duration as required by the design. After that, the specimen is cooled until it reaches room temperature, inside or outside the furnace.

The heat treatment process can be conducted in an inert gas or a controlled atmosphere. To minimise or avoid surface oxidation, the process can be performed at lower temperatures [Kalpakjian and Schmid, 2006].

The heating temperature is selected depending on the type of material and its melting temperature. Also the duration of soaking must be determined.

From the heat treatment cycle above, it can be concluded that three steps that must be considered during the heat treatment process, amely:

1. Heat treatment of the workpiece to a specific range of temperatures in a furnace
2. Soaking in which temperature and duration time of the work piece heated.
3. Cooling in air or in the furnace

As mentioned previously, the heat treatment of polymer materials has not in standardised, and so in this study information was collected from metal heat treatment as an initial reference point, to carry out and to suit the polymer heat treatment process.

Along with the above factors, the effect of distortion should also be considered.

2.5.1.1 Heating temperature / time

Heating temperature can be selected depending on the type of material and its melting temperature. Besides that, the time for soaking is determined based on the expected result of the process. For comparison, in metal heat treatment, there are several factors that must be taken into consideration in determining heat-up and soak times, as shown in Figure 2-26.

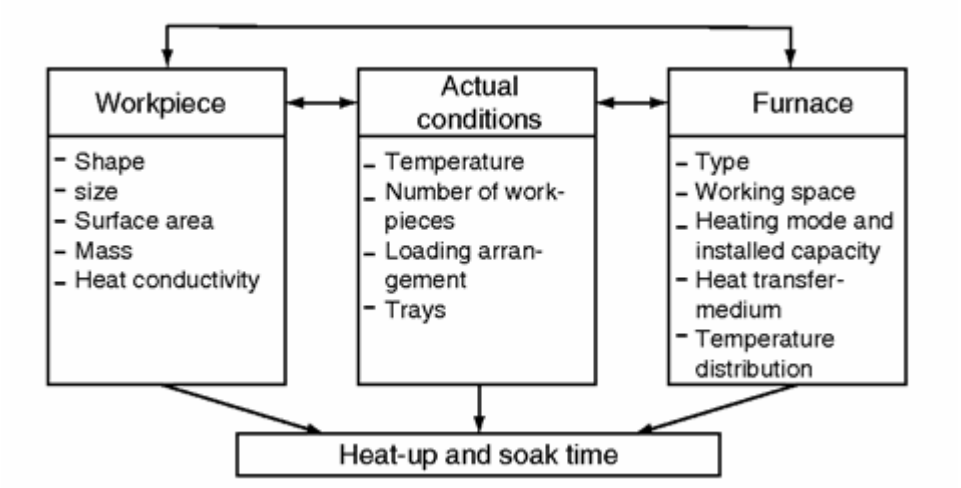

Figure 2-26 Main factors influencing heat-up and soak time [Totten, 2006]

In addition, Figure 2-27 shows another way to determine the thermal soak time for a packed load.

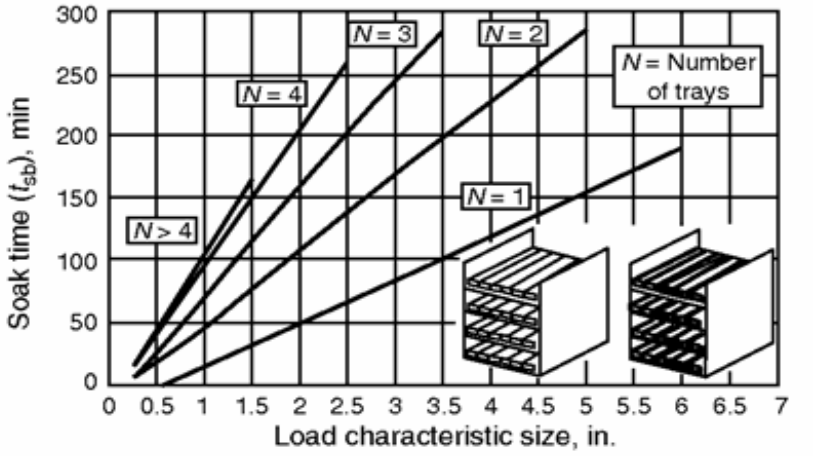

Figure 2-27 Thermal soak time for a packed load [Totten, 2006]

2.5.1.2 Heating media

The heating medium is another factor that must be considered when a heat treatment process is designed. Usually, a furnace is selected based on the capacity needed. The next choice concerns the atmosphere the heat treatment will be conducted in. Alternative furnaces are available on the market such as those fitted with inert gas or vacuum. Currently, in most furnaces start and end temperatures, heating rate and holding time are set as required using digital control.

The vacuum furnace is another alternative for the heat treatment process. Heat treatment in a vacuum has several advantages. It can prevent surface reactions such as

oxidation or decarburisation remove surface contaminants such as oxide films and residual traces of lubricants add a substance to the surface layers of the work or remove dissolved contaminating substances [Techpro, 2009].

2.5.1.3 Heating and cooling rates

Heating and cooling rates are also important. If the rate to slow, heat treatment will take more time. However, when it is too fast, it will affect the homogeneity of the structure, therefore, it is recommended to select slow heating/cooling rates.

2.5.1.4 Cooling medium

As shown in table 2-3, several cooling media are commonly used in the heat treatment of Nylon, each having advantages and disadvantages.

Table 2-3. Advantages and disadvantages of heat treatment fluid [Kohan, 1995]

Fluid	Advantages	Disadvantages
Gas General Air Nitrogen	 No clean up Low cost No oxidation	 Poor heat transfer Surface oxidation, discolouration Breathing hazard
Liquid General Boiling water Mineral Oil Glycerin Silicon Oil Polyglycol	 Heat transfer Low cost, clean Low cost Water soluble Chemically inert Water soluble	 Post-anneal cleaning Plasticisation High temperature limits Low boiling point: 182^{o}C Oxygen permeable Limited stability, use antioxidant
Hot wax General Paraffin Glyco wax S932	 -- Modest cost --	 -- Wax residue Wax residue

2.5.1.5 Distortion

The variations in the manufacturing process can cause distortion which creates an unexpected or inconsistent change in size or shape [Narazaki, M., 2006]. This must be carefully checked when the product needs the same dimensions after heat treatment.

Due to the improvement in properties, the post-processing analysis of distortion needs to be taken into account to ensure the consistent geometry of the end product.

2.5.2 Review of heat treatment of polymers and its impact

Many studies investigating polymeric materials have considered thermal condition and stability, microstructure, and the impact on the microstructure on the mechanical performance. In addition, experimental work effect of selective laser sintering (SLS) on material properties has also been conducted.

Zarringhalam and Hopkinson (2003) reported that using heat treatment as post-processing can improve the tensile strength and impact strength of SLS parts made from Nylon 12. In these studies, conventional heating in a Zwick temperature chamber was used to heat treat the specimen samples at different temperatures (155 to 183^{o}C) and for varying times (1 to 3 hours).

It was reported that impact strength increased by 60% compared to the standard value for the material after heat treatment at 183^{o}C for 3 hours. Tensile strength improved from 45.79 MPa to 52.69 MPa by 15% at these settings, whereas it increased to 47.24 MPa (3%) at 175^{o}C, and to 47.70 MPa (4%) at 180^{o}C for the same duration. In addition, the tensile modulus increased from 1796.17 MPa to 1904.47 MPa, 1863.19 MPa, and 1916.08 MPa when heat treated at 175^{o}C, 180^{o}C, and 183^{o}C respectively for 3 hours. Lower values of impact strength, tensile strength and tensile modulus were reported when heat treated at 155^{o}C, 165^{o}C, and 175^{o}C for 1 hour.

The effect of annealing on the thermal properties and crystalline structure of Nylon 11 (polyundecaneamide) and Nylon 12 (polylaurolactam) was investigated by Gogolewski [1979] and Gogolewski, et al [1980] respectively. It was reported that crystal size, melting temperature and the heat of melting rose with increased annealing temperature. For Nylon 11, the melting temperature and melting heat increased from 190^{o}C and 10cal/g to 211^{o}C and 20cal/g when treated at 180^{o}C for 2000 hours, whereas for Nylon 12 the values increased from 174^{o}C and 10cal/g to 187^{o}C and 23cal/g when treated for 1000 hours at 169^{o}C.

Scobbo and Hwang [1994] studied the effect of annealing on Poly(Phenylene Sulfide) using dynamic mechanical analysis (DMA). The annealing was performed in a vacuum oven for a constant duration of 4 hours, but in different temperatures of 160, 180, 200 and 220^{o}C. It was found that, as the annealing temperature increased, the

modulus also increased as a result of the increase in crystallinity. Moreover, the glass transition temperature increased with crystallinity. It was concluded that more of the amorphous material can gradually crystallise as the annealing temperature increases. The overall percentage crystallinity increased slightly with annealing, and modulus behaviour was influenced by thermal history.

Tregub, et al. [1993] investigated the effect of the degree of crystallinity on the static mechanical properties and fatigue performance of poly(etherether ketone) PEEK matrix composite material. A higher degree of crystallinity resulted in improved mechanical properties, and strength and flexural modulus were considerably higher for 35% compared to 10% crystallinity.

The effects of vacuum annealing on the physical properties of thermoplastics were studied by Ramazani and Mousavi [2005]. Their studies investigated the vacuum heat treatment of polystyrene at temperature between 60 to 90^{o}C and of Nylon 6 between 160 to 190^{o}C; and for durations between 24 to 72 hours with different degrees of vacuum (–700 to –900mbar). It was found that significant impacts on the mechanical properties of materials occured when heat treatment was conducted at higher levels of vacuum at high temperatures. The tensile strength of polystyrene increased by about 10% when heat treated at 80^{0}C or less at a vacuum level of –700 mbar. When nylon 6 was treated at about 190^{o}C (near the melting temperature of about 220^{o}C) for a short time in –900 mbar vacuum, tensile strength increased from 6.90 kgf/mm^{2} to 7.56 kgf/mm^{2} and the tensile modulus also increased from 190.12 kgf/mm^{2} to 223.88 kgf/mm^{2}.

Heat treatment to improve the mechanical properties of the polymer polyhydroxyamide was also performed by Chang, et al [1998]. It was reported that the values of the strength and initial modulus of the material were improved by increased the annealing temperature and time respectively.

Table 2-4 summarises the heat treatment studies on some relevant materials, nylon and polymer materials.

Table 2-4. Summary of Heat Treatment Studies of Nylon and Polymer Materials

Study by	Materials	Temp. (^{0}C)	Proximity to T_m	Atmos-phere	Time (Hours)	Outcome
1	Polystyrene	60 – 90	*N/A*	vacuum	24 – 72	At vacuum level (–700 mbar), tensile strength and modulus increased by about 10% when heat treated at 80^{o}C or less
	Nylon 6	160 – 190	30 (220)	vacuum	24 – 72	At 190^{o}C tensile strength and modulus increased at vacuum level (–900mbar)
2	Nylon 12 laser sintered	155 – 183	1 (184)	air	1 – 3	At 183^{o}C for 3 hours, ultimate tensile strength and tensile modulus increased
3	Polyhydro-xyamide (PHA)	250 – 500	*N/A*	vacuum	0.5–9	Strength and initial modulus increased when annealing temperature and annealing time increase
4	Poly(Phenylene sulfide)	160 – 220	65 (285)	vacuum	4	Modulus, crystallinity, glass transition temperature increased
5	Poly(ether ether ketone) (PEEK)	25 – 150	*N/A*	air	40 minutes	Higher crystallinity, give higher flexure modulus and strength
6	Nylon 11	175 – 180	40 (220)	air	5–2000	At 180^{o}C and 2000 hours, crystal size, melting temperature, heat of melting increased
	Nylon 12	165 – 173	36 (209)	air	10–2500	At 169^{o}C and 1000 hours, crystal size, melting temperature, heat of melting increased

Note: 1. Ramazani and Mousavi [2005]
2. Zarringhalam and Hopkinson [2003]
3. Chang, et al [1998]
4. Scobo and Hwang [1994]
5. Tregub, et al [1993]
6. Gogolewski [1979] and Gogolewski, et al [1980]

N/A = Not available

2.5.3 Review of geometry impact and scanning strategy on mechanical properties of SLS and SLM

It was noted that most researchers specialising in selective laser sintering (SLS) or selective laser melting (SLM) investigated and focused on the effect of processing parameters on mechanical properties. However, even though it has been studied extensively, there is still limited information on the effect of geometry on mechanical properties and thermal properties. In addition, studies that were conducted focused on the geometrical impact on mechanical properties using solid "dog bone" and solid round bar specimens with different setting parameters.

Research by Majewski and Hopkinson (2011) was carried out using solid "dog bone" specimens to investigate the geometrical impact on mechanical properties. They used tensile test specimens that were built in three different orientations in YX, YZ and ZY direction (where the first letter denotes the axis parallel to the longest dimension, and the second letter denotes the axis parallel to the second longest dimension) with six different thickness 2, 3, 4, 5 and 6mm. The results showed that at any build orientations, the section thickness had no significant effects to the tensile properties or on the repeatability of the properties. Thus, there was no significant effect on any mechanical properties on nylon-12 laser sintered materials.

In another study conducted by Hitt et al (2011), they investigated the effect of section thickness on fracture toughness. The study involved using a number of specimens made with different range of thicknesses. It was reported that an increase of around 48 per cent in the energy is required to initiate crack growth per unit area with increasing thickness for SLS nylon 12 specimens. Meanwhile, in the density observation there was a small increase (around 5 per cent) as the sample thickness increased from 2 to 10 mm each time.

The scanning strategy is another important factor besides process parameters to consider as described in section 2.3.2 when fabricating components using SLS and SLM. To optimise this function, the user or operator can select the scanning strategy before manufacturing the laser sintered parts. This could be a "fill only" or a "fill and outline" option. In the most recent established strategy, the laser beam does not only scan the entire cross section but also outlines its contour.

Three scanning strategies in SLS and SLM were introduced, which includes *roster scan*, *across scan* and *outline scan* applied in processing the parts [Yusoff and

Thomas, 2008]. The first one is *roster scan*, which involves scanner moving parallel to the X axis. The second one is called an *across scan*, where the scanning strategy is applied in perpendicular direction to each layer. The third scanning strategy is 'outline scan'. This is where the outer perimeter of the area is outlined.

Recently, research study on different scanning strategy in SLS and SLM became an interest due to the purpose of scanning itself in building the parts and material. From several investigations regarding this issue, the research finding shows and confirms that there were changes on their mechanical and other properties of laser sintered product and materials.

The influence of the laser scan strategy on grain structure and cracking behaviour in SLM powder-bed fabricated nickel super-alloy was investigated by Carter et al (2014). In this study, default scan strategy (Concept Laser M2 SLM) and the concept of a 'band' heating effect across each 'island' has been compared. 'Moving point' heating was suggested and supported by Electron Back Scattered Diffraction (EBSD) evidence. An EBSD map from a sample formed using a simple 'back-and-forth' strategy was also presented and a dramatic difference in grain structure and crystallographic orientation was found. It was confirmed that the condition undergone by the sample strongly influences the grain structure of the final material of specimen.

Bo, Qian et al (2012) stated in their research that laser scanning strategy can be used to determine the relationship of deformation magnitude and the shape of the residual stress profiles. However, in order to optimize manufacturing and reduce the deformation of manufactured metal layers, helix scan strategy and progressive scan strategy for selective laser melting technology was implemented, as illustrated in Figure 2.28. They have found that helix scan strategy was more able to reduce the deformation of melted layer compared to progressive scan strategy.

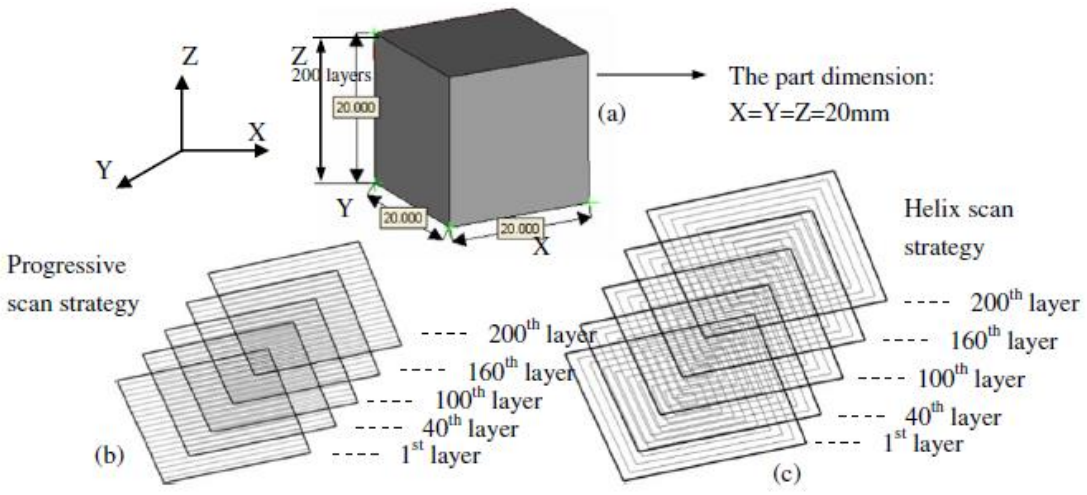

Figure 2-28 Illustration of technique and specifies of helix and progressive scanning strategy (a) the part model, (b) the random five scan layers with progressive scan strategy, (c) the random five scan layers with helix scan strategy [Bo, Qian et al, 2012]

The effect of laser scanning strategy and energy density on orange peel phenomenon of selective laser sintering process (SLS) was studied by Yussoff and Thomas (2008). In addition, Pham et al (2008) investigated the same issues that impacted the surface finish. They used recycled Polyamide 12 (PA12) powder on the manufacture of a Selective Laser Sintered (SLS) part.

Yusoff and Thomas (2008) found that by using recycled PA12 material, a poor and unacceptable surface finish was obtained. Then, they developed a strategy to eliminate the coarse surface texture known as “orange peel” by experimenting it on the specimens and controlling the most important SLS process parameters.

Pham et. al (2008b) used experimental design optimisation (DOE) to improve part of surface finish by observing the factors of laser scanning speed, scan spacing, laser power, scanning strategy and part bed temperature on the specimens . Their studies confirmed that SLS process parameters could enhance the surface quality making it better while using the proper scanning strategy.

The experimental results suggested that by implementing an effective laser scanning strategy and energy density value, the surface quality would be enhanced. Proposed method by Yusoff and Thomas (2008), states that a threshold MFR value of 18 is needed for the PA12 and any values lower than that created parts of poor and unacceptable surface quality.

Yadroitsev et al (2007) studied on parametric analysis of the selective laser melting process. They used different power and velocity (*P/V*) ratio to show the different influences of it on the properties. Their study reported that larger *P/V* ratio means larger re-melted line known as the "vector". Along with this, they also studied whether the shifting of consecutive single vectors had any impact on the process of forming the first layer. Different strategies were implemented to form objects with inner structures that are less than 1mm.

Ma, Liang and Bin, Hongzan (2007) studied the effect of laser scanning pattern on temperature, residual thermal stresses and distortion. They found that a layer created by a fractal scanning patterned processed by a moving laser beam has reduced amount of distortion. They concluded that in comparison with the 'S' scanning pattern, a more symmetrical temperature field and smaller distortion can be obtained by using fractal scanning pattern. In addition, their results demonstrated residual thermal stresses have insignificant effect on distortion in contrast to transient thermal stresses. Figure 2.29 shows the illustration of scanning strategy that investigated by Ma, Liang and Bin, Hongzan (2007).

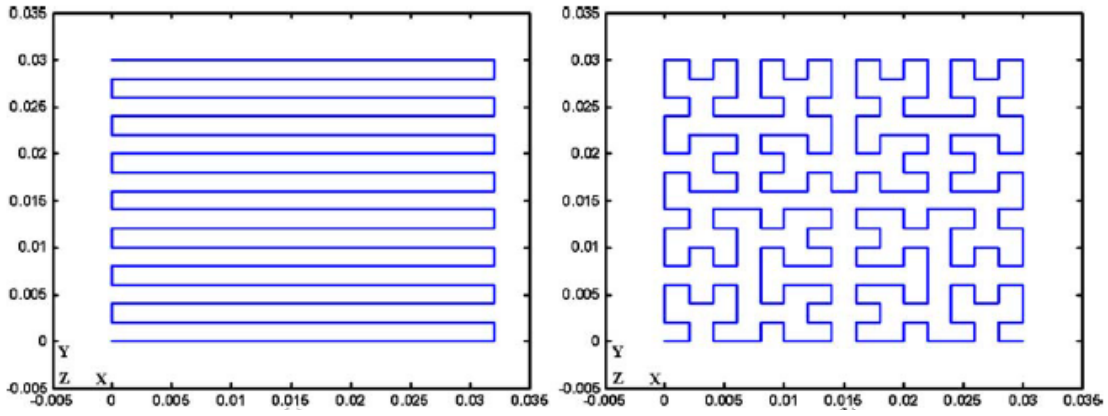

(a) (b)

Figure 2-29. Scanning strategy (a) with "S" scan pattern and (b) with Fractal scan pattern [Ma, Liang and Bin, Hongzan, 2007]

Kolosov et al (2006) studied homogeneity aspects in selective laser sintering (SLS). They examined the impact of the laser scanning strategy on the quality of sintered structure. They found that both sintering precision as well as the inner sintering quality is influenced significantly by the hatch distance. However, this fact has been often ignored in earlier studies.

Other related research regarding scanning strategy was also investigated by Yang et al (2003). They observed the relation between fractal scanning path generation and control systems for selective laser sintering (SLS). From the studies, they found that in comparison with the linear scanning path, the samples possessed an improvement in physical performance when using the fractal scanning.

Bugeda et al (1999) studied on numerical prediction of temperature and density distributions in selective laser sintering processes. Their investigation was based on a finite element model which has been developed for the 3D for simulations of single track SLS process. The model takes into account the thermal and sintering development in the process along with the temporary nature of the problem.

Stamp et al (2009) investigated the development of a scanning strategy for the manufacture of porous biomaterials by selective laser melting. Their aim was to develop a manufacturing process that is cost efficient as well as producing structures that meet the requirements. In order to do this, they developed a 'beam overlap' technique to create porous structures in commercially pure titanium using SLM.

2.6 Summary

The concept of additive manufacturing (AM) has been reviewed and discussed in this chapter. AM technology has developed using an additive approach that differs from conventional manufacturing processes. Selective laser sintering (SLS) is one of these technologies, using powder as raw material. Currently, SLS has become an option in the type of manufacture of end use products or components known as rapid manufacturing. Rapid manufacturing is a rapid process concept aiming to match market and customer demand rapidly.

However, this process produces inconsistent mechanical properties, even when using the same materials and the same machine. The mechanical properties of components are influenced by processing parameters, build orientation and the type of machine used. Scanning strategy is another factor that needed to consider when produce the part. One of the most common materials used in the SLS process is Nylon 12, commercially known as Duraform PA [3D Systems, 2006b]. Nylon 12 is a thermoplastic polymer which has a semi-crystalline microstructure. Crystallinity is the main factor that influences the properties of polymers, and particularly their

mechanical properties. Better mechanical properties, such as strength, modulus, hardness, and density, can be obtained when crystallinity is higher.

The degree of crystallinity of many polymers can be increased by using heat treatment to improve the molecular bonding in their chain structure. Nylon 12 has a semi-crystalline structure, and so it has the potential to be heat treated.

In rapid manufacturing and the SLS process, the final phase is post-processing. This phase is used to improve the quality of the product, for instance its surface quality or dimensional accuracy, as well as other finishing work as required.

From the fundamental theory and previous work in this area, the following conclusions can be drawn:

- Selective laser sintering is a technology developed for rapid manufacturing.
- Nylon 12 is one of the most popular polymers used in selective laser sintering (SLS).
- The material properties of Nylon 12 produced by SLS are anisotropic. Its characteristics also vary in different fabrication orientations. The mechanical properties are inconsistent.
- Crystallinity is an important factor affecting material properties, especially strength and modulus. In addition, scanning strategy is another alternative factor to alter the tensile properties.
- Heat treatment can be used to increase the degree of crystallinity.

2.7 Engineering context of research work

The main purpose of this research study is to understand the mechanical properties of Nylon SLS parts as an important step in aiding engineering design as one stage of the product realisation process. Then, post-processing methods are developed that can be used to improve the characteristics of the layer manufacture material. A heat treatment process is developed with the aim to generate consistent mechanical properties in the processing of Nylon 12 powders using selective laser sintering (SLS).

Analysis of rapid manufacturing has shown that there is a lack of data for materials used in rapid manufacturing systems. Such data is critical in the selection processes, particularly regarding failure analysis. Laser-sintered material produced using SLS has no consistent mechanical properties. As a consequence, to improve and generate more consistent mechanical properties in the process of producing objects

from Nylon 12 powder using SLS, the development of post-processing can be considered an alternative solution.

Therefore, in this research, heat treatment was selected as a post-processing method to improve the mechanical properties of laser sintered products. Figure 2-30 shows a flow diagram of the research into the heat treatment of nylon 12 laser sintered products conducted in this study.

Furthermore, this study also investigates the impact of fill and outline scanning strategy on the mechanical properties of closed hollow structures with different section thickness and solid specimens.

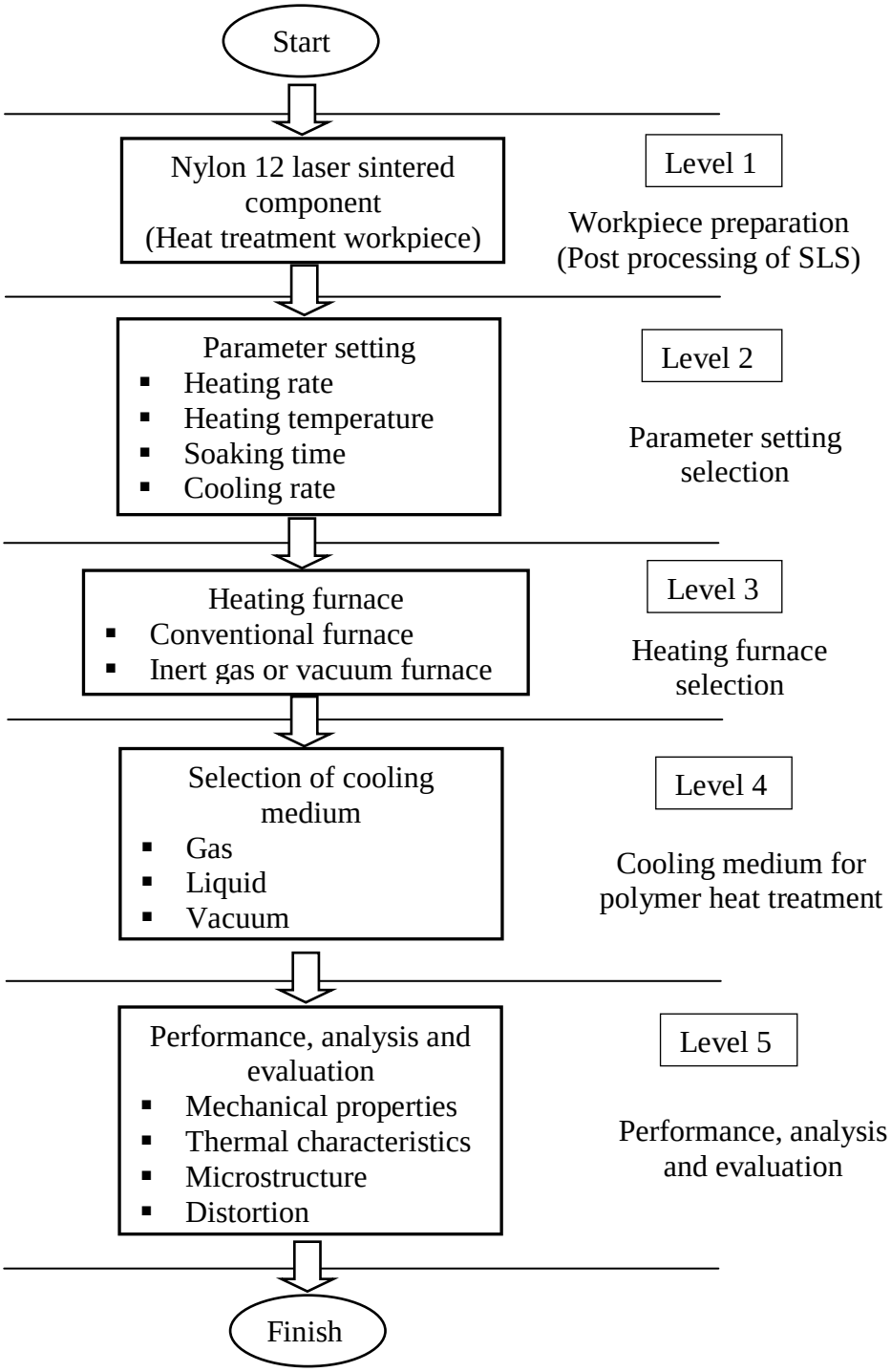

Figure 2-30 Flow diagram of heat treatment of nylon 12 laser sintered product

CHAPTER 3. EXPERIMENTAL STUDIES AND PROCEDURE

3.1 Introduction

This chapter gives details of the tests used to characterise mechanical properties and material conditions. Section 3.2 focuses on the SLS machine and material, while the subsequent section describes the specimen design and building for test samples. The mechanical testing equipment, and experimental test selection and procedures are described in sections 3.4–3.5. The heat treatment processes are then discussed in section 3.6 and the statistical tools employed for data analysis are explained at the end of this chapter.

3.2 SLS Machine and Material

A Sinterstation Vanguard^{TM} SLS machine from 3D Systems, as shown in figure 3-1 installed at the University of Leeds, was used to produce test samples in this study. The machine has a build volume as follows: width (X) = 370 mm, depth (Y) = 320 mm, and height (Z) = 445 mm. The machine has a maximum scan speed of 10,200 mm/sec. and was equipped with a 100 Watt CO_2 laser. More detailed specifications for the machine can be found at the 3D Systems website [3D systems, 2006a].

In this research, the study is focused on the investigation of heat treatment effect as a post processing and also the effect of different scanning strategy on their material characteristics of laser sintered product, rather than effect of different setting process parameters.

As described in the chapter 2 (literature review), setting process parameters of the SLS machine would influence the characteristics of laser sintered product, therefore to simplify and to reduce the risk of this consequence, in this research study, the default setting parameters was used to produce the test samples. Table 3-1 shows the default setting process parameters that were used in fabricating test specimens.

Duraform Polyamide (PA) material was chosen for the samples to be tested, because it is commonly used in industrial products. This material is commercially manufactured and supplied by 3D Systems Inc., and Table 3-2. shows the its typical properties [3D systems, 2006b].

Figure 3-1 Vanguard^{TM} SLS System [3D Systems, 2006a]

Table 3-1. Process parameters used for specimen fabrication

Parameters:	Setting:
1. Fill laser power	41 watt
2. Scanning speed	1778 mm/sec
3. Scan size	0.4 mm
4. Scan spacing	0.36 mm
5. Slice thickness	0.1 mm
6. Bed temperature	172^{o}C
7. Outline laser power	6 watt

Table 3-2. Duraform PA material properties [3D Systems, 2006b]

Properties	Units	Test Method	
Powder properties:			
• Density	g/cm^3	ASTM D4164	0.59
• Particle size average	μm	Laser Diffraction	58
• Specific gravity (20 ^{0}C)	g/cm^3	ASTM D792	0.97
• Moisture absorption (23 ^{0}C)	%	ASTM D570	0.41
Thermal properties:			
• Melting point: Tm	^{0}C	DSC	184
Mechanical properties:			
• Tensile strength	MPa	ASTM D638	44
• Tensile modulus	MPa	ASTM D638	1600
• Tensile elongation at break	%	ASTM D638	9
• Flexural modulus	MPa	ASTM D790	1285

3.3 Specimen Design for Testing

To create the CAD model and to generate the STL file for the test specimens, the Ideas 3D modelling software was used. The specimens were produced in a range of different fabrication orientations.

The basic building orientations are defined as the *x* orientation as the laser scanning orientation; the *y* orientation the plane perpendicular to scanning but in the scan plane; and the *z* orientation perpendicular to the *x*-*y* plane and manufactured along the short axis scan. Figure 3-2 shows the orientations used to fabricate the specimens for the bend/flexural and shear tests. The specimens built in the SLS machines were placed in 3 build orientations which are the *x*-axis, *y*-axis and *z*-axis orientations, with 2 variations of each orientation. Thus specimens test were produced in a total of 6 orientations in the XY, XZ, YX, YZ, ZX and ZY orientations as shown in Figure 3-2. The same orientations with a single variation were used to manufacture the specimens for tensile and compression tests were identified as X, Y and Z for each *x*, *y* and *z* direction. Six samples were built of each particular test specimen.

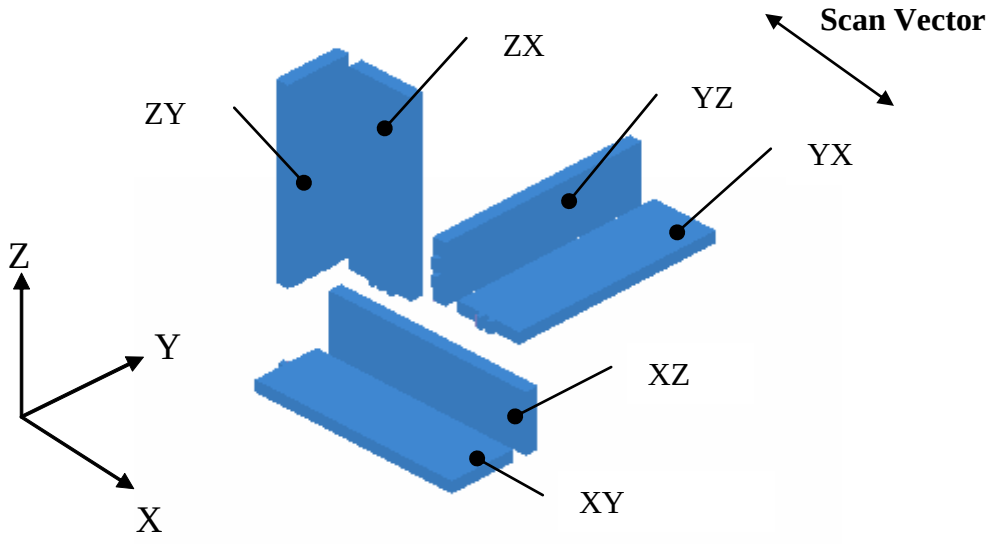

Figure 3-2 Orientation of fabrication of test specimens

3.4 Mechanical Testing Equipment

A INSTRON 4505 Universal Testing Machine, with max load of 100kN (in tension and compression), a maximum stroke of 1000 mm (approximate), and a maximum cross head speed of 20 mm/min., was used to carry out tensile, compression, shear and bending/flexure tests at room temperature.

The *Instron Strain Gauge* (25mm) extensometer was used to measure the strain or change in length. Moreover, these changes were recorded for each incremental change for continuous loading and computerised by using the software systems provided in the universal testing machine that was used to do the test.

3.5 Experimental tests selection

To characterise the materials, five basic types of mechanical tests were chosen. Tensile, compression and shear tests were carried out in order to characterise basic mechanical behaviour. Besides these, four- and three-point bend/flexure tests were used to investigate the structural responses of the material to more complex stress states.

Standard tests for layer manufactured structures are not yet available. Therefore, British and ASTM standards were reviewed, in particular those used for testing reinforced plastic composites which have similar structures to materials produced by SLS using layer manufacturing technology.

The standards used in defining the tests were:

1. BS EN ISO 527-1:1996 for tensile testing [BSI, 1996].
2. ASTM Designation: E 9-89a: 2000 [ASTM, 2000] for compression testing, and consulting ASTM Designation: E111-97 [ASTM, 2003].
3. BS EN ISO 15310: 2005 for shear test [BSI, 2005].
4. The four-point bend test and the three-point bend test based on standard BS EN ISO 14125:1998 [BSI, 1998] and consulting ASTM D6272-02 [ASTM, 2004].

3.5.1 Tensile test

The tensile tests were carried out to measure the tensile properties, include tensile strength and tensile modulus.

As shown in figure 3-3, the specimen was a round bar, which at the gauge

length has smaller diameter. The design of this specimen was based on the tensile specimen used on the Hounsfield Tensometer testing machine. However, BS EN ISO 527-1:1996 was used to determine the tensile properties. The detailed dimensions of the specimen are illustrated in Figure 3-3 and to fabricate it, the technique mentioned in section 3.3 was used. For this initial work, the specimen was manufactured for each different orientation in the X, Y and Z directions. Meanwhile, for heat treatment investigation, the tensile specimen was produced in the Y orientation in the y direction only (see chapter 5 and 6).

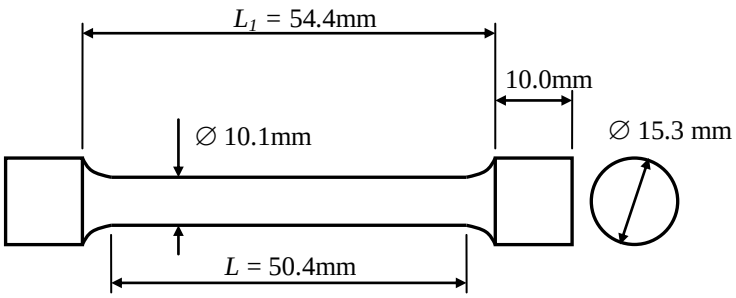

Figure 3-3 Tensile test specimen drawing

The specimen was placed on the testing equipment using a chuck as a gripper, as shown in figure 3-4a. The cross-head speed was set at 2mm/minute based on the BS EN ISO 527-1:1996 standard and the specimen was loaded continuously until it fractured. The tensile strength at break and tensile modulus were measured for all specimens. Figure 3-4b shows examples of fractured specimens after testing.

(a) (b)

Figure 3-4 Tensile test specimens: (a) on testing machine, (b) after testing

a. Tensile strength

All stress values are defined on the basis of the initial cross-sectional area of the specimen, and therefore the tensile strength is given by the maximum stress calculated using equation 3.1 by letting *F* equal the maximum load.

$$\sigma = \frac{F}{A} \quad \text{..... (3-1)}$$

where σ is stress (MPa), *F* is load / the measured force (N), and *A* is the initial cross-sectional area of the specimen (mm^2).

Tensile strength, σ_M, is the maximum tensile stress sustained by the test specimen during a tensile test (MPa).

b. Tensile modulus

Tensile modulus is determined by measuring the slope on a stress-strain diagram within the elastic range of deformation movement:

$$E = \frac{\sigma_2 - \sigma_1}{\varepsilon_2 - \varepsilon_1} \quad \text{..... (3-1)}$$

where *E* is tensile modulus, σ_2 is stress at strain ε_2 and σ_1 is stress at strain ε_1.

The strain was calculated using equation 3.2:

$$\varepsilon = \frac{\Delta L}{L} \quad \text{..... (3-2)}$$

where ε is strain value expressed as a dimensionless ratio or percentage (%), L is gauge length (initial length) of specimen (mm), ΔL is changes in length between gauge marks (mm). As shown in figure 3-5, the slope was taken on the straight line portion of the stress-strain curve. The slope for the line is b/a.

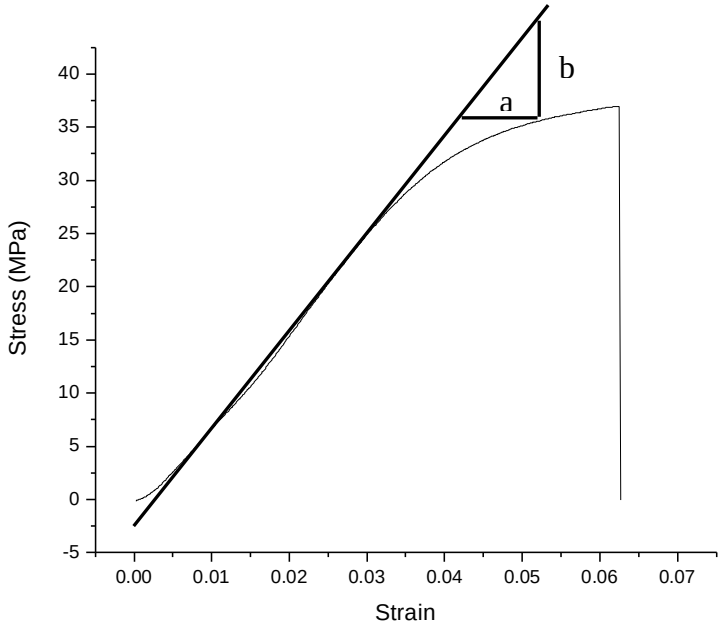

Figure 3-5 Slope measurement on stress-strain curve

3.5.2 Compression test

Compression tests were conducted to determine the compression modulus. The compression specimen design was based on the test specimen used in the standard ASTM Designation: E9-89a: 2000 [ASTM, 2000] for methods for the compression testing of metallic materials. The dimensions of the specimen with a L/D (length/diameter ratio) of 1.5 were taken, with diameter (D) 30 mm, and length (L) 45 mm. The detailed dimension of the specimen used with the test geometry is shown in Figure 3-6. The same technique was used to fabricate the specimen as is mentioned in section 3.3.

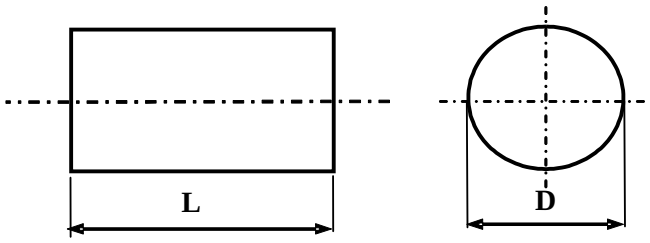

Figure 3-6 Compression test specimen drawing

The test machine with a cross-head speed of 0.3mm/min was used in testing. Tests progressed until the strain reached 10%. Figure 3-7 shows a compression test

specimen before testing and figure 3-8 shows it being tested. The equations used for the compression tests were those employed for tensile tests analysis.

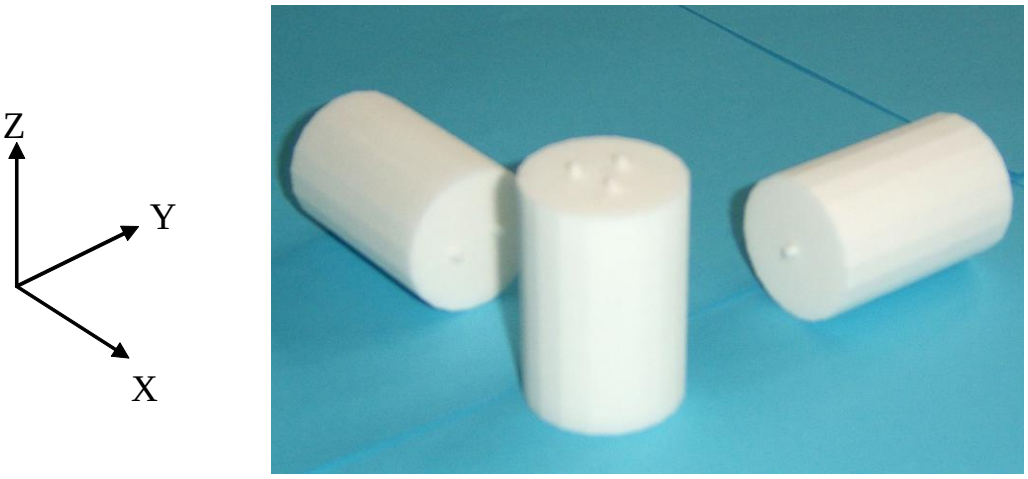

Figure 3-7 Compression test specimens for X, Y, and Z orientations

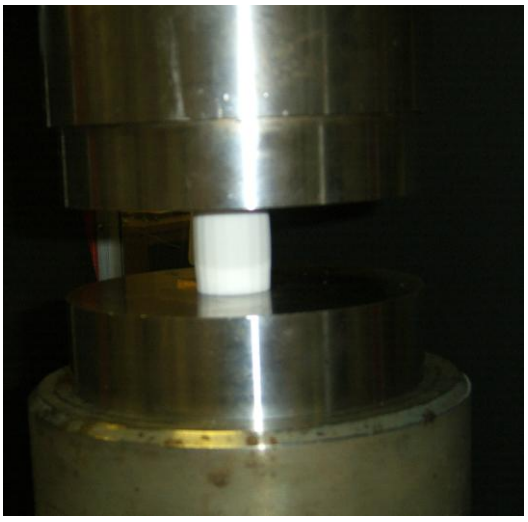

Figure 3-8 Compression specimen in the test equipment

3.5.3 Shear test

Shear tests were carried out to determine the shear modulus properties of the specimens. The same technique was used to manufacture the specimens as mentioned in section 3.3. The specimen design was based on standard BS EN ISO 15310 [BSI, 2005], as shown in Figure 3-9, on a square specimen of dimensions 150mm in length (*L*), 150mm width (*W*), and 4mm height (*H*).

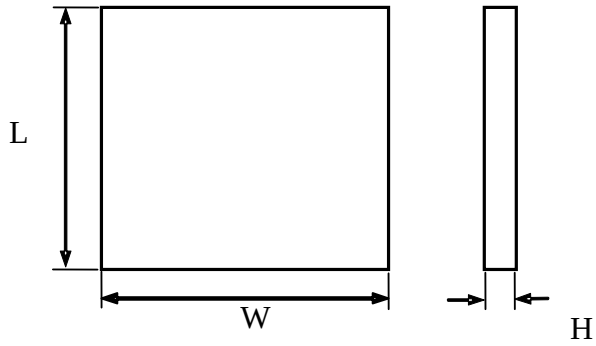

Figure 3-9 Shear test specimen drawing

In order to carry out the shear tests, a jig was designed based on the BS EN ISO 15310 standard [BSI, 2005] as shown in Figure 3-10. This jig was fixed to the INSTRON universal testing machine. Figure 3-11 shows a test being carried out. All the dimensions of this jig are shown in the appendix.

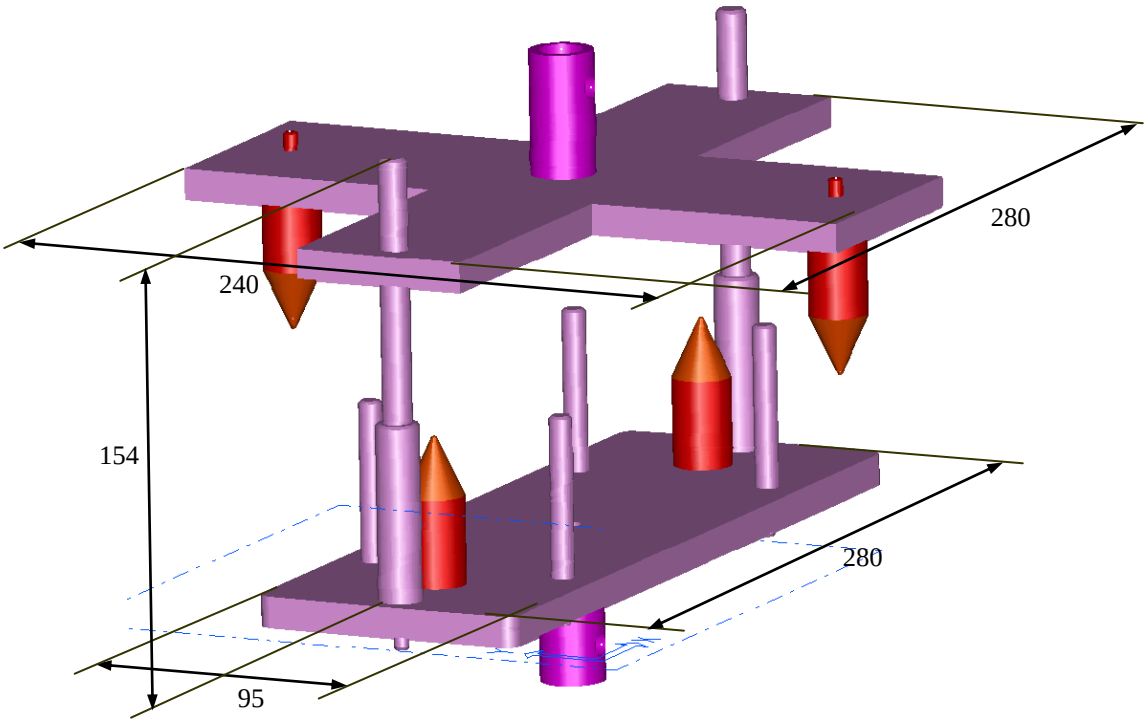

Figure 3-10 Jig fixture for shear test

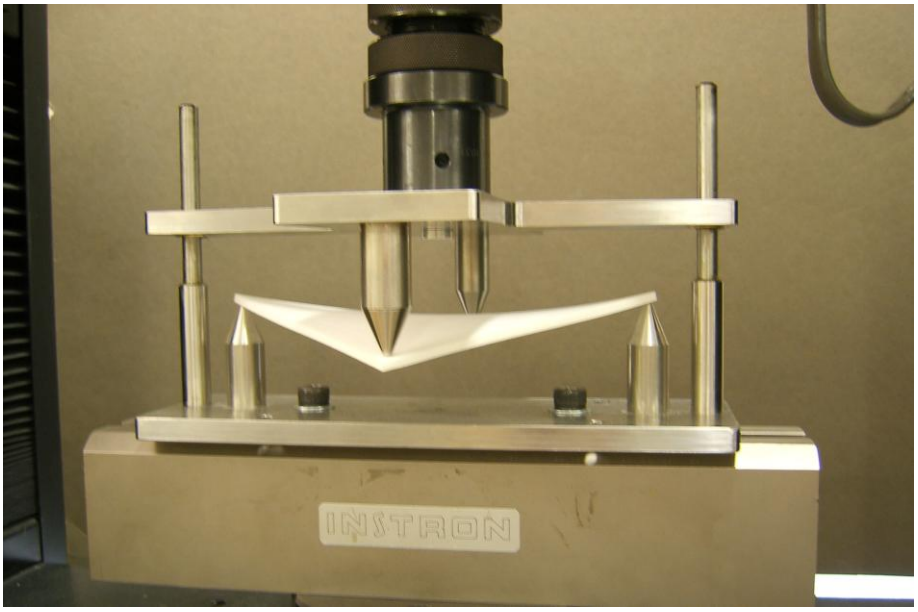

Figure 3-11 Shear specimen on the test equipment

According to the BS EN ISO 15310 standard [BSI, 2005], the following equation can be used to calculate the shear modulus:

$$G = \frac{3}{4} \times \frac{\Delta \times L \times W \times K}{1000 H^3} \quad \text{..... (3-3)}$$

where: $\Delta = \frac{F_2 - F_1}{w_2 - w_1}$

and where G is the plane shear modulus (GPa), L is the length of the specimen (mm), W is specimen width (mm), H is its thickness (mm), K is the geometric correction factor = 0.822; F_1 and F_2 are the corresponding loads (Newton); and w_1 and w_2 are the deflections (mm).

Shear modulus can be calculated using the loads F_1 and F_2 at the deflections w_1 and w_2 respectively, as shown in Figure 3-12. By defining the values of w_1 and w_2, then the deflection value recorded on the computer can be used to gain values of F_1 and F_2. The test progressed until the deflection reached 20mm, with a cross-head speed of 1 mm/min.

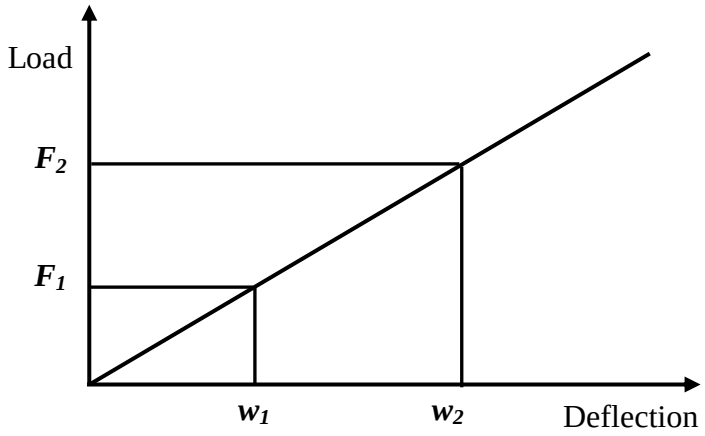

Figure 3-12 Load/deflection curve

3.5.4 Four-point bend/flexure test

Four-point bend/flexure tests were carried out to measure the flexural properties of the specimens. The specimen design was based on the EN ISO 14125:1998 standard [BSI, 1998], and a rectangular bar (beam) of 80mm length, 10mm width and 4mm depth was fabricated using the same technique as mentioned in section 3.3. Standard ASTM D6272-02 (ASTM, 2004) was used as a guide for the determination of the properties. The loading set-up for the test is shown in Figure 3-13.

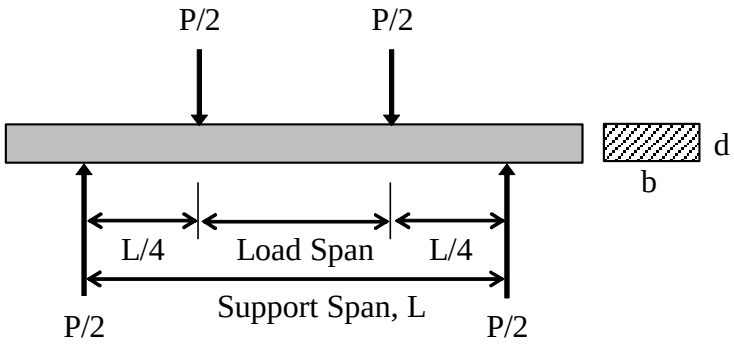

Figure 3-13 Four-point bend/flexure test specimen loading set-up

Based on the ASTM D6272-02 standard, the rate of crosshead motion, *R*, can be determined using equation 3-4:

$$R = \frac{0.167ZL^2}{d} \quad \text{..... (3-4)}$$

where R is the rate of cross-head motion (mm/min), L is the support span length (65 mm), d is the depth of the beam (mm), Z is the rate of straining of the outer fibres (mm/mm), and min Z = 0.01. The rate of cross-head motion used for the test was R = 1.76 ≈ 2 mm/min. This cross-head speed is recommended in the BS EN ISO 14125: 1998 standard.

The tests were carried out after specimen were placed on the testing equipment using a jig designed by a previous researcher [Yubero, 2004], as shown in figure 3-14.

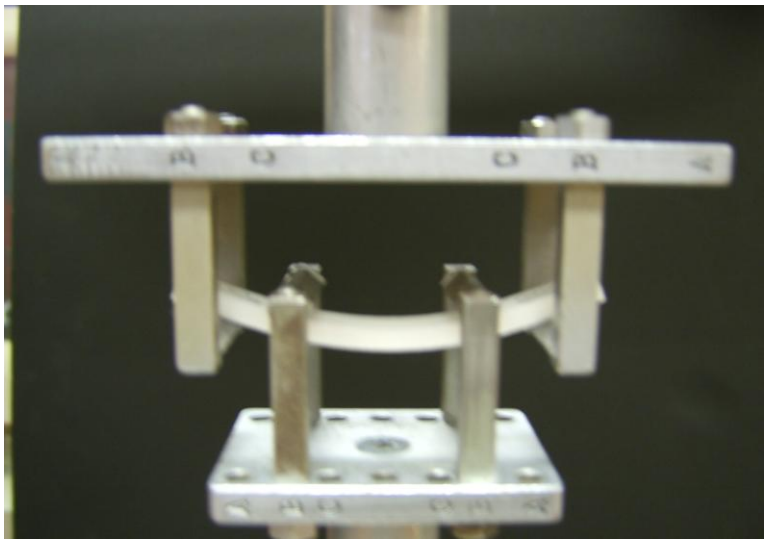

Figure 3-14 Four-point bend/flexure test specimen being tested

a. Flexural strength

For a load span of one half of the support span as shown in Figure 3-13 and as confirmed by the ASTM D6272-02 standard (ASTM, 2004), for relatively small deflections at any point along the load deflection curve, the flexural stress can be determined using equation 3-5:

$$S = \frac{3PL}{4bd^2} \quad \text{..... (3-5)}$$

where S is the stress (MPa), P is the load at a given point on the load deflection curve (N), L is the support span length (mm), b is the width of the beam (mm), and d is the depth of the beam (mm).

Then, the flexural strength of the specimen is equal to the maximum stress in the outer fibres at the moment of break, which is calculated by letting P equal the load at the moment of break. However, if the resultant deflection occurrs at more than 10%

of the support span length, the maximum stress from equation 3-6 is applied (ASTM, 2004):

$$S = \frac{3PL}{4bd^2} \times \left[1 - \left(\frac{10.91Dd}{L^2}\right)\right] \quad \text{..... (3-6)}$$

where P, L, b, and d are the same as for equation 3-5, but D is the maximum deflection of the centre of the beam (mm); and the maximum strain, r, is determined using equation 3-7:

$$r = \frac{4.36Dd}{L^2} \quad \text{..... (3-7)}$$

The value of deflection at the centre of the beam (D) must be calculated and was estimated through analysis of beam deflection. The value of deflection recorded on the computer was the deflection value at the loading point which resulted from the machine test.

The deflection at any point on the beam is based on the loading diagram (Figure 3-13) and can be determined using equation 3-8 (William, 1994):

$$EI\ y(x) = \frac{P}{12}\left[(x)^3 - \left(x - \frac{l}{4}\right)^3 - \left(x - \frac{3l}{4}\right)^3 + (x - l)^3\right] - \left(\frac{3Pl^3}{64}\right) \quad \text{..... (3-8)}$$

where E is the modulus of elasticity, I is the second moment of area, P is the load, l is the support span length, and x is the loading position at a given point.

From equation 3-8, by substituting $x = l/4$, the value of the deflection at the loading point can be calculated as:

$$y_{l/4} = \frac{-Pl^3}{96EI} \quad \text{..... (3-9)}$$

and then by substituting $x = l/2$, the value of the deflection at the centre can be calculated as:

$$y_{l/2} = \frac{-11Pl^3}{768EI} \quad \text{.....(3-10)}$$

Then, dividing equation 3-10 by 3-9, the ratio for deflection at both points can be determined. Therefore, the value of deflection at the centre was calculated as 1.375 times the value of the deflection at the loading point.

b. Flexural modulus

The flexural modulus was determined using the same procedure as for measuring tensile modulus as shown in Figure 3-5.

3.5.5 Three-point bend/flexure test

Three-point bending tests were also carried out to determine the flexural properties of the specimen. The same technique was used to fabricate the specimen as mentioned in section 3.3. The specimen design based on the EN ISO 14125:1998 standard [BSI, 1998] was a rectangular beam of 80mm length, 25mm width and 5mm depth. The same standard was used to determine the properties. The loading set-up for the test is shown in Figure 3-15, with a support span length of 65 mm. The cross-head speed used was 1 mm/min.

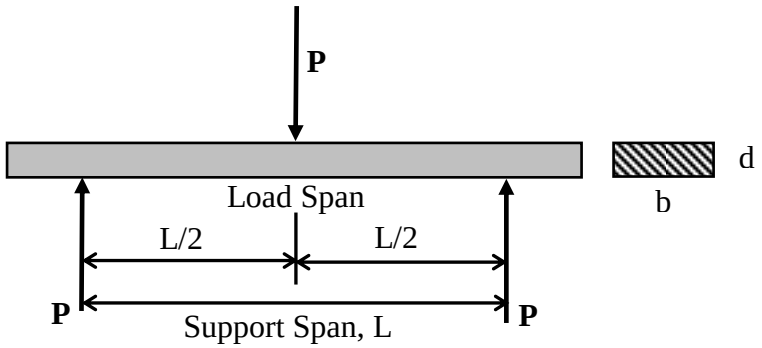

Figure 3-15 Three-point bend/flexure test specimen loading set-up

The tests for three-point bending were carried out after the specimen was placed on the testing equipment using a jig designed by a previous researcher [Yubero, 2004], as shown in figure 3-16.

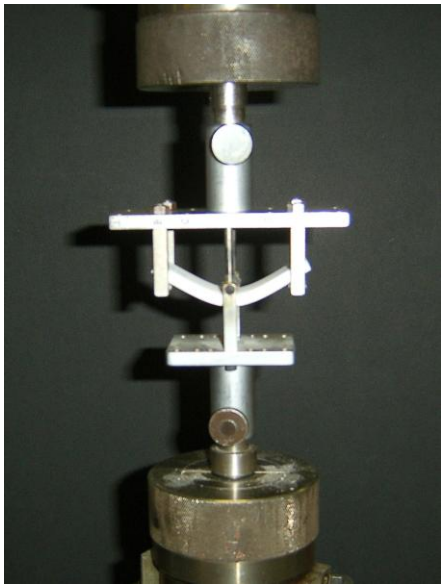

Figure 3-16 Three point bend/flexure test specimen being tested

a. Flexural strength

As shown in Figure 3-15, the load in the three point bending test is applied at the mid support span and so will cause maximum deflection at the mid point of the beam.

According to the BS EN ISO 14125:1998 standard [BSI, 1998], the following procedure can be used to calculate the flexural strength and strain of the specimen.

The flexural stress σ_f is given by the following equation [BSI, 1998]:

$$\sigma_f = \frac{3PL}{2bd^2} \quad \text{.....(3-11)}$$

where σ_f is the flexural stress in megapascals (MPa), P is the load in newtons (N), L is the span length in millimetres (mm), d is the thickness of the specimen, in millimeters (mm), and b is the width of the specimen in millimeters (mm)

And the strain in the outer surface of the specimen can be calculated as follows:

$$\varepsilon = \frac{6sd}{L^2} \quad \text{.....(3-12)}$$

where s is the beam mid-point deflection in millimetres (mm)

b. Flexural modulus

The flexural modulus was determined using the same procedure as for measuring tensile modulus as shown in Figure 3.5.

3.6 Differential Scanning Calorimetry (DSC)

To analyse thermal conditions and crystallinity, a Mettler Toledo Differential Scanning Calorimetry (DSC) 823e was used, as shown in Figure 3-17.

Figure 3-17 DSC Mettler Toledo 823e

The degree of crystallinity and melting point were measured for samples prepared by cutting a small amount of material from the tensile test specimens (after the tests were carried out). The amount of material used for each DSC run was ~7±0.1mg. Each sample for measurement was positioned in a 100µl aluminium crucible before being placed in a heat flux cell.

The measurements were made under nitrogen flow with a Mettler FP90 controller connected to a FP85 heat flux cell. A heating rate of 10^{o}C/minute was used to heat the sample from 30 to 220^{o}C, with then a hold of 2 minutes. After that, the instrument was set up to cool at the same rate from 220 to 30^{o}C, and a melting and crystallisation thermogram recorded.

To determine the degree of crystallinity and melting point, software analysis was used with the value of $\Delta H_{PA\text{-}12}$ as the melting enthalpy per gram of 100% crystalline. A value of $\Delta H_{PA\text{-}12}$ had to be inputted and the value used was 209.3J/g, based on the measurement of Gogolewski et al [1980]. Then the value of degree of crystallinity or melting point can be obtained.

3.7 Statistical analysis tool

Confidence intervals were used to estimate the reliability of results. A confidence interval gives an estimated range of values which is likely to include the unknown population average, the estimated range being calculated from a given set of sample data.

Minitab software was used to calculate confidence intervals, using the function: CONFIDENCE (alpha, standard_dev, size), in which alpha is the significance level used to compute the confidence level, standard_dev. is the population standard deviation for the data range and is assumed to be known and size is the sample size.

In this study, the confidence interval was chosen to be 95 %, and therefore alpha is 0.05. The function of standard deviation is $S = \sqrt{\frac{\sum (X - M)^2}{N - 1}}$, where *s* is the standard deviation, *X* is the value from the each test results. *M* is the average of all test results from all samples and *N* is the sample size.

Furthermore, in order to analyse the result of the experiment, the analysis of variance (ANOVA) is also used. ANOVA is used to identify the performance of group of parameters under investigation. The purpose of ANOVA is to investigate the parameter, whose combination to total variation is significant. One-way analysis of variance (abbreviated one-way ANOVA) is a technique used to compare means of three or more samples (using the F distribution). This technique can be used only for numerical data.

Source of variation	Sums of squares (SS)	Degrees of freedom (DF)	Mean square (MS)	F
Treatments	$\sum_{Treatments} I_j(m_j - m)^2$	$J - 1$	$\frac{SS_{Treatment}}{DF_{Treatment}}$	$\frac{MS_{Treatment}}{MS_{Error}}$
Error	$\sum_{Treatments} (I_j - 1)s_j^2$	$I - J$	$\frac{SS_{Error}}{DF_{Error}}$	
Total	$\sum_{Observations} (y_{ij} - m)^2$	$I - 1$		

In ANOVA, sum of squares or SS is calculated by $\sum_{Treatment} Ij\ (mj - m)^2$ where I is the number of experimental unit, and m is the mean. The mean square of a factor (*MSj*) or error (*MSe*) is found by dividing its sum of squares with its degree of freedom. The three DFs are calculated from the summaries. Then the MSs are calculated and a ratio determines F. The F-value of each design parameter is found by dividing MS treatment with MS error. The calculated probability *(p*-value) says the probability of rejection the null hypothesis in case the null hypothesis holds. In case of $\rho < \alpha$, where α *(0.05)* is chosen significance level (0.05), the null hypothesis or Ho is rejected. On the other hand, in case of $\rho > \alpha$ then the result is valid and Ho is accepted [Ostertagová and Ostertag, 2015].

3.8 Scanning Electron Microscope (SEM).

For morphological analysis, Scanning Electron Microscope (SEM), Hitachi S2400 SEM with an Oxford Instruments Isis 200 ultra-thin window X-ray detector was used in this study.

CHAPTER 4. MECHANICAL PROPERTY CHARACTERISATION

4.1 Introduction

The purpose of this chapter is to present the results of the tests of mechanical properties on Selective Laser Sintered Nylon 12 (Duraform PA) carried out to provide a benchmark of mechanical performance. The specimens were produced based on those described in section 3.3, in which different fabrication orientations were defined. All specimens were produced using the commercial Sinterstation Vanguard SLS machine at Leeds University, as described in section 3.2.

To characterise material performance, the responses of the material to load in different conditions need to be on determined, such as in tensile, bending and shear testing. Tensile testing is used to measure the resistance of a material to tensile load, and flexural testing is used to measure the durability in terms of wear, pressure, or damage of a material to withstand bending load, while shear testing is used to measure shear resistance of a material. All these tests are important in knowing how the material will behave in service conditions.

The effects of different fabrication orientations on the mechanical properties of specimens were characterised, as described in the next section. For each test result obtained, an analysis on variance (ANOVA) was carried out to investigate the significance of variations in the mechanical characteristics of specimens according to orientation.

For the initial work described in this chapter, all specimens were tested as non-heat-treated samples.

4.2 Tensile test

Tensile tests were carried out for three different fabrication orientations, X, Y and Z. For each orientation, six samples were tested. The values of stress and strain were calculated using equations 3.1 and 3.2. The stress-strain graphs were then plotted as shown in Figure 4-1.

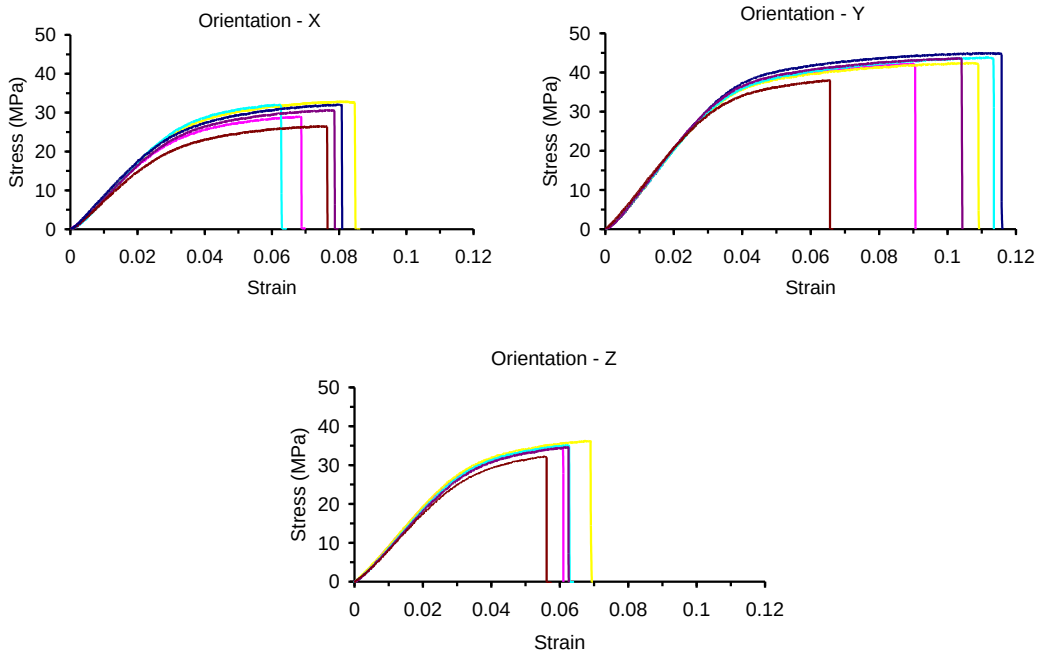

Figure 4-1 Stress-strain graphs for each of the tensile tests for the different part orientations.

From these stress-strain graphs, tensile strength was determined from the maximum stress value. The results for specimens fabricated in different orientations are summarised in Table 4-1. The table also show the average values and confidence intervals for each orientation of the specimens. Sample number one in the Z orientation failed when it was tested, and therefore no value is given.

Table 4-1. Tensile strength results (MPa)

Orientation	Sample						Average (MPa)	95 % Confidence interval
	1	2	3	4	5	6		
X	28.98	32.75	32.00	30.55	26.45	31.90	30.44	±1.89
Y	44.88	42.11	42.44	43.70	43.60	37.99	42.45	±1.92
Z	-	34.63	36.16	35.02	34.56	32.25	34.52	±1.25

The confidence intervals in table 4-1 show that there were small variations in tensile strength within the specimens fabricated in the same orientations. For specimens fabricated in different orientations (Figure 4-2) there are significant differences in tensile strength. The ANOVA results also indicate that the differences in average strength for different orientations were significant, where the *p* value is 0.00 smaller than 0.05.

The X orientation has the lowest mean tensile strength, while Z is slightly higher. However, the Y orientation gives the highest values of mean tensile strength, which is consistent with other research findings (Gibson and Shi, 1997; Hague et al, 2004).

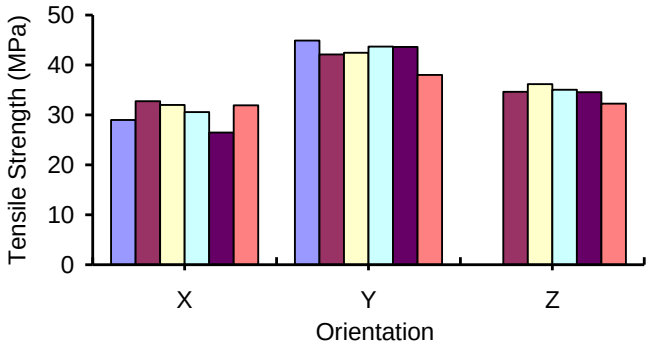

Figure 4-2 Tensile strength of different fabrication orientations (distribution for all specimens)

The tensile modulus for each test was calculated from the initial slope of the straight line on the stress-strain curves shown in Figure 4-1. The slope was measured at strain value by constructing a linear fit line on selected data, as shown in Figure 4-3 which illustrates the plot for the Y orientation. The tensile modulus for each orientation was found from the linear fit equation, and the results are summarised in Table 4-2.

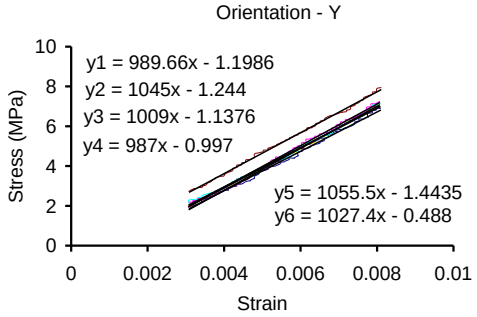

Figure 4-3 Linear fit line on stress-strain relationship of specimen in tensile test for the Y oriented parts

Table 4-2. Tensile modulus results (MPa)

Orientation	Sample						Average (MPa)	95 % Confi-dence interval
	1	2	3	4	5	6		
X	853.20	876.15	870.21	866.18	765.09	938.84	861.61	±44.78
Y	989.66	1045.00	1009.00	987.00	1055.50	1027.40	1018.93	±22.81
Z	-	964.06	934.17	921.35	912.02	841.10	914.54	±39.89

It can be seen from the confidence intervals in table 4-2 that the tensile modulus also varies within each orientation. The results shown in Figure 4-4 give the highest mean tensile modulus value in the Y orientation (1018.93 MPa), while the lowest is in the X orientation (861.61 MPa) which represents 15.4% of variation in the different build orientations. From the ANOVA results, it is also confirmed that the *p*-value is 0.00 < 0.05, meaning that tensile modulus is influenced by build orientation.

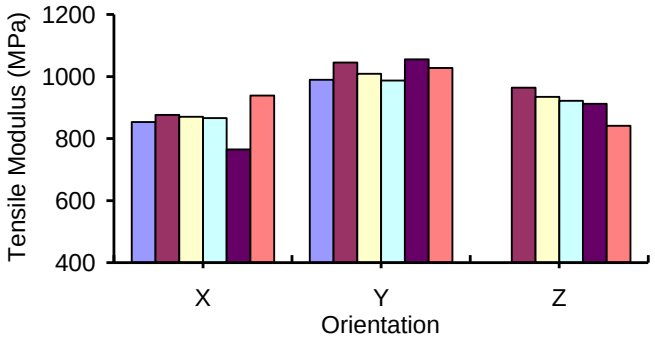

Figure 4-4 Tensile modulus of different fabrication orientations (distribution for all specimens)

Tensile elongation at break was determined by calculating the strain value at the point where the break was found, then multiplying it by 100 (%), as shown in Figure 4-1 for each different fabrication orientations, and the results are summarised in table 4-3.

Table 4-3. Tensile elongation at break (%)

Orientation	Sample						Average (%)	95 % Confidence Interval
	1	2	3	4	5	6		
X	6.80	8.30	6.20	7.60	7.50	8.00	7.40	±0.62
Y	11.50	8.60	10.70	11.20	10.30	6.50	9.80	±1.53
Z	-	6.10	6.90	6.20	6.10	5.50	6.16	±0.44

From table 4-3, the results show that the tensile elongation for the Y orientation has the highest of average value followed by those X and for Z. This result is slightly different from the results for average tensile strength, in which the Z orientation had a slightly higher value than that for the X orientation. However, the tensile elongation for the Y orientation was still the highest for both average tensile elongation and average tensile strength. As shown in Figure 4-5, for specimens fabricated with different orientations, there are significant differences in tensile elongation at break. This

observation is confirmed by the statistical analysis (ANOVA) where the *p*-value is less than 0.05.

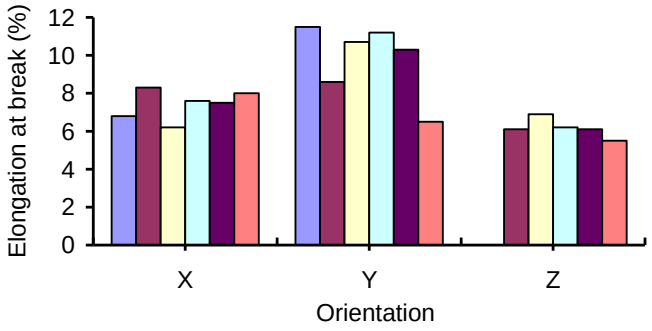

Figure 4-5 Tensile elongation at break of different fabrication orientations (distribution for all specimens)

As shown in Figure 4-1 and Figure 4-5, the variations in the results of elongation at break (strain) almost 100% in the Y-orientation and only 15% in the Z-orientation. Meanwhile the variations in the results of tensile strength (Table 4.1 and Figure 4-2) and tensile modulus (Table 4.2 and Figure 4-4) are not bigger than 18% and 7% for Y direction; 12% and 14.6% for Z direction, respectively.

When the direction of loading during tensile testing is perpendicular to the scan direction, the average elongation at break was found to be greater. Loading for specimen in Y and Z are perpendicular to the direction of scan, while for X is it parallel to the direction of scan. The scanning laser in the perpendicular specimen is only traveling at the same width of the specimen. Thus this could cause faster fusing of scan lines. In comparison, for parallel specimen the laser must travel the full length of the specimen before scanning the next line. Thus delaying the fusion time. As a result, the difference in time between scan lines causes different particle-to-particle bonding during sintering and therefore causes a variation in material properties depending on the direction of loading during tensile testing [Nelson J.A., et al, 2014].

Besides that, the differences of the variations might be due to that all areas of the powder bed were used to position specimens with different quality of powder used whilst they were being built.

4.3 Compression test

Compression tests were carried out on the three different fabrication orientations X, Y and Z. The properties of six samples were evaluated for each orientation of the specimens. The values of stress and strain were calculated using similar equations to those used for tensile stress and strain. The stress–strain graphs were plotted as shown in Figure 4-6 for the X, Y and Z orientations.

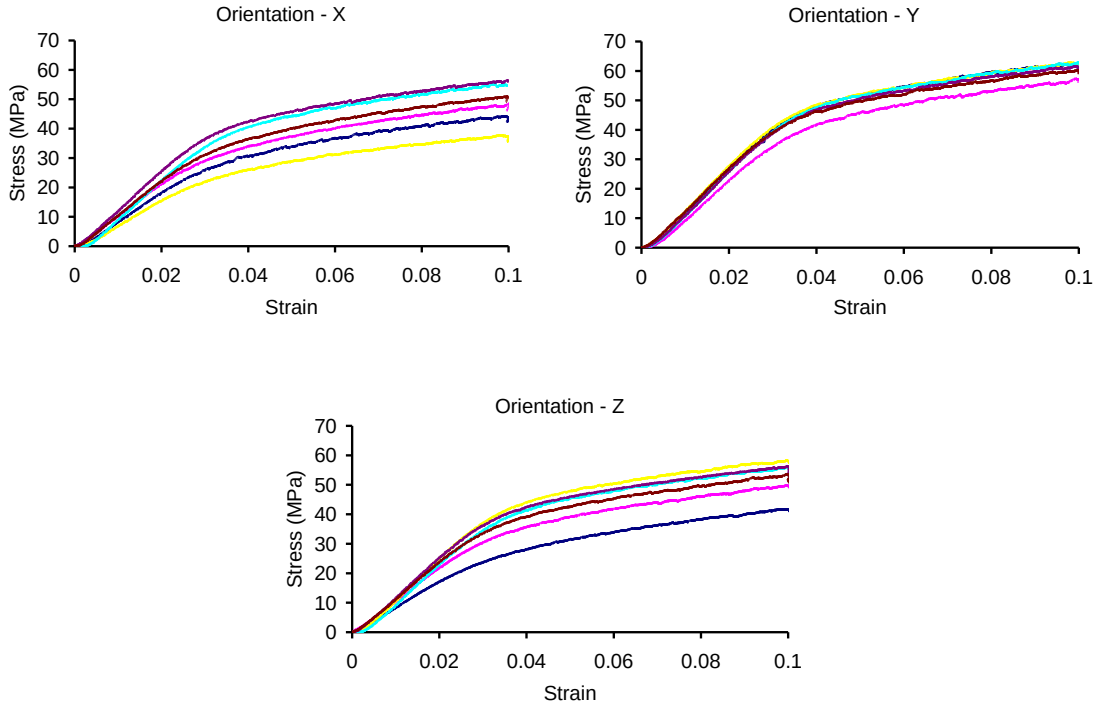

Figure 4-6 Stress-strain graphs for each of the compression tests for the different orientation of parts

Using the same procedure as applied for tensile properties, the compression modulus of each orientation was determined by measuring the slope of the straight line on the stress-strain curve. As mentioned in section 3.5.2, the compression tests were progressed until the strain reached 10%. The slope was measured at strain by constructing a linear fit line on selected data, as shown in Figure 4-7 which illustrates results for the Y orientation. The compression modulus for specimens in each orientation (X, Y and Z) was found from the linear fit equation, and the results are summarised in Table 4-4.

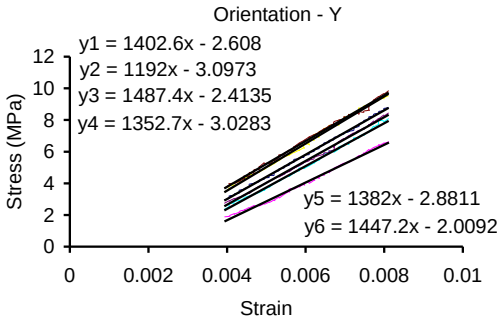

Figure 4-7 Linear fit line on stress-strain relationship of specimen in compression test for the Y-oriented parts

Table 4-4 shows the compression modulus from the specimens produced with different orientations.

Table 4-4. Compression modulus results (MPa)

Orienta-tion	Sample						Average (MPa)	95 % Confi-dence interval
	1	2	3	4	5	6		
X	1036.10	1162.90	857.16	1310.10	1369.10	1226.80	1160.36	±150.88
Y	1402.60	1192.00	1487.40	1352.70	1382.00	1447.20	1377.32	±82.08
Z	882.44	1115.10	1298.50	1221.70	1243.00	1191.00	1158.62	±118.62

As shown by the confidence intervals in Table 4-4 and Figure 4-8, the average value of compression moduli in different fabrication orientations vary. The Y orientation still gives the highest average value (1377.32 MPa) and the X and Z orientation values (1160.36 MPa and 1158.62 MPa) are similar. From the ANOVA results, it can be seen that the *p*-value is 0.036 which is less than 0.05, meaning that compression modulus also differs with the orientation of the specimen.

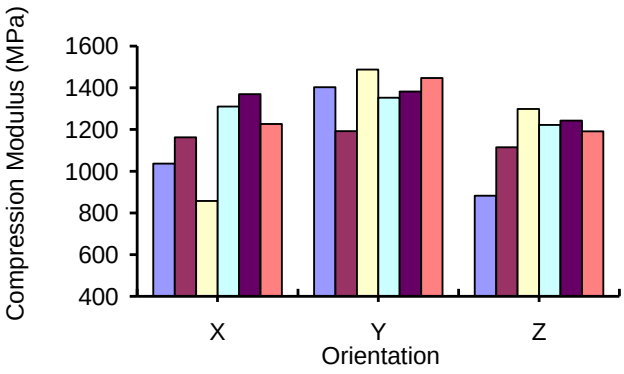

Figure 4-8 Compression modulus of different fabrication orientations (distribution for all specimens)

4.4 Shear test

Shear tests were carried out on six samples each of the six different fabrication orientations to evaluate the material properties in each individual orientation. Figure 4-9 shows load-deflection plot for the YZ and ZY orientations. Results for other orientations (XY, XZ, YX, ZX), can be found in appendix A.

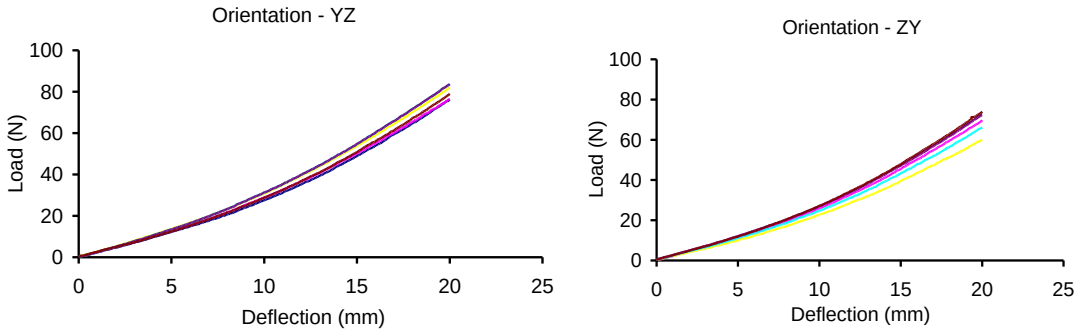

Figure 4-9 Load-deflection graphs for each of the shear tests for the YZ and ZY oriented parts

The shear modulus of a specimen was calculated by using equation 3-3 as described in section 3.5.3, in which loading F_1 at deflection w_1 and loading F_2 at deflection w_2 were used for the calculation. Here, by defining w_1=2mm and w_2=6mm, and then by interpolating the load from the data recorded, F_1 and F_2 can be determined. The data was recorded until the deflection reached 20 mm. Table 4-5 shows the shear modulus the specimens produced in different orientations.

Table 4-5. Shear Modulus Results (GPa)

Orientation	Sample						Average (GPa)	95 % Confidence interval
	1	2	3	4	5	6		
XY	0.59	0.38	0.46	0.35	0.31	0.44	0.42	±0.08
YX	0.62	0.60	0.54	0.66	0.54	0.55	0.58	±0.04
ZX	0.62	0.58	0.56	0.57	0.59	0.59	0.59	±0.02
XZ	0.56	0.54	0.56	0.50	0.49	0.52	0.53	±0.02
YZ	0.51	0.53	0.56	0.58	0.57	0.51	0.54	±0.02
ZY	0.48	0.47	0.42	0.45	0.48	0.48	0.46	±0.02

Table 4-5 and Figure 4-10 shows that the highest average shear modulus values are achieved in the YX and ZX orientation while the lowest values are in XY and ZY. The highest and lowest average values differ by 28.8%. This shows that the shear modulus is also influenced by build orientation, as confirmed by the *p*-value from the

ANOVA result which is less than 0.05. Figure 4-10 illustrates the distribution of shear modulus value for all specimens from different fabrication orientations.

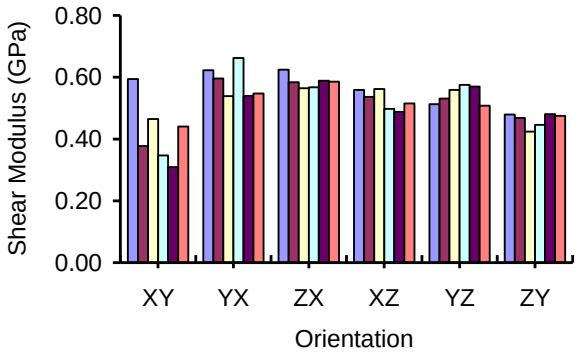

Figure 4-10 Shear modulus of different fabrication orientations (distribution for all specimens)

4.5 Three-point bending/flexure test

Three-points bending tests were carried out on the six different fabrication orientations. To evaluate the properties for each individual orientation, six samples were tested. Figure 4-11 shows the full test results of the three point bending/flexure test for the YX and ZX orientations. For other results in the XY, XZ, YZ, ZY orientation, see in the appendix A.

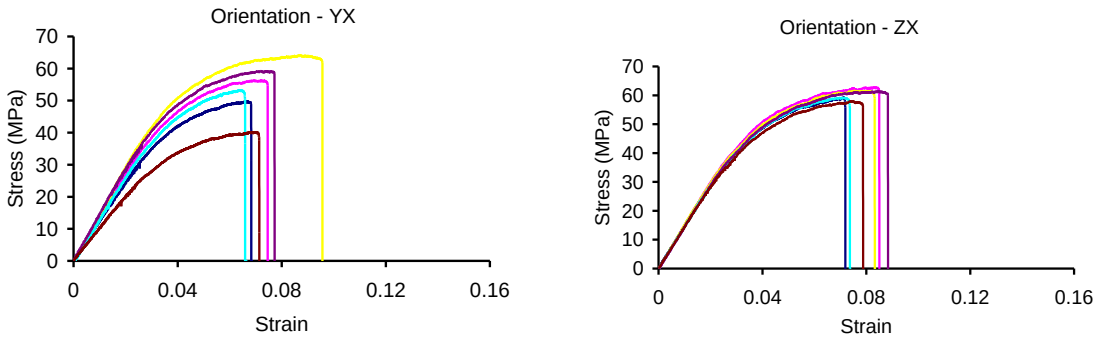

Figure 4-11 Stress-strain graphs for each of the three point bending tests for the YX and ZX oriented parts

To determine the flexural modulus properties of the specimen, the three-point bending test was carried out using the procedure as described in section 3.5.5.

Using a similar procedure as that to determined tensile modulus as described in section 3.5.1, the flexural modulus was determined. The slope was measured at a strain

value by constructing a linear fit line on selected data, as shown in Figure 4-12 for the ZX orientation**.** Results for all specimens are summarised in Table 4-6.

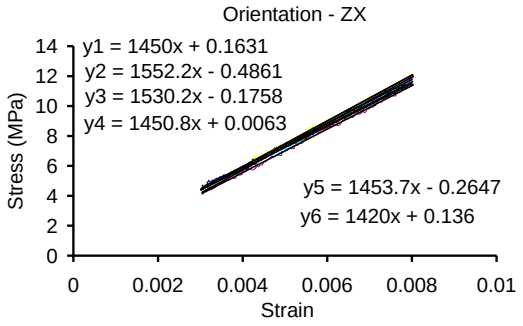

Figure 4-12 Linear fit line on stress-strain relationship of specimen in three point bending/flexure test for the ZX-oriented parts

Table 4-6. Three point flexural modulus results (MPa)

Orientation	Sample						Average (MPa)	95 % Confi-dence Interval
	1	2	3	4	5	6		
XY	1428.60	1150.20	1179.40	1336.20	1033.00	847.50	1162.48	±166.85
YX	1224.20	1401.00	1444.10	1336.10	1417.30	1005.20	1304.65	±133.20
ZX	1450.00	1552.20	1530.20	1450.80	1453.70	1420.00	1476.15	±41.87
XZ	989.08	1107.20	998.92	866.58	1059.00	1153.10	1028.98	±81.04
YZ	-	1562.50	1597.00	1551.60	1547.70	1537.80	1559.32	±20.02
ZY	1487.70	1518.60	1452.60	1412.50	1428.90	1433.70	1455.67	±32.12

Figure 4-13 shows a graphical representation of the flexural modulus results.

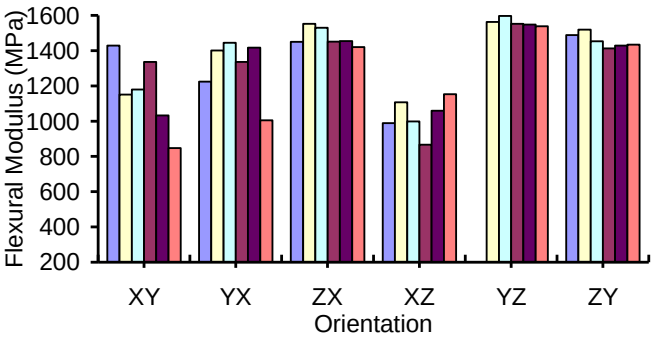

Figure 4-13 Three point flexural modulus of different fabrication orientations (distribution for all specimens)

As shown in Table 4-6 and Figure 4-13, the flexural modulus of the different fabrication orientations also varies. From the average value, the YZ orientation has the highest average modulus, followed by ZX, ZY and then YX. From the ANOVA results,

it can be confirmed that the *p*-value is 0.000, which is less than 0.05 and means that modulus varies with different orientations.

The high YZ orientation average value is thought to be caused by the scan factor in this orientation being short. According to Gibson and Shi [1997], the average sintering temperature is uniform when the scan vector is short. This condition can provide better mechanical properties in the sintered part. The XZ orientation then has the lowest mean modulus (1028.98MPa) due to the long scan vector.

4.6 Four-point bending/flexure test

Four-point bending tests were carried out on the six different fabrication orientations. For each individual orientation, six samples were tested to evaluate the material properties. Figure 4-14 shows the full test results of the four point bending/flexure tests for the XY and YZ orientations. Other results can be seen in appendix A.

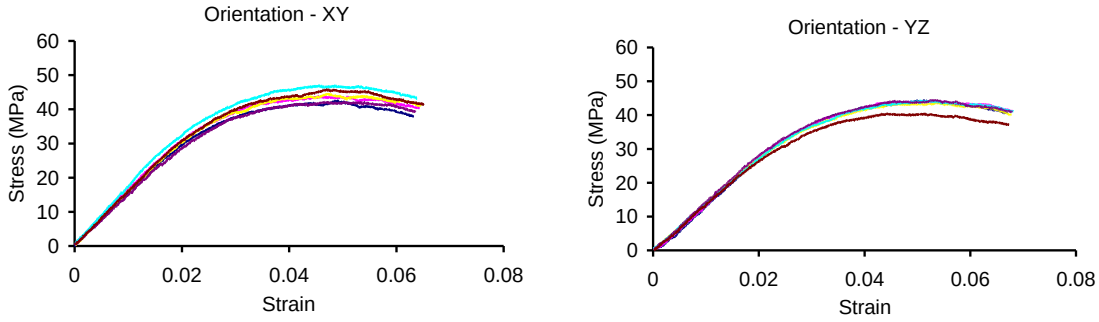

Figure 4-14 Stress-strain graph for each of the four point bending tested for the XY and YZ oriented parts

The flexural modulus from the four-point bending test was determined using the same procedure as described in section 3.5.4. During the test the specimens did not fracture, except for one YZ specimen. This happened due to a slip of the specimen between the spans, resulting in the specimen not breaking and generating an error in the results.

The slope was measured at a strain value by constructing a linear fit line on selected data, as shown in Figure 4-15 for the XY orientation. The results for all specimens are summarised in Table 4-7.

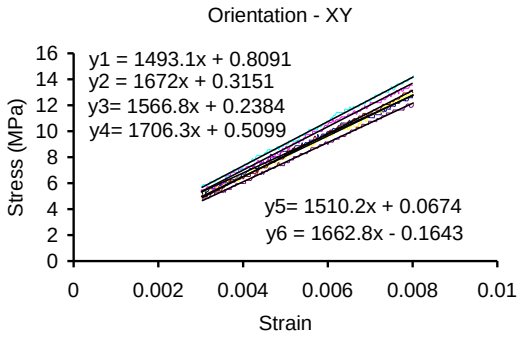

Figure 4-15 Linear fit line on stress-strain relationship of specimen in four point bending/flexure test for the XY-oriented parts

Table 4-7. Four point flexural modulus results (MPa)

Orientation	Sample						Average (MPa)	95 % Confiden-ce Interval
	1	2	3	4	5	6		
XY	1493.10	1672.00	1566.80	1706.30	1510.20	1662.80	1601.87	±72.46
YX	1466.40	1437.30	1322.40	1480.40	1475.40	1293.50	1412.57	±66.34
ZX	1573.90	1538.60	1665.20	1656.30	1510.60	1659.70	1600.72	±54.77
XZ	1326.90	1202.80	1276.60	1326.80	1163.40	1289.90	1264.40	±53.79
YZ	1460.90	1408.10	1418.00	1460.10	1522.60	1508.00	1462.95	±36.89
ZY	1535.90	1748.90	1668.30	1619.30	1689.60	1709.90	1661.98	±60.27

The results for flexural modulus of the different fabrication orientations are shown graphically in Figure 4-16.

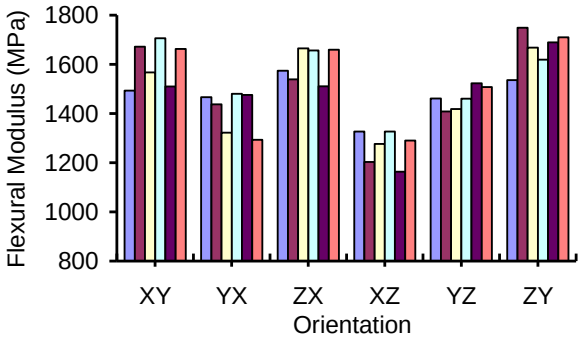

Figure 4-16 Four point flexural modulus of different fabrication orientations (distribution for all specimens)

From Table 4.7 and Figure 4-16, it can be seen that the highest average flexural modulus value is in the ZY orientation, followed by XY and ZX. This also shows that

flexural modulus varies with the orientation of specimens. This observation is supported by the results from the ANOVA where the *p*-value is less than 0.05.

A part with a position in the shorter laser scanning direction will produce a high flexural modulus, whereas a part in the longer laser scanning direction will have a low flexural modulus. This is shown in Figure 4-16. The laser scanning direction was described in Figure 3-2 and section 3.3.

4.7 Summary, Benchmarking and Discussion

4.7.1 Summary of test results

The mechanical properties of Nylon 12 laser sintered components has been characterised, and the results for all modulus values are shown in Figure 4-17.

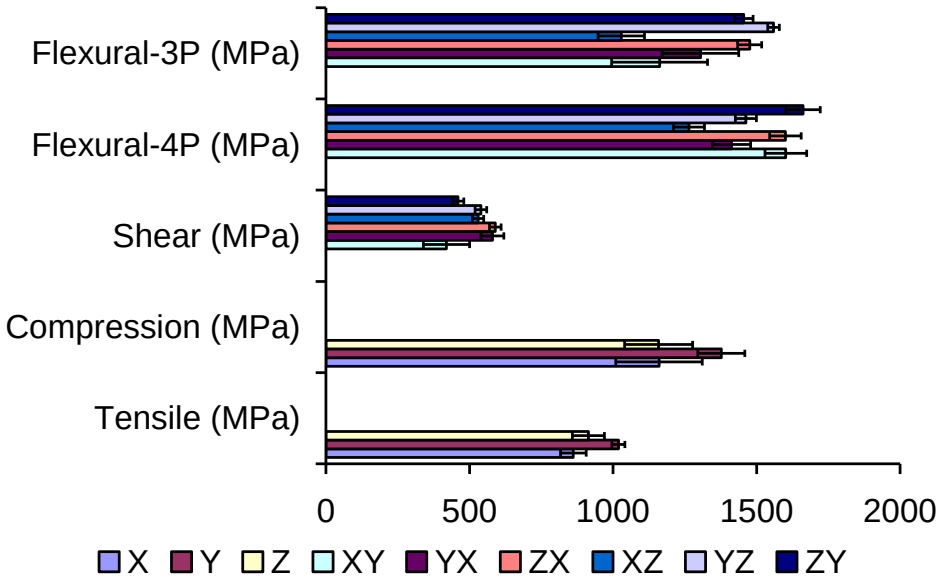

Figure 4-17 Summary of result for tensile, compression, shear and flexural modulus (three- and four-point) of nylon 12 laser sintered material in the X, Y, Z, XY, YX, ZX, XZ, YZ and ZY orientations

Tensile strength, tensile modulus, tensile elongation at break and compression modulus were highest in the Y orientation.

In the other tests conducted, the modulus values in different orientations showed some variation. However, the values of the shear modulus were always smaller than other modulus values, even for different orientations.

4.7.2 Comparison of present results with those of previous research

The values of modulus and strength resulting from the tests were compared with the values found by other researchers [Hague et al, 2004; Yubero, 2004; Hou, 2005] and reported by 3D Systems [2006b], as shown in Tables 4-8 to 4-11, and Figures 4-18 to 4-22. Even though other researchers used different names for each of their specimen orientations, the general directions of how the specimens are placed are similar.

Table 4-8. Comparison of results of tensile and compression modulus of Duraform PA (SLS) material

Data from	Tensile Modulus (MPa)			Compression Modulus (Mpa)		
	X	Y	Z	X	Y	Z
This research	861.61	1018.93	914.54	1160.36	1377.32	1158.62
Hou [2005]	1582.89	1547.34	1507.52	1572.01	1574.18	1328.94
3D Systems [2006b]	1600			-		
Hague et al [2004]	Flat		Upright	-		-
	2047.0		1817			
Yubero [2004]	Horizontal		Vertical	Horizontal		Vertical
	1575.46		1316.29	1518.55		1405.36

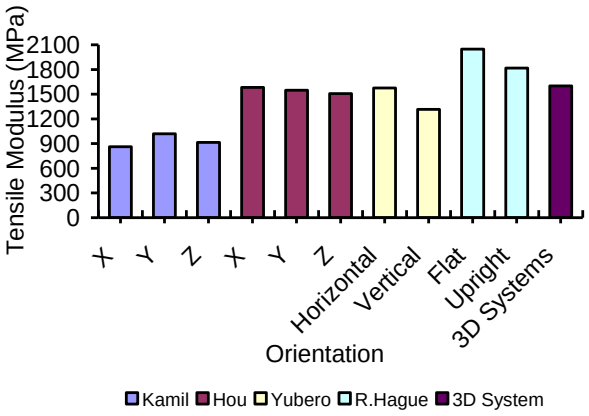

Figure 4-18 Comparison of results of tensile modulus test

Figures 4-18 and 4-19 shows that the test results for tension and compression in this study were low compared to those reported by other authors. However, from the results as a whole, it is clear that there are significant variations between researchers.

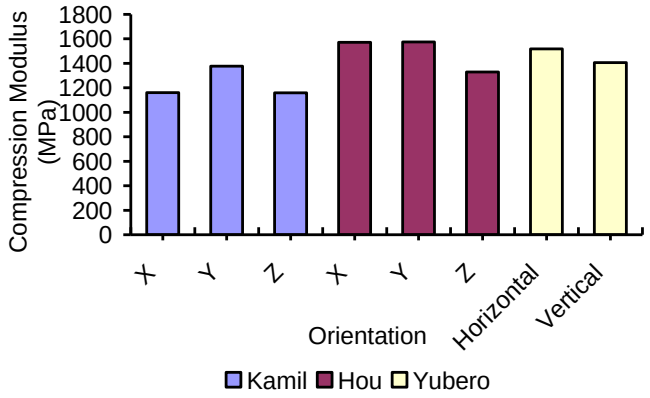

Figure 4-19 Comparison of results of compression modulus tests

It can be seen that the value of tensile modulus does, in general, vary with orientation, as does the compression modulus. Both sets of results illustrate that the highest values are in the Y orientation, while the values in the X or Z directions differ only slightly.

In addition, table 4-9 illustrates the flexural modulus results from the three-point bend/flexure tests found in this research and by other researchers.

Table 4-9. Comparison of results of flexural modulus of Duraform PA (SLS) Material (Three-point test)

Data from	Flexural Modulus (3 Point) (MPa)					
	XY	YX	ZY	XZ	YZ	ZX
This research	1162.48	1304.65	1476.15	1028.98	1559.32	1455.67
Hou [2005]	X	Y	Z	-	-	-
	1515.9	1747.0	1386.92	-	-	-
3D Systems [2006b]	1285					

It should be noted that 3D Systems conducted the test based on the ASTM D790 (three-point bend/flexure test) standard, while this research (and also Hou's) used BS EN ISO 14125:1998. Moreover, table 4-10 shows the results of the four-point bend/flexure test with different fabrication orientations.

Table 4-10. Comparison of results of flexural modulus of Duraform PA (SLS) material (Four-point test)

Data from	Flexural Modulus (4 Point) (MPa)					
	XY	YX	ZY	XZ	YZ	ZX
This research	1601.87	1412.57	1600.72	1264.40	1462.95	1661.98
Hou [2005]	X	Y	Z	-	-	-
	1727.77	2052.13	1398.04	-	-	-
Yubero [2004]	Horizontal			Vertical		
	1443.91			1347.09		

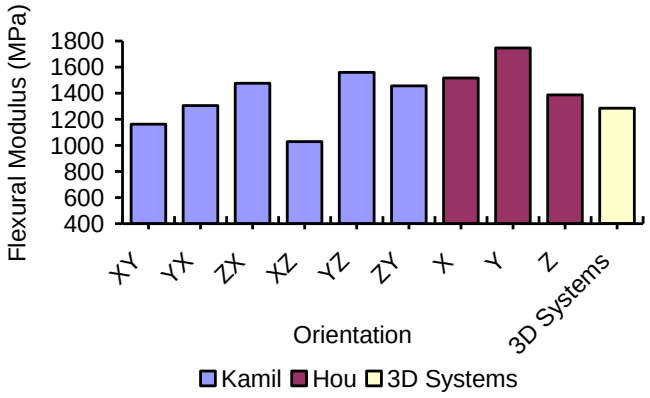

Figure 4-20 Comparison of results of test of flexural modulus (three-point)

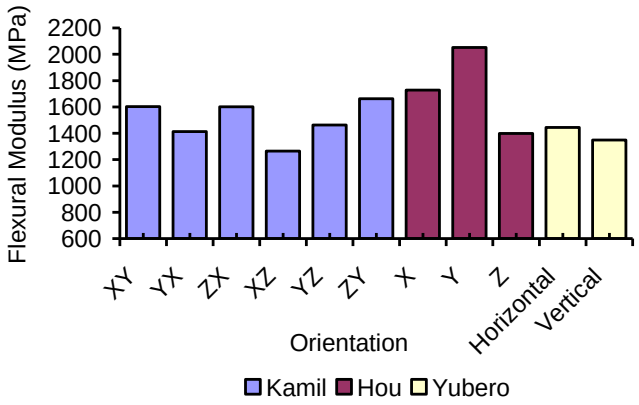

Figure 4-21 Comparison of results of test of flexural modulus (four-point)

From tables 4-9 and 4-10 and Figures 4-20 and 4-21, it is also clear that the values of flexural modulus for different fabrication orientations are different. The highest value from the three point test is in the YZ direction, while the ZY orientation has the highest value in the 4-point test. The lowest values from both sets of result are in the XZ direction.

Furthermore, table 4-11 and Figure 4-22, compare the tensile strengths found in this research with findings by other researchers.

Table 4-11. Comparison of tensile strength results

Data from	Tensile Strength (MPa)		
	X	Y	Z
This Research	30.44	42.45	34.52
Hou [2005]	41.93	42.36	37.35
3D Systems [2006b]	44		
R.Hague [2004]	48.7	-	40.9
Yubero [2004]	Horizontal		Vertical
	44		34.4

In this research, the highest tensile strength is in the Y direction, while the values of X and Z are similar, as was noted for tensile modulus.

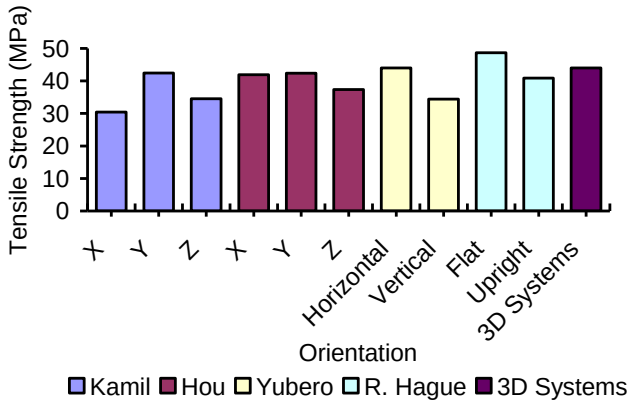

Figure 4-22 Comparison of tensile strength results

It can be concluded that the variations in results between researchers are greater than the variations between fabrication orientations in the X, Y or Z directions. It is clear that there are significant variations between researchers, which means that the results are inconsistent even using the same materials. In addition, there is a significant factor to account for in the general repeatability of the results, such as sample preparation and test conditions.

The test results as a whole also show that both strength and modulus vary between different fabrication orientation. Therefore the material is anisotropic, and this is a second significant factor that needs to be taken into account.

4.7.3 Discussion

The mechanical property test results have demonstrated that the part built in the Y orientation showed highest modulus values, while the parts produced in the X and Z

orientations showed lower values. This is thought to be the result of the different densities of the build material. In the Y direction, a short scan vector causes higher density, which gives improved mechanical properties. Generally, for laser fabricated material a single spot laser is focused to consolidate the powder grains. However, when the scan vector is short; this single laser spot that is moving back and forth very rapidly with a high level of overlap between each scan line could potentially heat an entire 'band' or 'length of motion' of the materials instantaneously. The cooling rate and direction of heat flow caused the adjacent materials to have less difference in thermal gradient during solidification and generate a more homogenous material [Carter et al, 2014]. Therefore, shorter scan vectors can offer uniform temperatures in sintering, resulting in good mechanical properties. This is as reported by Gibson and Shi [1997].

The same trend was also observed for the shear modulus. Shorter laser scanning in YX yielded the highest modulus, while longer scanning in the XY direction produced a lower modulus. However, for the part produced in the YZ orientation the modulus values were higher than those in other orientations in the three-point bending test and for the four-point bending test. This is according to the direction of loading applied to each specimen, which also has an effect on the mechanical properties.

The results also indicated that there exist some variations in the modulus between other researchers. Since different standard is used by different researchers, slight changes in term of layer thickness, height/thickness of the samples geometry, the state of the material used, and the samples position within the build envelope during build will have impact on the mechanical properties [Rusenberg and Schmid, 2014; Rusenberg et al, 2014]. As materials used (polyamide Nylon-12) during SLS process is susceptible to material ageing which is dependent on, job height and position of the samples [Rusenberg and Schmid, 2014; Rusenberg et al, 2014].

In addition, the results obtained indicated that the variations in the different tests in this analysis could be due to the different geometries of the specimen samples.

From the results presented in this chapter and also from the literature review, it is clear that the mechanical properties of laser-sintered material vary and are not consistent across machines or fabrication orientation. Besides that, variations also occur due to the process parameters used for powder material.

For crystalline materials, such as Nylon 12, they are often brittle. This property makes it difficult to get yield point, but easy to get the ultimate tensile strength (UTS).

Yield stress is mostly used in design application, mainly for ductile material. Yield strength is an important factor to consider during design to ensure safety factor is maintained. Meanwhile UTS is used for quality control of products that are manufactured, as it easy to carry out the test.

Therefore, in this study, the ultimate tensile strength is being used as a criterion for comparing the performance of tensile specimens and not the elastic modulus or the yield stress.

CHAPTER 5. HEAT TREATMENT STUDIES

5.1 Introduction

This chapter is to present details of the heat treatment regimes applied to selective laser sintered nylon 12 and their impact on the material's mechanical properties. Section 5.2 describes heat treatment selection factors and related matters. Following sections are the descriptions of samples preparation and characterisations. The furnaces and equipment used in this work, procedures and results are reported in section 5.5. At the end of the chapter, a discussion is presented. All samples used in this chapter were solid structure samples.

As initial work, in chapter 4, characterisation was carried out to provide a benchmark of mechanical performance. It is to show the responses of the material to load in different condition, such as the resistance of a material to tensile load, bending load and shear load.

In practice, humidity and temperature, the effect of type of loads, strain and creep play a big role in the properties, characteristics and behaviour of a plastic material and the moulded product performance. However, since it is expensive to test all the available properties of a plastic material, the test are carried out to ensure that the properties meet the minimum requirement needed for our intended purpose.

Therefore, in chapter 5 and 6, it was decided to do the tensile test rather than other tests, to minimise the research cost. It was believed that with the tensile properties results obtained, it can be used to observe the different characteristics of laser sintered specimens with and without heat treatment; and from different scanning strategy applied.

5.2 Heat Treatment Selection

As discussed in the literature review, several researchers have investigated the use of heat treatment to improve materials' properties, in particular; nylon and polymer.

These heat treatment studies were conducted using different setting of temperature, time and environment. In general, it can be seen that better mechanical properties were obtained when the heat treatment was carried out close to the melting temperature. All these studies used materials produced using conventional processes, except for the nylon 12 SLS material used by Zarringhalam and Hopkinson [2003].

In their investigation, Zarringhalam and Hopkinson [2003] conducted conventional heating in a Zwick temperature chamber. In this research, heat treatments in air and heat treatments in vacuum conditions has been assessed. Both conditions were studied in order to establish the optimum condition for heat treatment of SLS Nylon 12.

Heat treatment at lower temperature and duration is preferable from practical perspective. Therefore, in this research, the temperature was selected for 140^{o}C with two hours heat treatment duration as initial work. This was later increase to 180^{o}C with 16 hours duration. Then, the heat treatment was conducted with the same temperature for 100 hours duration. Two heat treatment environments in air and vacuum were selected to find out the effect of heat treatment on the mechanical properties of SLS made parts. A slow heating rate of 2-3^{o}C/minute was selected in order to achieve homogeneous heating conditions.

5.3 Specimen Preparation

Tensile test samples were produced using the SLS Sinterstation Vanguard at Leeds University, Leeds (see section 3.2.). These specimens were used for comparing the properties with and without heat treatment. The tensile test specimens were fabricated in three different built orientations; X,Y and Z using specimen design and processing conditions as described in section 3.3 and 3.4.

5.4 Characterisations

In this study, three characteristics were measured using heat treated and non heat treated specimens. Tensile tests were used to examine the mechanical properties, while DSC analysis was used to determine the crystallinity and melting temperature. Furthermore, the optical microscopy was used to observe the microstructure of the specimens.

5.5 Experimental Work and Procedures

5.5.1 Heat Treatment in Air

A conventional heating oven, the “BINDER”, was used to heat treat the tensile specimens from room temperature with a heating rate of 2^{o}C/minute up to 140^{o}C. Then the temperature was held constant for 120 minutes before cooling at the natural

rate of the furnace to 27^{o}C. The specimens were placed in the oven as shown in figure 5-1.

Figure 5-1 Heating oven and tensile specimen

5.5.1.1 Tensile Test Results

Tensile tests were carried out as described in section 4.4 on all three different fabrication orientations. Six samples for each orientation were tested in order to evaluate the tensile properties. The values of stress and strain were calculated using equation 3.1 and 3.2. Figure 5-2 shows the stress-strain curves of heated and non-heated specimens for all orientations while table 5-1 summarises the tensile strengths obtained. The curves indicated that the material under-goes plastics failure, which typical of behaviour of polymer materials.

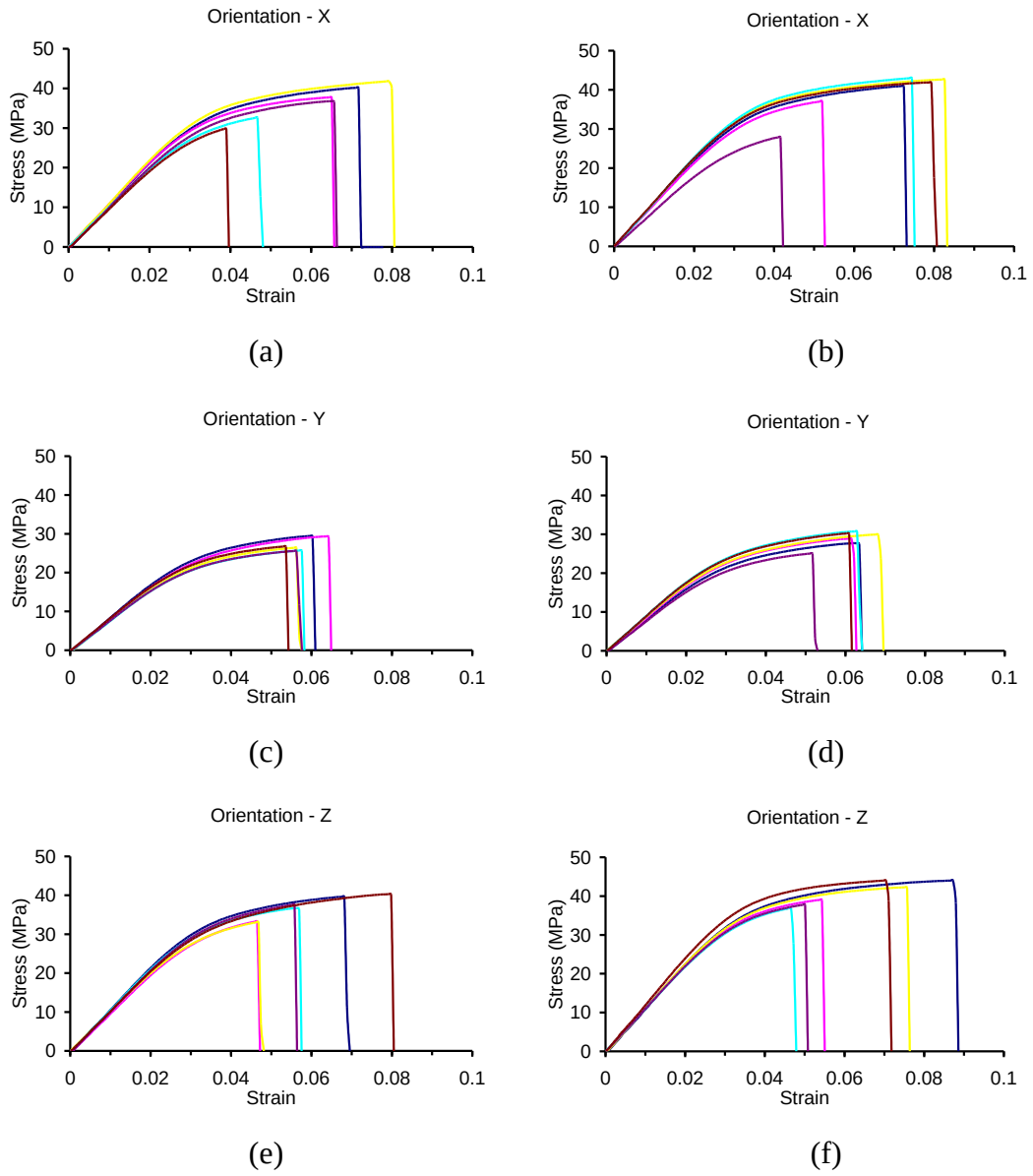

Figure 5-2 Stress-strain graphs for each of the tensile tests in X, Y and Z orientation (a), (c) and (e) without heat treatment; (b), (d) and (f) with heat treatment.

Table 5-1. Tensile Strength Results (MPa) – With and Without Heat Treatment

Orientation	Sample						Average (MPa)	95 % Confidence Interval
	1	2	3	4	5	6		
X	40.1	37.7	41.7	32.6	36.6	29.7	36.4	±3.62
X_{ht}	40.9	37.1	42.6	43.0	27.9	41.8	38.9	±4.63
Y	29.4	29.2	26.4	25.6	25.6	26.7	27.2	±1.38
Y_{ht}	27.5	28.9	29.9	30.7	25.0	30.2	28.7	±1.70
Z	39.7	33.3	33.1	36.4	37.6	40.3	36.7	±2.45
Z_{ht}	44.0	39.0	42.2	36.9	37.8	44.0	40.7	±2.52

The graphical comparison of the results with and without heat treatment in air can be seen in figure 5-3.

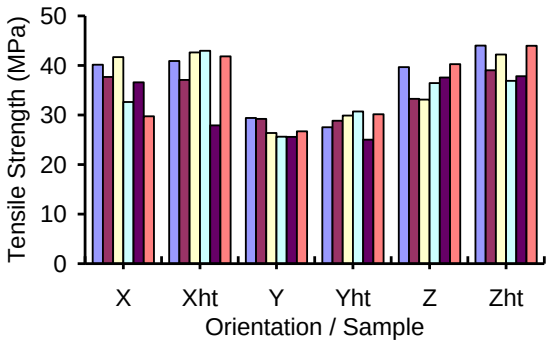

Figure 5-3 Tensile strength of different fabrication orientations with and without heat treatment (distribution for all specimens**)**. The suffix ht indicates heat treatment.

From Table 5-1, it can be seen that the average tensile strength in the X, Y and Z orientations after heat treatment in air improved slightly. The average increases are 6.8% in the X orientation, 5.71% in Y and 10.59% in Z. However, the overlaps in 95% confidence intervals mean that, at a 95% confidence level, the differences are not statistically significant.

The tensile modulus for each test was calculated from the initial slope of the straight line on the stress-strain curves and this is summarised in tables 5-2.

Table 5-2. Tensile Modulus Results (MPa) - With and Without Heat Treatment

Orientation	Sample						Average (MPa)	95 % Conf. Interval
	1	2	3	4	5	6		
X	1093.7	1065.4	1069.5	998.6	1030.5	984.6	1040.4	±34.5
X_{ht}	1079.8	1077.8	1124.0	1136.4	919.2	1111.8	1074.8	±63.8
Y	874.1	846.0	814.4	790.8	789.3	839.1	825.6	±26.8
Y_{ht}	824.0	871.1	871.1	903.7	786.8	902.0	859.8	±36.8
Z	1092.7	1013.9	1009.8	1078.4	1061.9	1034.3	1048.5	±27.5
Z_{ht}	1121.7	1122.6	1143.4	1082.9	1089.2	1167.0	1121.1	±25.5

The graphical comparison of the tensile modulus results for Duraform PA (Nylon 12) with and without heat treatment in the air environment is illustrated in figure 5-4.

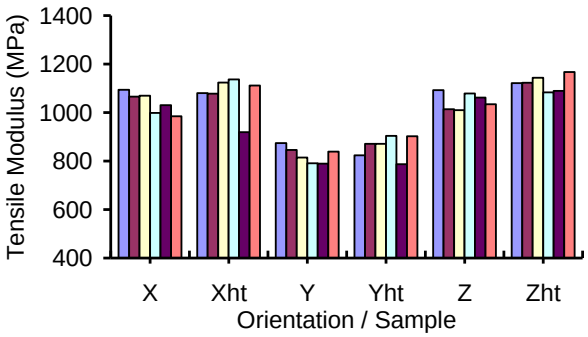

Figure 5-4 Tensile modulus result with and without heat treatment (distribution for all specimens**).** The suffix ht indicates heat treatment.

Table 5-2 shows that the average tensile modulus in the X, Y and Z orientations with heat treatment increased slightly compared with those without heat treatment. The increases are 3.31% in the X orientation, 4.14% in Y and 6.93% in Z. Again, there are overlaps in the 95% confidence intervals for the X and Y orientations, but not for the Z orientation. Therefore, at a 95% confidence level, the increase is significant in Z but not in X and Y.

Tensile elongation at break for each test was determined by calculated from strain value at point where the break found as shown in Figure 5-2 for each different fabrication orientation, with and without heat treatment, then multiplied with 100(%) and the results is summarised in table 5-3. Figure 5-5 illustrates the graphical comparison of the tensile elongation at break results.

Table 5-3. Tensile Elongation at Break (%)

Orientation	Sample						Average (%)	95 % Confidence Interval
	1	2	3	4	5	6		
X	7.20	6.50	8.10	4.70	6.60	3.90	6.17	±1.26
X_{ht}	7.20	5.20	8.30	7.40	4.20	7.90	6.70	±1.30
Y	5.90	6.40	5.60	5.80	5.60	5.40	5.78	±0.28
Y_{ht}	6.30	6.10	6.80	6.20	5.20	6.00	6.10	±0.42
Z	6.80	4.60	4.70	5.70	5.60	7.90	5.88	±1.02
Z_{ht}	8.70	5.40	7.50	4.60	5.00	7.00	6.37	±1.29

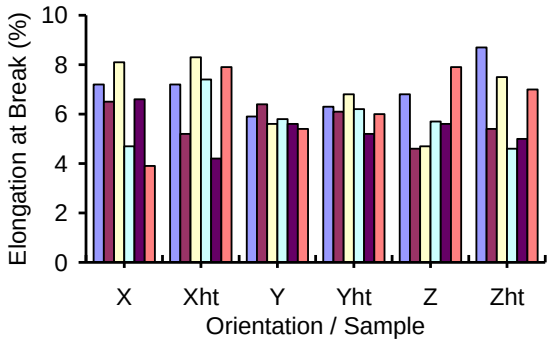

Figure 5-5 Tensile elongation at break result with and without heat treatment (distribution for all specimens**).** The suffix ht indicates heat treatment.

From Table 5-3, it can be seen that the average tensile elongation at break improved slightly, in which the average increases are 8.6% in the X orientation, 5.5% in Y and 8.3% in Z after heat treatment in air. However, the differences are not statistically significant at a 95% confidence level, as it shown that there are overlaps in 95% confidence intervals.

5.5.1.2 Distortion Performance

In order to make sure that there were no geometric changes, the dimensions of each specimen for different fabricated orientations were measured before and after heat treatment using a vernier calliper. All dimensions that measured are shown in Figure 5-6 that illustrates the solid tensile specimens.

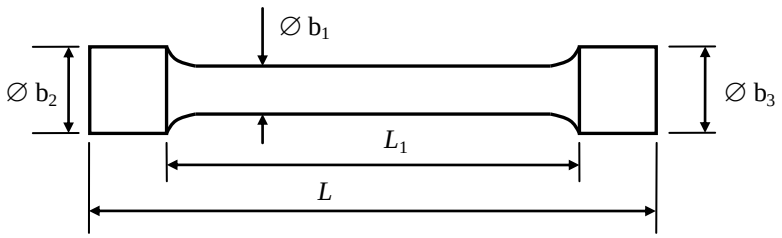

Figure 5-6 Solid tensile specimen

For each dimension L, L_1, b_1, b_2 and b_3, it was measured three times at three different positions and then an average was calculated. To determine the distortion before and after heat treatment the equation (5.1) was used and the results was summarised in tables 5.4 – 5.6.

$$Distortion = \frac{dimension_{after} - dimension_{before}}{dimension_{before}} \times 100\% \quad \ldots\ldots\ldots\ldots (5.1)$$

Table 5-4. Distortion for Heat Treated Sample (X Orientation)

Orientation /Sample	Distortion (%)				
	L	L_1	b_1	b_2	b_3
$X1_{ht}$	0.00	0.00	0.33	0.33	0.00
$X2_{ht}$	0.00	0.00	0.00	0.33	0.00
$X3_{ht}$	0.13	0.18	0.33	0.33	0.00
$X4_{ht}$	0.13	0.18	1.00	0.33	0.00
$X5_{ht}$	0.00	0.00	1.00	0.66	0.00
$X6_{ht}$	0.00	0.00	0.00	0.99	0.00

Table 5-5. Distortion for Heat Treated Sample (Y Orientation)

Orientation /Sample	Distortion (%)				
	L	L_1	b_1	b_2	b_3
$Y1_{ht}$	0.00	0.00	0.00	0.33	0.00
$Y2_{ht}$	0.00	0.00	0.33	0.33	0.00
$Y3_{ht}$	0.00	0.00	0.00	0.33	0.00
$Y4_{ht}$	0.00	0.00	0.00	0.00	0.00
$Y5_{ht}$	0.00	0.00	0.00	0.33	0.00
$Y6_{ht}$	0.00	0.00	0.00	0.33	0.00

Table 5-6. Distortion for Heat Treated Sample (Z Orientation)

Orientation /Sample	Distortion (%)				
	L	L_1	b_1	b_2	b_3
$Z1_{ht}$	0.00	0.00	0.00	0.33	0.99
$Z2_{ht}$	0.00	0.00	0.00	0.33	0.99
$Z3_{ht}$	0.00	0.00	0.00	0.33	0.33
$Z4_{ht}$	0.00	0.00	0.33	0.00	0.33
$Z5_{ht}$	0.00	0.00	0.00	0.33	0.00
$Z6_{ht}$	0.00	0.00	0.00	0.00	0.00

From table 5-4 to 5-6 it was concluded that there were no significant dimensional changes.

5.5.1.3 DSC test results

Thermal characterisations were conducted on six samples of each individual orientation. Figure 5-7 shows DSC plots of specimens in X orientation, without heat treatment in air, which were obtained. DSC analysis focused on melt region between 130°C and 210°C to determine crystallinity and melting temperature. All others DSC plots (test) results can be seen in Appendix.

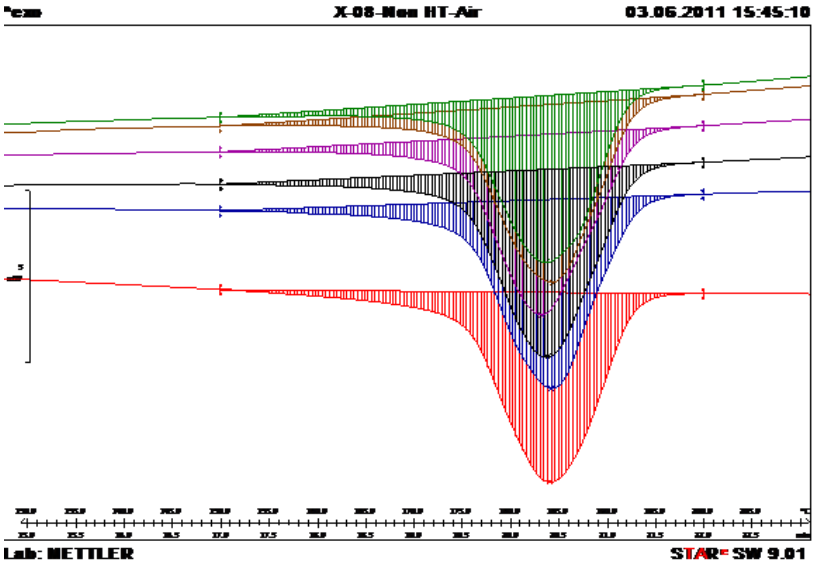

Figure 5-7 DSC plots for X orientation specimen sample without heat treatment

Figure 5-7 shows that all of the DSC plots show a similar trend with single peak and the results from other test samples were equally consistent. From DSC plots, the degree of crystallinity can be determined (see section 3.6).

All the values of degree of crystallinity of heat treated and non-heat treated specimens material in the X, Y and Z orientations are shown in tables 5-7 and Figure 5-8.

Table 5-7. Crystallinity Results (%) – With and Without Heat Treatment

Orientation	Sample						Average (%)	95 % Conf. Interval
	1	2	3	4	5	6		
X	24.8	27.3	27.6	27.3	27.2	26.3	26.8	±0.86
X_{ht}	27.4	25.8	25.9	25.9	25.6	25.9	26.1	±0.51
Y	25.3	27.1	28.1	26.7	24.3	27.7	26.5	±1.18
Y_{ht}	27.9	25.9	25.9	28.1	28.2	28.8	27.5	±1.00
Z	28.6	25.3	25.4	27.4	26.9	26.3	26.7	±1.00
Z_{ht}	25.8	20.8	26.7	22.5	25.7	25.9	24.6	±1.88

Table 5-7 and Figure 5-8 shows that the degree of crystallinity is not significantly changed by heat treatment.

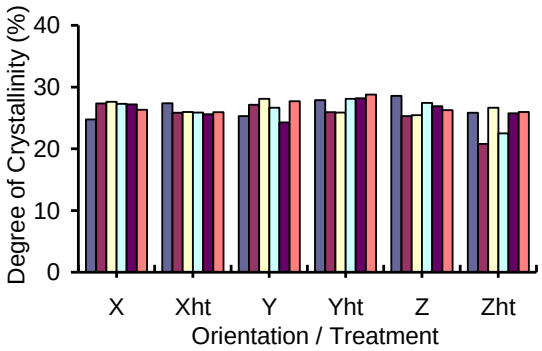

Figure 5-8 Crystallinity results with and without heat treatment (distribution for all specimens). Suffix ht indicates heat treatment.

The melting peak temperature was also determined from the DSC plots and the results are tabulated in tables 5-8 and illustrated in figure 5-9.

Table 5-8. Melting Peak Temperature (^{o}C) – With and Without Heat Treatment

Orientation	Sample						Average (^{o}C)	95 % Conf. Interval
	1	2	3	4	5	6		
X	183.6	184.0	183.7	183.7	184.3	183.1	183.7	±0.32
X_{ht}	184.1	184.7	186.3	184.5	182.5	184.0	184.4	±0.98
Y	183.9	183.3	184.7	183.7	183.7	182.5	183.7	±0.58
Y_{ht}	183.6	183.2	184.7	183.6	184.6	183.0	183.8	±0.59
Z	183.8	184.4	183.6	185.7	182.9	186.1	184.4	±1.00
Z_{ht}	185.2	184.0	183.1	183.0	182.8	183.6	183.6	±0.70

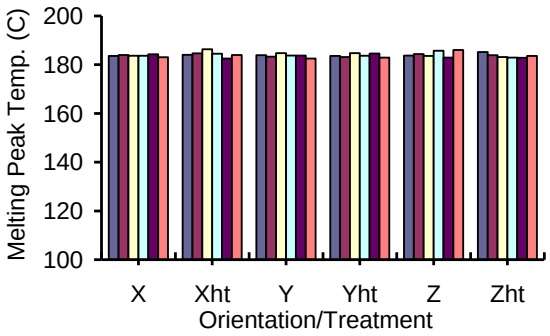

Figure 5-9 Melting peak temperature result with and without heat treatment (distribution for all specimens). The suffix ht indicates heat treatment.

Tables 5-8 and Figure 5-9 show that there is no significant change in the value of the peak melting temperature due to heat treatment in air.

5.5.1.4 Optical Microscopy

In order to observe the microstructure of the specimens with and without heat treatment, an optical light microscope was used. An Olympus BX60M optical microscope fitted with an adjustable micrometer was set up to observe the specimen and a JVC digital camera (KY-F55BE) fitted to the optical microscope and connected to a PC was used to capture the images.

The samples were prepared using a cold mounting technique. 16ml of Araldite resin and 2ml of Vantico hardener were mixed together and then poured into a mould, and left at room temperature. The samples were released from the mould after 24 hours.

To analyse microstructure polished flat surfaces were required. The specimens were ground using silicon carbide grinding paper, starting from a low grit number (320), and then using progressively finer paper (grit number 500 and 1200). The specimens were then thoroughly polished using a diamond polisher of 3 micron grit. This was then followed by the use of 1 micron grit as a final stage of the polishing process to remove all scratches.

The microstructures of specimens with and without heat treatment then were observed to compare the effect of the heat treatment in air, as shown in Figure 5-10.

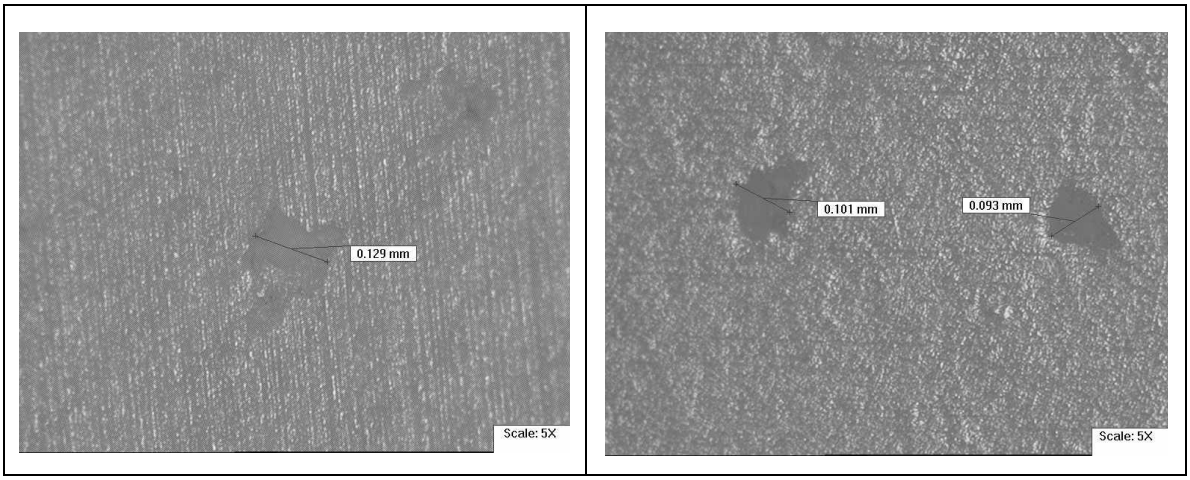

(a). X3 (b). XA3

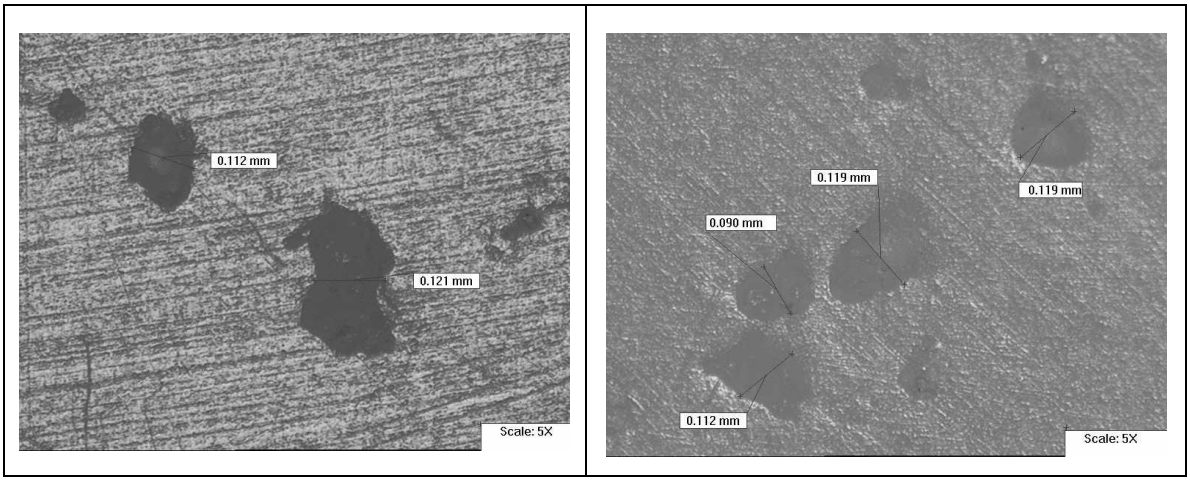

(c). Z2 (d). ZA2

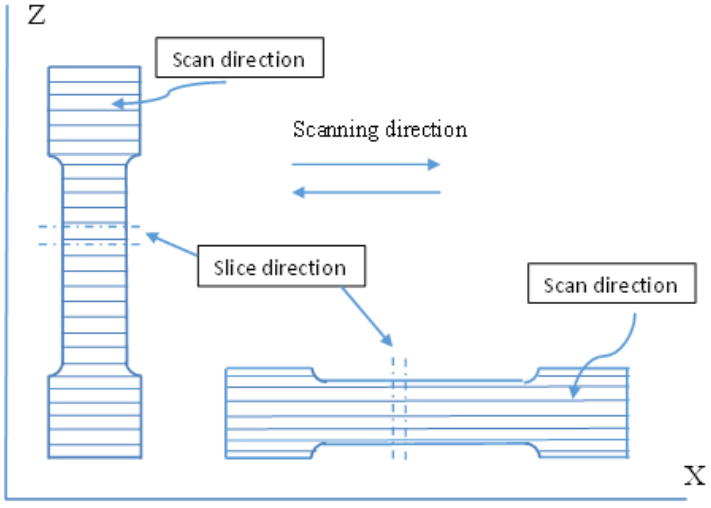

(e)

Figure 5-10 Microstructure samples with and without heat treatment in air, with 5X magnification: (a) sample no.3-X orientation without heat treatment; (b) sample no.3-X orientation with heat treatment; (c) sample no.2-Z orientation without heat treatment; (d) sample no.2-Z orientation with heat treatment; (e). The slicing direction of the sections.

The micrograph of heat treated and non-heat treated specimens as shown in Figure 5.10, the porosity seems not to have reduced much in size after heat treatment of the specimens in air environment.

5.5.1.5 Heat Treatment in Air (at 180°C, time of 100 hours)

Heat treatment in air at temperature 180°C with 100 hours time setting was also conducted using the drying oven. However, all specimens were burned/charred, presumably by oxidation which occurred during heat treatment. Figure 5-11 shows selected samples after treatment. Consequently, this approach was not considered useful.

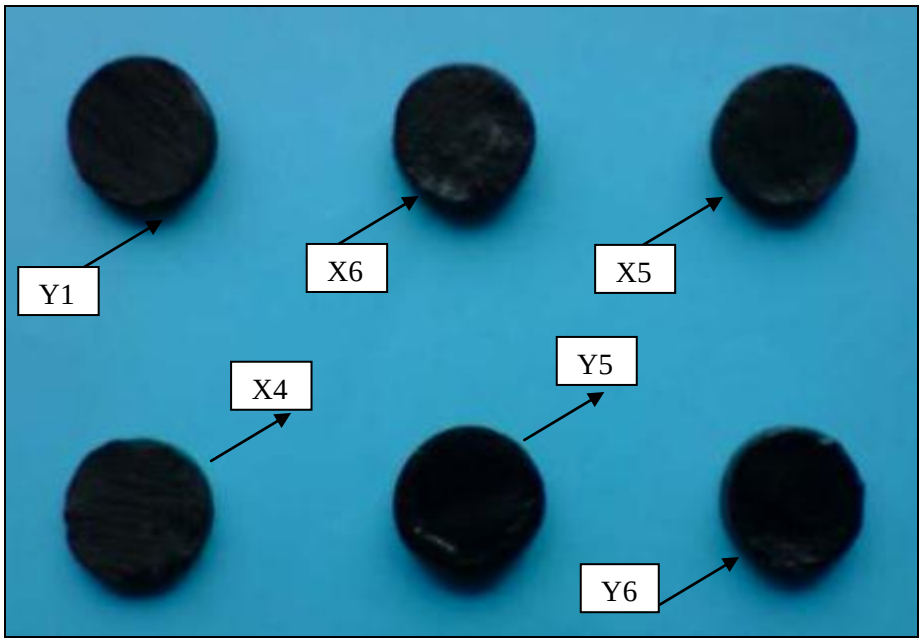

Figure 5-11 Cut-off specimens that burned after heat treated in air atmosphere for 180°C and 100 hours.

5.5.2 Heat Treatment in Vacuum

In order to avoid oxidation, heat treatment in a vacuum environment was undertaken. This was at 180°C for 16 and 100 hours, with a vacuum level of 1018mbar.

A vacuum oven, "***Technico***", installed at Metaltech Ltd., Consett, Durham, was used to heat treat the tensile specimens. The heat treatment was conducted with a heating rate of 3.3°C/minute. This temperature was held for 16 or 100 hours before cooling naturally in vacuum conditions to a temperature of 27°C. The specimens were placed in the vacuum oven as shown in Figure 5-12.

Figure 5-12 Vacuum oven facilities and tensile specimens

To avoid the repetition of the tests, reduce build time and also reduce experimental cost, tensile tests were carried out on one built orientation; Y-axis only. In addition, if mechanical properties can be improved for specimens produced in a single orientation, then the study can be extended further to other built orientation of specimens.

5.5.2.1 Test results at holding time 100 hours

A. Tensile Tests Results

Using the same equipment and procedure as described in section 5.5.1.1, tensile tests were carried out and Figure 5-13 shows the stress-strain plots with and without heat treatment. The results shown in Table 5-9 and Figure 5-14 illustrate the tensile strength with and without heat treatment.

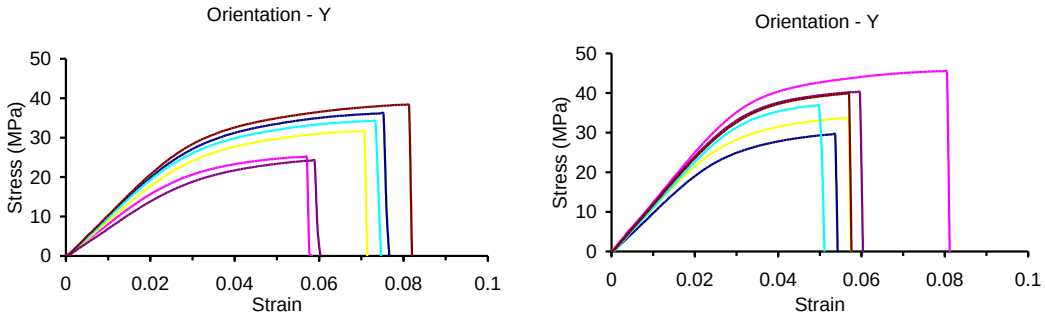

(a) (b)

Figure 5-13 Stress-strain graphs for each of the tensile tests for Y oriented parts, (a) without heat treatment and (b) with heat treatment in vacuum for 100 hours

Table 5-9. Tensile Strength Results (MPa) – With and Without Heat Treatment

Orientation	Sample						Average (MPa)	95 % Confidence Interval
	1	2	3	4	5	6		
Y	36.1	25.1	31.6	34.1	38.2	24.2	31.6	±4.63
Y_{ht}	29.6	45.4	33.6	36.9	40.2	39.8	37.6	±4.44

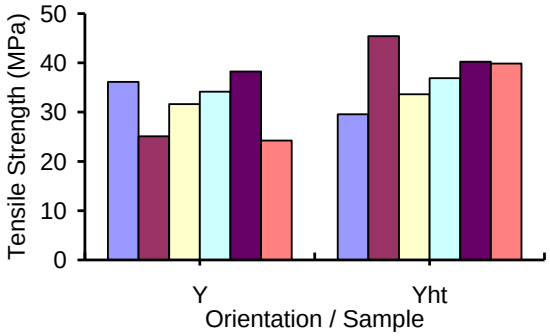

Figure 5-14 Tensile strength result with and without heat treatment (distribution for all specimens). The suffix ht indicates heat treatment.

Table 5-9 shows that the mean tensile strength increased, but that the difference was not significant at a 95% confidence level.

Tensile modulus values for each individual specimen were also determined. The results are summarised in Table 5-10 and Figure 5-15.

Table 5-10. Tensile Modulus Results (MPa) – With and Without Heat Treatment

Orienta-tion	Sample						Averag e (MPa)	95 % Conf. Interval
	1	2	3	4	5	6		
Y	1020.6	797.1	924.5	1007.0	1060.6	712.5	920.4	±110.7
Y_{ht}	1002.3	1209.4	1099.9	1161.1	1202.7	1208.8	1147.4	±66.2

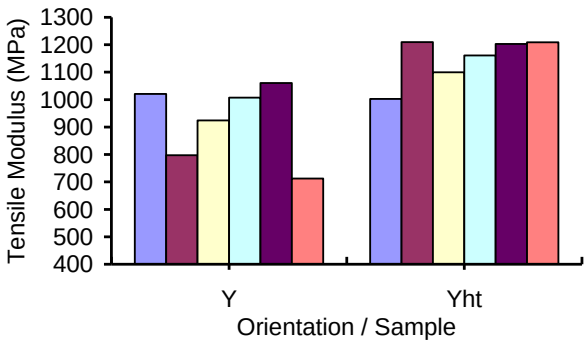

Figure 5-15 Tensile modulus result with and without heat treatment (distribution for all specimens). The suffix ht indicates heat treatment.

From Table 5-10, it can be concluded that the average tensile modulus of the heat treated samples increased by 24.66% compared to the non-heated samples, and that this increase is significant at a 95% confidence level.

For each individual specimen, tensile elongation at break was also determined and the results are summarised in Table 5-11 and Figure 5-16.

Table 5-11. Tensile Elongation at Break (%) – With and Without Heat Treatment

Orientation	Sample						Average (%)	95 % Confidence Interval
	1	2	3	4	5	6		
Y	7.50	5.70	7.00	7.30	8.10	5.80	6.90	±0.77
Y_{ht}	5.30	8.00	5.70	4.90	5.90	5.70	5.92	±0.87

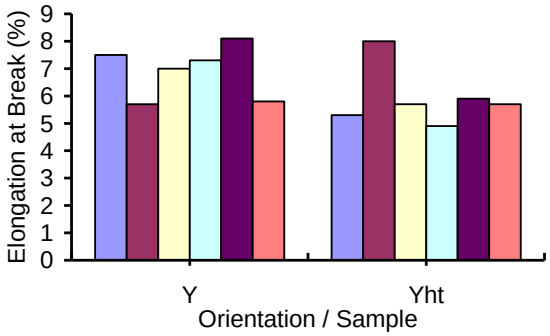

Figure 5-16 Tensile elongation at break result with and without heat treatment (distribution for al specimens). The suffix ht indicates heat treatment.

From Table 5-11, it can be seen that the average tensile elongation at break of the heat treated samples decreased by 14.20% compared to the non-heated samples, but was not significant at 95% confidence interval.

B. Distortion Performance

For heat treatment in 100 hours, any changes in the dimensions of specimens before and after heat treatment, as shown in table 5-12, were not significant.

Table 5-12. Distortion for Heat Treated Sample (Y Orientation)

Orientation /Sample	Distortion (%)				
	L	L_1	b_1	b_2	b_3
$Y1_{ht}$	0.08	0.11	0.00	0.00	0.00
$Y2_{ht}$	0.13	0.18	0.06	0.07	0.00
$Y3_{ht}$	0.11	0.15	0.13	0.06	0.07
$Y4_{ht}$	0.15	0.20	0.07	0.00	0.03
$Y5_{ht}$	0.03	0.04	0.03	0.03	0.00
$Y6_{ht}$	0.05	0.07	0.07	0.00	0.03

C. DSC Test Results

Using the same procedure as described in section 5.5.1.3, the degree of crystallinity was determined and all the results are shown in Table 5-13 and Figure 5-17.

Table 5-13. Crystallinity Results (%) – With and Without Heat Treatment

Orientation	Sample						Average (%)	95 % Confidence Interval
	1	2	3	4	5	6		
Y	27.9	25.9	28.2	28.0	24.5	25.5	26.7	±1.28
Y_{ht}	27.0	28.2	30.0	29.5	29.9	24.9	28.3	±1.62

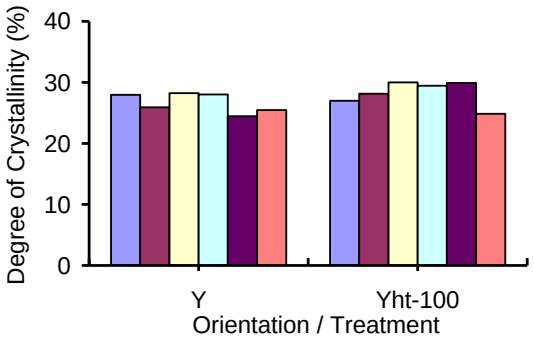

Figure 5-17 Crystallinity result with and without heat treatment (distribution for all specimens). The suffix ht indicates heat treatment.

Table 5-13 shows that the average degree of crystallinity of the heat treated samples increased by 5.81% compared to the non-heat treated samples, but was not significant at 95% confidence interval.

The procedure described in section 5.5.1.3 was also used to obtain the values of melting peak temperature (T_{peak}) with and without heat treatment in the vacuum environment. The results are shown in Table 5-14 and Figure 5-18.

Table 5-14. Melting Peak Temperature (^{o}C) – With and Without Heat Treatment

Orientation	Sample						Average (^{o}C)	95 % Conf. Interval
	1	2	3	4	5	6		
Y	184.5	183.4	183.1	184.8	182.4	183.6	183.6	±0.71
Y_{ht}	185.1	187.5	186.4	186.9	186.3	189.1	186.9	±1.08

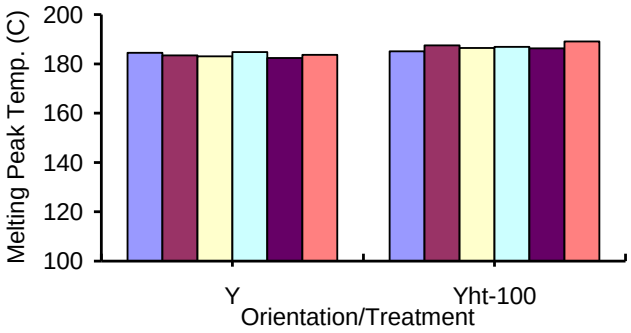

Figure 5-18 Melting peak temperature result with and without heat treatment (distribution for all specimens). The suffix ht indicates heat treatment.

Table 5-14 shows significantly increased values of melting peak temperature.

D. Optical Microscopy

To observe and analyse microstructure, the same equipment and procedure as described in section 5.5.1.4 were used. Figure 5-19 shows the microstructure of some specimens with and without heat treatment in the vacuum environment.

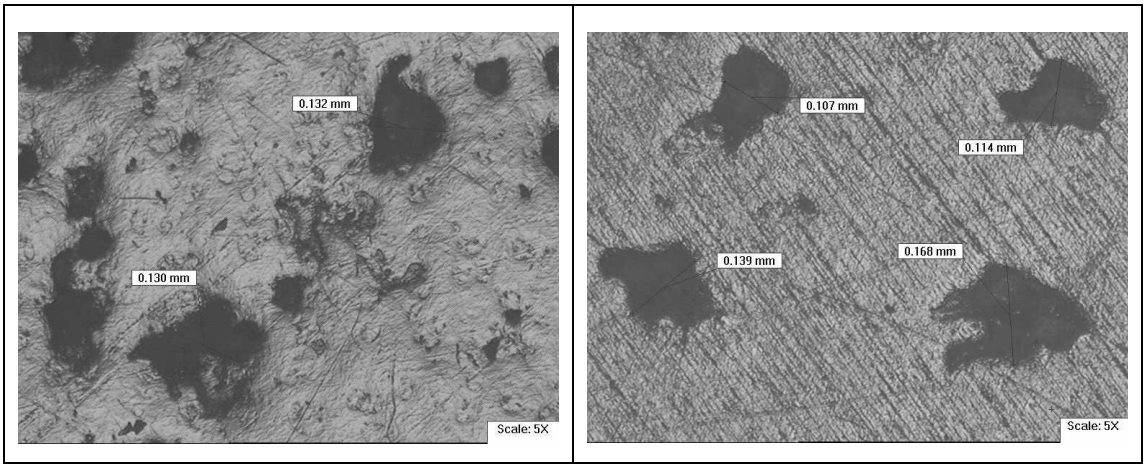

(a). Y2 (b). Y2V

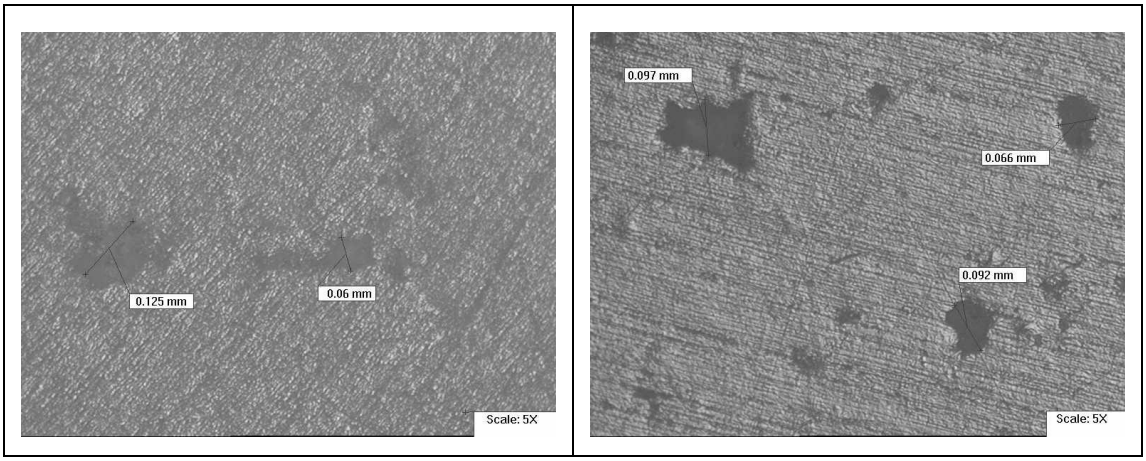

(c). Y6 (d). Y6V

Figure 5-19 Microstructure samples with and without heat treatment in vacuum, with 5X magnification: (a) sample no.2-Y orientation without heat treatment; (b) sample no.2-Y orientation with heat treatment; (c) sample no.6-Y orientation without heat treatment; (d) sample no.6-Y orientation with heat treatment

From Figure 5.19 shown the micrograph of heat treated and non-heat treated specimens and it seems that the porosity was not to have reduced much in size after heat treatment of the specimens.

From overall heat treatment in vacuum with 100 hours holding time, it can be summarised, the results show that heat treatment has increased the average melting temperature and the average tensile modulus, with this change being significant at a 95% confidence level. The average tensile strength and the average crystallinity also show an increase, but this result is not significant at a 95% confidence level. However, the average tensile elongation at break shows a decrease.

5.5.2.2 Test results at holding time 16 hours

A. Tensile Tests Results

The tensile strengths of these specimens were determined from stress-strain plots as shown in Figure 5-20 and all the results are shown in Table 5-15. The graphical comparison of tensile strength results from specimens with and without heat treatment is shown in Figure 5-21.

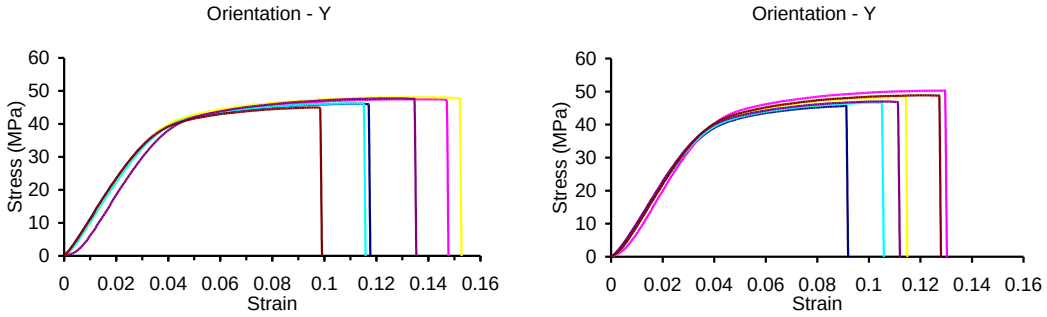

(a) (b)

Figure 5-20 Stress-strain graphs for each of the tensile tests for Y oriented parts, (a) without heat treatment and (b) with heat treatment in vacuum for 16 hours

Table 5-15. Tensile Strength Results (MPa) – With and Without Heat Treatment

Orientation	Sample						Average (MPa)	95 % Confidence Interval
	1	2	3	4	5	6		
Y	45.9	47.0	47.7	46.1	47.5	44.7	46.5	±0.91
Y_{ht}	45.6	50.2	48.3	46.6	46.8	48.7	47.7	±1.34

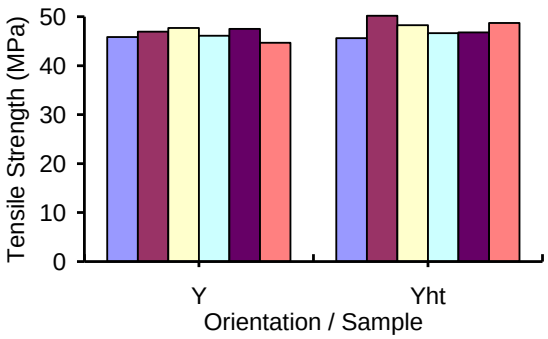

Figure 5-21 Tensile strength result with and without heat treatment (distribution for all specimens). The suffix ht indicates heat treatment.

Table 5-15 shows that the average tensile strength not increased after heat treatment, even though there were slightly different around 2.57%, but at a 95% confidence interval there were overlaps.

Tensile modulus values for each individual specimen were also determined, The results are summarised in Table 5-16 and Figure 5-22.

Table 5-16. Tensile Modulus Results (MPa) – With and Without Heat Treatment

Orienta-tion	Sample						Averag e (MPa)	95 % Conf. Interval
	1	2	3	4	5	6		
Y	1256.8	1238.3	1245.0	1225.2	1167.1	1294.2	1237.8	±33.5
Y_{ht}	1225.1	1221.9	1272.0	1258.7	1267.4	1271.5	1252.8	±18.6

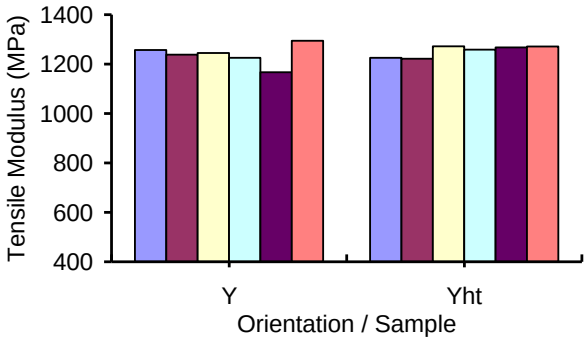

Figure 5-22 Tensile modulus result with and without heat treatment (distribution for all specimens). The suffix ht indicates heat treatment.

From Table 5-16, it can be concluded that the average tensile modulus of the heat treated samples not increased significantly compared to the non heated samples. The increase is only 1,19%. Again, there was overlap in the 95% confidence interval.

Tensile elongation at break for each individual specimen was also determined. The results are summarised in Table 5-17 and Figure 5-23.

Table 5-17. Tensile Elongation at Break (%) – With and Without Heat Treatment

Orientation	Sample						Average (%)	95 % Confidence Interval
	1	2	3	4	5	6		
Y	11.7	14.7	15.2	11.5	13.4	9.80	12.7	±1.66
Y_{ht}	9.10	12.9	11.4	10.5	11.1	12.7	11.3	±1.13

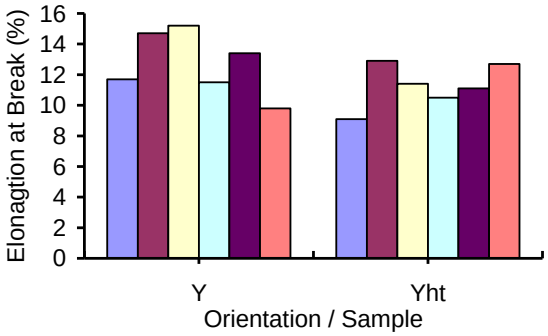

Figure 5-23 Tensile elongation at break result with and without heat treatment (distribution for all specimens).The suffix ht indicates heat treatment

Table 5-17 shows that the average tensile elongation at break was decrease around 11.3% after heat treated.

B. Distortion Performance

Dimensions before and after heat treatment for 16 hours were measured and the results showed there is no significant impact, as shown in table 5-18.

Table 5-18. Distortion for Heat Treated Sample (Y Orientation)

Orientation /Sample	Distortion (%)				
	L	L_1	b_1	b_2	b_3
$Y1_{ht}$	0.01	0.02	0.00	0.03	0.03
$Y2_{ht}$	0.03	0.00	0.03	0.03	0.03
$Y3_{ht}$	0.00	0.00	0.00	0.03	0.00
$Y4_{ht}$	0.00	0.00	0.03	0.03	0.03
$Y5_{ht}$	0.01	0.00	0.06	0.00	0.03
$Y6_{ht}$	0.00	0.02	0.00	0.00	0.03

C. DSC Test Results

Using the same procedure as described in section 5.5.1.3, the degree of crystallinity was determined and all the results are shown in Table 5-19 and Figure 5-24.

Table 5-19. Crystallinity Results (%) – With and Without Heat Treatment

Orientation	Sample						Average (%)	95 % Confidence Interval
	1	2	3	4	5	6		
Y	25.4	25.4	24.3	25.4	27.1	26.0	25.6	±0.74
Y_{ht}	28.5	25.8	28.2	27.9	28.9	27.3	27.8	±0.87

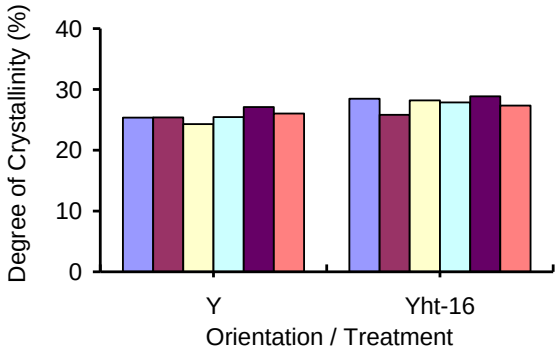

Figure 5-24 Crystallinity result with and without heat treatment (distribution for all specimens). The suffix ht indicates heat treatment.

Table 5-19 shows that the average degree of crystallinity of the heat treated samples increased by 8.44% compared to the non-heat treated samples.

The procedure described in section 5.5.1.3 was also used to obtain the values of melting peak temperature (T_{peak}) with and without heat treatment for 16 hours in the vacuum environment. The results are shown in Table 5-20 and Figure 5-25.

Table 5-20. Melting Peak Temperature (^{o}C) – With and Without Heat Treatment

Orientation	Sample						Average (^{o}C)	95 % Conf. Interval
	1	2	3	4	5	6		
Y	182.6	183.5	183.7	182.9	183.9	183.5	183.35	±0.39
Y_{ht}	185.1	183.7	184.1	184.4	184.6	184.4	184.36	±0.38

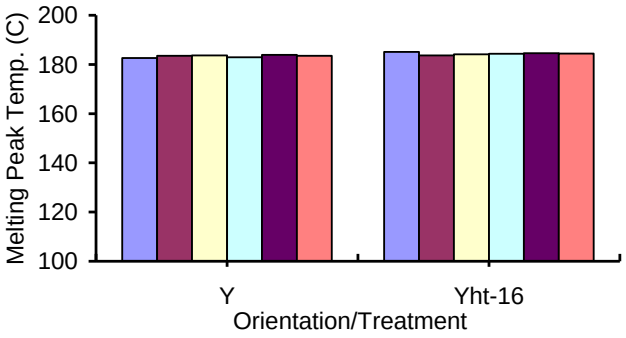

Figure 5-25 Melting peak temperature result with and without heat treatment (distribution for all specimens). The suffix ht indicates heat treatment.

Table 5-20 shows that there was no significantly increased values of melting peak temperature of heat treated compared to non-heat treated specimens.

It can be concluded all the results show that heat treatment in vacuum with holding time of 16 hours has significantly increased the average crystallinity, but not significantly increased any of the other parameter.

5.6 Summary and Discussion

The results for heat treatment in air and vacuum atmosphere as determined in section 5.5.1 and 5.5.2 summarised in Figure 5-26 to 5-30.

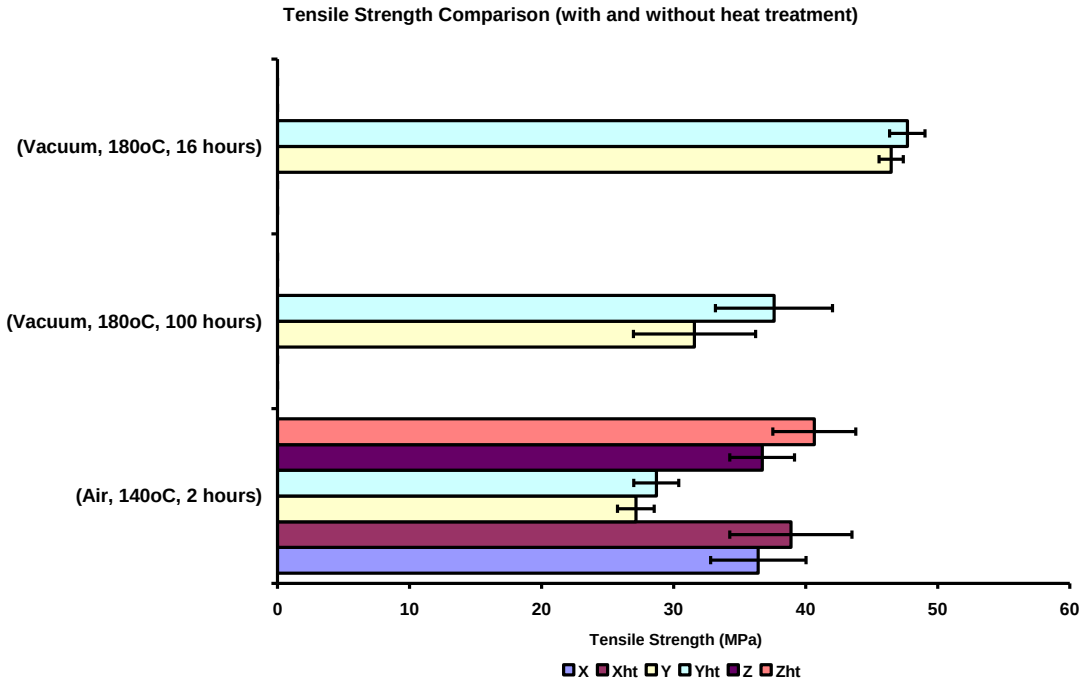

Figure 5-26 Summaries of test results: average tensile strength with and without heat treatment. The X, Y and Z indicate fabrication orientation. The suffix ht indicates heat treatment. Error bars are 95% confidence interval

The overall conclusion from figure 5-26 is that none of the heat treatment regimes has significantly increased the tensile strength. ANOVA also indicated that the differences in average tensile strength with and without heat treatment for all heat treatment conducted were not significant effect, with all p values greater than 0.05.

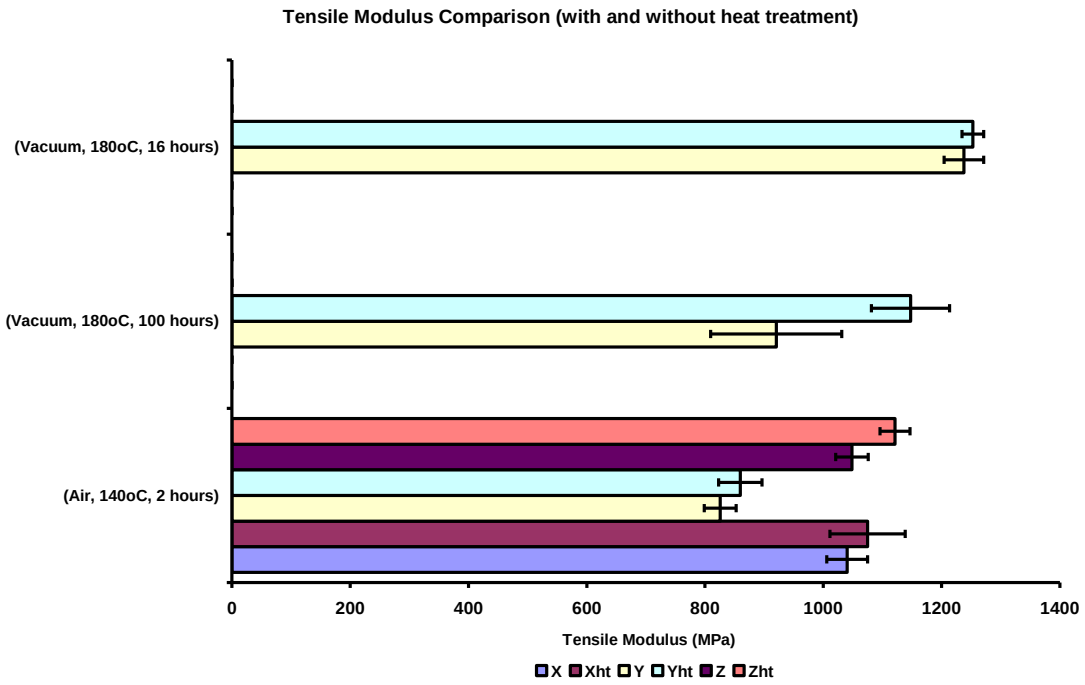

Figure 5-27 Summaries of test results: average tensile modulus with and without heat treatment. The X, Y and Z indicate fabrication orientation. The suffix ht indicates heat treatment. Error bars are 95% confidence interval

From Figure 5-27 we can conclude that the effect of the heat treatment on tensile modulus was mixed, with significant improvements in two out of five comparisons. This was confirmed by ANOVA for a *p*-value of 0.05.

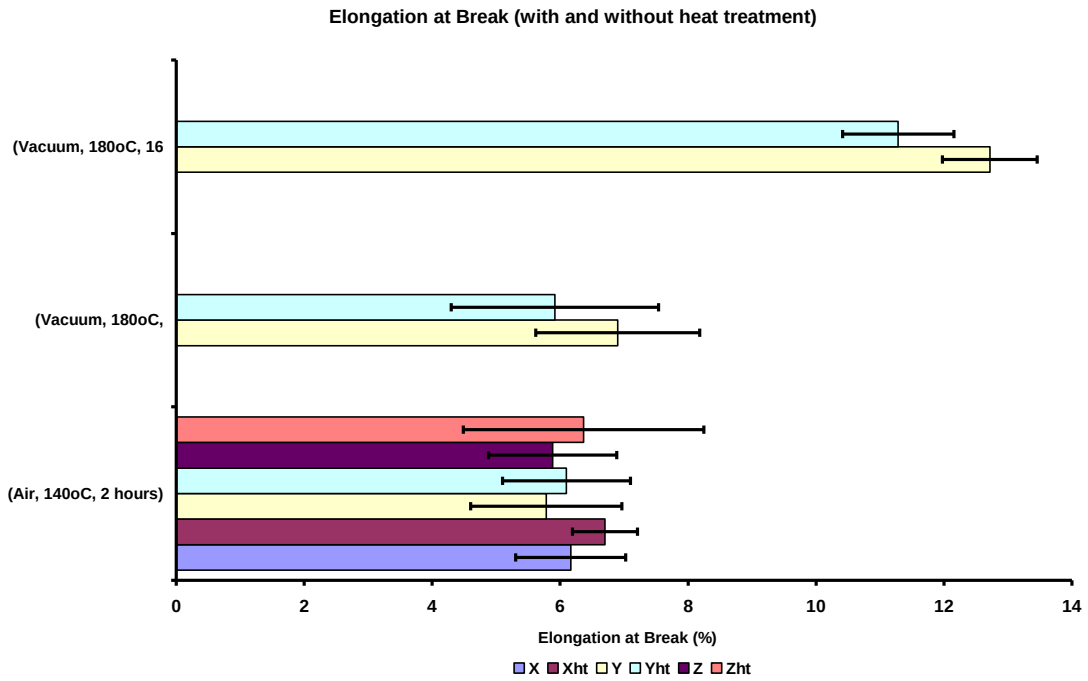

Figure 5-28 Summaries of test results: average elongation at break with and without heat treatment. The X, Y and Z indicate fabrication orientation. The suffix ht indicates heat treatment. Error bars are 95% confidence interval

From figure 5-28, it can be seen that the overall conclusion that none of the heat treatment regimes has significantly effects on elongation at break. This observation is also confirmed by ANOVA for a *p*-value of 0.05.

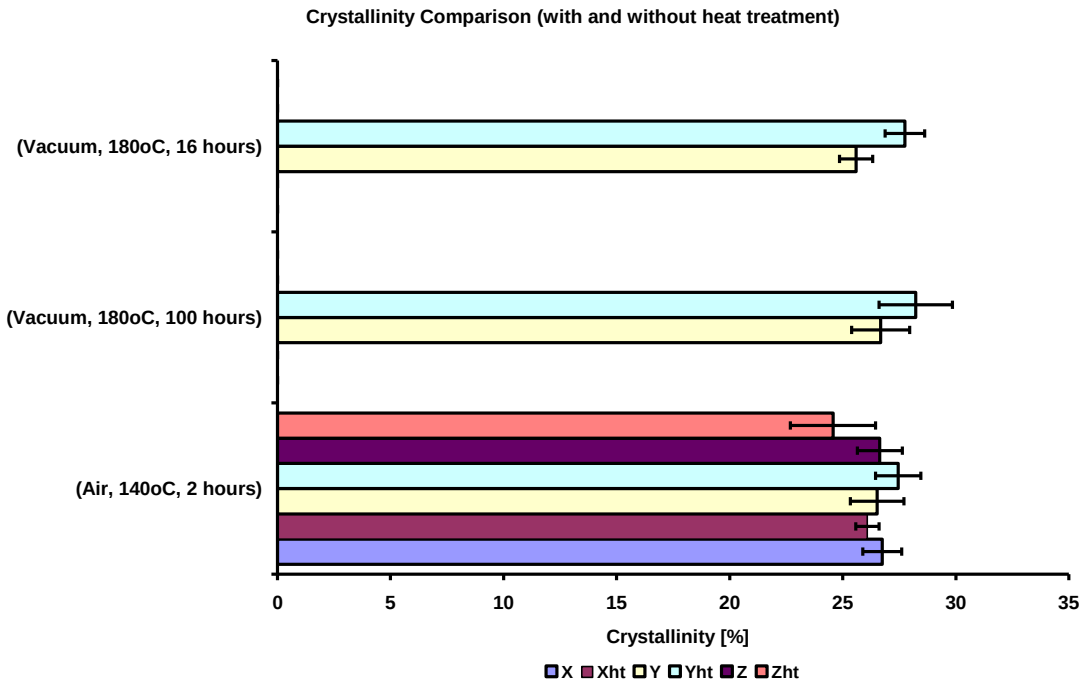

Figure 5-29 Summaries of test results: average crystallinity with and without heat treatment. The X, Y and Z indicate fabrication orientation. The suffix ht indicates heat treatment. Error bars are 95% confidence interval

From Figure 5-29 it can be seen that the effect of heat treatment on degree of cristallinity is small and was only significant in one comparison. ANOVA confirmed this.

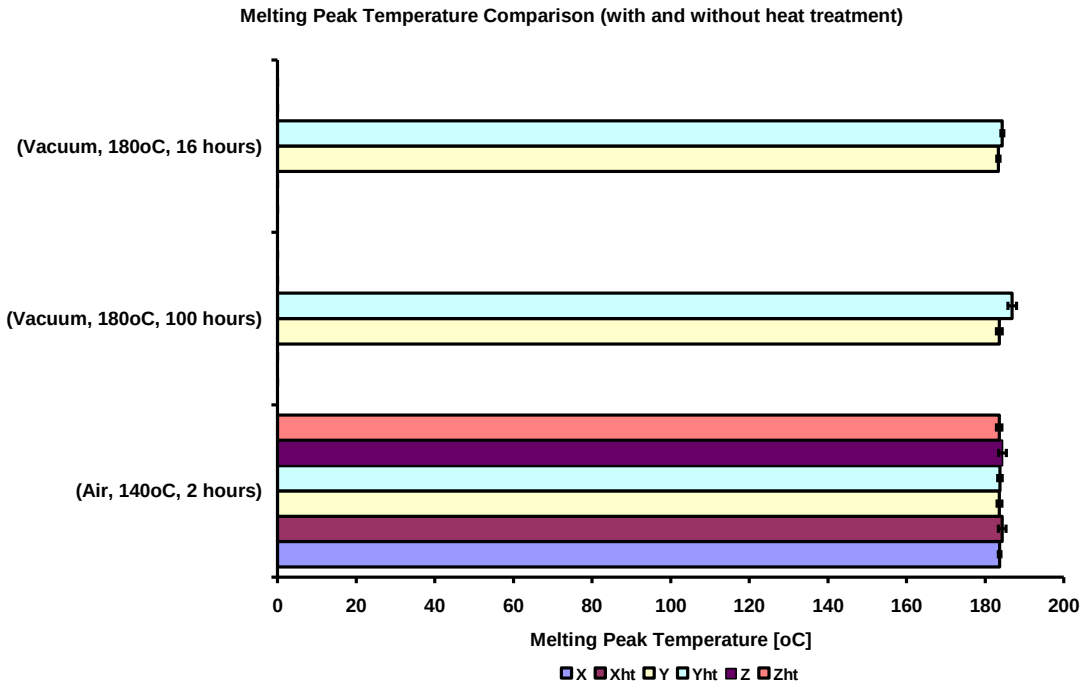

Figure 5-30 Summaries of test results: average melting peak temperature with and without heat treatment. The X, Y and Z indicate fabrication orientation. The suffix ht indicates heat treatment. Error bars are 95% confidence interval

Figure 5-30 demonstrates the melting peak temperature value of samples that heat treated and non-heat treated samples. The effect is small, and significant in two of five comparisons. This observation is also supported by ANOVA for a *p*-value is of 0.05.

From Figure 5-26 to 5-30 shown that heat treatment in air has generally been established to have an insignificant effect on the mechanical properties of the specimens; therefore there was no difference in the degree of crystallinity between specimens with or without heat treatment. Moreover, the melting peak temperatures were also similar. Although some small increases overall were shown between heat treated and non-heat treated components, but these were not statistically significant. It is also clear that the heat treatment in air has not had any impact on the anisotropy present in the samples. This contrasts with the results from Zarringhalam and Hopkinson [2003].

This condition may be caused by the lower amount of heat melting in the air environment, which was not enough to completely melt the particles, and to improve the bonding between them. This did not show a different result when compared with and without heat treatment of the specimens. This is also confirmed by observation of

the microstructure of the specimens, which were heat treated and non-heat treated (Figure 5-10).

Heat treatment in vacuum with 16 hours holding time and at 180^0C heating temperature shows that there was also no improvement in all aspects involving tensile strength, tensile modulus and elongation at break, even though there were slight differences, but not at a 95% confidence interval. However, there was a significant difference with the degree of crystallinity and melting peak temperature although the increase was small. This is because, there is a possibility that the initial characteristics of the fully sintered samples were already high prior to heat treatment and there was no impact from further heat treatment.

However, when heat treatment is carried out in a vacuum, particularly when the samples were heat treated with 100 hours holding time; the modulus and melting peak temperature improved as a result of increased crystallinity. But not the tensile strength and elongation at break even though the values increased and decreased, respectively. These results are comparable with those obtained in previous work [Scobbo and Hwang, 1994; Chang et al., 1998; Ramazani and Mousavi, 2005].

The observation of microstructures of the specimens with and without heat treatment in the vacuum environment shows very similar results compared to the microstructure heat treated in the air environment. These figures (Figures 5-10 and 5-19), explain that even though the amount of heat melting in the vacuum is higher than the heat melting in the air environment, but the results still show that the particles did not bond effectively.

From the results of the experiment conducted, it demonstrates that the mechanical properties and thermal characteristics of SLS material are different for each orientation of fabrication (in air heat treatment and in vacuum heat treatment). This condition is caused related to the particular characteristics of SLS material. These differences may be due to the fact that they are produced at different times, and whether the same machine and material were used. As a result, in this research study, each different experimental work used for fabrication of the specimens was produced from the same batch as a control of material properties in order to be fairly compared.

Tables 5-4 to 5-6, 5-12 and 5-19 (distortion performances) show that even though the position of placement of the specimens in furnace was changed, the dimensions of all samples did not change. These conditions confirmed that the position of the product did not influence the distortion performance. This situation

means that using heat treatment to improve mechanical properties and thermal characteristics has no relative impact on the geometry of the parts.

In vacuum heat treatment, the specimens used were built in Y orientation only. This condition has some impact on mechanical properties and thermal characteristics but not crystalinity, as compared to X and Z orientations. In addition, the position of building specimen in building area was another factor that affected the characteristics. Furthermore, the setting up of building parameters can possibly influence the results.

From all the results, the comparison of the values of tensile strength and tensile modulus were bigger when obtained from a vacuum heat treatment rather than the results in air heat treatment. This is because of the higher amount of energy absorbed (heat melting) when it occurs in vacuum heat treatment. Another possibility is that, reaction in vacuum condition causes the polymer chain to be easily released as compared to in air environment. In addition, heat treatment in air with higher temperature and longer time has an effect on degradation and oxidation, as shown in Figure 5-11.

The values of crystallinity and heat melting for specimens in X, Y and Z orientation in air heat treatment are different, in which the highest values is in Z orientation, whereas the lowest is in X orientation. This condition shows that in Z orientation, more energy (melting heat) was used to melt the particles in order for more bonding to form, which can improve the mechanical properties. This condition can be confirmed by observation of the tensile strength and modulus of Z, which is the highest as compared to the tensile strength and modulus of X and Y orientations.

Heat treatment can provide more absorption energy and time due to dependent phenomena to get equilibrium condition. As compared to heat treatment in air environment, heat treatment in vacuum environment can provide more energy absorption and can avoid / eliminate oxidative degradation. Thermal/residual stress that occurred during fast temperature in cooling and crystallisation, stress relaxation phenomena, re-orientation of macromolecules can be removed which was completed during cooling in machine process [Ramazani and Mousavi, 2005].

Compare to the previous results in chapter 4 with the results in chapter 5, in the first set of results; the tensile strength in the Y-direction is greater than that in the Z- and X-directions. But in the second and third set of results, the tensile strength in the Y-direction is lower than that in the X- and Z-direction.

This is thought to be the result of different densities of the build material, as confirmed by Ho et al [1999] the strength of sintered part is closely related to the density. As stated on page 95, chapter 4, in the Y-direction, a short scan vector causes higher density, which gives the higher tensile strength. The shorter scan vectors can offer uniform temperatures in sintering [Gibson and Shi, 1997].

The laser power plays the role of energy density, which means that when laser power is higher it would give the higher energy density. When higher energy density was produced, the powder fused thoroughly which allowed a more dense structure to be built. However, when lower laser power was used, there is a lower energy density and therefore there was not enough energy to melt the powder particle to create a better bonding.

Therefore, in the first set of results, the values show that there was enough laser energy to melt the particles and make it bond better. The lower values in the second and third set of results might be caused by insufficient laser power. The fracture tends to occur between the polymer particles, when specimens built under a low energy density [Ho et al, 1999].

For instance, the ultimate tensile strength results on page 100 are very different from the earlier results. The Y values were much smaller than those in the X and Z directions. As reported in heat treatment in the air with a temperature of 140^{o}C for 2 hours in chapter 5, the Y value for tensile strength and tensile modulus was the lowest compared to X and Z direction, and also the lowest compared to the results in chapter 4. This might be because of insufficient laser power when setting up the machine, due to the inaccurate default power settings. With limited laser power, it was not high enough to melt the particle completely and the limited fusion of the particle powder resulted in weak bonding.

The same trend, on page 111, the tensile modulus in the Y-direction was reported as being 920.4MPa, which was very different from the values of 1018 and from 825 reported earlier in the thesis. This means that there was also the variation in the tensile modulus. This also might be because of insufficient laser power when setting up the machine, due to the faulty default power settings.

In addition, all these variations in the results is due to the test being done of different specimens, which were produced from different batch of production with different quality of the material used [Gibson and Shi, 1997; Zarringhalam, 2007]. During produce, the samples are often mixed with used powder as well as virgin

powder. However, it is unknown which material contained recycled powder and how many times that powder has been used. The quality of the component is reduced when recycled powder is used during production; particularly when the recycled powder has been used for a number of times [Gornet, T.J., et al, 2002].

It was not anticipated that the values of tensile strength and tensile modulus in the Y orientation would be the lowest when compared to X and Z in the tests of heat treatment in air and in vacuum atmosphere. A comparison of the results (in Figures 4-2 and 4-4 and Figures 5-3 and 5-4) would suggest that the Y orientation specimens used in the chapter 5 were flawed in some way, meaning that the results in chapter 5 for these specimens should not be considered representative.

However, since the purpose of the experiment was to investigate the influence of heat treatment, the result of the sample can still be used as part of the study.

It is of note that no special constraints were applied in this work to reduce inconsistency. A mixture of old and new powder was used in fabricating specimens, and all areas of the powder bed were used to position specimens, whilst they were being built. Work by Zarringhalam and others [Gibson and Shi, 1997; Zarringhalam, 2007] has shown that this can reduce variability; however, such strategies were not considered in this work as they were thought to represent unreasonable constraints for the typical user.

CHAPTER 6. HEAT TREATMENT AND MECHANICAL PROPERTIES OF CLOSED AND OPEN HOLLOW STRUCTURES

6.1 Introduction

This chapter describes the effect of outline/cross-section thickness on properties of laser sintered hollowed parts. In particular, their impacts on the material's mechanical properties of closed and opened end hollow structure, and their thermal properties. Moreover, an in depth description of the impact of heat treatment, on different thicknesses of laser sintered parts of closed hollow structure.

The purpose of performing this experiment was to investigate if any changes of mechanical properties when their crystallinity increases after heat treatment as a post process. This observation was conducted through different geometry, particularly on different outline/cross-section thickness.

In addition, in Section 6.6 reports the scanning strategy studies that was applied to improve the mechanical properties of closed hollow structure on different thicknesses. The methodology applied in this chapter is as described in Section 6.2 and Section 6.3 for samples preparation and equipment used. All characterisations, tests, procedures and results are reported and at the end of the chapter, a summary and brief discussion is presented.

6.2 Specimens Preparation and Material

To observe the impact of different section thickness on the mechanical and thermal properties of closed and opened hollow structure, the tensile test specimens were produced with hollow structure in different section thickness and solid specimens. In addition, a similar design of specimens of closed hollow structure was also produced to observe the effect of heat treatment on their mechanical and thermal characteristics.

All specimens were produced using the SLS Sinterstation Vanguard SLS at Leeds University, as described in section 3.2. Basically, tensile test specimens were built with a similar design of specimen as described in section 3.3. However, to achieve one of the objectives of this research, the samples were then modified with different part geometry. Hollow structure with different section thickness 1mm, 2mm and 3mm were used.

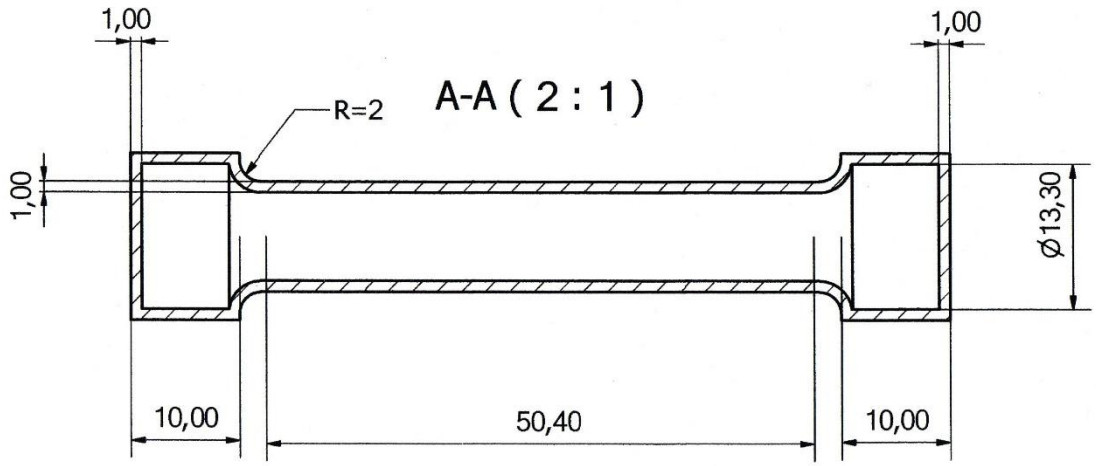

(a)

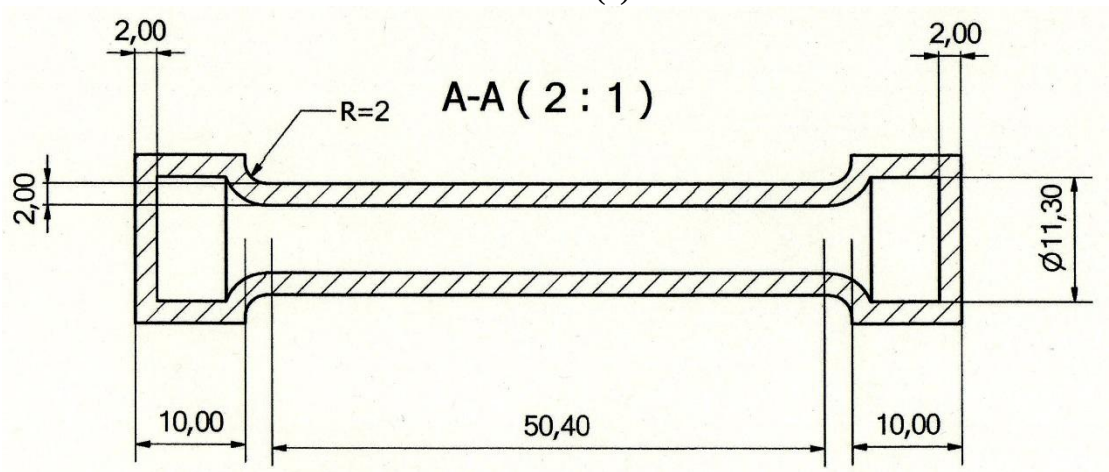

(b)

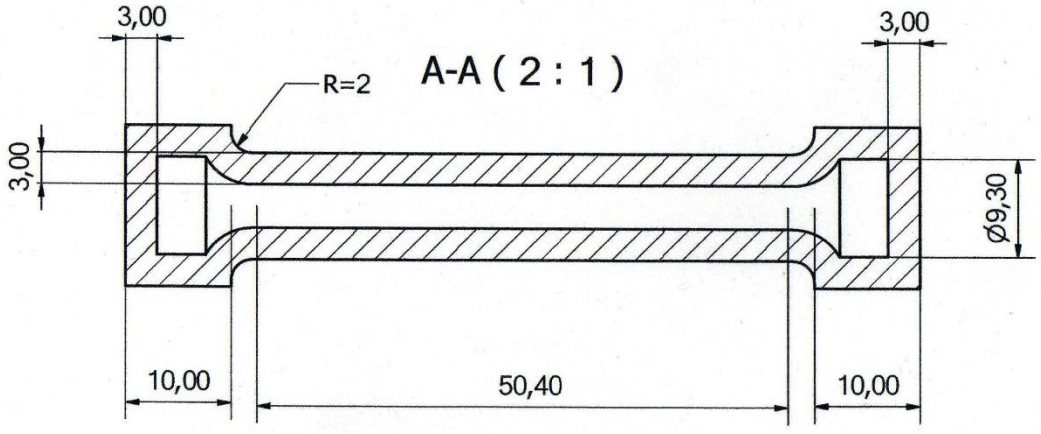

(c)

Figure 6-1 Tensile test specimens drawing with shell and closed hollow structure with different section thickness (a) 1mm, (b) 2mm and (c) 3mm

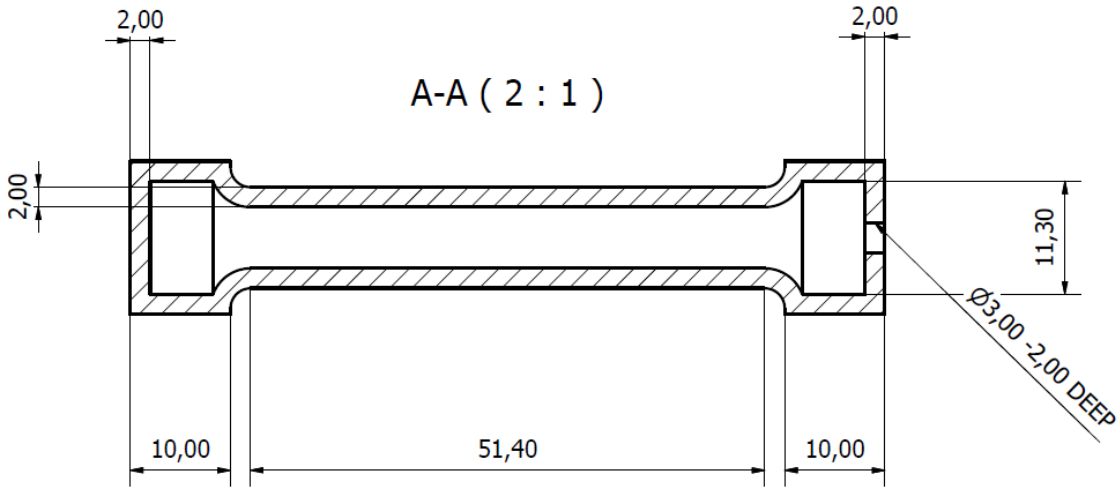

Figure 6-2 Tensile test specimens drawing with shell and open hollow structure with 2mm section thickness

Figure 6-1 showed the technical drawing of closed hollow structure, while Figure 6-2 for opened hollow with a 2mm section thickness. The closed hollow structure specimen contains un-sintered material trapped inside the hollow shell, whereas the opened end hollow structure is the specimen without un-sintered material; the un-sintered material is removed from inside the specimen after completely built from SLS machine.

For comparison, the similar design of solid specimens as control specimens, as reported in previous chapters (chapter 4 and 5); were also manufactured from this same batch of material to observe any changes on the properties between the solid and the hollow specimens. All these specimens were produced in the same batch as to avoid and minimise any differences that will affect their properties in order to maintain the accuracy (Zarringhalam et al, 2006).

For these studies, twelve specimens were produced for each of the 1mm, 2mm, 3mm section thickness of closed hollow structure and solid section, respectively. Six of the specimens with individual different section thickness and solid were used for the analysis of the impact of section thickness on mechanical and thermal characteristics and also used as a reference of non-heat treated specimens. The other six specimens with individual different section thickness and solid were used for analysis of the impact of non-heat treatment and heat treatment on the different areas in terms of mechanical and thermal properties. Moreover, an additional six specimens of 2mm section thickness of opened hollow structure (Figure 6-2) were fabricated for investigation of the effect of closed and opened hollow structure on their tensile

properties. This was produced from a different batch. The same Nylon 12 material was used to produce all the 54 specimens using the default setting process parameters and default fill scanning strategy, as described in section 3.2.

Due to the hollow geometry of the specimens as shown in Figure 6-1, the specimens have two sections or areas. One section is sintered by the laser during sintering process while the other section consists of trapped un-sintered powder in the hollow section of the specimens. This is because the un-sintered powders were entrapped in the shell hollow of the specimens.

All of the designed specimens were then placed in the building envelope of the SLS machine as shown in Figure 6-3 and were produced using default setting with built direction along the Y-axis orientation.

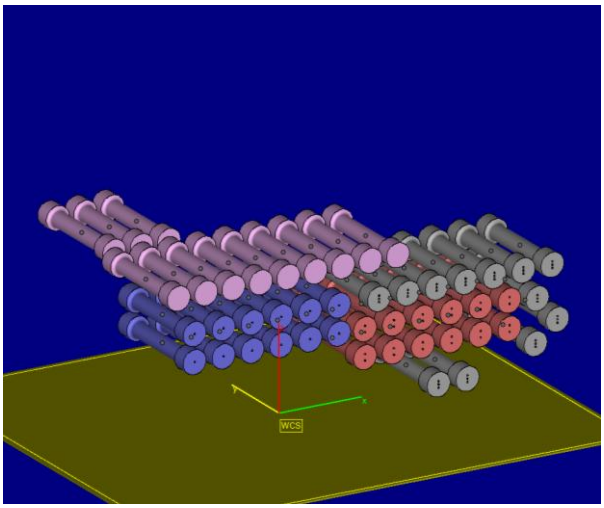

Figure 6-3 Specimens position and orientation in the Vanguard SLS machine

6.3 Equipments, Experimental Work and Procedures

The same experimental work and procedures as described in chapter 3 were also used in this study. Universal testing machine was used to carry out tensile tests and DSC equipment was used to measure the crystallinity and melting peak temperature. In addition, the morphology/microstructure of the specimens was observed using Scanning Electron Microscope (SEM).

Tensile tests were carried out as described in section 3.4. From those tests, the behaviour of the layer material on different section thickness and solid specimens was determined. Tensile tests were carried out on one built orientation; Y-axis only. As mentioned in chapter 5, Y-orientation of specimens was used to avoid the repetition of the tests, reduce build time and also reduce experimental cost. Moreover, if

mechanical properties can be improved for specimens produced in a single orientation, then the study can be extended further to other built orientation of specimens.

Each individual different section thickness and solid was tested for six samples to evaluate tensile properties, as described in chapter 4. The values of stress and strain were calculated using equation 3.1 and 3.2. The area of the sintered section was determined by using the original formula for the determining the area of solid round bar. To calculate the area of the solid round bar, the outer diameter (d_o) is squared, multiplied by phi (π) and then divided by four ($\pi/4*d^2$). However, to work out the area of the hollow specimen, the formula has been modified by subtracting the inner diameter (d_i) from the outer diameter (d_o) of the hollow structure specimen. Therefore, the formula to find out the measurement of the area of hollow specimen is = $\pi/4*(d_o^2-d_i^2)$. Figure 6-4 shows the cross section of hollow specimen.

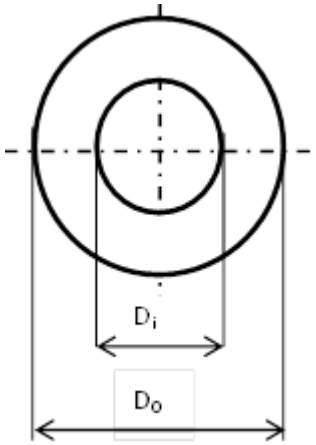

Figure 6-4 Cross section of hollow specimen

The measurement of the outer diameter for solid and hollow structure specimens was measured before the specimen were tested, meanwhile for the inner diameter for specimens with hollow structure; it were measured (approximately) after the specimens broke. The measurement was conducted three times at three different positions and then an average was calculated.

The mechanical and thermal properties results were then analysed using statistical analysis tool (Minitab software), in which the p value, average and confidence interval can be determined, as described in chapter 3 section 3.7.

6.4 Impact of Section Thickness

6.4.1 Tensile Test Results for Non-heat treated Specimens

Stress strain graphs of all the specimens for 1mm, 2mm, 3mm, and solid are shown in Figure 6-5 and Figure 6-6. In addition, Figure 6-7 shows the specimen of each section thickness after tensile test. The tensile test results for different thickness of section, closed and opened hollow structure and solid section in non-heat treated specimens are shown in Figure 6-8 to Figure 6-13.

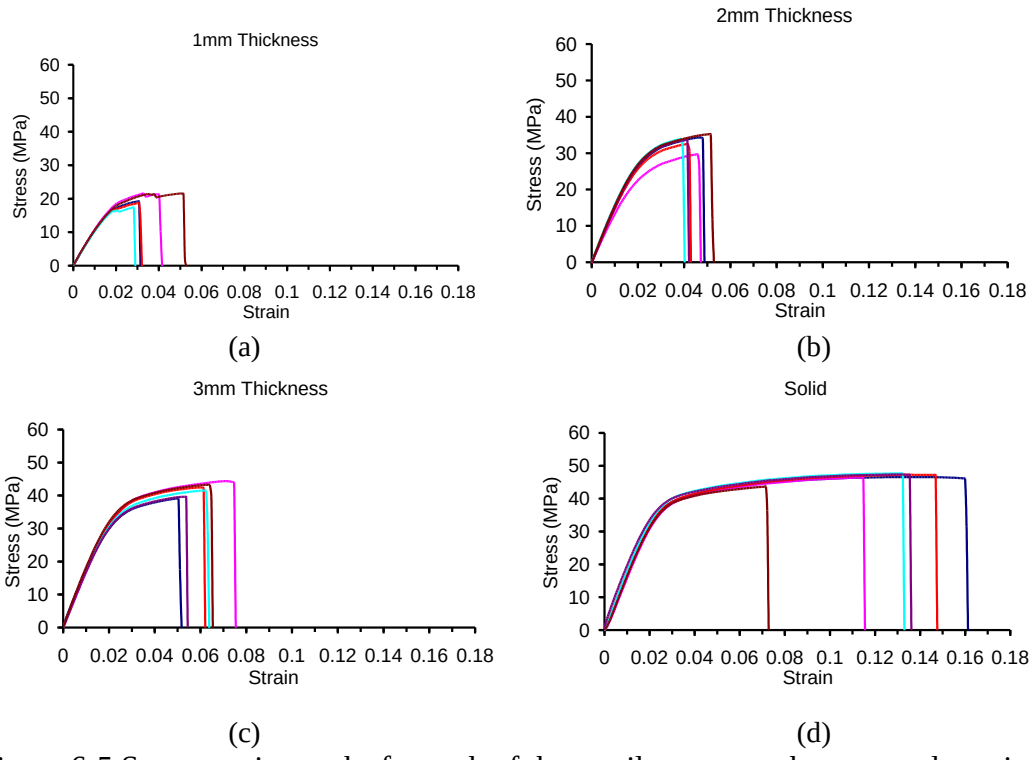

Figure 6-5 Stress-strain graphs for each of the tensile tests non-heat treated specimens for closed hollow with section thickness (a) 1mm, (b) 2mm, (c) 3mm and (d) solid

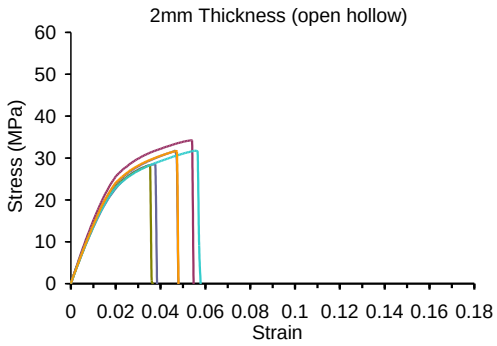

Figure 6-6 Stress-strain graphs for each of the tensile tests non-heat treated specimens for open hollow with 2mm section thickness

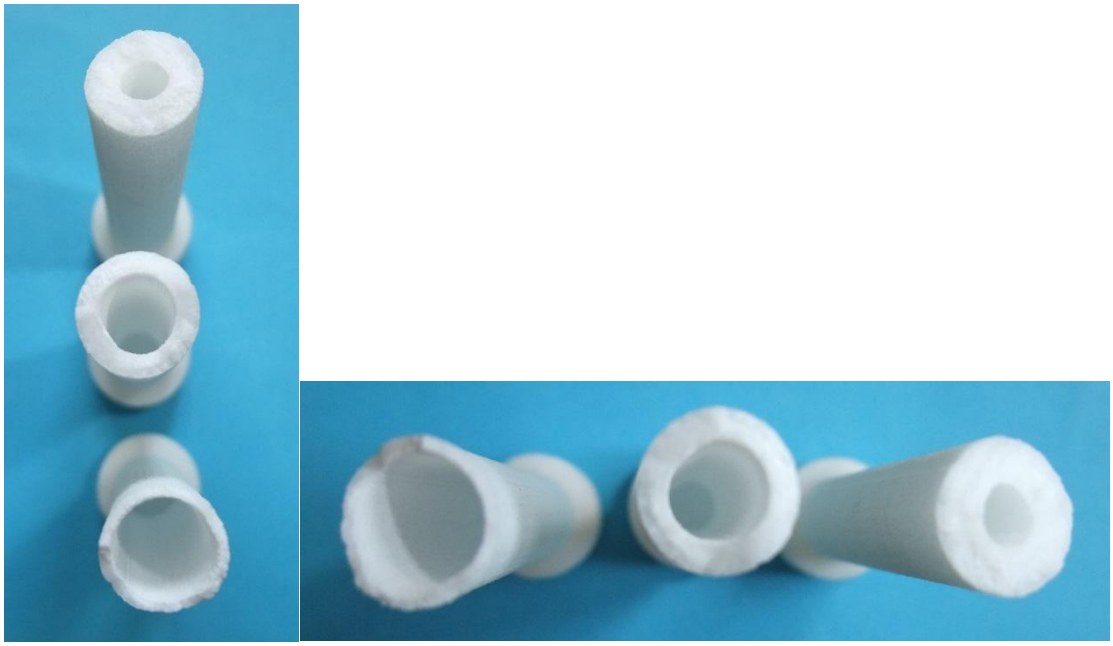

Figure 6-7 Tensile test specimens (after testing) for closed hollow structure with 1mm, 2mm and 3 mm section thickness

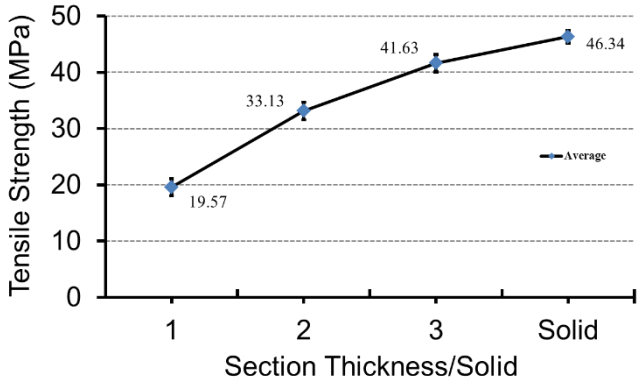

Figure 6-8 Tensile strength result of different section thickness of closed hollow and solid non-heat treated specimens. Error bars are at 95% confidence interval

Based on Figure 6-5 and Figure 6-6 all the specimens displayed a linear elastic behaviour within the same region of strain values between 0.0 and 0.02. It can be observed Figure 6-8 that the smaller thickness section created a lower average tensile strength and the solid specimens promoted the highest average tensile strength. The ANOVA confirms that the average tensile strength on each different section thickness and solid specimens increased significantly, in which the p value was smaller than 0.05. This indication confirmed that section thickness have effect on average tensile strength significantly.

The tensile modulus for each specimen with different wall thickness and solid samples were then determined from the initial slope of the straight line on the stress-strain curves as explained in section 3.5.1.b. Tensile modulus results for all specimens then are shown in Figure 6-9.

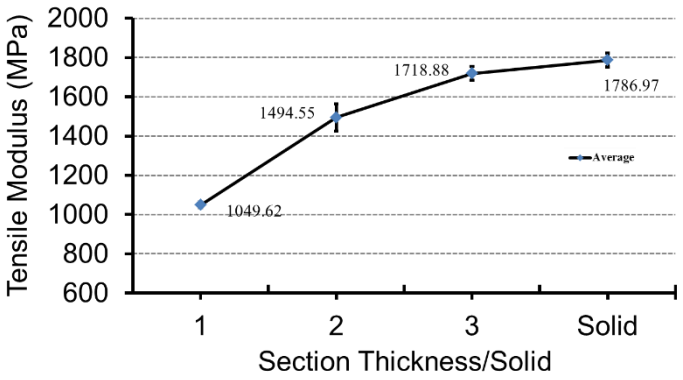

Figure 6-9 Tensile modulus result of different section thickness of closed hollow and solid non-heat treated specimens. Error bars are at 95% confidence interval

It was clear that the solid specimens promoted the highest average tensile modulus, while the smaller section thickness specimens created a lower average tensile modulus, in which the smallest average tensile modulus occurred when the smallest thickness of 1mm section specimens were used. The ANOVA confirmed that the p value was smaller than 0.05 when the average tensile modulus on each different section thickness and solid specimens increased significantly. This indication showed that the outline/cross-section thickness and solid have an effect on average tensile modulus significantly.

The elongation at break for each specimen with different section thickness and solid were then determined as described in section 3.5.1.b. Elongation at break results for all specimens are illustrated in Figure 6-10.

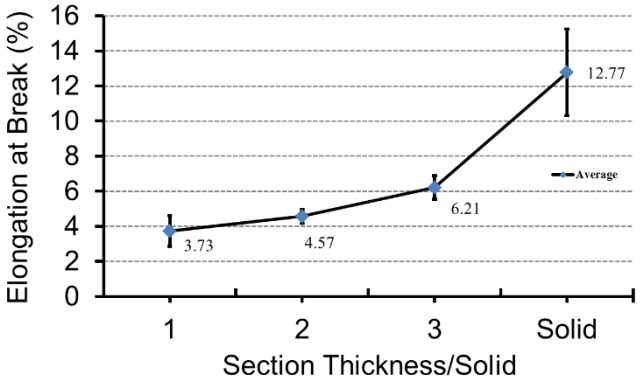

Figure 6-10 Elongation at break results of different section thickness of closed hollow and solid non-heat treated specimens. Error bars are at 95% confidence interval

The smaller the sections thickness, the lower the average elongation at break obtained. While the solid specimens promoted highest average elongation at break. However, for section thickness 1mm and 2mm, there was not significantly difference, whereas for the 3mm section thickness and solid, it was significantly different.

The results of tensile properties of opened end hollow structure were obtained and shown in Figure 6-11 to Figure 6-13. As described in previous section 6.2, these result then compare to the closed hollow structure to observe if there is any different impact of closed and opened end hollow structure.

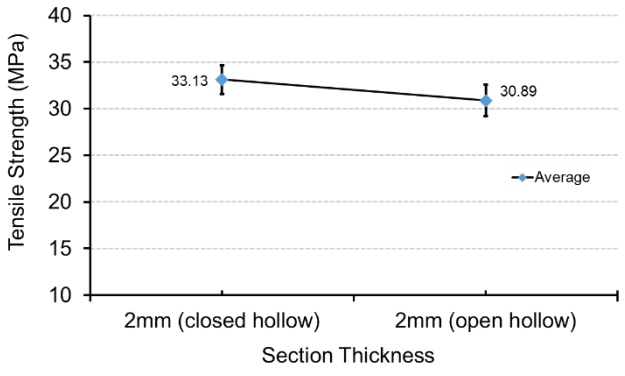

Figure 6-11 Summaries of test results: average tensile strength of closed and open hollow structure specimens. Error bars are at 95% confidence interval

Figure 6-11 illustrates the tensile strength for 2mm section thickness of open hollow specimens. From Figure 6-11 and Figure 6-8 It can be seen that there was no

significant change in the average tensile strength between closed and open hollow 2mm section thickness specimens, as it was also confirmed by ANOVA in which the p value was greater than 0.05.

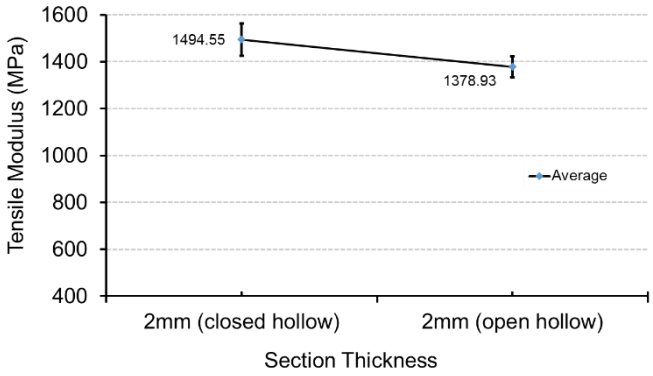

Figure 6-12 Summaries of test results: average tensile modulus of closed and open hollow structure specimens. Error bars are at 95% confidence interval

Figure 6-12 shows the average tensile modulus results of open hollow specimens with 2mm section thickness. From these evidences, it can be observed that there were no significant changes between the average tensile modulus of open hollow specimen and closed specimen. This was confirmed by ANOVA for a p value that was greater than 0.05.

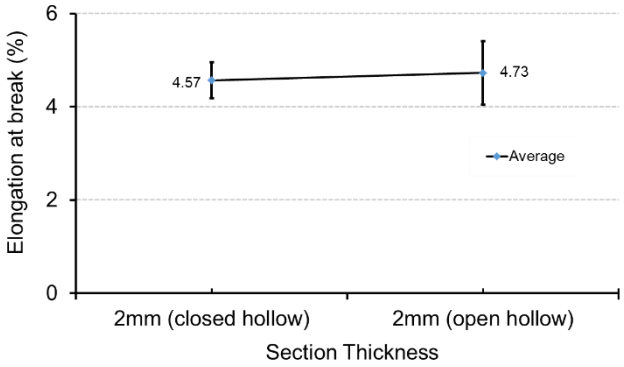

Figure 6-13 Summaries of test results: average elongation at break of closed and open hollow structure specimens. Error bars are at 95% confidence interval

Figure 6-13 shows the average elongation at break of closed and open hollow specimens with 2mm section thickness. it can be seen that there was no changes of elongation at break for open hollow structure, although there were small differences

of average at around 0.16 %, but not significant enough at a 95 % confidence level. The ANOVA confirmed this by showing a p value that was greater than 0.05.

Figure 6-11 to Figure 6-13 show that there were no differences in the tensile properties of the specimens with closed and open hollow structure. Even though there were slight different in average tensile strength by 2.24 MPa, average tensile modulus by 115.62MPa and average elongation at break by 0.16%, but they were not significant at 95% confidence level. Therefore, it can be summarised that whether the structure of the specimen were open or closed hollow, it had no effect on the mechanical characteristics. These differences possibly occurred due to the fact that both specimens of closed and open structure were manufactured in different batch of production, as it was confirmed by Zarringhalam et al. [2006] in their research.

6.4.2 Crystallinity Characterisation Results for Non-heat treated Specimens

Using the same procedure as described in section 3.7, the degree of crystallinity of sintered and un-sintered material from different section thickness specimens and sintered material from solid specimens were determined and all the results are shown in Figure 6-14. All these specimens were non-heat treated specimens.

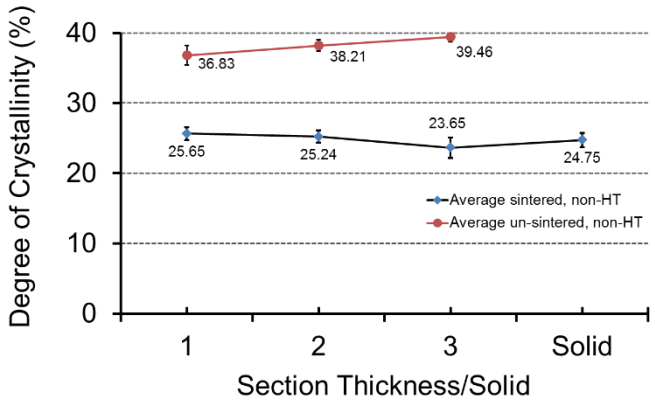

Figure 6-14 Degree of crystallinity of sintered and un-sintered material of non-heat treated specimens with different section thickness and solid. Error bars are at 95% confidence interval

From Figure 6-14 it can be seen that the average degree of crystallinity for sintered material were between the range of 23.65 % and 25.65 % for the all specimens, even though there was slight difference for the specimens with 1mm, 2mm, 3mm section thickness and solid specimens, but the difference was not

significant. Moreover, as it can be observed that the degree of crystallinity for un-sintered material of each specimen in each different section thickness were also not significantly different. However, the average degrees of crystallinity of un-sintered material were higher compared to sintered material. As indicated Figure 6-14, the difference was not significant for each specimen in 1mm, 2mm, 3mm section thickness and solid specimens.

6.4.3 Melting Peak Temperature (T_{peak}) Results for Non-heat treated Specimens

This section describes the impact of crystallinity on melting peak temperature (T_{peak}) of each specimen with different wall thickness and solid, for non-heat treated specimens. This was determined from the DSC plot.

The comparison of melting peak temperatures for sintered and un-sintered material, with different section thickness is illustrated in Figure 6-15.

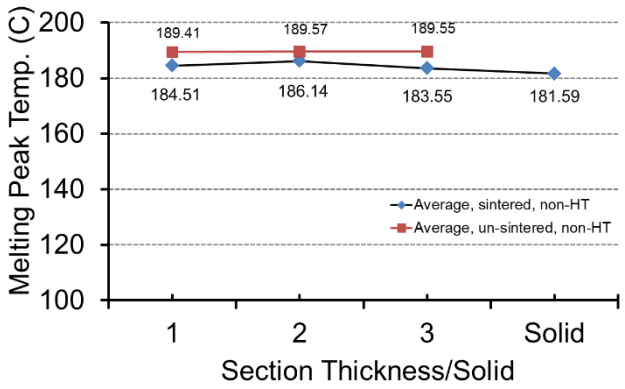

Figure 6-15 Melting peak temperature sintered and un-sintered material of non-heat treated specimens with different wall thickness and solid. Error bars are at 95% confidence interval

Figure 6-15 show that there was no significant change in the value of the peak melting temperature on the different section thickness of the specimens, for un-sintered material, in which the temperature was between 189.41^{o}C to 189.57^{o}C. However, for sintered material, the average melting peak temperature was significantly different for each individual section thickness and solid specimens. The average temperature were 184.51^{o}C, 186.14^{o}C, 183.55^{o}C and 181.59^{o}C for 1mm, 2mm, 3mm section thickness and solid, respectively. It was clear that the melting temperatures for all section thickness and solid were not consistent and did not follow

a specific pattern. Furthermore, by comparing to the melting peak temperature for un-sintered specimens, sintered specimens have lower melting peak temperature.

6.4.4 Morphology and Microstructure for Non-heat treated Specimens

To observe and analyse the morphology of the fabricated parts, a Scanning Electron Microscope (SEM) as described in section 3.8 were used. Figure 6-16 shows the microstructure of selected specimens that were observed by using SEM. In addition, 6-17 illustrates un-sintered material particle grain (without heat treatment).

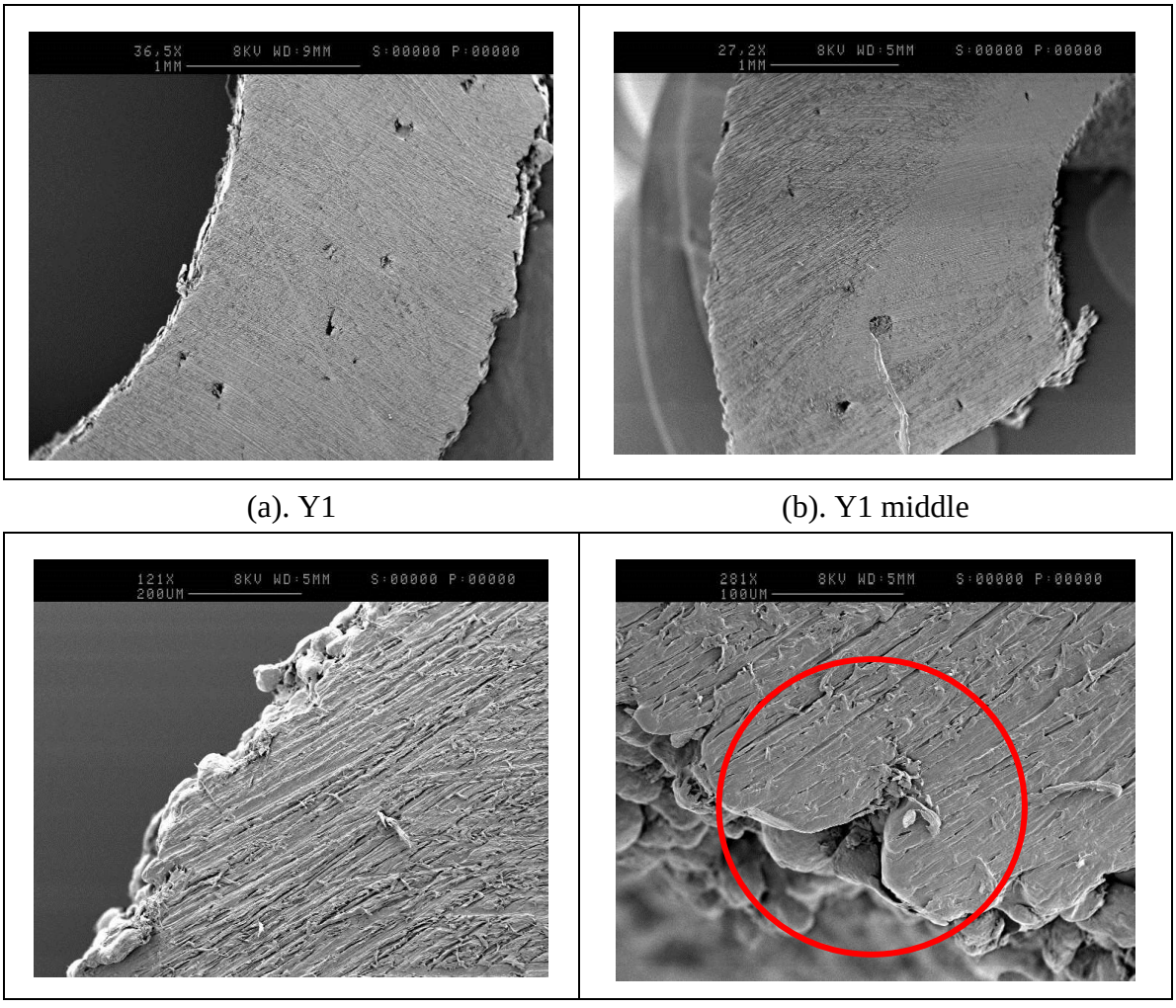

(a). Y1 (b). Y1 middle

(c). Y1 outer edge (d). Y1 inner edge

Figure 6-16 Microstructure samples without heat treatment in vacuum; sample with 3mm section thickness (a) surface cutting, (b) in the middle, (c) outer edge (d) inner edge of specimen

Figure 6-16 (a) and (b) show parts of the surface of specimens made with the default setting of SLS machine. It can be seen that the specimens consists of porous surface, which probably occurred during the sintering process. From Figure (c) and

(d), it can also be seen that the presence of rough surface may be due to ineffective sintering or low degree of powder particle melting during the laser sintering. Furthermore, there was an increase of serration in the surface texture and this was possibly due to the un-sintered particle grain size (d).

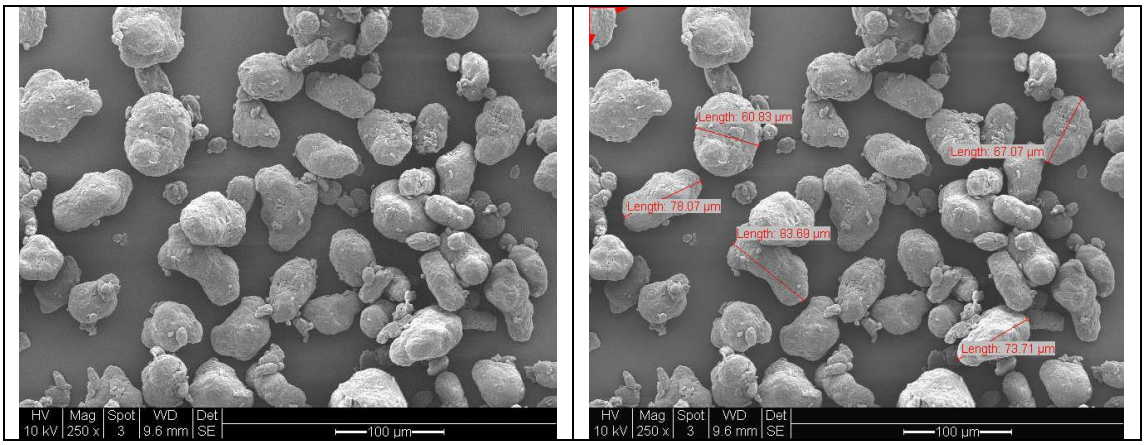

Figure 6-17 Un-sintered material particle grain (without heat treatment)

Figure 6-17 shows the un-sintered particle grain without heat treatment. It can be seen that the un-sintered particle have spherical shapes with diameter of between 60-80micron. Due to the condition of this is un-sintered material, it means that during the SLS process, this particle was not affected by laser and remained like the original powder of Nylon 12. Therefore, the SEM showed that between the particles, there was no bonding amongst each other. However, when compared with the previous Figure 6-16, all particles bonded as a result of laser sintering process.

6.5 Impact of Heat Treatment on Properties of Different Section Thickness

As further experimental work in this research study, impact of heat treatment on mechanical and thermal properties on different wall thickness on closed hollow structure were investigated. The same material Nylon 12 was also used and produced in the same methods as the material used in the non-heat treated specimens. The specimens were then heat treated in vacuum environment by using the same vacuum furnace as described in sub-section 5.5.2. This experimental work was conducted to observe if there was an impact on each individual different section thickness and solid specimens after heat treatment in term of mechanical and thermal properties as compared to non-heat treated specimens.

From the previous studies in Chapter 5, when specimens were heat treated for 2 hours at 140°C and for 16 hours at 180°C there was no significant effect on mechanical and thermal properties as observed. Therefore, in this heat treatment the temperature setting was selected directly at 180°C (near melting point of Nylon 12), for 100 hours with the vacuum level setting at -1018mbar (the maximum capacity of the available vacuum oven).

6.5.1 Tensile Tests Results for Heat treated Specimens

Figure 6-18 shows the plot of stress-strain heat treated specimens for different section thickness and solid. From this Figure, the tensile strengths of these specimens were determined and all the results are shown in Figure 6-19.

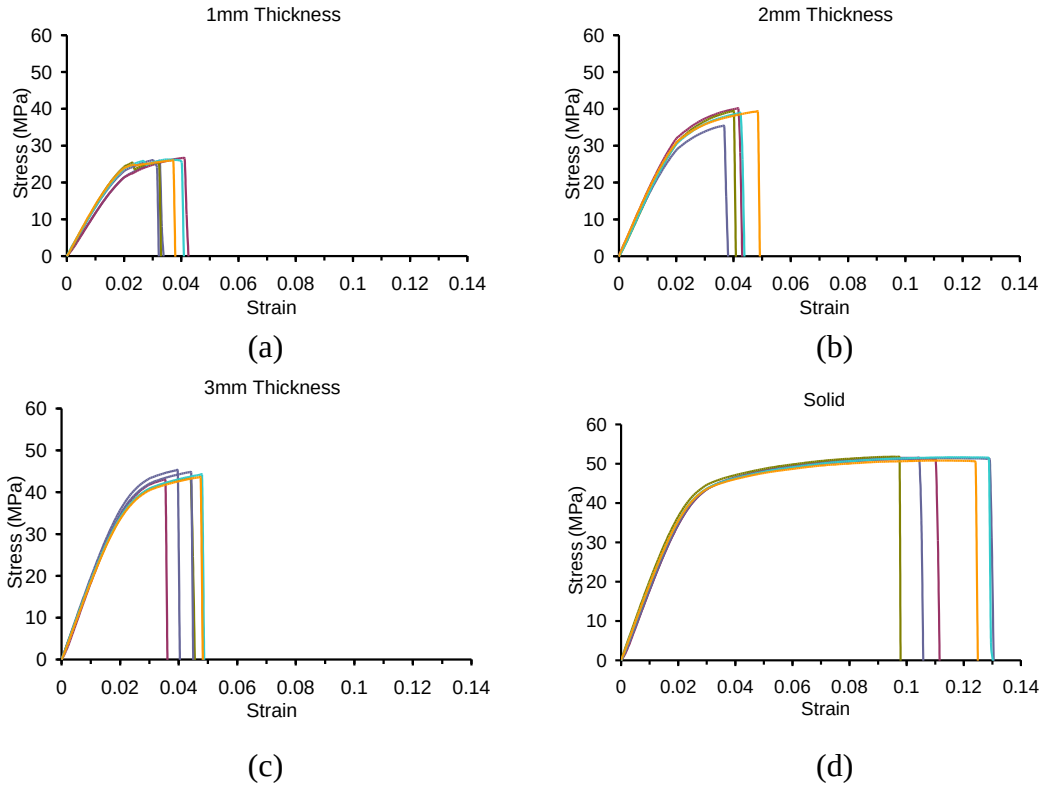

Figure 6-18 Stress-strain plots for each of the tensile tests of heat treated specimens with section thickness, (a) 1mm, (b) 2mm, (c) 3mm and (d) solid

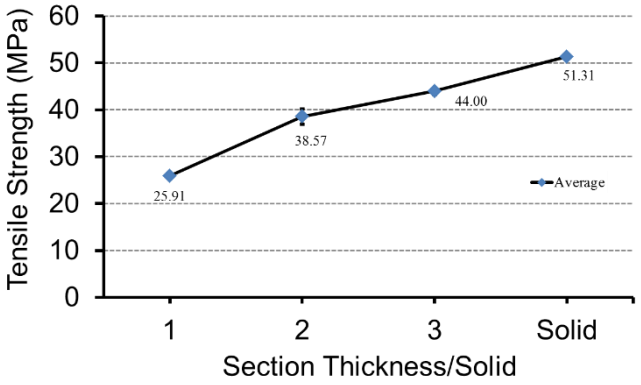

Figure 6-19 Tensile strength results of different section thickness of closed hollow and solid heat treated specimens. Error bars are at 95% confidence interval

Figure 6-19 shows the average of tensile strength obtained from all heat treated specimens. It was clear that the average tensile strength of each different section thickness and solid specimens were significantly different. This observation confirmed that there is a correlation between thickness and tensile strength where tensile strength increases from smallest thickness section to solid. The ANOVA confirmed this with the p value of 0.05.

Tensile modulus values for each individual specimen after heat treatment was determined and the results are summarised Figure 6-20.

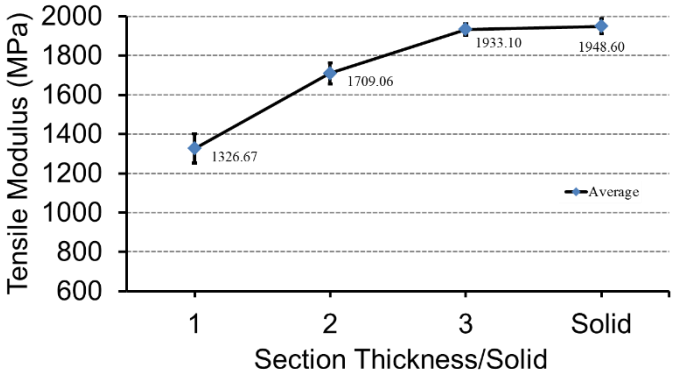

Figure 6-20 Tensile modulus results of different section thickness of closed hollow and solid heat treated specimens. Error bars are at 95% confidence interval.

Figure 6-20 illustrates the average tensile modulus obtained after heat treatment. This observation confirmed again that this a correlation between thickness

and tensile modulus where tensile modulus increases from smallest thickness section to solid. The ANOVA confirmed that the p value was smaller than 0.05.

Elongation at break values for each individual heat treated specimen was determined and the results are summarised in Figure 6-21.

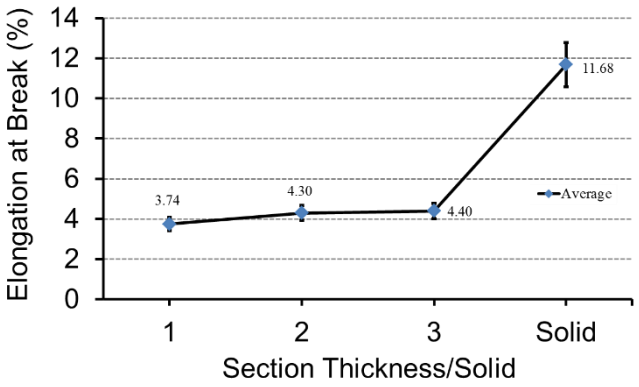

Figure 6-21 Elongation at break results of different section thickness of closed hollow and solid heat treated specimens. Error bars are at 95% confidence interval

Figure 6-21 demonstrates that the average elongation at break for 1mm, 2mm, 3mm section thickness and solid specimens after heat treatment. This indicated that they were not significantly different, even though there were small differences of the distribution elongation at break among them in each individual section thickness. However, compared to 1mm, 2mm and 3mm section thickness, the average elongation at break of solid specimens was 11.68 % increased dramatically.

6.5.2 Crystallinity Characterisation Results for Heat Treated Specimens

Using the same procedure as described in section 3.6, the degree of crystallinity of sintered and un-sintered material of heat treated specimens was determined and all the results are shown in Figure 6-22.

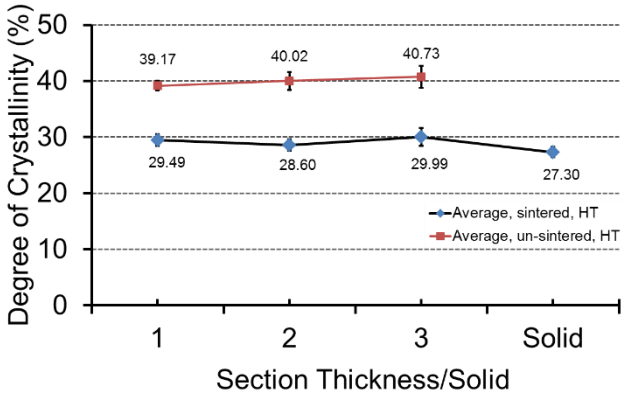

Figure 6-22 Degree of crystallinity of sintered and un-sintered material result of heat treated specimens with different section thickness and solid. Error bars are at 95% confidence interval

It can be seen from Figure 6-22 that the average degree of crystallinity for sintered material were between the ranges of 27.30% and 29.99 %. Even though there was slight differences as illustrated in, but they are not significant. It also shows that the average degree of crystallinity for un-sintered material for all section thickness was also not significantly different. The average degree of crystallinity ranges from 39.17 % to 40.73 %. However, the average degree of crystallinity of un-sintered material is higher than the sintered material for all heat treated specimens.

6.5.3 Melting Peak Temperature (T_{peak}) Results for Heat treated Specimens

The same procedure as described in section 3.7 was used to obtain the values of melting peak temperature (T_{peak}) with and without heat treatment in the vacuum environment. The results are shown in Figure 6-23.

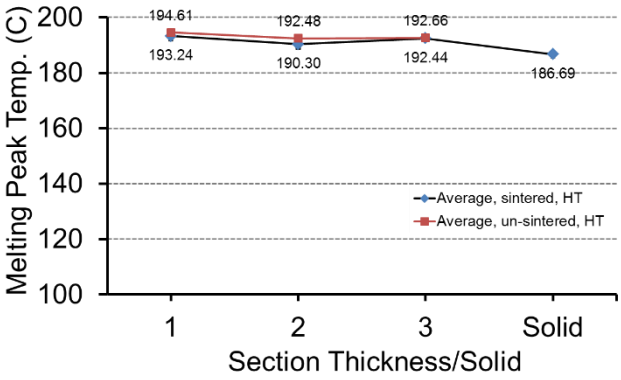

Figure 6-23 Melting peak temperature of sintered and un-sintered material heat treated specimens with different section thickness and solid. Error bars are at 95% confidence interval

Figure 6-23 shows the average melting temperature for sintered and un-sintered material for all heat treated specimens. The average melting peak temperature for sintered material and un-sintered is not significantly different. The average melting temperature for sintered specimens ranges from 186.69 ^{o}C to 193.24 ^{o}C while for un-sintered is from 192.48^{o}C to 194.61^{o}C. The range different constitute less than 5% difference which is not significant.

6.5.4 Morphology and Microstructure for Heat treated Specimens

To observe and analyse microstructure, the same equipment and procedure as described in section 3.8 were used. Figure 6-24 shows the microstructure of some selected specimens after heat treatment in the vacuum environment.

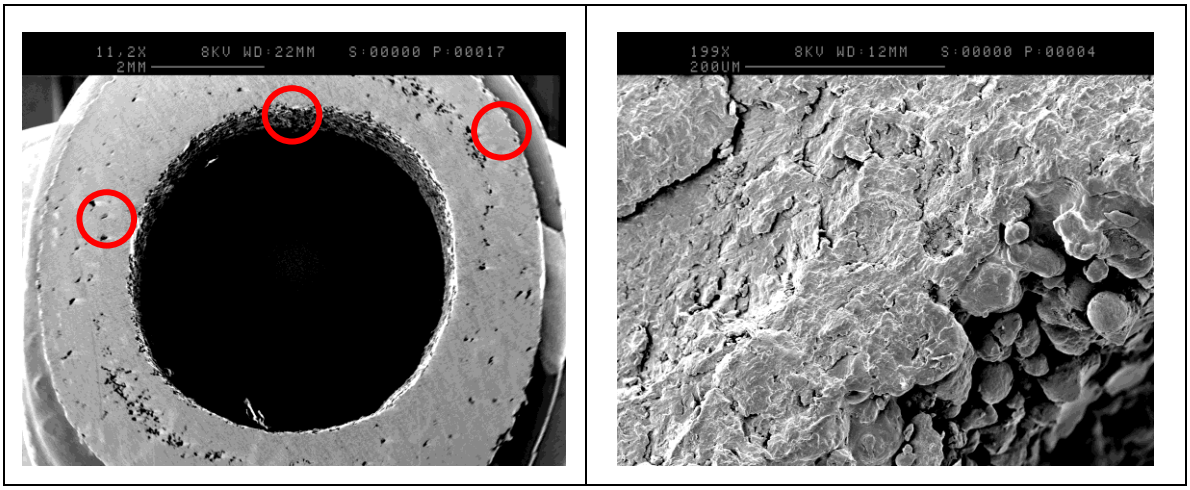

(a). Y3h5 (b). Y3h5-outer edge

(c). Y3h5 inner edge (d). Y3h5 middle

Figure 6-24 Microstructure specimens with heat treatment in vacuum, sample with 3mm section thickness (a) surface cutting; (b) outer edge (c) inner edge (d) in the middle of specimen

Figure 6-24 (a) shows part of the surface of specimens made with default setting on SLS machine, but after being heat treated in a vacuum environment. As it can be seen in the photograph, the porous surface still appeared even though it was heat treated. This probably occurred during the sintering process. From Figure (b) and (c), it can also be seen in the outer and the inner edge of 3mm section thickness specimens that the surface seems to be more solid even though uneven surface texture was still present. Again, the presence of uneven surface texture may be due to ineffective sintering or a low degree of powder particle melting during laser sintering. Even though it was heat treated, there was probably insufficient amount of energy to melt the powder particle and form a smoother surface. Moreover, it was also observed that (d) had similar surface roughness in the middle area to (b) and (c).

6.6 Impact of Scanning Strategy (fill and Outline Scanning) on Mechanical Properties

In this sub-section, the characteristics of mechanical properties of Nylon 12 laser sintered material with different methods of scanning strategy are reported.

Six numbers of the closed hollow specimens with similar design as described in section 6.2 produced in different section thickness (1mm, 2mm and 3mm) and solid using the SLS Vanguard machine. However, in this study, the different setting of outline scanning strategy was applied.

The default process setting for the study in this section is as shown in table 3-1, except the setting for the laser power in outline scanning was altered from the default of 6watt (default) to 41watt. This condition was selected to observe if any impact on mechanical properties if outline laser power similar as fill laser power of 41watt. This was intended to use this outline strategy in built the specimens rather than repeated fill scanning motion again (for secondly or after). Therefore, this laser magnitude was the same as the default setting for laser power of fill scanning. In addition, the fill and outline scanning traced in one motion only following the design of the specimen. The laser scan moved in the same direction as the fill scanning as discussed in the previous chapters (4 and 5) and previous sections (6.4 and 6.5) of this thesis.

The tensile test was then carried out using the same universal testing machine that was also used to examine the mechanical characteristics as reported in the previous chapter 4 and 5, and previous section 6.4 and 6.5 . The mechanical properties of specimens were then measured to analyse whether there was any changes and impact on the different thickness of section and solid.

Figure 6-25 illustrates the scanning path of fill and outline scanning strategy for solid and different section thickness specimens when it was produced.

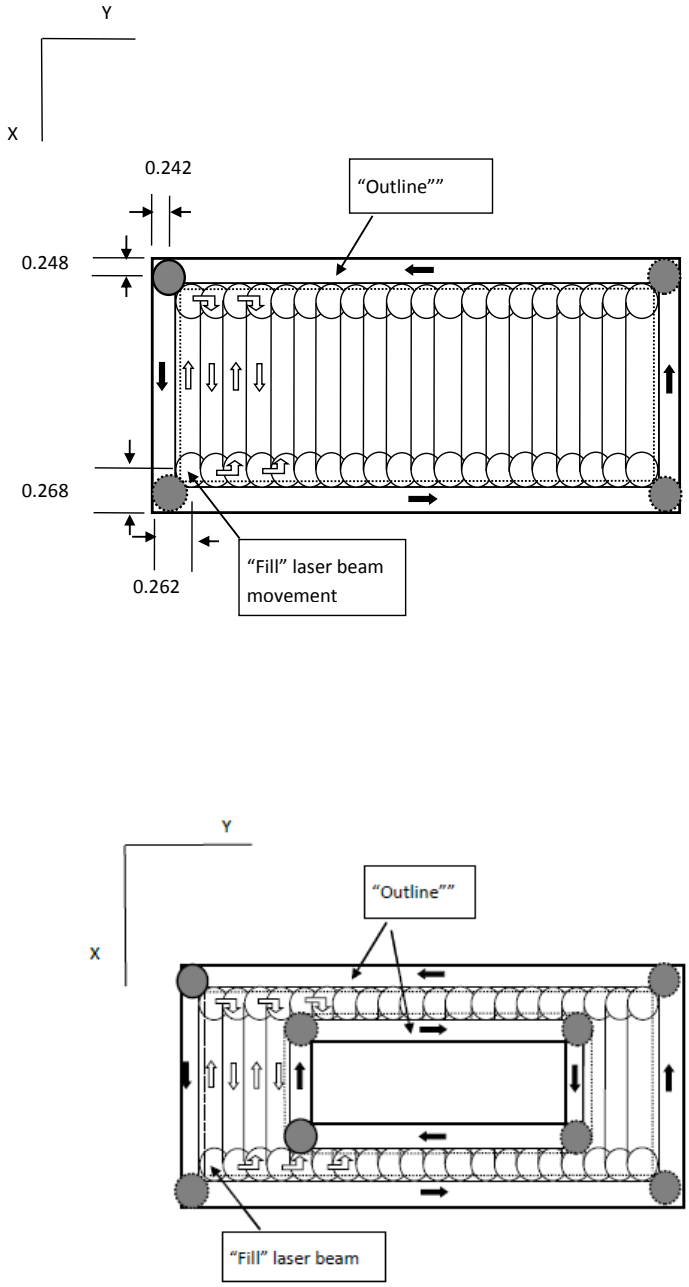

Figure 6-25 Scan path of fill and outline scanning strategy for (a) solid and (b) section thickness specimens

The obtained results from this implementation of different scanning strategy were then compared with the previous results as described in section 6.4 that was built using the default scanning strategy (it was also mentioned as non-heat treated specimens).

6.6.1 Tensile tests results

For specimens with different section thickness 1mm, 2mm, 3mm of closed hollow structure and solid with fill and outline scanning strategy, tensile strengths were determined and all the results are shown in Figure 6-27. Meanwhile Figure 6-26 shows the plot of stress-strain relationship. In addition, the average of tensile modulus and elongation at break is presented in Figure 6-28 and Figure 6-29.

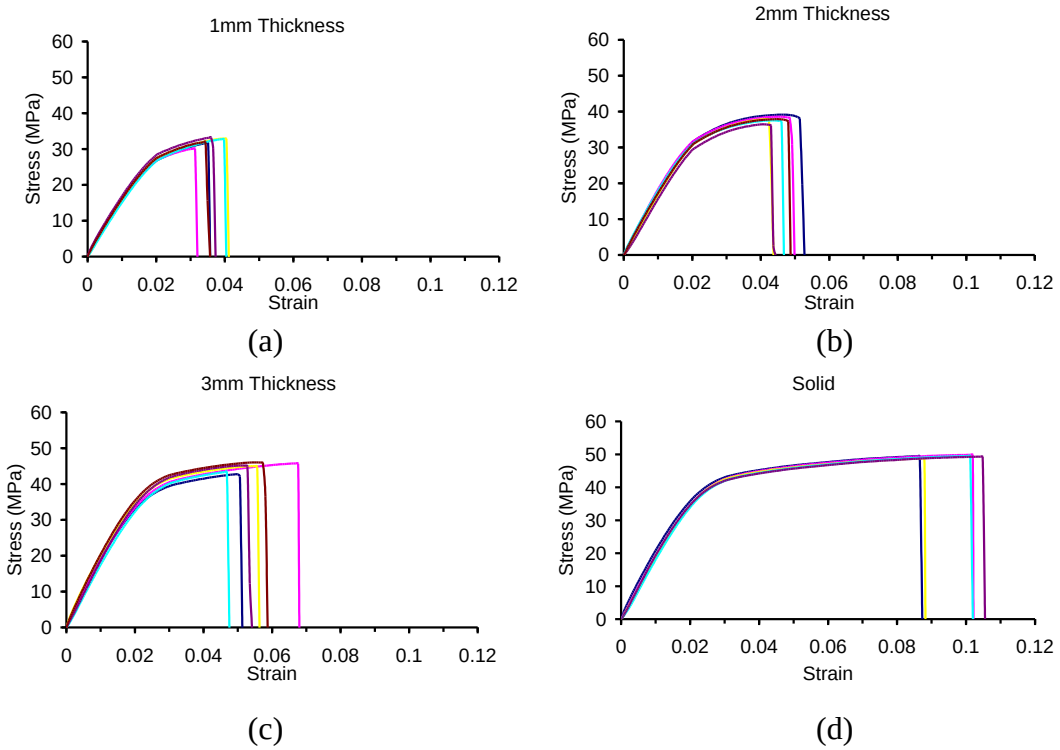

Figure 6-26 Stress-strain graphs for each of the tensile tests with fill and outline scanning specimens for closed hollow with section thickness, (a) 1mm (b) 2mm, (c) 3mm and (d) solid

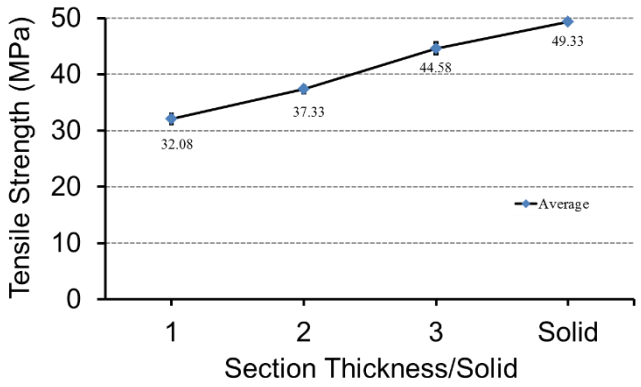

Figure 6-27 Tensile strength results of different section thickness of closed hollow and solid specimens with fill and outline scanning. Error bars are at 95% confidence interval

Figure 6-27 shows the average of tensile strength obtained from all specimens with fill and outline strategy implemented. It can be seen that the distribution of tensile strength on each individual different section thickness and solid specimens was almost similar. In addition, it was clear that the average tensile strength tend to increase from smallest section thickness to solid specimens. The ANOVA confirmed this with the p value of 0.05.

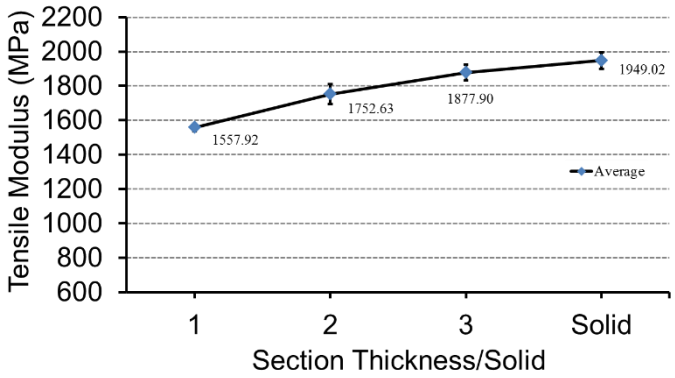

Figure 6-28 Tensile modulus results of different section thickness of closed hollow and solid specimens with fill and outline scanning. Error bars are at 95% confidence interval

Figure 6-28 illustrates the average tensile modulus obtained from the specimens with fill and outline implemented. In addition, the average modulus was different on each different section thickness and solid specimens. This indicated an increasing trend with the changes in section thickness. This observation confirmed that the average tensile modulus of fill and outline scanning samples increases as the thickness of section of the specimens increases up to solid. The ANOVA confirmed that the p value was smaller than 0.05.

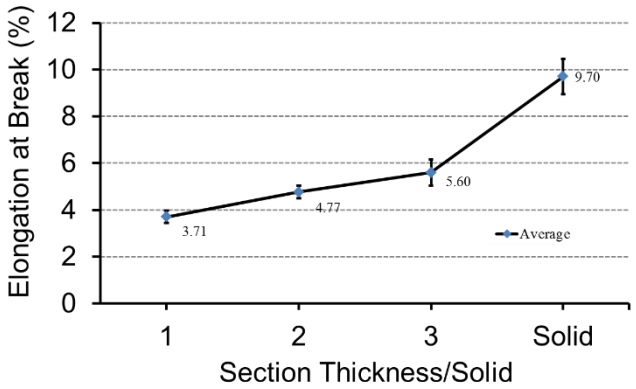

Figure 6-29 Elongation at break results of different section thickness of closed hollow and solid specimens with fill and outline scanning. Error bars are at 95% confidence interval

Figure 6-29 demonstrates that the average elongation at break for 1mm, 2mm, 3mm section thickness and solid specimens with fill and outline scanning strategy.. This indicated that there was an increase in the average of elongation as the thickness increased. This indication was also confirmed by The ANOVA in which the p value was smaller than 0.05.

6.6.2 Energy Density

As described in section 2.2, energy density is one important and direct processing parameter. This research investigates the effect of implementation of different scanning strategy on their mechanical properties, on different section thickness and solid specimens. The total energy density in each individual different section thickness, with fill scanning can be determined by using the equation (6.1), meanwhile for fill and outline scanning by using the equation (6.2):

$$\text{Total energy} = \frac{ED}{A} \text{ x L x d} \qquad \text{……..} \quad (6.1)$$

$$\text{Total energy} = [\frac{ED}{A} \text{x L x d}] + \frac{Po}{A} \qquad \text{……...} \quad (6.2)$$

ED is Energy density as shown in equation 2.1 = $\frac{P}{BS * SP}$ (Joule/cm^2), where *P* is fill laser power (watt), *BS* is laser beam speed (cm/s), *SP* is scan spacing (cm), A is area

scanned, L is scan path length (cm), d is diameter of beam of laser (cm), P_o is outline laser power (watt).

The scan path length is the total number of length of laser scanning that traces the material in the designated area in order to sinter it. This is then repeated until all layers of the specimens have been completely sintered. Scanning pattern of scan path as described in section 3.3, in which the laser moves parallel to X axis and perpendicular of Y axis, was also applied in this study when producing the specimens. When referred to the theory of scanning laser traces, as shown in Figure 2-11 and 2-12 the scan path length can be determined. Using the pictures as shown in Figure 6-30 and Figure 6-31, the scan path length can be calculated due to the nature of the shape of the specimens, which are round hollow bars and solid.

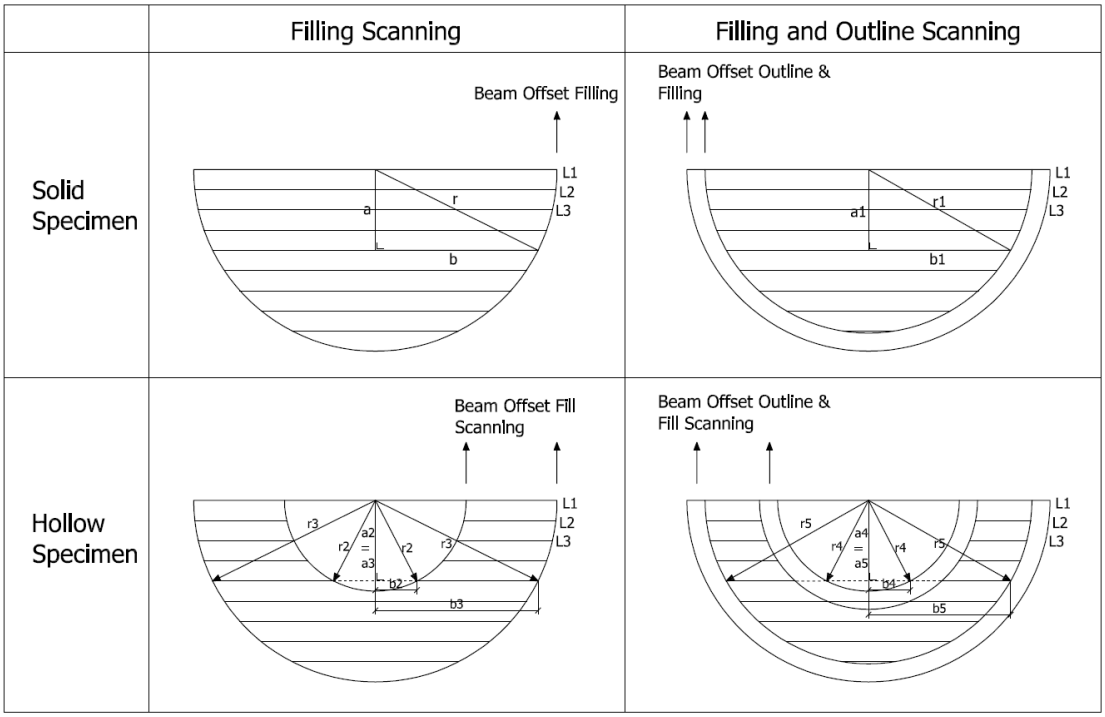

Figure 6-30 Scan path length of Fill (F) and Fill and outline (F/O) for different section thickness and solid specimens

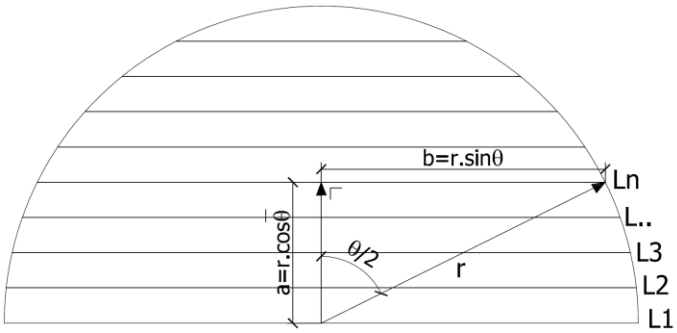

Figure 6-31 Pythagorean theory of each layer

To calculate the scan path length for each layer, from Figure 6-30, it can be determined that the chord is 2rsinϴ. It is then calculated by multiplying this number with the length of the specimen in Y direction (see Figure 6-3 specimens' position and orientation in the Vanguard SLS machine). In X direction, the number of scan path length is the area of specimens divided to scan spacing for each layer then multiply with the number of layers.

All the results obtained were presented in Figure 6-32 for specimens with fill and fill and outline scanning strategy, with different section thickness and solid.

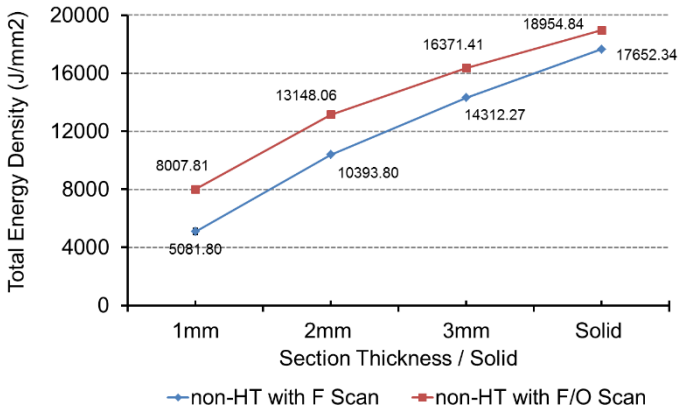

Figure 6-32 Total energy density of different section thickness and solid specimens for non-heat treated with fill (non-HT with F scan) and non-heat treated with fill and outline (non-HT with F/O scan) strategy.

Figure 6-32 shows the average total energy density obtained from all specimens that was built with the fill scanning strategy (default) and with fill and outline scanning strategy. It also can be observed that the average total energy density was different on each different section thickness and solid specimens. The average total

energy density increased when there was a greater section thickness and it was the highest with the solid specimens. This means that the sections with the smaller thicknesses had a lower energy density compared to the solid specimen, which had the highest energy density even though they were built using the fill scanning method. This pattern was also seen when the specimens were produced by using fill and outline strategy. The ANOVA confirmed this as both of the p values was smaller than 0.05.

6.7 Summary and Discussions

The tensile characteristics results for specimens with different section thickness of closed and opened hollow structure and solid, for non-heat treated and heat treated, for specimens with the implementation of different setting of fill and outline scanning strategy as determined in section 6.4, 6.5 and 6.6 are summarised in Figure 6-33 to Figure 6-35. Moreover, the summaries of their thermal characteristics are demonstrated in Figure 6-36 to 6-39.

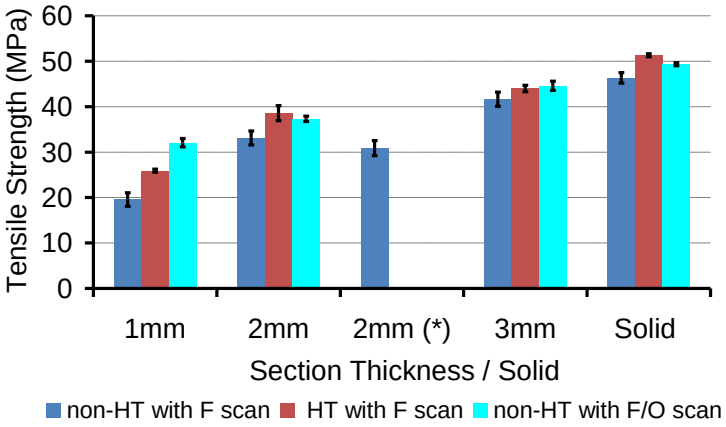

Figure 6-33 Comparison of average tensile strength of different section thickness and solid specimens of non-heat treated (non-HT) with fill (F) scan, heat treated (HT) with fill (F) scan and non-heat treated (non-HT) with fill and outline (F/O) scan. (*) open hollow and others are closed hollow structure. Error bars are at 95% confidence interval.

From Figure 6-33 it can be seen that the average tensile strength of heat treated and non-heat treated specimens, in individual section thickness and solid specimens were different. As it was described in section 6.4 and 6.5 , the smaller average value of tensile strength can be seen on the smaller section thicknesses and the highest average value of the tensile strength was for the solid specimens, for both heat treated

and non-heat treated specimens. This observation confirmed that the average tensile strength was influenced by the different section thickness.

Furthermore, heat treated specimens have a higher value of tensile strength on average compared to all non-heat treated specimens for individual different section thickness and solid. From this Figure, it can be concluded that section thicknesses and the heat treatment effects the average tensile strength and making them increase significantly at a 95% confidence level. ANOVA also indicated that there was significant increase on the average tensile strength on difference section thicknesses with all p values smaller than 0.05. For all samples with a different section thickness and solid, average tensile strength improved in the range of 2 – 6.34 MPa even when samples that have been and have not been heat treated were used.

From Figure 6-33 it can be seen that there was significant effect of the implementation of fill and outline scanning strategy on average tensile strength. The average tensile strength increases as the section thickness increases up to solid specimens compared to the specimens that were built using fill scanning strategy only. This indication confirmed that there was an improvement in the average tensile strength for 1mm section thickness by 12.50 MPa, while for 2mm it was by 4.20 MPa and for 3mm and solid it was by around 2.99 MPa for both. ANOVA confirmed this condition, in which the p value was smaller than 0.05.

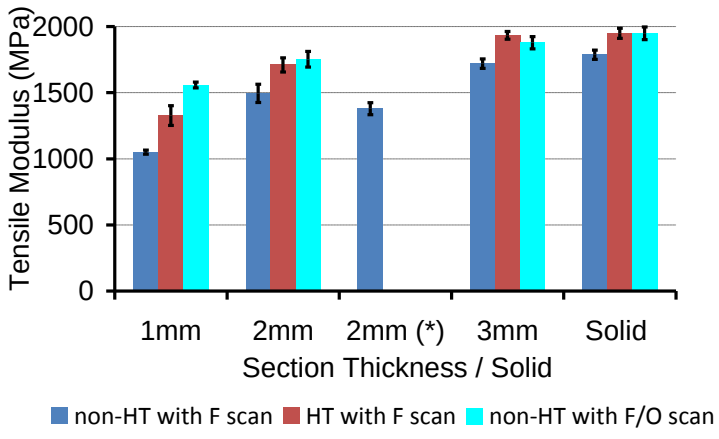

Figure 6-34 Comparison of average tensile modulus of different section thickness and solid specimens of non-heat treated (non-HT) with fill (F) scan, heat treated (HT) with fill (F) scan and non-heat treated (non-HT) with fill and outline (F/O) scan. (*) open hollow and others are closed hollow structure. Error bars are at 95% confidence interval.

From Figure 6-34 it can be observed that the average tensile modulus increased with the increase of section thickness, for all specimens with and without heat treatment. This indication has also been described in section 6.4 and 6.5. However, the average value of tensile modulus of the heat treated specimens was higher compared to the values of non-heated specimens, in each different individual section thickness and solid. Again, this confirmed that average tensile modulus depended on the section thickness and whether heat treatment was carried out on the specimen. From this figure, it can be concluded that heat treatment influences the average tensile modulus and the significant is at a 95% confidence level. The ANOVA confirmed this significant increase with the p value being smaller than 0.005. Compared to the specimens without heat treatment, the improvement of heat treated specimens increased by 277.05MPa, 214.51MPa, 214.22MPa and 161.63MPa for 1mm, 2mm, 3mm and solid samples, respectively.

From Figure 6-34, it can be observed that the specimens built with fill and outline scanning strategy has higher average tensile modulus compared to the specimens that was built with fill scanning strategy only. It was clear that the average tensile modulus increased significantly at a 95% confidence interval. ANOVA confirms this because the p value was smaller than 0.05.

It can be summarised that there was a significant effect of fill and outline scanning strategy on the average tensile modulus on each different section thickness and solid specimens. This was indicated by the increase of the average tensile modulus by 508.30 MPa, 258.08 MPa, 159.02 MPa and 162.05 MPa for 1mm, 2mm, 3mm section thickness and solid specimens, respectively.

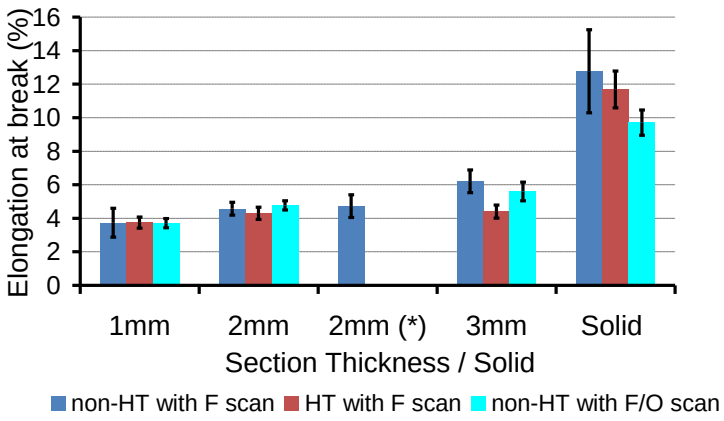

Figure 6-35 Comparison of average elongation at break of different section thickness and solid specimens of non-heat treated (non-HT) with fill (F) scan, heat treated (HT) with fill (F) scan and non-heat treated (non-HT) with fill and outline (F/O) scan. (*) open hollow and others are closed hollow structure. Error bars are at 95% confidence interval.

As shown in Figure 6-35, the trend of elongation at break in all heat treated and non-heat treated specimens were different to the trend of tensile strength and tensile modulus. It can be seen that the average elongation at break for heat treated hollowed specimens were similar. However, the elongation at break value decreased when heat treated specimens were used as compared to non-heat treated specimens. Although the value decreased, it is not significant enough to be at a 95% confidence level, except for specimens with 3mm section thickness where there was a significant decrease in the value. This indicated that there was no effect of heat treatment on elongation at break.

Figure 6-35 demonstrates that the implementation of fill and outline scanning strategy did not significantly affect the average elongation at break on each different section thickness and solid specimens. It seems that there was no increase on the average elongation at break for specimens with 1mm and 2mm. However, the average elongation for 3mm section thickness and solid specimens decreased. Even though there was a slight increase and decrease, they were not significantly at 95% confidence level. ANOVA confirmed this condition, in which the p value was greater than 0.05. It can be summarised that there was no impact on average elongation at break by using fill and outline scanning strategy.

From Figure 6-33 to 6-35 in can be summarised that the section thickness of the specimens influenced the average tensile strength and average tensile modulus, but

not fully impact the elongation at break. Furthermore, it also can be summarised from the results obtained that the heat treatment at 180^{o}C for 100 hours in vacuum environment brought about an improvement, particularly for tensile strength and tensile modulus for each different section thickness and solid specimens.

From Figure 6-33 to Figure 6-35 it can be summarised that compared to specimens that built using fill scanning strategy, the average tensile strength and average tensile modulus of specimens that built with fill and outline scanning strategy were increased for each individual different section thickness and solid specimens. However, this was not the case for elongation at break. This also indicated that the implementation of different set of fill and outline scanning obtained a higher total energy density as shown Figure 6-32. The total energy density increased with the greater section thickness and the highest occurred with solid specimens.

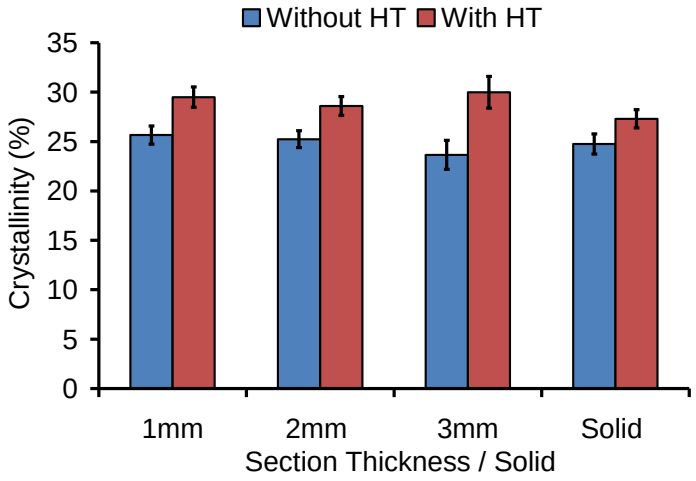

Figure 6-36 Summaries of test results: average crystallinity sintered material with and without heat treatment of different section thickness and solid specimens. Error bars are 95% confidence interval

Figure 6-36 shows that the average degree of crystallinity of sintered material with heat treated were higher compared to average degree of crystallinity of the same material but non-heat treated. It was clear that the increase of average degree of crystallinity after heat treatment was significantly at a 95% confidence level. This was also confirmed by ANOVA which showed that the p value was smaller than 0.05.

It can be summarised that the heat treatment affected the average degree of crystallinity for sintered material. Compared with and without heat treatment, the

improvement of degree of crystallinity by 14.97%, 13.31%, 26.81% and 10.30% for 1mm, 2mm, 3mm and solid specimens, respectively.

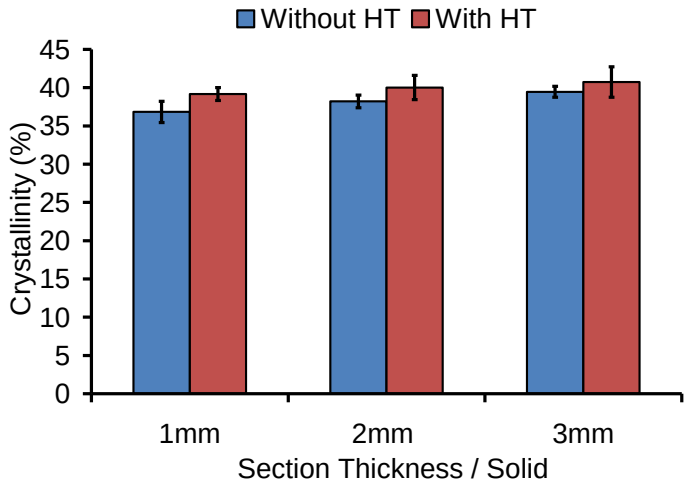

Figure 6-37 Summaries of test results: average crystallinity un-sintered material with and without heat treatment of different section thickness and solid specimens. Error bars are 95% confidence interval

From Figure 6-37, although there was a slight improvement on the average degree of crystallinity on thickness of section 1mm (2.34%), 2mm (1.82%) and 3mm (1.28%), it can be observed that there were no significant differences for un-sintered material, for each of the different section thickness, from heat treated and non-heat treated specimens. This indicated that there was no significant effect of heat treatment on the average degree of crystallinity for un-sintered material. ANOVA confirmed this conclusion by showing a p value which was greater than 0.05.

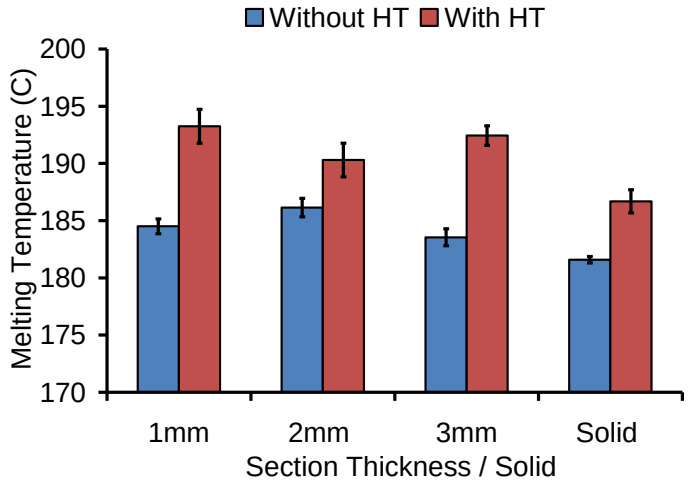

Figure 6-38 Summaries of test results: average melting peak temperature sintered material with and without heat treatment of different section thickness and solid specimens. Error bars are 95% confidence interval

From Figure 6-38, it shows that for sintered material, the average melting peak temperature increased significantly at a 95% confidence level by 8.73^{o}C, 4.16^{o}C, 8.89^{o}C and 3.10^{o}C for 1mm, 2mm, 3mm and solid specimens, respectively. This indication confirmed that there was an increase of the average melting temperature compared to non-heat treated specimens, even though in all specimens the improvement was lower than 5%. This was clear that the heat treatment affected the average melting peak temperature. The ANOVA confirmed this with a p value was smaller than 0.05.

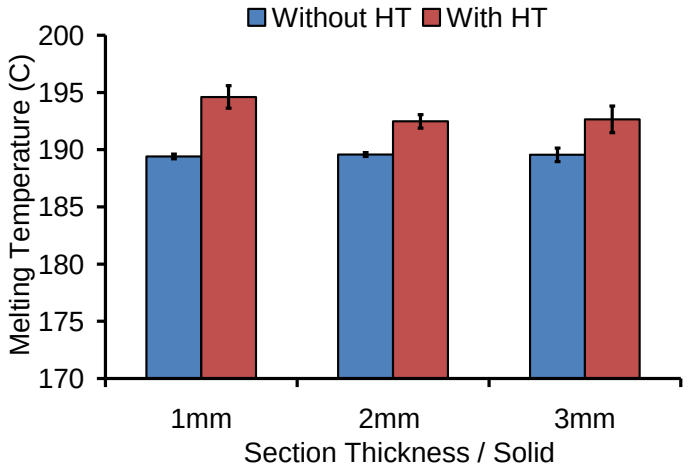

Figure 6-39 Summaries of test results: average melting peak temperature un-sintered material with and without heat treatment of different section thickness of specimens. Error bars are 95% confidence interval

Figure 6-39 illustrates that heat treatment affected the average melting peak temperature for un-sintered material significantly at a 95% confidence level. ANOVA confirmed this condition, in which the p value was smaller than 0.05. Compared to the specimens without heat treatment, the average melting peak temperature increased by 5.20^{o}C, 2.91^{o}C, 3.10^{o}C for the specimens with 1mm, 2mm and 3mm section thickness, respectively. However, the improvement was lower than 5% in all specimens.

From Figure 6-36 to Figure 6-39, it can be summarised that the section thickness had no effect on the average degree of crystallinity, either for heat treated or non-heated specimens. However, the degree of crystallinity was higher after heat treatment was carried out. This indicated that the heat treatment at 180^{o}C for 100 hours in vacuum environment provoked an improvement in degree of crystallinity, particularly for laser sintered material.

6.7.1 Effect of Section Thickness of Closed and Open Hollow Structure

Figures 6-33 to 6-39 show the comparison of mechanical properties and thermal properties of different outline/cross-section thickness and solid specimens of Nylon 12 laser sintered material.

It can be seen that the outline/cross-section thickness influences the mechanical properties. The figures demonstrated that the tensile properties increased when the thickness of the outline/cross-sections were greater.

As shown in Figure 6.5(d) on page 134, the variation in the maximum tensile strength of the solid sample is not huge. However, the variation in the elongation at break of the same sample is huge for the solid sample.

The layer-to-layer bonding region in solid specimen is larger than for hollow specimen. Thus greater energy is needed to break the layer-to-layer bonding. In addition the laser scan lines on the solid samples are longer than the close-hollow samples. Longer scan lines allows the previously scanned line time to cool and solidify while shorter laser scan lines limits the cooling time between lines. This resulted in stronger fusion of particle-to-particle bonds that increases ductility and are more difficult to break [Nelson J.A., et al, 2014]. Furthermore in the region of effect of end of vector (EoV) for hollow specimens are very together which exposure the specimens to longer and higher intensity laser. This will causes greater sintering and

increased densification and affect the mechanical properties [Ajoku, U. et al, 2006]. This is illustrated by Figure 6-40 below.

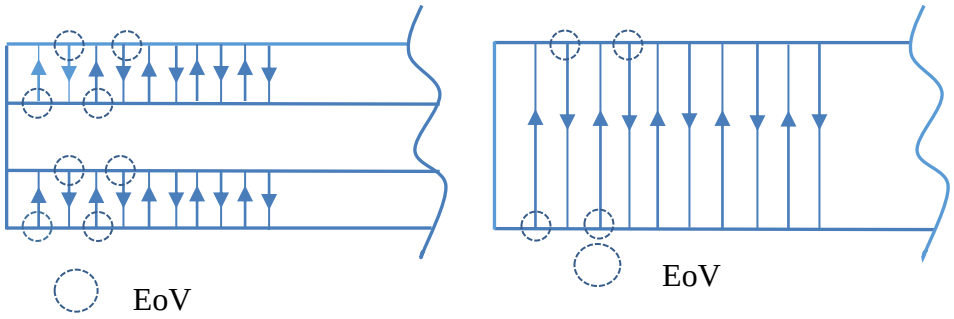

(a) Hollow structure (b) Solid structure

Figure 6-40. End of vector effect (a). Hollow structure (b). Solid structure

Moreover, the variation in the tensile modulus changes with the different section thickness. Laser sintered materials such as Nylon 12 exhibits anisotropy behaviour (Faes, M. et al, 2015, Ajoku, U. et al, 2006b] due to the influence of processing parameter. This is different from most polymer materials that are manufacture from bulk material through moulding or extrusion processes that tend to produce isotropy behaviour [Griskey, 1995]. Beside the orientation, secondary effect of end-of-vector (EoV) during the sintering process will produce different tensile modulus for varying cross section [Ajoku, U. et al, 2006b]. When the cross section of sintering area (as view from above toward the build platform) is bigger, the tensile strength and modulus will be different from smaller cross section as EoV causes greater sintering and increased densification. And in more prevalent in small feature or crossection [Ajoku, U. et al, 2006b]. This behaviour occurs due to the build orientation of the components and different temperature changes which occur within the parts during the LS process.

However, as shown in Figure 6-36 for sintered material, it was confirmed from the crystallinity characterisation results there was no significant difference for each section thickness and solid for either non-heat treated or heat treated specimens. This signifies that the crystallinity was not affected by the different section thickness or solid. In contrast, the crystallinity became increasingly higher when each of individual specimens was heat treated compared to non-heat treated specimens.

In addition, the peak melting temperature, as revealed in Figure 6-37 for the sintered material, illustrated that for each different section thickness and solid, non-

heat treated or heat treated specimens, the peak melting temperature was significantly different and the peak temperature of the heat treated specimens were higher compared to non-heat treated specimens. This is possible, because of the variation in crystallinity of each different section thickness and solid. The peak melting temperature of heat treated specimens was higher due to the increase in crystallinity when the specimens were heat treated.

Regarding the closed and open hollow structures, there was no significant difference because in the un-sintered area from both specimens there were no melted particles due to the design of the specimens. This means the original (input) powders were still in the same particle condition (see Figure 6-18, morphology of particle), even though the specimens were heat treated. In the SLS process, the laser will scan the design area only (the outline parameter/profile of the parts), as a sintering process to melt a powder particle when components or parts are produced.

Figures 6-11 to 6-13 show the results of the 2mm section thickness; the closed and open hollow structure confirm that there was no impact, as there was no significant difference of their mechanical properties for both results. It can be described that the mechanical properties occurs as an effect of force on the sintered area. In the closed hollow structure, the original powder material is enclosed in the hollow area; it is not sintered. This indicates, that this material can be observed as the original powder. Meanwhile, for the open hollow structure, the original powder was also not sintered during the SLS process. This trapped powder, which was the original powder that was removed prior to conducting the tensile test. Therefore, it can be seen that the force on the sintered area was similar. As a result, with respect to the un-sintered area, this area has become un-melted (particle) material. In addition, this un-melted material does not fuse with the sintered material area; therefore, when the reaction force occurred during the tensile test, there was no distribution of force on this area.

In this research, the specimens that were used were round bars with hollow structures, which confirmed that the larger sintered area gave higher tensile properties. This case is different with the results demonstrated by Majewski and Hopkinson [2011] that used dog bone as the specimens in their investigation. Their results demonstrated that there was no influence of section thickness on the mechanical properties [Majewski and Hopkinson, 2011].

However, from Majewski and Hopkinson [2011] and this particular research, the results confirm that there were no effects on the tensile properties, even though there was a small increase in crystallinity at the larger section thickness. This is because slight increase in crystallinity is not enough to have a significant effect on them.

6.7.2 Effect of heat treatment on properties

Heat treatment conducted in this research has an impact on mechanical properties, given that it has more (enough) energy to melt the particles. In processing the SLS material, the amount of heat melting was lower, and not enough to melt the particles completely. However, the bonding of the particles improved when the heat energy is increased, as it is being heat treated, mainly when treated in vacuum condition. This condition was confirmed by the DSC traces with heat treated materials, in the vacuum environment. In the air heat treatment, the amount of heat melting energy was slightly lower than the amount of energy that occurs in the vacuum condition, and this resulted in the improvements of the mechanical properties and the thermal characteristic constantly increases. Therefore, in order to change the semi-crystalline materials that are of high ordered molecular structure with sharp melt points into a viscous liquid, a given quantity of heat need to be absorbed. As semi-crystalline materials do not gradually soften with a temperature increase but rather remain hard until the molten polymer flows in between the powder particles, forming sintering necks, enough heat must be provided and maintained for complete layer is fully molten and overlaps to the previous layer. Since the rate of crystallization is minimum near Tg and Tm, and reaches a maximum between those two temperatures. SLS process is something between partial and full melting. The melt viscosity is linearly related to the molecular weight (MW). For good interfusion of the polymer chains, sufficient to provide particle necking and layer to layer adhesion, a low melt viscosity is desirable. However, low viscosity results in high shrinkage and poor part accuracy. Thus an optimum MW range exists but is not easily controllable, neither at the polymer production nor during aging in process.

The thermal degradation over time when re-using the same powder repeatedly, results in the decay of the MFI (Mold Flow Index) hence a drop in powder flowability

and a rise in melt viscosity preventing proper sintering and a drop in mechanical properties can be observed as well.

It was believed that the porosity occurred as there was not enough energy to melt the particle structure. It was expected that the heat treatment can be used to reduce the porosity of the specimen, in which the amount of particle structure melting would increase.

The use of heat treatment as a processing of laser sintered material can reduce the porosity and shrinkage problem. This is a consequence of the greater energy of melting after heat treatment. The greater energy of melting results in better fusion of the particles and builds a more compact structure. Therefore, the tensile strength and tensile modulus improved in the heat treated specimens rather than the non-heat treated specimens.

Basically, in polymers science, molecular weight is an essential factor to form microstructure in order to bond effectively. In this situation, the molecular weight is increased relatively by increasing the heat melting temperature. This DSC indicated that the increasing heat melting temperature was enough to melt the polymer microstructure. Due to this effect, the increasing molecule weight would also increase the melting viscosity and density of polymer structures. This significant trend was observed by the degree of crystallinity.

The DSC traces of each specimen in different fabrication shows a different heat melting energy to melt the polymer particle. From these conditions it can be described that the heat treatment methods can give different amount of energy, which was caused by the different settings of temperature and time of treatment for each heat treatment in air and in vacuum environment.

Theoretically, the values of crystallinity are influenced by the shape of specimens, the position in which the material was cut and then placed in pan or crucible [Craig and White, 2005]. In this research study, the material cutting was taken from the centre of the tensile specimens and used it as the tensile specimen test. Therefore, the values of crystallinity in this study are different with the values of crystallinity that was studied by Zarringhalam [2007]. He reported that he used the specimens which were built in X orientation, with flat shape and different settings of building parameters. However, the result values, when compared are relatively the same.

The results that were obtained in chapter 6 have different impact and relationship on the properties after heat treatment compared to the results obtained in chapter 4 and 5. The results show that on different section thickness 1mm, 2mm, 3mm and solid, either for heat treated or non-heat treated specimens, the mechanical properties increase while section thickness increases up to solid. In addition, in all individual different section thickness and solid specimens, it can be confirmed that the mechanical properties were higher after heat treatment. Moreover, the crystallinity of all heat treated were higher than non-heat treated specimens.

Figures 6-36 and 6-37 shows that the average degree of crystallinity and melting temperature for sintered material of heat treated specimens was higher compared to non-heat treated specimens. This condition confirms that heat treatment has effect on crystallinity and melting temperature.

Table 6.1 show the relationship of changes in mechanical property and changes in degree of crystallinity after heat treated.

Table 6.1. Relationship of changes in mechanical property and changes in degree of crystallinity after heat treated

Specimen	Degree of Crystallinity			Percentage Changes in Mechanical Property after heat treated (%)		
	Without Heat treatment	With Heat treatment	Percentage Changes (%)	Strength	Modulus	Elongation
Section 1mm	25.65	29.49	14.97	32.40	26.40	0.21
Section 2mm	25.24	28.60	13.31	16.42	14.35	-5.87
Section 3mm	23.65	29.99	26.81	5.69	12.46	-29.17
Solid	24.75	27.30	10.30	10.73	9.04	-8.55

From Table 6.1, it was clear that when crystallinity was higher, tensile strength and tensile modulus would increase. This is due to enhanced secondary inter-chain bonding which results from adjacent aligned chain segments as percent crystallinity increases. This enhanced inter-chain bonding inhibits relative inter-chain motion.

However, the elongation at break was lower or similar when crystallinity is higher. The reduction in elongation is due the changes in the molecular structure of the materials where disordered quasi-amorphous interlamellar (IL) regions between the crystal lamellae were reduced. This is as confirmed by research study by Bessel et al [1975], Majewski et al [2008] and Hopkinson et al [2009].

Heat treatment of semi-crystalline polymers can lead to an increase in the percent crystallinity and in crystallite size and perfection, as well as to modification of the spherulite structure. For undrawn materials that are subjected to constant time heat treatments, increasing the annealing (heat treatment) temperature lead to the following: (1) an increase in tensile modulus, (2) an increase in yield strength and (3) reduction in ductility [Callister and Rethwisch, 2012].

For a specific polymer, the degree of crystallinity can have a significant influence on the mechanical properties because it affects the extent of the intermolecular secondary bonding. For crystalline regions in which molecular chains are closely packed in an ordered and parallel arrangement, extensive secondary bonding typically exists between adjacent chain segments. As a consequence, for semi-crystalline polymers, tensile modulus increases significant with degree of crystallinity [Callister and Rethwisch, 2012].

In addition, these results confirm that the heat treatment has impact on thermal properties of Nylon 12 laser sintered material and consequently influenced their mechanical properties.

From Figures 6-38 and 6-39 for un-sintered material, where raw particle powder of Nylon 12 is trapped in a hollow structure of each individual 1mm, 2mm and 3mm section thickness; the degree of crystallinity of non-heat treated and heat treated did not significantly change at 95% confidence level, even though there was a small increase in the heated specimens. However, the melting temperature significantly changes at 95% confidence level. This may be because of the size of the grain particles of the original raw material used were not from the same batch and not originally from fresh or re-used or might be mixture of fresh and re-used material. Therefore, there was no effect of heat treatment on un-sintered material and in this case on raw powder material. Due to this, there was insufficient heat supplied on the powder particle to form as to a sintered area that fused with laser sintered area.

The degree of crystallinity and melting temperature of sintered material were always lower compared to un-sintered material, either for non-heat treated and heat treated specimens. Figures 6-38 and 6-39, demonstrated that the average degree of crystallinity was between 27.30% and 29.99% for sintered material, while for un-sintered material it was between 39.17% and 40.73%. This result confirms that the degree of crystallinity of sintered material were lower than degree of crystallinity of un-sintered material, for each individual 1mm, 2mm and 3mm section thickness. This

is because a melted solid material has lower particle crystallisation during SLS process.

In addition for specimens with heat treatment as shown in Figures 6-37 and 6-39, the average melting temperature was between 186.69^{o}C to 193.24^{o}C for sintered material and between 192.48^{o}C to 194.61^{o}C for un-sintered material. This result confirms that the melting temperature of sintered material were lower than melting temperature of un-sintered material, for each individual 1mm, 2mm and 3mm section thickness.

Furthermore, since different in melting temperature between all the difference section thickness is so small; it shows that there was no effect of crystallinity on melting temperature with and without heat treatment on un-sintered material. However, it is difference for sintered material as the result confirms that there was effect of crystallinity on melting temperature.

For sintered and un-sintered material, melting temperature of heat treated specimens was higher compared to non-heat treated specimens.

6.7.3 Effect of Scanning Strategy on Mechanical Properties

This experimental study on the effect of different setting of scanning strategy on mechanical properties Nylon 12 laser sintered material has been implemented. As mentioned previously, the setting of laser power of outline scanning was set up bigger, to observe if there was an impact.

The implementation demonstrated that there was an impact on mechanical properties. It is believed that this is because there are the relationship between the energy density and mechanical properties. Figure 6-41 to 6-43 shows the relationship between average total energy density and average tensile strength, average tensile modulus and average elongation at break.

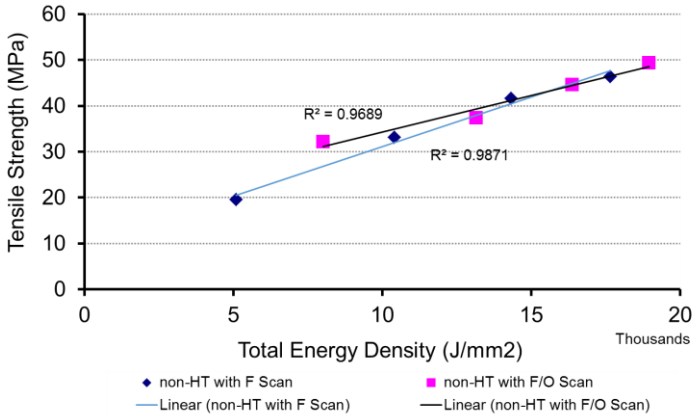

Figure 6-41 Average energy density and average tensile strength relationship for specimens with default fill scanning and fill and outline scanning, with 1mm, 2mm, 3mm section thickness and solid

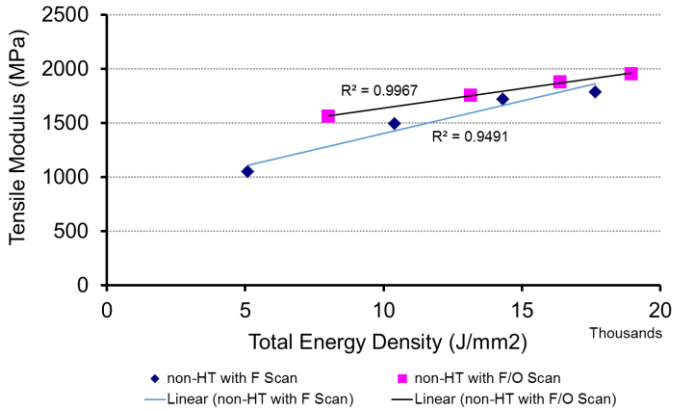

Figure 6-42 Average total energy density and average tensile modulus relationship for specimens with default fill scanning and fill and outline scanning, with 1mm, 2mm, 3mm section thickness and solid

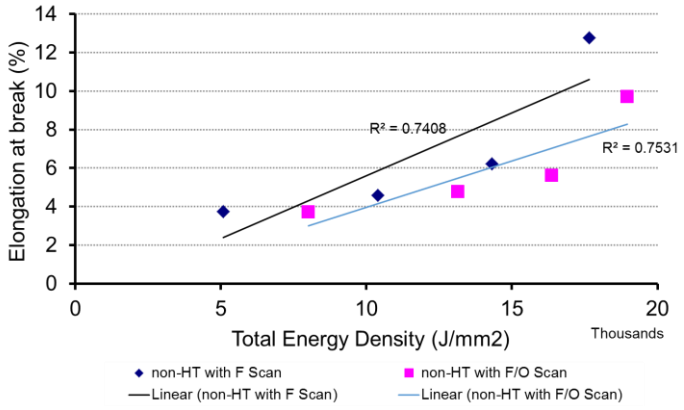

Figure 6-43 Average total energy density and average elongation at break relationship for specimens with default fill scanning and filling and outline scanning, with 1mm, 2mm, 3mm section thickness and solid

This was also confirmed by the research of others, which shows that when energy density is higher the mechanical properties of laser sintered material are also higher [Tontowi and Childs, 2001; Gibson and Shi, 1997, Caulfield, et al, 2007].

It is clear that when the energy density increases, this means that the number of particles melted is increasing and the particle bonding is stronger. This relation is higher when it comes to mechanical properties.

The implementation of bigger laser power setting for outline scan made a stronger bonding of the particle that melted. With higher laser energy, particles tend to coalesce and had larger necking area between particles. Similar finding by Salmoria [2014] was also reported on polymer sintering of PC using different laser energy and particles size. Furthermore, when the particles were laser sintered once and then it was laser scanned again resulting in an overlap of scanning, the heat dispersed in the '$-Z$' direction and the X-Y plane were almost uniform and instantaneously heated up the successive slice layer thickness [Carter, et al, 2014]. That is why the specimens with 1mm section thickness make bigger improvements compared to section 2mm and 3mm.

It is clear that when the length of scanning path increases, this means that the number of particles melted is increasing and the particle bonding is stronger. This relation is higher when it comes to mechanical properties.

CHAPTER 7. CONCLUSIONS AND FUTURE WORK

7.1 Summary of Findings and Conclusion on Practical implications of the work

The summary and conclusion of the works that were performed in this research are as outline in section 7.1.1 and section 7.1.2.

7.1.1 Summary of Findings

From the present research findings, the following conclusions can be drawn:

A. Material characterisation

- Nylon 12 laser sintered components can be considered as anisotropic material.
- The variation of the test results from those of other researchers indicates inconsistent characteristics of materials, even though the same material and same machine type was used.
- Tensile strength and tensile modulus are higher when it is heat treated compared to non-heat treated for each individual different cross-section of thickness and solid, while the average degree of crystallinity were approximately similar for each individual section thickness and solid, heat treated and non-heat treated specimens. The larger sintered area gives higher mechanical properties, in which the solid specimens were the highest when it comes to tensile strength and tensile modulus. Crystallinity is higher when heat treated compared to non-heat treated specimens. However, when compared to each individual section thickness and solid specimens, the crystallinity is approximately the same for all non-heat treated and heat treated specimens.
- Compared to the default setting strategy, better mechanical properties were obtained when different (bigger) setting of laser power was applied to outline the contour of scanning in the fill and outline scanning strategy implemented.
- The increase of tensile strength, tensile modulus and crystallinity of 1mm section thickness was higher when heat treated compared to the other different section thickness even when heat treated or non-heat treated. This is maybe because more particles melt during sintering process due to the fact that it

occurs in a bigger sintered area. This condition is due to more availability of energy to sinter the melting material rather than sintering a larger surface area. This condition also appeared when fill and outline scanning strategy was applied for 1mm section thickness, which also resulted in the in the increase of their tensile strength and tensile modulus which were higher than the other section thickness.

B. Heat treatment studies

- Heat treatment in air at short hour (2 hours) within the Tg and Tm temperature range did not promote sufficient changes in crystallinity to significantly change the mechanical properties. However, longer hours (100 hours) at $180^{O}C$ of heat treatment in vacuum condition (as reported in chapter 6) promote a slight difference in crystallinity, where the average degree of crystallinity increased in the average of 11.63% significantly at a 95% confidence level and melting peak for both different section thickness and solid specimens.
- Crystallinity for heat treated specimens was higher compared to non-heat treated specimens. However, compared to each individual different section thickness and solid specimens, the crystallinity was approximately similar within the non-heat treated specimens and the heat treated un-sintered material.
- Increase in crystallinity from heat treatment influenced the mechanical properties of tensile strength, tensile modulus and elongation at break.

C. **Scanning strategy implementation**

- Tensile properties increased when scanning strategy was implemented on different section thickness and solid specimens (as reported in chapter 6). The results showed that there was an improvement on their tensile strength and tensile modulus. Compared to the initial specimens that was produced with default fill scanning strategy and non-heat treated, at a 95% confidence level tensile strength significantly increase in the average of 63.92%, 12.68%, 7.09% and 6.45% for specimens with 1mm, 2mm, 3mm section thickness and solid respectively. In addition, average tensile modulus also increased

significantly at a 95% confidence level by 48.43%, 17.27%, 9.25% and 9.07% for each individual specimen respectively.

7.1.2 Conclusion on Practical implications of the work

It might be considered that vacuum heat treatment could be adopted on an industrial scale. The method is simple and only limited facilities are required. However, the initial cost is relatively expensive, especially when a specific furnace or other equipment is needed. In addition, the additional lead time might be considered too long. As a result, such work requires more costly components and the time to market can be longer. Even though the mechanical properties are better, the extra time required does not justify the additional cost required.

Heat treatment in a vacuum environment can be a suitable option in order to improve the mechanical properties of laser sintered Nylon 12 material. However, when the component is fully sintered, the increase of properties is not sufficient enough when heat treatment is used.

Another alternative proposed from this research work by alterations in different setting of scanning strategy during building the specimens or the actual parts or component to gain better mechanical properties. This approach is shorter and more economical than using the heat treatment approach to gain better mechanical properties. Furthermore, no additional equipment are required since in this setup the existing SLS machine is used.

Table 7.1 summarises the results of tensile properties of Nylon 12 laser sintered material, for closed hollow structure with different section thickness and solid, with different build up scanning strategy, non-heat treated and heat treated specimens.

Table 7.1 Comparison of Mechanical Properties of Specimens with: default fill scanning strategy and non-heat treated (A); default fill scanning strategy and heat treated (B); fill and outline scanning strategy and non-heat treated (C)

Specimens	Build up and Post processing Treatment			Changes/Improvement	
	A	B	C	A to B (%)	A to C (%)
Section 1mm					
• Strength (MPa)	19.57	25.91	32.08	32.40	63.92
• Modulus (MPa)	1049.62	1326.67	1557.92	26.40	48.43
• Elongation (%)	3.73	3.74	3.71	0.27	-0.54
Section 2mm					
• Strength (MPa)	33.13	38.57	37.33	16.42	12.68
• Modulus (MPa)	1494.55	1709.06	1752.63	14.35	17.27
• Elongation (%)	4.57	4.30	4.77	-5.91	4.38
Section 3mm					
• Strength (MPa)	41.63	44.00	44.58	5.69	7.09
• Modulus (MPa)	1718.88	1933.10	1877.90	12.46	9.25
• Elongation (%)	6.21	4.40	5.60	-29.15	-9.82
Solid					
• Strength (MPa)	46.34	51.31	49.33	10.73	6.45
• Modulus (MPa)	1786.97	1948.60	1949.02	9.04	9.07
• Elongation (%)	12.77	11.68	9.70	-8.54	-24.04

Table 7.1 shows that the improvement and the changes of mechanical properties by using outline scanning strategy was better than heat treatment and fill scanning except for 1mm section thickness. However for both alternatives, when the outline/cross-section thickness increases, the improvement and the changes tend to be reduced. This is due to the fact that the amount of sintered material area had increased. Hence, for solid part the improvement is less significant as compared to thin hollowed cross-section.

But with scanning strategy there could be another problem that needs to be anticipated regarding the nominal and dimensional accuracy. The surface roughness can be impacted as suggested by other studies that scanning strategy can cause of dimensional inaccuracy and surface roughness (Yusoff and Thomas, 2008). Due to the

limitation of time and budget, this was not investigated further nor observed in this current study.

With heat treatment of 100 hours, the process is too long, defeating the concept of rapid manufacturing (RM). As a result, the fill and outline scanning strategy process can be used as an alternative to improve the mechanical properties. However, further investigation is still needed to develop a more effective strategy in reality. Another important issue to consider when the designer or user needs to confirm which technology approach is more acceptable in order to obtain the right specimen and for the process to be cost effective.

As a concluding remark, scanning strategy is more beneficial to be used on thin outline/cross-section thickness and be taken into consideration during SLS process.

7.2 Achievement of objectives

The overall aim and objectives of this research is to achieve a greater understanding of the factors that have effects on properties of Nylon 12 laser sintered material. Moreover, from this understanding it can be used to control the behaviour of the parts or component produced. This knowledge is useful for designer and other users in order to achieve suitable performances of the parts and components.

This study was expected to achieve some objectives in particular to determine the mechanical performance of one SLS material (Duraform PA), over a range of stress states; to develop post processing methods for the material; to determine and understand the impact that the post-processing methods have on the consistency of the mechanical properties.

From chapter 4 it is clear that all the results obtained show that the mechanical properties of Nylon 12 laser sintered material were varied and anisotropic. In addition, as it was reported in chapter 6, their mechanical properties also changed when different section thickness of specimens were used. Moreover, the implementation of different setting of scanning strategy in manufacturing the parts shows different mechanical properties compared to the default setting of scanning strategy. These results confirm that first objective “to determine the mechanical performance of one SLS material (Duraform PA), over a range of stress states” is achieved.

From chapter 5, it can be summarised that heat treatment did not show any improvement on properties when the specimens were heat treated either in air or in a

vacuum environment, particularly when specimens were heat treated for 2 hours in air and 16 hours in vacuum. However, as shown in chapter 6, there were some different results obtained. For all specimens that were heat treated in vacuum for 100 hours, the results confirm that there were effects of heat treatment on mechanical and thermal properties on Nylon 12 laser sintered material. This means, the heat treatment can be used as an alternative solution to improve their mechanical properties. All evidences can be used as an approval for the second objective "to develop post processing methods for the material".

The third objective of this study is "to determine and understand the impact that the post-processing methods have on the consistency of the mechanical properties". The impact of heat treatment shows that the crystallinity of specimens increased after heat treated compared to non-heat treated specimens. During the sintering process in SLS machine, the number of particle melted were still low, due to limited energy density and sintering process occurred quickly, laser scanning or scanning process to sinter the material done quickly. This mean that the amount of energy still insufficient to complete to sinter the materials which better results. As a results the degree of crystallinity were also low. However, after heat treated it was confirmed that the degree of crystallinity increased. This mean that the melted particles after being heat treated, increases compare to non-heat treated specimens. All of these conditions confirm about the achievement of the third objective.

7.3 Research Contributions:

Very little information is available in published literature about mechanical properties of Nylon 12 laser sintered material on hollow structure with different section thickness and solid specimens. In addition, available information after different types of heat treatment on this laser sintered material are also very limited, particularly heat treatment in vacuum environment. Results from this study can fill some of this gap.

This experimental study clearly contributes to the novelty and originality. Firstly, the mechanical properties of laser sintered product with different section thickness of closed hollow structure and solid specimens create different result of tensile strength and tensile modulus.

Secondly, identify the possibility of the use of heat treatment approach to improve mechanical properties in vacuum environment. This study show that degree of crystallinity can be increased by using heat treatment approach.

In addition, effects of scanning strategy in sample preparation were obtained and showed different values of tensile strength and tensile modulus. Therefore, another possibility to improve the mechanical properties is by using different fill and scanning strategy when manufacturing the product. The results show that when the product is manufactured using a combination of fill and outline scanning strategy, the results were better.

From laser sintered product that was manufactured using a combination of fill and outline scanning strategy, it is believed that the mechanical properties will be higher and can be improved even more when also heat treated (with vacuum environment).

7.4 Future work

From the research findings and conclusions described above, it is recommended that further research work can be continued to provide more information and understanding of the possible ways to improve and make more consistent characteristics of laser sintered components. The following further research is recommended:

1. From material characterisation (chapter 4), suggests that there is a need to develop a standard method for measuring the mechanical properties of laser sintered materials in order to provide greater consistency in methods between researchers.

2. In the present research, heat treatment was conducted at 140^{o}C for 120 minutes in the air environment and at 180^{o}C for 960 minutes and 6000 minutes in vacuum conditions at −1018mbar level. Future experimental work in vacuum heat treatment should be conducted using the same temperature, but for shorter periods. This future work can be used to observe or find the optimal time to achieve the same degree of improvement in mechanical properties.

3. Another suggestion for heat treatment in vacuum would be to conduct heat treatment with different cooling rates and different cooling media to observe the effect on crystallinity and mechanical properties.

4. To investigate the effect of different setting of scanning strategy on degree of crystallinity and how far their impact will be compared to when the default setting of scanning strategy is used in producing the component or part. Moreover, to observe the effect on surface roughness and accuracy of dimensions.

5. Theoretically, in polymer science, crystallinity does not only depend on crystallisation rate and molecular weight, but it also depends on the shape of specimens parts [Craig and White, 2005] and also the cutting position of the specimen. Therefore, further experiment using different shape of specimens can be used to observe and to ensure if the outcome of SLS components is different or same.

6. Another potential idea, the experiment can be conducted by using chemical solution / chemical solvent to infiltrate the specimen. It would be useful to use solvent based chemical, such as Buehler Epo-kwick fast cure epoxy (Epoxy base solvent) or Polyurethane in which the specimens will soak in for limited duration of time before being heat treated in vacuum condition.

LIST OF PUBLICATION RELATED THIS STUDY:

- Ahmad Kamil, K.W. Dalgarno, *Material Model for Design Analysis of Laser Sintered Products*, Proceedings of the Eighth National Conference on Rapid Design, Prototyping and Manufacture, Buckhinghamshire, United Kingdom, 15 June 2007.

- Ahmad Kamil, K.W. Dalgarno, *The Effects of Heat Treatment on the Mechanical Properties of Laser Sintered Product Material*, Proceeding of The 32nd Japan Rapid Prototyping Symposium, Tokyo, Japan, 23-24 June 2008.

REFERENCES

3D Systems (2006a), Vanguard SLS systems, available online from: http:/www.3dsystems.com/products/sls/vanguard/index.asp [Accessed April 2006]

3D Systems (2006b), SLS materials, available online from: http:/www.3dsystems.com/products/solidimaging/lasersintering/datasheets.asp [Accessed April 2006]

3D Systems (2010b), SLS materials, available online from: http://www.3dsystems.com/products/materials/sls/index.asp [Accessed February 2010]

Agarwala, Mukesh, Bourell, David, Beaman, Joseph, Marcus, Harris, Barlow, Joel. (1995). "Direct selective laser sintering of metals." Rapid Prototyping Journal **1**(1): 26-36.

Ajoku, Uzoma; Hopkinson, Neil; Caine, Mike. (2006a). "Experimental measurement and finite element modelling of the compressive properties of laser sintered Nylon-12". Material Science and Engineering A 428: 211-216.

Ajoku, U., Saleh, N., Hopkinson, N., Hague, R., Erasenthiran, P. (2006b). "Investigating mechanical anisotropy and end-of-vector effect in laser-sintered nylon parts." Proc. IMechE, Part B: J. Engineering Manufacture **220**: 1077-1086.

Anderson, J. C., Leaver, K. D., Leevers, P., Rawlings, R.D. (2003). Materials Science for Engineers, 5th edition. Cheltenham, Nelson Thornes Ltd.

ASTM Designation: E 9-89a: 2000 (2000). Standard Test Methods of Compression Testing of Metallic Materials at Room Temperature. ASTM International, West Conshohocken, USA.

ASTM Designation: E111-97 (2003). Standard Test Methods for Young's Modulus, Tangent Modulus, and Chord Modulus. ASTM International, West Conshohocken, USA.

ASTM Designation D6272-02 (2004). Standard Test Methods for Flexural Properties of Unreinforced Plastics and Electrical Insulating Materials by Four-Point Bending. ASTM International, West Conshohocken, USA.

Baker, Anne Marie M., Mead, Joey (2002). "Thermoplastics" in Handbook of Plastics, Elastomers and Composites, fourth edition, editor in chief: Harper, C. A., New York, McGraw-Hill.

Beaman, Joseph J., Barlow, Joel W., Bourell, David L., Crawford, Richard H., Marcus, Harris, McAlea, Kevin P. (1997). Solid freeform fabrication: A new direction in manufacturing. Dordrecht, London: Kluwer Academic Publisher.

Bessell, T. J., Hull, D., Shortall, J.B. (1975). "The effect of polymerization conditions and crystallinity on the mechanical properties and fracture of spherulitic nylon 6." Journal of Materials Science **10**: 1127-1136.

Bo, Qian, Yu-sheng, Shi, Qing-song, Wei, Hai-bo,Wang (2012). "The helix scan strategy applied to the selective laser melting". Int. Journal Advanced Manufacturing Technology, 63: 631-640

British Standards Institution. (1996). BS EN ISO 527-1:1996. Plastics. Determination of tensile properties. General Principles. London, BSI.

British Standards Institution. (1998). BS EN ISO 14125:1998. Fibre-reinforced plastic composites. Determination of flexural properties. London, BSI.

British Standards Institution. (2005). BS EN ISO 15310:2005, amendment no.1 to BS ISO 15310:1999. Reinforced plastic. Determination of the in-plane shear modulus by the plate twist method. London, BSI.

Brydson, John A. (1999). Plastics Materials, seventh edition. Oxford, Auckland, Boston, Johannesburg, Melbourne, New Delhi, Butterworth-Heinemann.

Bugeda, Gabriel; Cervera, Miguel; Lombera, Guillermo. (1999). "Numerical prediction of temperature and density distributions in selective laser sintering processing". Rapid Prototyping Journal 5(1): 21-26

Callister, W.D. and Rethwisch, D.G. (2012). Fundamental of Materials Science and Engineering: An Integrated Approach. 4th Ed., p290-293, John Wiley & Sons, New Jersey.

Carter, Luke N.; Martin, Christopher; Withers, Philip J.; Attallah, Moataz M. (2014). "The influence of the laser scan strategy on grain structure and cracking behaviour in SLM powder-bed fabricated nickel superalloy". Journal of Alloys and Compounds 615: 338- 347.

Castle Island's (2010), Worldwide Guide to Rapid Prototyping, available online from: http://www.additive3d.com [Accessed February 2010]

Caulfield, B., McHugh, P.E., Lohfeld, S. (2007). "Dependence of mechanical properties of polyamide components on build parameters in the SLS process." Journal of Materials Processing Technology **182**: 477-488.

Cee Kai, Chua, K. F. Leong, C.S., Lim. (2003). Rapid Prototyping: Principles and Applications. New Jersey, World Scientific.

Chang, Jin Hae, Chen, Michael J., Farris, Richard J. (1998). "Effect of heat treatment on the thermal and mechanical properties of a precursor polymer: polyhydroxyamide." Polymer **39**(23): 5649-5654.

Craig, I.H and White, J.R. (2005). "Crystallization and Chemi-Crystallization of Recycled Photodegraded Polyethylenes". Polymer Engineering and Science, **45** (4): 588-595.

Dalgarno, K. W., Stewart, T.D. (2001). "Manufacture of production injection mould tooling incoporating conformal cooling channels via indirect selective laser sintering." Proc. Instn Mech Engrs, Part B **215**: 1323-1332.

Dalgarno, K. W., Wright, C.S. (2003). "Approaches to Processing Metals and Ceramics Through the Laser Scanning of Powder Beds." Society of Manufacturing Engineers (Technical Paper).

Dutta, Debasish, Prinz, Fritz B., Rosen, David, Weiss, Lee. (2001). "Layered Manufacturing: Current Status and Future Trends." Journal of Computing and Information Science in Engineering **1**(March): 60-71.

Faes, Matthias, Wang, Ya, Lava, P., Moens, David (2015).”Variability in the mechanical properties of laser sintered PA-12 components”. Proceedings of the 26th Annual International Solid Freeform Fabrication Symposium, Austin, Texas, USA, 10-12 August 2015: pp 847-856

Gibson, Ian (2002). Software solutions for rapid prototyping. London, Professional Engineering Pub.

Gibson, Ian, Shi, Dongping (1997). "Material properties and fabrication parameters in selective laser sintering process." Rapid Prototyping Journal **3**(4): 129-136.

Gogolewski, S. (1979). "Effect of annealing on thermal properties and crystalline structure of polyamides. Nylon 11(polyundecaneamide)." Colloid & Polymer Science **257**: 811-819.

Gogolewski, S., Czerniawska, K., Gasiorek, M. (1980). "Effect of annealing on thermal properties and crystalline structure of polyamides. Nylon 12 (polylaurolactam)." Colloid & Polymer Science **258**: 1130-1136.

Gornet, T.J, Davis, K.R, Starr, TL, Mulloy, K.M (2002).”Characterisation of selective laser sintering materials to determine proses stability”. Solid Freeform Fabrication Symposium Proceedings, pp 546-553.

Griskey, Richard G. (1995). Polymer Process Engineering. New York, USA, Chapman and Hall.

Hague, Richard, Mansour, Saeed., Saleh, Naguib. (2003a). "Design opportunities with rapid manufacturing" Assembly Automation **23**(4): 346-356.

Hague, R., Campbell, I., Dickens, P. (2003b). "Implications on Design of rapid manufacturing" Special issue paper, Proc. Instn. Mech.Engrs. Part C: Journal Mechanical Engineer Science **217**: 25-30.

Hague, R., Mansour, S., Saleh, N. (2004). "Material and design considerations for Rapid Manufacturing." International Journal of Production Research **42**(22): 4691-4708.

Hague, R., (2006). "Unlocking the Design Potential of Rapid Manufacturing" in Rapid manufacturing : an industrial revolution for the digital age, editors: Hopkinson, N., Hague R. J. M., Dickens, P.M., Chichester, England, John Wiley.

Hitt, D.J., B. Haworth, and N. Hopkinson (2011)"Fracture mechanics approach to compare laser sintered parts and Injection mouldings of Nylon -12. Proc. IMechE Part B: J. Engineering Manufacture, 225: 1663-1672.

Ho, H. C. H., Gibson, I., Cheung, W.L. (1999). "Effects of energy density on morphology and properties of selective laser sintered polycarbonate." Journal of Materials Processing Technology **89-90**: 204-210.

Hopkinson, N. and P. Dickens (2001). "Rapid prototyping for direct manufacture." Rapid Prototyping Journal **7**(4): 197-202.

Hopkinson, N. and P. Dickens (2003). "Analysis of rapid manufacturing-using layer manufacturing process for production" Proc. IMechE, Part C, Journal of Mechanical Engineering Science **217**: 31-39.

Hopkinson, N., Hague, R., Dickens, P. (2006). "Introduction to Rapid Manufacturing" in Rapid manufacturing : an industrial revolution for the digital age, editors: Hopkinson, N., Hague R. J. M., Dickens, P.M., Chichester, England, John Wiley.

Hopkinson, N., Majewski, C.E., Zarringhalam, H. (2009). "Quantifying the degree of particle melt in Selective Laser Sintering" CIRP Annals-Manufacturing Technology **58**: 197-200

Hou, Xiaonan (2005). Material models for FEA of SLS component. MPhil Thesis, University of Leeds.

Kalpakjian, Serope, Schmid, Steven R. (2006). Manufacturing Engineering and technology, 5th edition. London, Pearson Prentice Hall

Kim, J., Creasy, T.S. (2004). "Selective laser sintering characteristics of nylon 6/clay re-inforced nanocomposite" Polymer Testing **23**: 629-636

Kohan, Melvin I. (1995) Nylon Plastics Handbook. Munich, Vienna, New York, Cincinnati, Hanser Publishers Hanser/Gardner Publications, Inc.

Kolosov, S.; Vansteenkiste, G.; Boudeau, N.; Gelin, J.C.; Boillat, E,. (2006). "Homogeneity aspects in selective laser sintering (SLS)". Journal of Materials Processing Technology 177: 348-351.

Kridli, Ghassan T. (2006). "Material properties and characterization" in Rapid prototyping: Theory and practice, edited by Kamrani, Ali, Nasr, Emad Abouel, New York, N.Y., Springer.

Kruth, J. P., Leu, M.C., Nakawa, T. (1998). "Progress in Additive Manufacturing and Rapid Prototyping." CIRP Annals - Manufacturing Technology **47**(2): 525-540.

Kruth, J. P., Mercelis, P., Froyen, L., Rombouts, Marleen. (2005a). "Binding Mechanisms in Selective Laser Sintering and Selective Laser Melting". Rapid Prototyping Journal **11**(1): 26-36.

Kruth, J. P., Wang, X., Laoui, T., Froyen, L. (2003). "Lasers and materials in selective laser sintering." Assembly Automation **23**(4): 357-371.

Kruth, J. P., Vandenbroucke, B., Vaerenbergh, J.Van, Mercelis, P. (2005b). "Benchmarking of different SLS/SLM processes as rapid manufacturing techniques". International Conference Polymers and Moulds Innovations (PMI). Gent, Belgium.

Levy, G. N., Schindel, R. (2002). "Overview of layer manufacturing technologies, opportunities, options and applications for rapid tooling". Proc. Instn. Mech. Engrs **Part B**: Journal Engineering Manufacture, **216,** 1621-1633.

Levy, G. N., Schindel, Ralf, Kruth, J.P. (2003). "Rapid manufacturing and rapid tooling with layer manufacturing (LM) technologies, state of the art and future perspectives." CIRP Annals **52**(2): 589-609.

Ma, Liang; Bin, Hongzan. (2007). "Temperature and stress analysis and simulation in fractal scanning-based laser sintering". Int J Adv Manuf Technol. 34: 898-903.

Majewski, Candice; Hopkinson, Neil. (2011). "Effect of section thickness and build orientation on tensile properties and material characteristics of laser sintered nylon-12 parts". Rapid Prototyping Journal 17(3): 176-180.

Majewski, C.E.; Zarringhalam, H.; Hopkinson, N. (2008). "Effects of the degree of particle melt and crystallinity in SLS Nylon-12 parts". Proceedings of the 19th Annual International Solid Freeform Fabrication Symposium, Austin, Texas, USA, 2008: pp 45-54.

Mansour, S., Hague, R. (2003). "Impact of rapid manufacturing on design for manufacture for injection moulding" Proc. Instn. Mech.Engrs. Part B: Journal Engineering Manufacture **217**: 453-461.

Mateva, R., Delev, O., Rousseva, S. (1997). "Structure of poly-ω-dodecalactam obtained in bulk by an anionic mechanism." European Polymer Journal **33**(8): 1377-1382.

Narazaki, Michiharu and Totten, George E. (2007). Distortion of Heat-treated Components in Steel Heat Treatment, Metallurgy and Technologies (Handbook), Editor: Totten, George E, Second Edition, Boca Raton, USA CRC Press, Taylor and Francis Group.

Nelson, J.A, Galloway, G, Rennie, A. E. W., Abram, T. N (2014). "Effect of scan direction and orientation on mechanical properties of laser sintered polyamide-12". Int. Journal Advanced Design and Manufacturing Technology, Vol. 7/No.3: 19-25

Nelson, J.C. (1993). Selective laser sintering: A definition of the process and a empirical sintering model. PhD Thesis, University of Texas at Austin, USA.

Noorani, Rafiq. (2006). Rapid Prototyping: Principles and Applications. Los Angeles, CA, John Wiley & Sons, Inc.

Ostertagová, Eva, Ostertag, Oskar, (2015), Methodology and Application of Oneway ANOVA, http://pubs.sciepub.com/ajme/1/7/21/ (Accessed at 17.00 on 29 Sept 2015)

Pham, D. T. and Dimov, S. S. (2001). Rapid manufacturing : the technologies and applications of rapid prototyping and rapid tooling. London, Berlin, Heidelberg, Springer.

Pham, D. T., Ji, C., Dimov, S.S., (2004). "Layer manufacturing technologies". Proc.of the 1st International Conference on New Forming Technology (ICNFT), Harbin, China, 317-324.

Pham, D. T., Dotchev, K.D., Yusoff, W.A., (2008a). "Deterioration of polyamide powder properties in the laser sintering process." Proc. IMechE, Part C, Journal of Mechanical Engineering Science **222**: 2163-2176.

Pham, D. T.; Dotchev, K.D.; Yusoff, W.A. (2008b). "Improvement of part surface finishing in laser sintering by experimental design optimisation (DOE)." Conference.iproms.org/sites/conference.iproms/org/files/papers2007/112.pdf. accessed: 9/9/2011, at 12.40

Ramazani SA, A. and Mousavi S, S.A. (2005). "Investigation of vacuum annealing effects on physical-mechanical properties of thermoplastic parts" Materials and Design **26**: 89-93.

Rosenzweig, N. and Narkis, M. (1981). "Dimensional variations of two spherical polymeric particles during sintering". Polymer Engineering and Science, 21 (10): pp582-585

Rusenberg, S.; Schmid. H.J. (2014). "Advanced characterization method of nylon 12 materials for application in laser sinter processing" AIP conference Proceedings 1593: 713-718. DOI: 10.1063/1.4873877

Rusenberg, S, Josupeit, S and Schmid, H. (2014), "A method to characterize the Quality of a Polymer Laser Sintering Process", in Advances in Mechanical

Engineering, p7-10, Hindawi Publishing Corporation,(http:// dx.doi.org/10.1155/2014/640496)

Salmoria, G.V, Hotza, D, Klauss, P, Kanis, L.A, and Roesler, C.R.M. (2014), "Manufacturing of porous polycaprolactone prepared with different particle sizes and infrared laser sintering conditions: Microstructure and Mechanical Properties", in Advances in Mechanical Engineering, pages 7, Hindawi Publishing Corporation, 2014. (http:// dx.doi.org/10.1155/2014/640496)

Scobbo Jr, J. J. and Hwang, C.R. (1994). "Annealing Effects in Poly(Phenylene Sulfide) as Observed by Dynamic Mechanical Analysis." Polymer Engineering and Science 34(23).

Shi, Y., Chen, J., Wang, Y., Li, Z., Huang, S. (2007). "Study of selective laser sintering of polycarbonate and postprocess for parts reinforcement." Proc. IMechE, Part L, Journal of Materials: Design and Applications **22**: 37-42.

Shi, Y., Li, Z., Sun, H., Huang, S., Zeng, F. (2004). "Effect of the properties of the polymer materials on the quality of selective laser sintering parts." Proc. Instn. Mech. Engnr Part L, Journal of Materials: Design and Applications **218**(3): 247-252.

Stamp, R.; Fox, P.; O'neill, W.; Jones, E.; Sutcliffe, C. (2009). "The development of a scanning strategy for the manufacture of porous biomaterials by selective laser melting". J Mater Sci: Mater Med 20: 1839- 1848.

Technopro, Energy (2009). Vacuum Furnace, available online from: http:/www.energytechpro.com/Demo-IC/Gas_Technology/ Heat_Treat_Vacuum.htm [Accessed 24/08/2009]

Tolochko, N.K., Khlopkov, Y.V., Mozzharov, S.E., Ignatiev, M.B., Laoui, T., Titov, V.I. (2000). "Absorptance of powder materials suitable for laser sintering." Rapid Prototyping Journal **6**(3): 155-161.

Tontowi, Alva. E., Childs, T. H. C. (2001). "Density prediction of crystalline polymer sintered parts at various powder bed temperatures" Rapid Prototyping Journal **7**(3): 180-184.

Totten, George E. (2006). Steel Heat Treatment, Equipment and Process Design. Boca Raton, USA, FL: Taylor and Francis.

Tregub, Alexander, Harel, Hannah, Marom, Gad (1993). "The influence of thermal history on the mechanical properties of poly(ether ether ketone) matrix composite materials." Composites Science and Technology **48**: 185-190.

Upcraft, S. and R. Fletcher (2003). "The rapid protoyping technologies." Assembly Automation **23**(4): 318-330.

Venuvinod, Patri K., Ma, Weiyin (2004). Rapid Prototyping: Laser-based and other technologies. Norwell, Kluwer Academic Publishers.

Wikipedia, (2009a). Rapid manufacturing, definition, available online: http://en.wikipedia.org/wiki/Rapid_manufacturing. [Accessed July, 2009].

Wikipedia. (2009b). Selective laser sintering, definition, available online: http://en.wikipedia.org/wiki/Selective_laser_sintering [Accessed July, 2009].

Williams, A.N. (1994). Schaum's outline of theory and problems of strength of materials, Third Edition, McGraw-Hill, New York, USA.

Williams, John D.; Deckard, Carl R. (1998). "Advances in modelling the effects of selected parameters on the SLS process". Rapid Prototyping Journal 4(2): 90-100.

Wohlers, T.T. (2006), Wohler Reports 2006: Rapid Prototyping and Manufacturing State of the Industry, Fort Collins, Co, USA: Wohlers Associates.

Wunderlich, Bernhard. (1976). Macromolecular Physics: Crystal Nucleation, Growth, Annealing. New York, San Fransisco, London, Academic Press.

Wunderlich, Bernhard (1980). Macromolecular Physics: Crystal Melting. New York, London, Toronto, Sydney, San Fransisco, Academic Press.

Yadroitsev, I.; Bertrand, Ph.; Smurov, I. (2007). "Parametric analysis of the selective laser melting process". Applied Surface Science 253: 8064- 8069.

Yang, J., Bin, H., Zhang, X, Liu, Z., (2003). "Fractal scanning path generation and control system for selective laser sintering (SLS)". International Journal of Machine Tools and Manufacture 43: 293-300.

Young, R. J. (1983). Introduction to polymers. London ; New York, Chapman and Hall.

Yubero, Victor (2004). Development of material model for selective laser sintering components. Final report: MECH 3810 Individual Project, University of Leeds.

Yusoff, W.A.Y.; Thomas, A.J. (2008). "The effect of employing an effective laser sintering scanning strategy and energy density value on eliminating "orange peel" on a selective laser sintered part". International Association for Management of Technology. IAMOT 2008 Proceeding

Zarringhalam, H. and N. Hopkinson (2003). "Post-Processing of Duraform^{TM} Parts for Rapid Manufacture". Solid Freeform Fabrication Symposium, Austin, Texas, USA.

Zarringhalam, H., Hopkinson, N., Kamperman, N.F., Vlieger, J.J. de. (2006). "Effects of processing on microstructure and properties of SLS Nylon 12." Materials Science and Engineering A **435-436**: 172-180.

Zarringhalam, H. (2007). "Investigation into Crystallinity and Degree of Particle Melt in Selective Laser Sintering". Doctoral Thesis, Loughborough University.

Zarringhalam, H., Majewski, C., Hopkinson, Neil. (2009). "Degree of particle melt in Nylon-12 selective laser-sintered parts." Rapid Prototyping Journal **15**(2): 126-132.

A: SHEAR AND BENDING TEST RESULTS

Three-point bending:

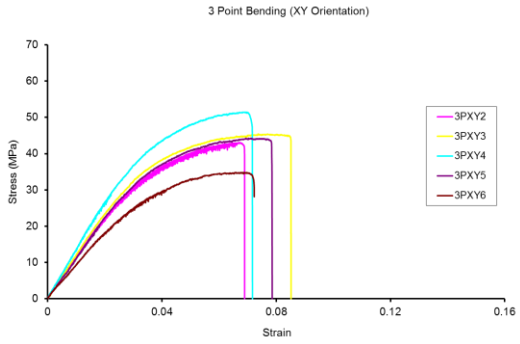

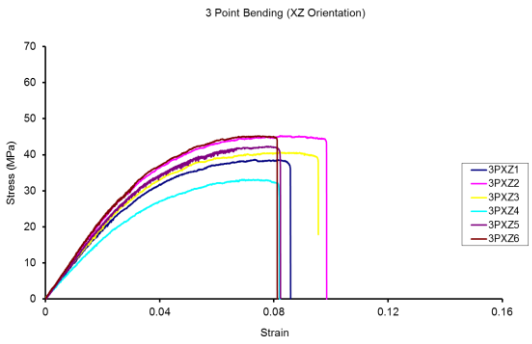

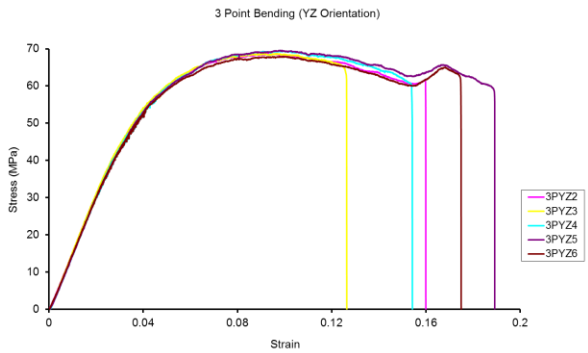

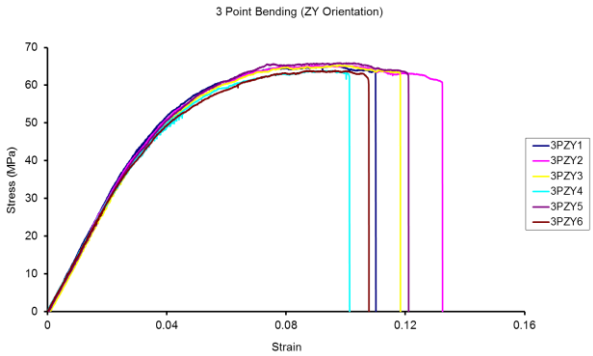

Four-point bending:

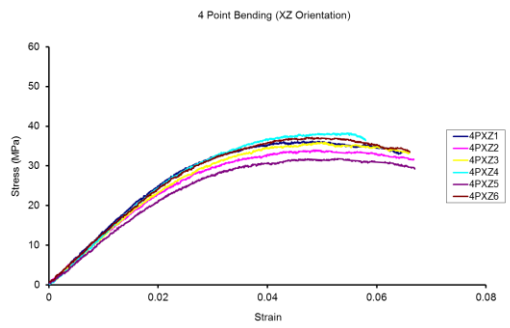

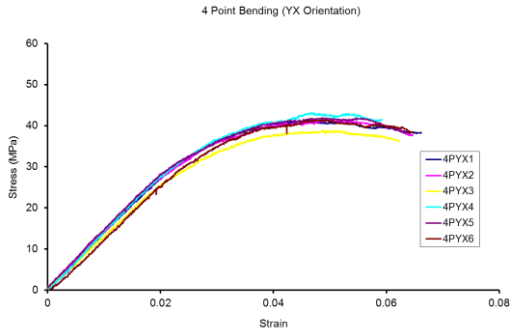

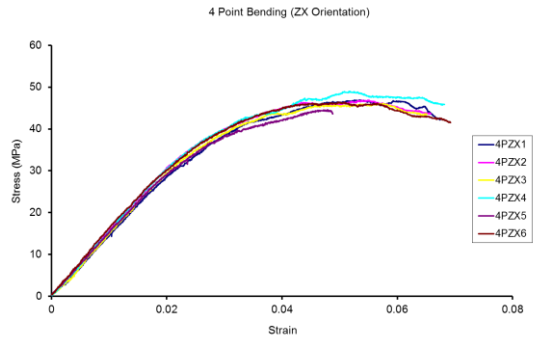

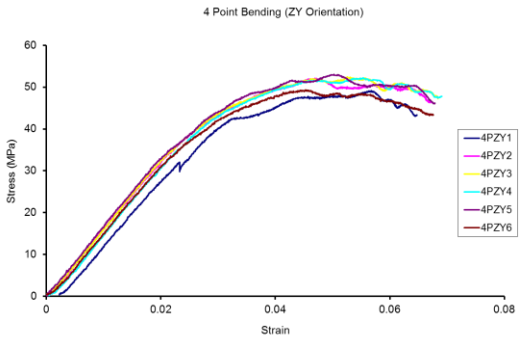

Shear Test:

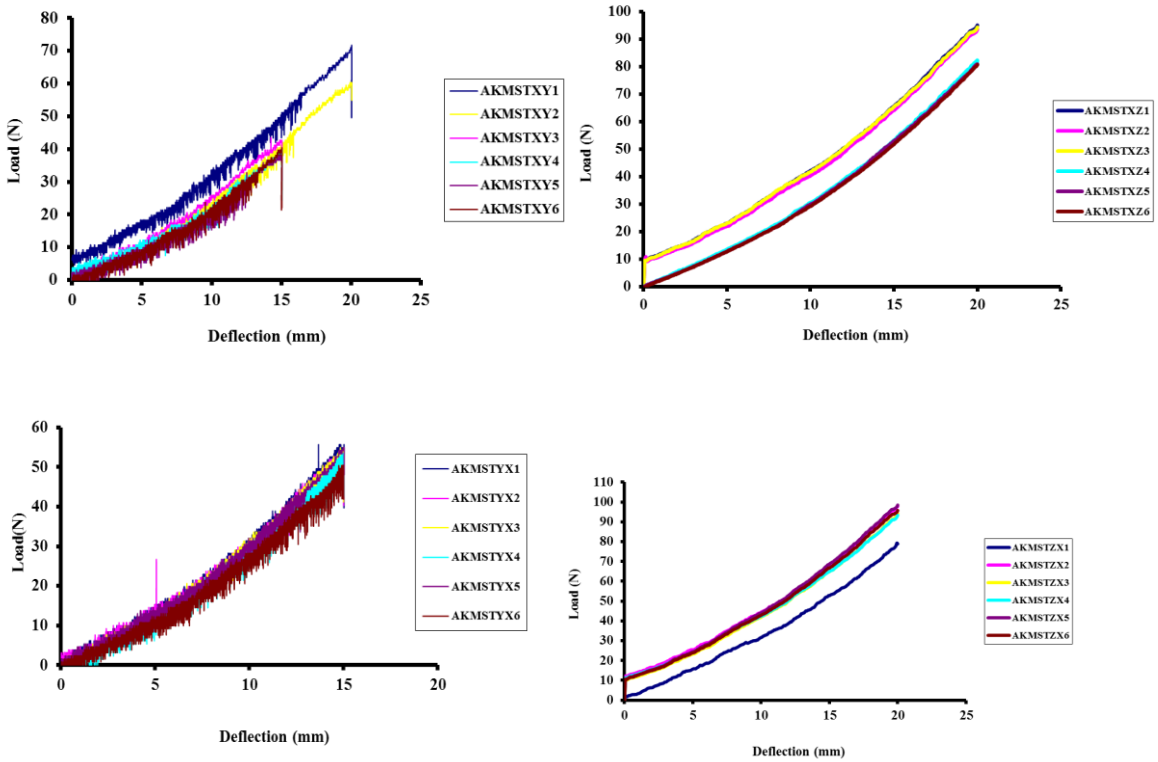
Load (N)
Deflection (mm)
AKMSTXY1
AKMSTXY2
AKMSTXY3
AKMSTXY4
AKMSTXY5
AKMSTXY6
Load (N)
Deflection (mm)
AKMSTXZ1
AKMSTXZ2
AKMSTXZ3
AKMSTXZ4
AKMSTXZ5
AKMSTXZ6
Load(N)
Deflection (mm)
AKMSTYX1
AKMSTYX2
AKMSTYX3
AKMSTYX4
AKMSTYX5
AKMSTYX6
Load (N)
Deflection (mm)
AKMSTZX1
AKMSTZX2
AKMSTZX3
AKMSTZX4
AKMSTZX5
AKMSTZX6

B: ANOVA RESULTS

CHAPTER 4

A. Tensile Strength

One-way ANOVA: TStrength - X, TStrength - Y, TStrength - Z

Analysis of Variance

Source	DF	Adj SS	Adj MS	F-Value	P-Value
Factor	2	446.12	223.058	48.14	0.000
Error	14	64.87	4.633		
Total	16	510.98			

B. Tensile Modulus

One-way ANOVA: T Mod - X, T Mod - Y, T Mod - Z

Analysis of Variance

Source	DF	Adj SS	Adj MS	F-Value	P-Value
Factor	2	76580	38290	19.14	0.000
Error	14	28005	2000		
Total	16	104585			

C. Tensile Elongation at Break

One-way ANOVA: T Elong - X, T Elong - Y, T Elong - Z

Analysis of Variance

Source	DF	Adj SS	Adj MS	F-Value	P-Value
Factor	2	38.29	19.146	12.05	0.001
Error	14	22.25	1.589		
Total	16	60.54			

D. Compression Modulus

One-way ANOVA: C Mod - X, C Mod - Y, C Mod - Z

Analysis of Variance

Source	DF	Adj SS	Adj MS	F-Value	P-Value
Factor	2	189800	94900	4.18	0.036
Error	15	340281	22685		
Total	17	530081			

E. Shear Modulus

One-way ANOVA: Shear Mod - , Shear Mod - , Shear Mod - , Shear Mod - , ...

Analysis of Variance

Source	DF	Adj SS	Adj MS	F-Value	P-Value
Factor	5	0.13166	0.026332	9.97	0.000
Error	30	0.07920	0.002640		
Total	35	0.21087			

F. 3Point Flexural Modulus

One-way ANOVA: 3 P Flex Mod, 3 P Flex Mod, 3 P Flex Mod, 3 P Flex Mod,

Analysis of Variance

Source	DF	Adj SS	Adj MS	F-Value	P-Value
Factor	5	1200768	240154	16.16	0.000
Error	29	431093	14865		
Total	34	1631862			

G. 4Point Flexural Modulus

One-way ANOVA: 4 P Flex Mod, 4 P Flex Mod, 4 P Flex Mod, 4 P Flex Mod, ...

Analysis of Variance

Source	DF	Adj SS	Adj MS	F-Value	P-Value
Factor	5	667683	133537	24.98	0.000
Error	30	160387	5346		
Total	35	828071			

CHAPTER 5

A. Tensile Strength:

A.1. Heat treatment in Air, 140°C, 2 hours

One-way ANOVA: TX2, TXht-2

Source	DF	SS	MS	F	P
Factor	1	18.3	18.3	0.68	0.430
Error	10	269.6	27.0		
Total	11	287.9			

One-way ANOVA: TY2, TYht-2

Source	DF	SS	MS	F	P
Factor	1	7.21	7.21	1.92	0.196
Error	10	37.59	3.76		
Total	11	44.80			

One-way ANOVA: TZ2, TZht-2

Source	DF	SS	MS	F	P
Factor	1	46.53	46.53	4.82	0.053
Error	10	96.49	9.65		
Total	11	143.02			

A.2. Heat treatment in Vacuum, 180°C, 100 hours

One-way ANOVA: TY100, TYht-100

Source	DF	SS	MS	F	P
Factor	1	108.8	108.8	3.38	0.096
Error	10	321.5	32.2		
Total	11	430.3			

A.3. Heat treatment in Vacuum, 180°C, 16 hours

One-way ANOVA: TY16, TYht-16

Source	DF	SS	MS	F	P
Factor	1	4.54	4.54	2.22	0.167
Error	10	20.45	2.05		
Total	11	25.00			

B. Tensile Modulus:

B.1. Heat treatment in Air, 140°C, 2 hours

One-way ANOVA: MoX2, MoXht-2

Source	DF	SS	MS	F	P
Factor	1	3560	3560	0.87	0.374
Error	10	41092	4109		
Total	11	44652			

One-way ANOVA: MoY2, MoYht-2

Source	DF	SS	MS	F	P
Factor	1	3496	3496	2.16	0.172
Error	10	16182	1618		
Total	11	19678			

One-way ANOVA: MoZ2, MoZht-2

Source	DF	SS	MS	F	P
Factor	1	15827	15827	14.38	0.004
Error	10	11007	1101		
Total	11	26834			

B.2. Heat treatment in Vacuum, 180°C, 100 hours

One-way ANOVA: MoY100, MoYht-100

Source	DF	SS	MS	F	P
Factor	1	154576	154576	11.91	0.006
Error	10	129818	12982		
Total	11	284394			

B.3 Heat treatment in Vacuum, 180°C, 16 hours

One-way ANOVA: MoY16, MoYht-16

Source	DF	SS	MS	F	P
Factor	1	675	675	0.59	0.460
Error	10	11440	1144		
Total	11	12115			

Elongation at Break

C.3 Elongation at break, 140C, 2 hours

One-way ANOVA: Elong. X2, Elong.Xht-2

Analysis of Variance

Source	DF	Seq SS	Contribution	Adj SS	Adj MS	F-Value	P-Value
Factor	1	0.8533	3.22%	0.8533	0.8533	0.33	0.577
Error	10	25.6333	96.78%	25.6333	2.5633		
Total	11	26.4867	100.00%				

One-way ANOVA: Elong. Y2, Elong.Yht-2

Analysis of Variance

Source	DF	Seq SS	Contribution	Adj SS	Adj MS	F-Value	P-Value
Factor	1	0.3008	13.26%	0.3008	0.3008	1.53	0.245
Error	10	1.9683	86.74%	1.9683	0.1968		
Total	11	2.2692	100.00%				

One-way ANOVA: Elong. Z2, Elong.Zht-2

Analysis of Variance

Source	DF	Seq SS	Contribution	Adj SS	Adj MS	F-Value	P-Value
Factor	1	0.7008	3.21%	0.7008	0.7008	0.33	0.577
Error	10	21.1217	96.79%	21.1217	2.1122		
Total	11	21.8225	100.00%				

C.4 Elongation at break, 180C, 100 hours

One-way ANOVA: Elong. Y100, Elong.Yht-100

Analysis of Variance

Source	DF	Seq SS	Contribution	Adj SS	Adj MS	F-Value	P-Value
Factor	1	2.901	21.70%	2.901	2.901	2.77	0.127
Error	10	10.468	78.30%	10.468	1.047		
Total	11	13.369	100.00%				

C.5.Elongation at break, 180C, 16 hours

One-way ANOVA: Elong.Y16, Elong.Yht-16

Analysis of Variance

Source	DF	Seq SS	Contribution	Adj SS	Adj MS	F-Value	P-Value
Factor	1	6.163	16.31%	6.163	6.163	1.95	0.193
Error	10	31.637	83.69%	31.637	3.164		
Total	11	37.800	100.00%				

D. Crystallinity:

D.1. Heat treatment in Air, 140^{o}C, 2 hours

One-way ANOVA: CX-08, CX140-120-08

Source	DF	SS	MS	F	P
Factor	1	1.307	1.307	1.68	0.224
Error	10	7.763	0.776		
Total	11	9.069			

One-way ANOVA: CY-08, CY140-120-08

Source	DF	SS	MS	F	P
Factor	1	2.55	2.55	1.37	0.269
Error	10	18.59	1.86		
Total	11	21.14			

One-way ANOVA: CZ-08, CZ140-120-08

Source	DF	SS	MS	F	P
Factor	1	12.81	12.81	3.60	0.087
Error	10	35.61	3.56		
Total	11	48.42			

D.2. Heat treatment in Vacuum, 180°C, 100 hours

One-way ANOVA: CY100, CYht-100

Source	DF	SS	MS	F	P
Factor	1	7.21	7.21	2.17	0.172
Error	10	33.24	3.32		
Total	11	40.45			

D.3. Heat treatment in Vacuum, 180°C, 16 hours

One-way ANOVA: CY16, CYht-16

Source	DF	SS	MS	F	P
Factor	1	14.02	14.02	13.80	0.004
Error	10	10.16	1.02		
Total	11	24.17			

E. Melting Peak Temperature:

E.1. Heat treatment in Air, 140°C, 2 hours

One-way ANOVA: MX-08, MX140-120-08

Source	DF	SS	MS	F	P
Factor	1	1.300	1.300	1.55	0.241
Error	10	8.382	0.838		
Total	11	9.682			

One-way ANOVA: MY-08, MY140-120-08

Source	DF	SS	MS	F	P
Factor	1	0.051	0.051	0.09	0.765
Error	10	5.379	0.538		
Total	11	5.430			

One-way ANOVA: MZ-08, MZ140-120-08

Source	DF	SS	MS	F	P
Factor	1	1.96	1.96	1.69	0.223
Error	10	11.60	1.16		
Total	11	13.56			

E.2. Heat treatment in Vacuum, 180°C, 100 hours

One-way ANOVA: MY100, MYht-100

Source	DF	SS	MS	F	P
Factor	1	31.98	31.98	24.54	0.001
Error	10	13.03	1.30		
Total	11	45.01			

E.3. Heat treatment in Vacuum, 180°C, 16 hours

One-way ANOVA: MY16, MYht-16

Source	DF	SS	MS	F	P
Factor	1	3.070	3.070	13.20	0.005
Error	10	2.327	0.233		
Total	11	5.397			

CHAPTER 6

A. Effect of section thickness on Tensile Strength
One-way ANOVA: 1mm (w/o HT), 2mm (w/o HT), 3mm (w/o HT), Solid (w/o HT)

Source	DF	SS	MS	F	P
Factor	3	2229.92	743.31	236.75	0.000
Error	19	59.65	3.14		
Total	22	2289.57			

B. Effect of heat treatment on Tensile Strength

One-way ANOVA: 1mm (w/o HT), 1mm (HT), 2mm (w/o HT), 2mm (HT), ...

Source	DF	SS	MS	F	P
Factor	7	4493.59	641.94	308.39	0.000
Error	38	79.10	2.08		
Total	45	4572.69			

A. Effect of section thickness on Tensile Modulus
One-way ANOVA: 1mm (w/o HT)_1, 2mm (w/o HT)_1, 3mm (w/o HT)_1, Solid (w/o HT)_1

Source	DF	SS	MS	F	P
Factor	3	1771458	590486	192.62	0.000
Error	19	58245	3066		
Total	22	1829704			

B. Effect of heat treatment on Tensile Modulus
One-way ANOVA: 1mm (w/o HT), 1mm (HT)_1, 2mm (w/o HT), 2mm (HT)_1, ...

Source	DF	SS	MS	F	P
Factor	7	3732995	533285	150.87	0.000
Error	38	134320	3535		
Total	45	3867316			

A. Effect of section thickness on Crystallinity (sintered)
One-way ANOVA: 1mm (w/o HT), 2mm (w/o HT), 3mm (w/o HT), Solid (w/o HT)

Source	DF	SS	MS	F	P
Factor	3	13.40	4.47	2.41	0.097
Error	20	37.09	1.85		
Total	23	50.50			

One-way ANOVA: 1mm (HT), 2mm (HT), 3mm (HT), Solid (HT)

Source	DF	SS	MS	F	P
Factor	3	25.01	8.34	3.86	0.025
Error	20	43.18	2.16		
Total	23	68.19			

B. Effect of heat treatment on Crystallinity (sintered)
One-way ANOVA: 1mm (w/o HT), 1mm (HT), 2mm (w/o HT), 2mm (HT), ...

Source	DF	SS	MS	F	P
Factor	7	232.46	33.21	16.55	0.000
Error	40	80.27	2.01		
Total	47	312.73			

A. Effect of section thickness on Crystallinity (un-sintered)
One-way ANOVA: 1mm (w/o HT)_1, 2mm (w/o HT)_1, 3mm (w/o HT)_1

Source	DF	SS	MS	F	P
Factor	2	20.69	10.34	6.41	0.010
Error	15	24.21	1.61		
Total	17	44.90			

B. Effect of heat treatment on Crystallinity (un-sintered)
One-way ANOVA: 1mm (w/o HT), 1mm (HT)_1, 2mm (w/o HT), 2mm (HT)_1, ...

Source	DF	SS	MS	F	P
Factor	5	54.66	10.93	4.40	0.004
Error	29	72.07	2.49		
Total	34	126.73			

A. Effect of section thickness on Melting Peak Temperature (sintered)
One-way ANOVA: 1mm (w/o HT)_2, 2mm (w/o HT)_2, 3mm (w/o HT)_2, Solid (w/o HT)_1

Source	DF	SS	MS	F	P
Factor	3	65.289	21.763	33.12	0.000
Error	20	13.140	0.657		
Total	23	78.429			

One-way ANOVA: 1mm (HT)_2, 2mm (HT)_2, 3mm (HT)_2, Solid (HT)_1

Source	DF	SS	MS	F	P
Factor	3	154.34	51.45	21.60	0.000
Error	20	47.63	2.38		
Total	23	201.97			

B. Effect of heat treatment on Melting Peak Temperature (sintered)
One-way ANOVA: 1mm (w/o HT), 1mm (HT)_2, 2mm (w/o HT), 2mm (HT)_2, ...

Source	DF	SS	MS	F	P
Factor	7	761.73	108.82	71.63	0.000
Error	40	60.77	1.52		
Total	47	822.50			

A. Effect of section thickness on Melting Peak Temperature (un-sintered)
One-way ANOVA: 1mm (w/o HT)_3, 2mm (w/o HT)_3, 3mm (w/o HT)_3

Source	DF	SS	MS	F	P
Factor	2	0.092	0.046	0.21	0.812
Error	15	3.267	0.218		
Total	17	3.359			

One-way ANOVA: 1mm (HT)_3, 2mm (HT)_3, 3mm (HT)_3

Source	DF	SS	MS	F	P
Factor	2	16.39	8.19	6.59	0.010
Error	14	17.41	1.24		
Total	16	33.80			

B. Effect of heat treatment on Melting Peak Temperature (un-sintered)
One-way ANOVA: 1mm (w/o HT), 1mm (HT)_3, 2mm (w/o HT), 2mm (HT)_3, ...

Source	DF	SS	MS	F	P
Factor	5	140.752	28.150	39.48	0.000
Error	29	20.677	0.713		
Total	34	161.429			

Effect of open and closed hollow structure (2 mm) on Tensile Strength

One-way ANOVA: 2mm (powder), 2mm (w/o powder)

Source	DF	SS	MS	F	P
Factor	1	15.05	15.05	3.45	0.093
Error	10	43.63	4.36		
Total	11	58.68			

Effect of open and closed hollow structure (2 mm) on Tensile Modulus

One-way ANOVA: 2mm (powder)_1, 2mm (w/o powder)_1

Source	DF	SS	MS	F	P
Factor	1	40102	40102	7.22	0.023
Error	10	55539	5554		
Total	11	95641			

C: DSC TEST RESULTS

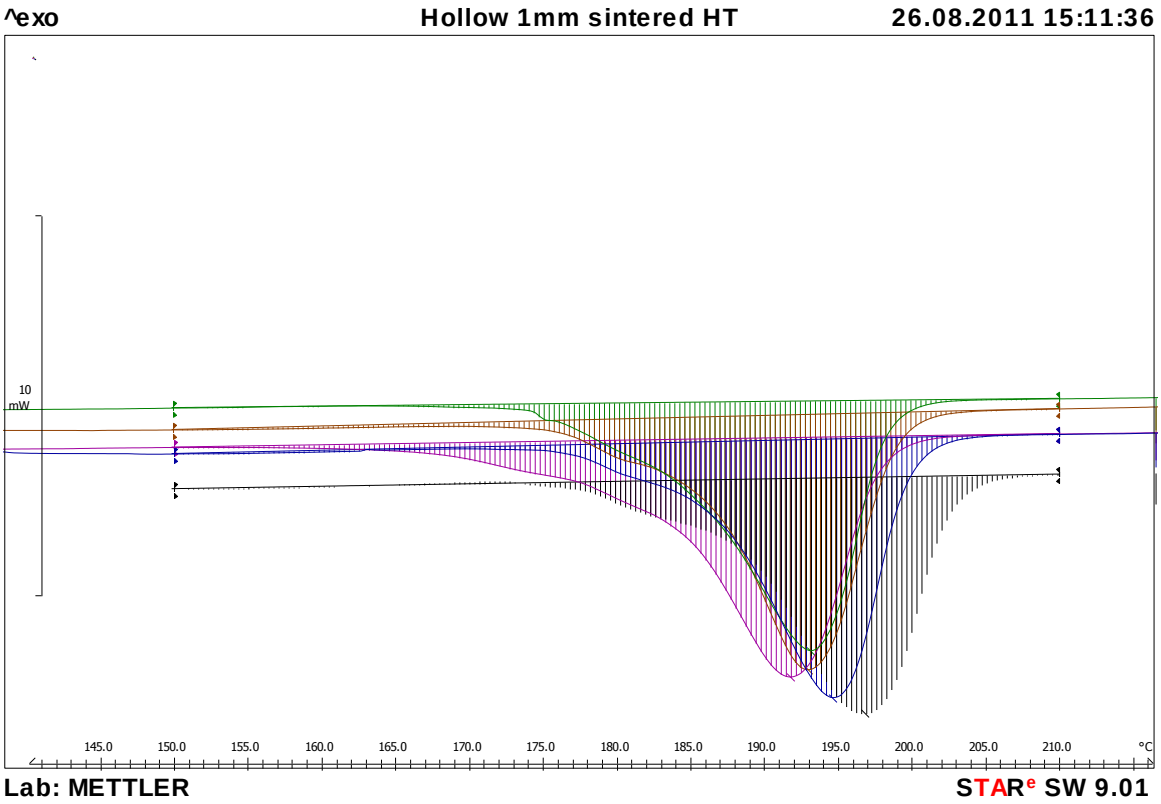

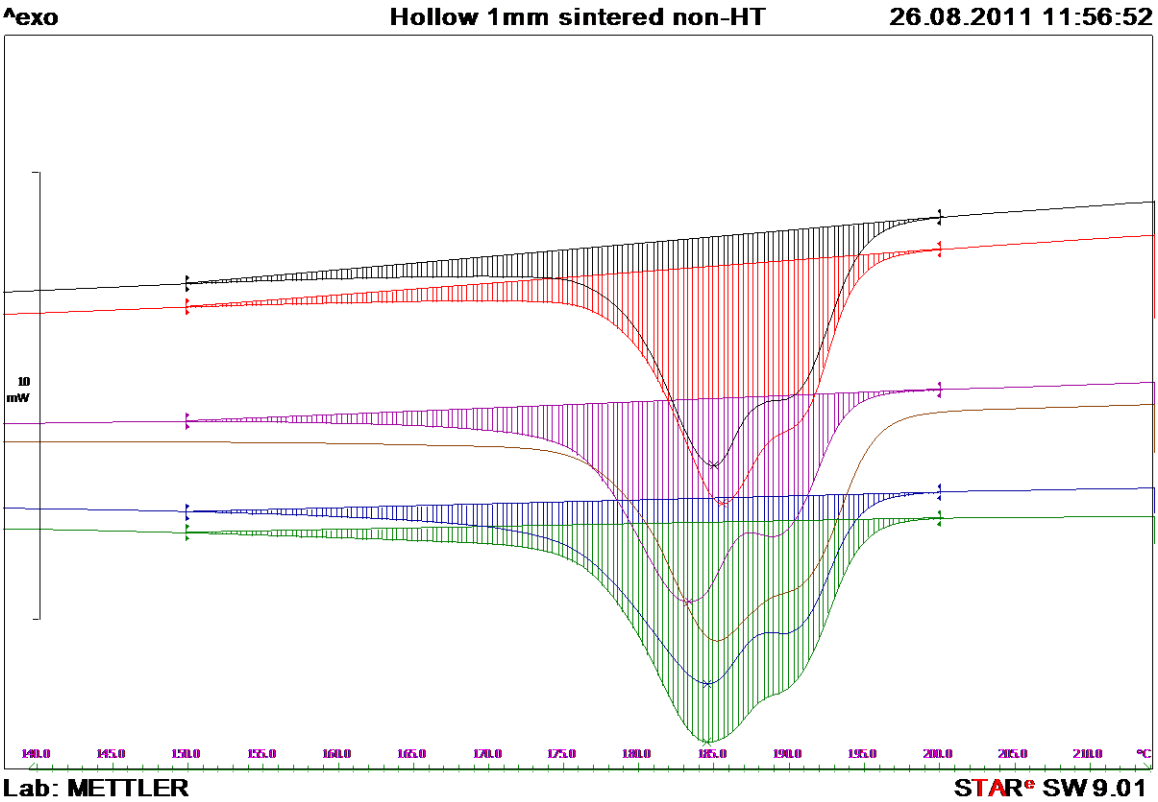

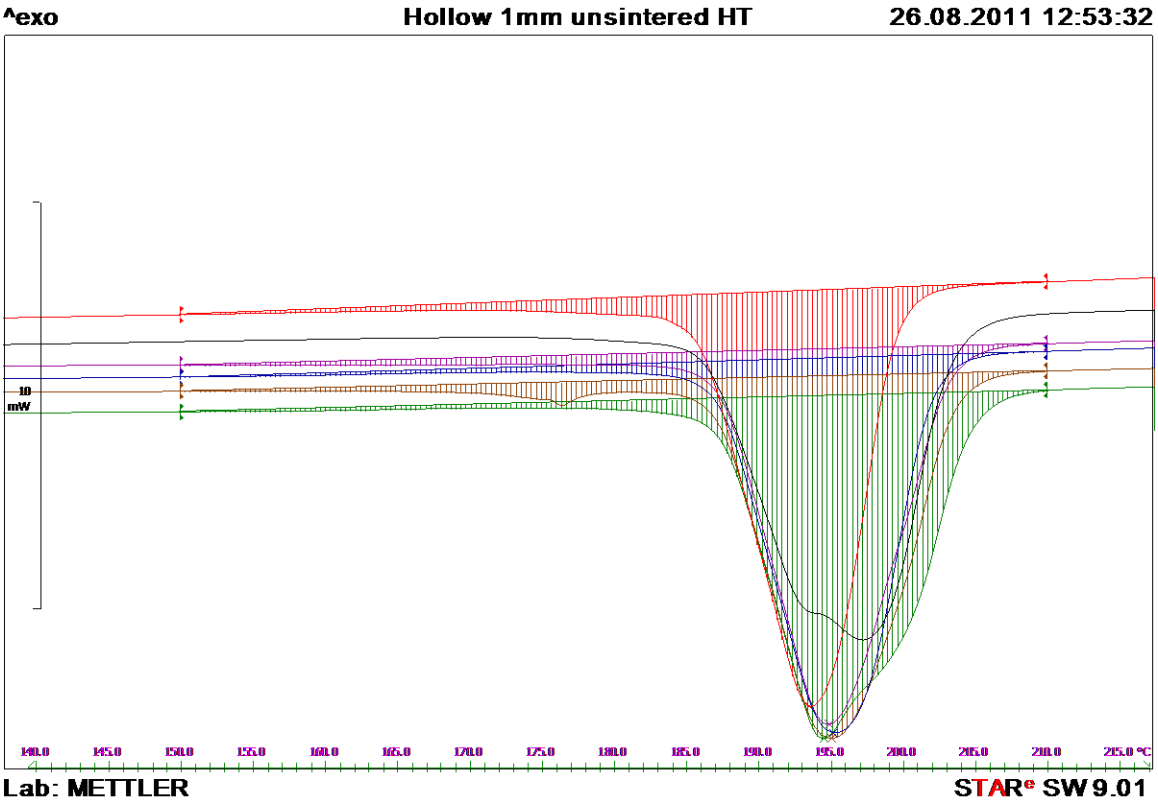
^exo
Hollow 1mm unsintered HT
26.08.2011 12:53:32
10
mW
140.0 145.0 150.0 155.0 160.0 165.0 170.0 175.0 180.0 185.0 190.0 195.0 200.0 205.0 210.0 215.0 °C
Lab: METTLER
STARe SW 9.01

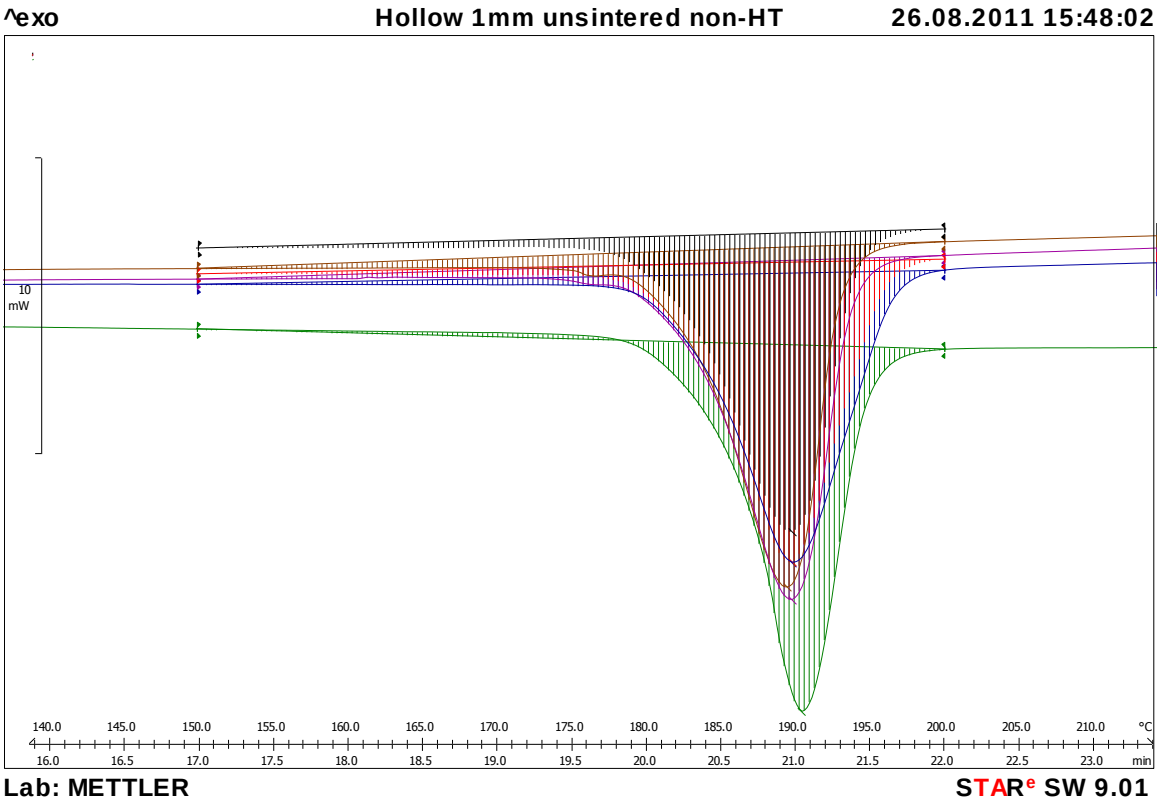
^exo
Hollow 1mm unsintered non-HT
26.08.2011 15:48:02
10
mW
140.0 145.0 150.0 155.0 160.0 165.0 170.0 175.0 180.0 185.0 190.0 195.0 200.0 205.0 210.0 °C
16.0 16.5 17.0 17.5 18.0 18.5 19.0 19.5 20.0 20.5 21.0 21.5 22.0 22.5 23.0 min
Lab: METTLER
STARe SW 9.01

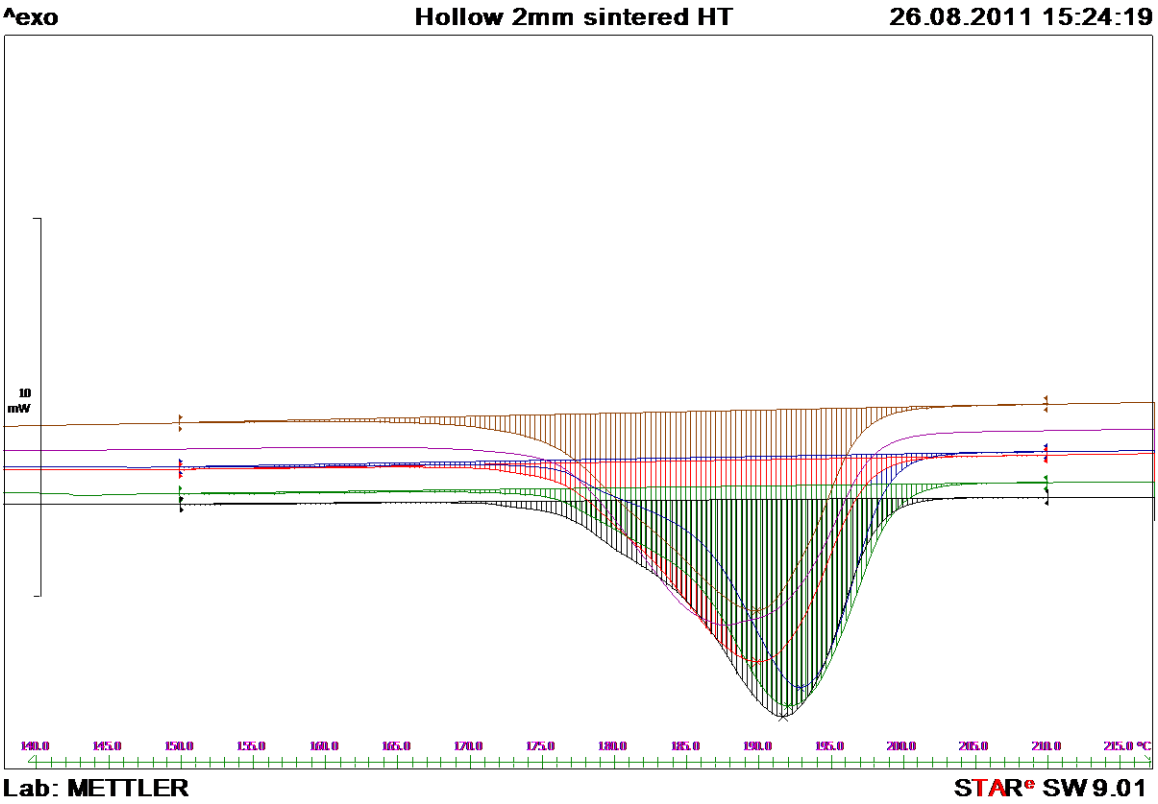
^exo
Hollow 2mm sintered HT
26.08.2011 15:24:19
10
mW
Lab: METTLER
STARe SW 9.01

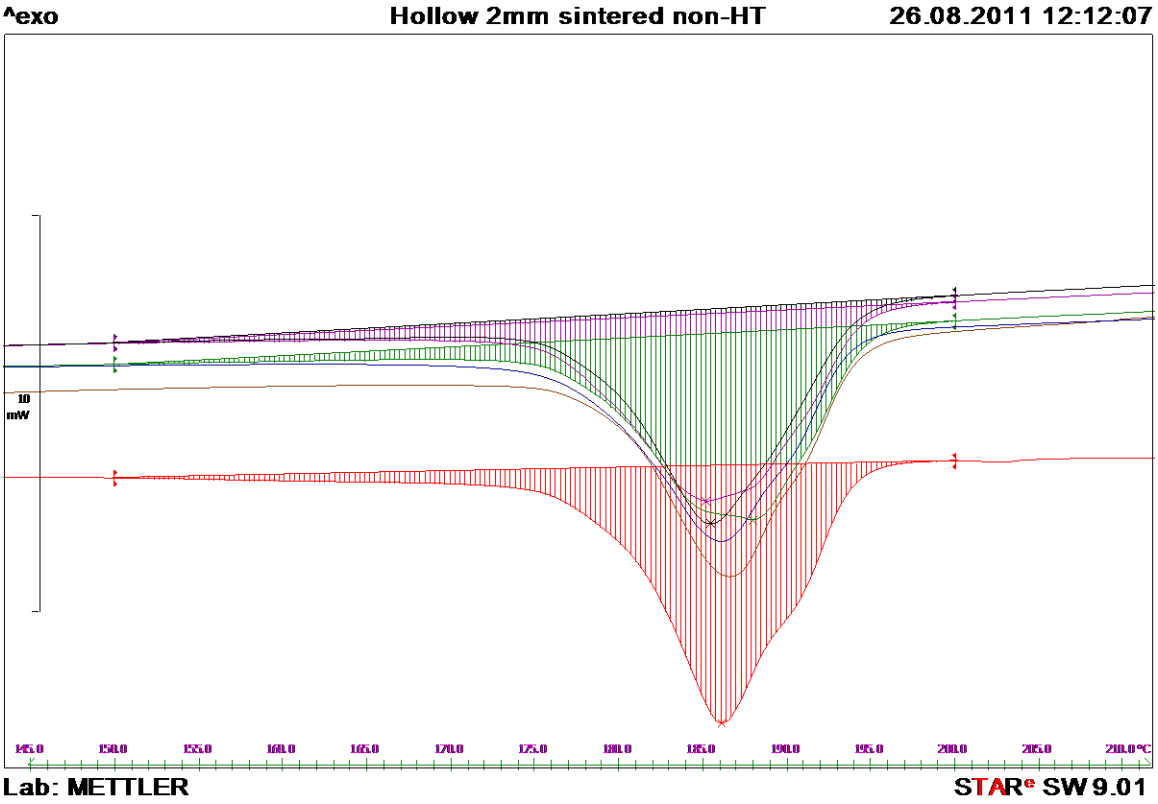
^exo
Hollow 2mm sintered non-HT
26.08.2011 12:12:07
10
mW
Lab: METTLER
STARe SW 9.01

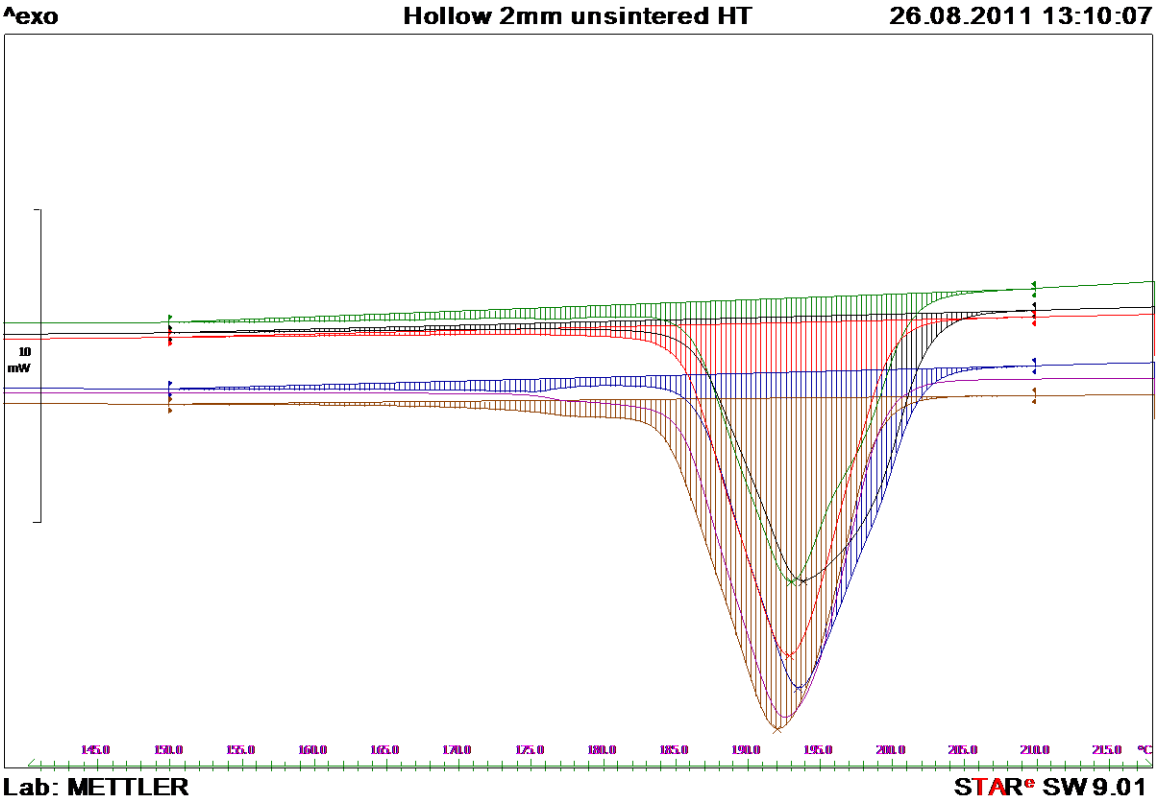
^exo
Hollow 2mm unsintered HT
26.08.2011 13:10:07
10
mW
Lab: METTLER
STARe SW 9.01

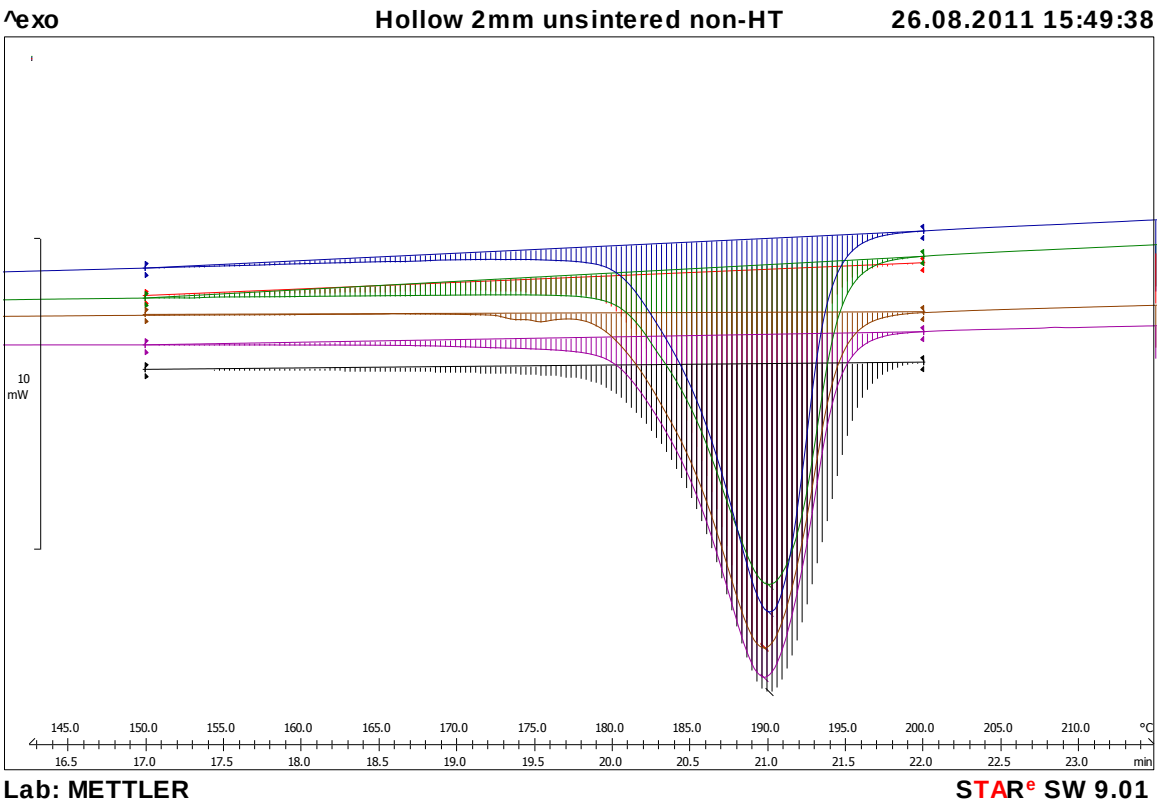
^exo
Hollow 2mm unsintered non-HT
26.08.2011 15:49:38
10
mW
145.0 150.0 155.0 160.0 165.0 170.0 175.0 180.0 185.0 190.0 195.0 200.0 205.0 210.0 °C
16.5 17.0 17.5 18.0 18.5 19.0 19.5 20.0 20.5 21.0 21.5 22.0 22.5 23.0 min
Lab: METTLER
STARe SW 9.01

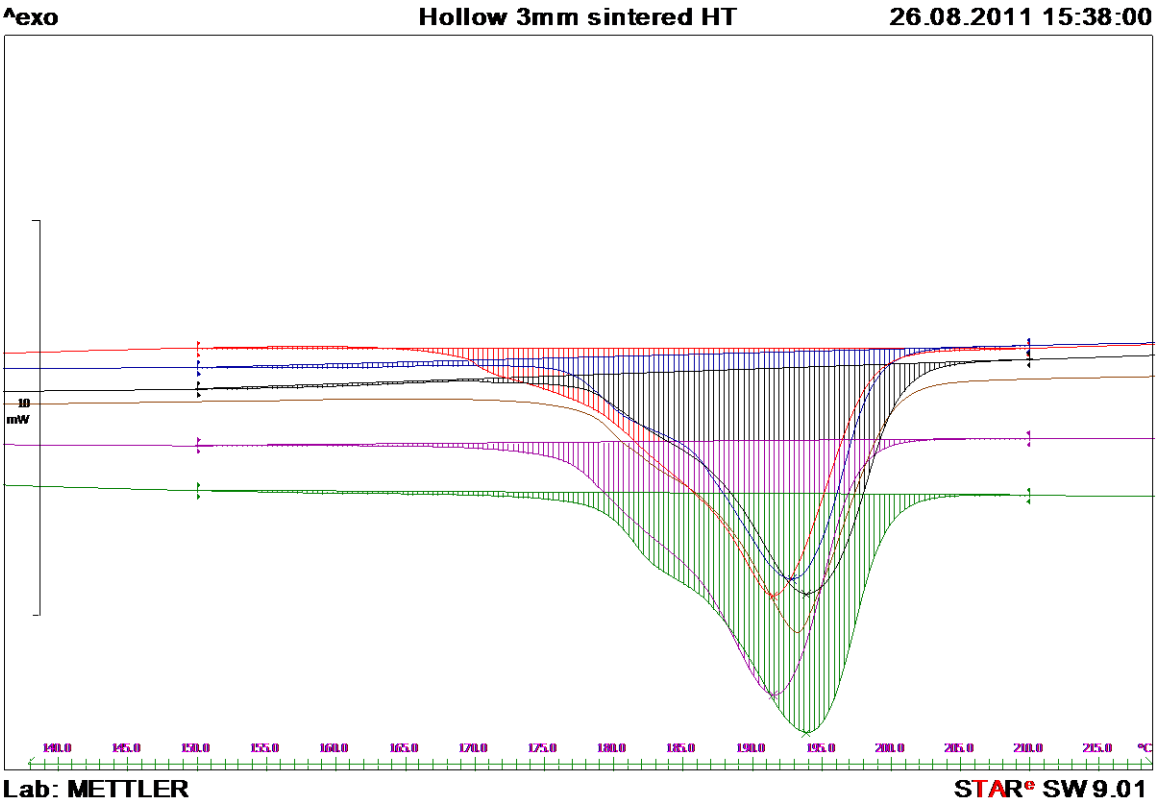
^exo
Hollow 3mm sintered HT
26.08.2011 15:38:00
10
mW
Lab: METTLER
STARe SW 9.01

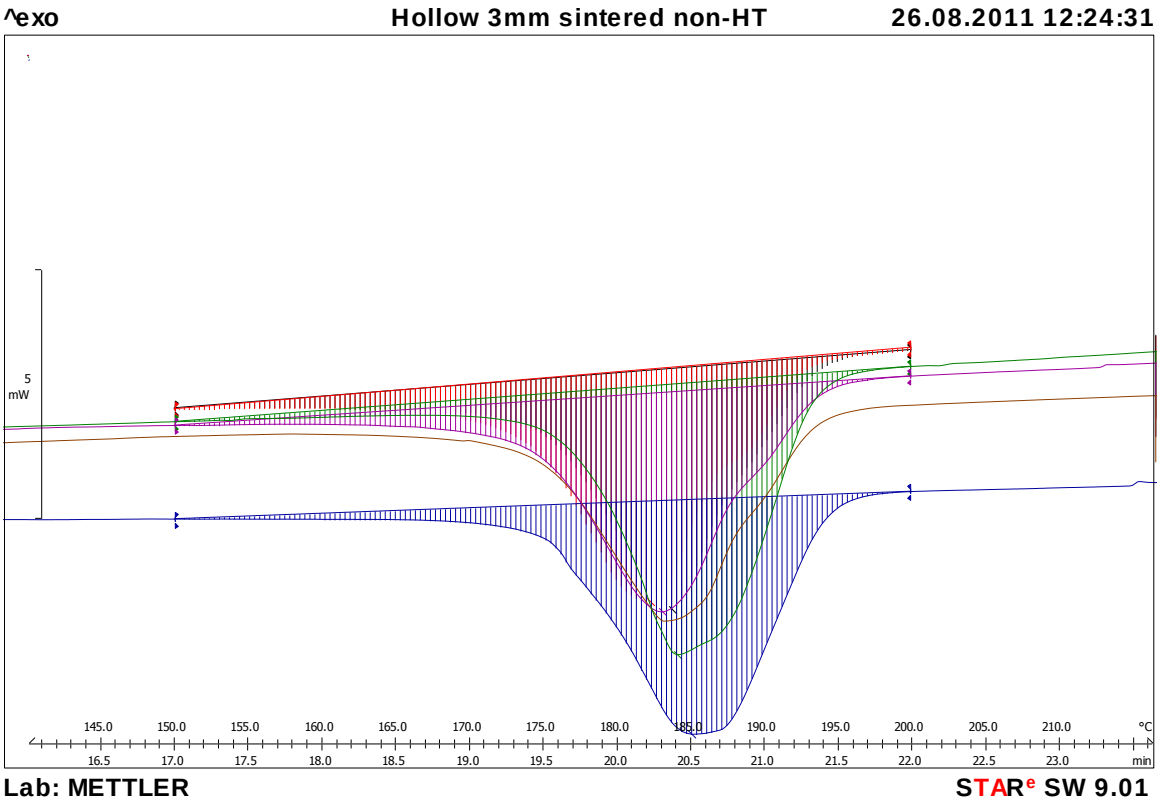
^exo
Hollow 3mm sintered non-HT
26.08.2011 12:24:31
5
mW
145.0 150.0 155.0 160.0 165.0 170.0 175.0 180.0 185.0 190.0 195.0 200.0 205.0 210.0 °C
16.5 17.0 17.5 18.0 18.5 19.0 19.5 20.0 20.5 21.0 21.5 22.0 22.5 23.0 min
Lab: METTLER
STARe SW 9.01

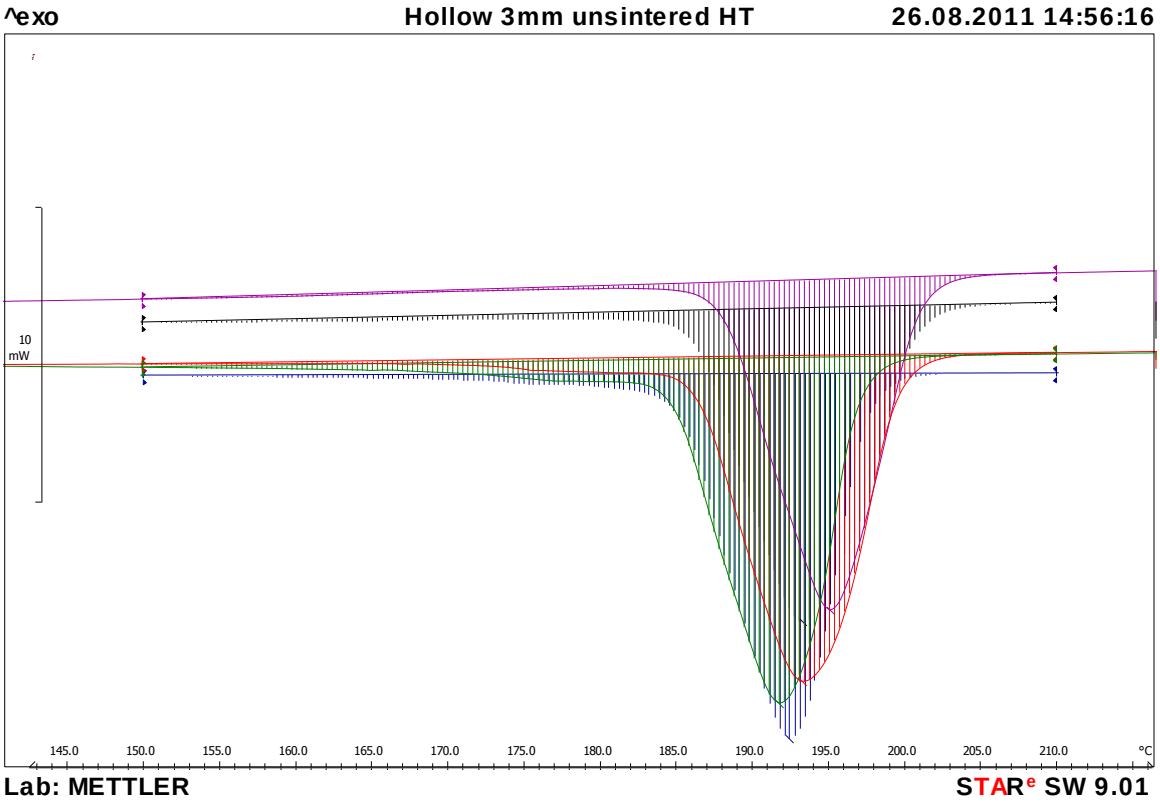
^exo
Hollow 3mm unsintered HT
26.08.2011 14:56:16
10
mW
145.0
150.0
155.0
160.0
165.0
170.0
175.0
180.0
185.0
190.0
195.0
200.0
205.0
210.0
°C
Lab: METTLER
STARe SW 9.01

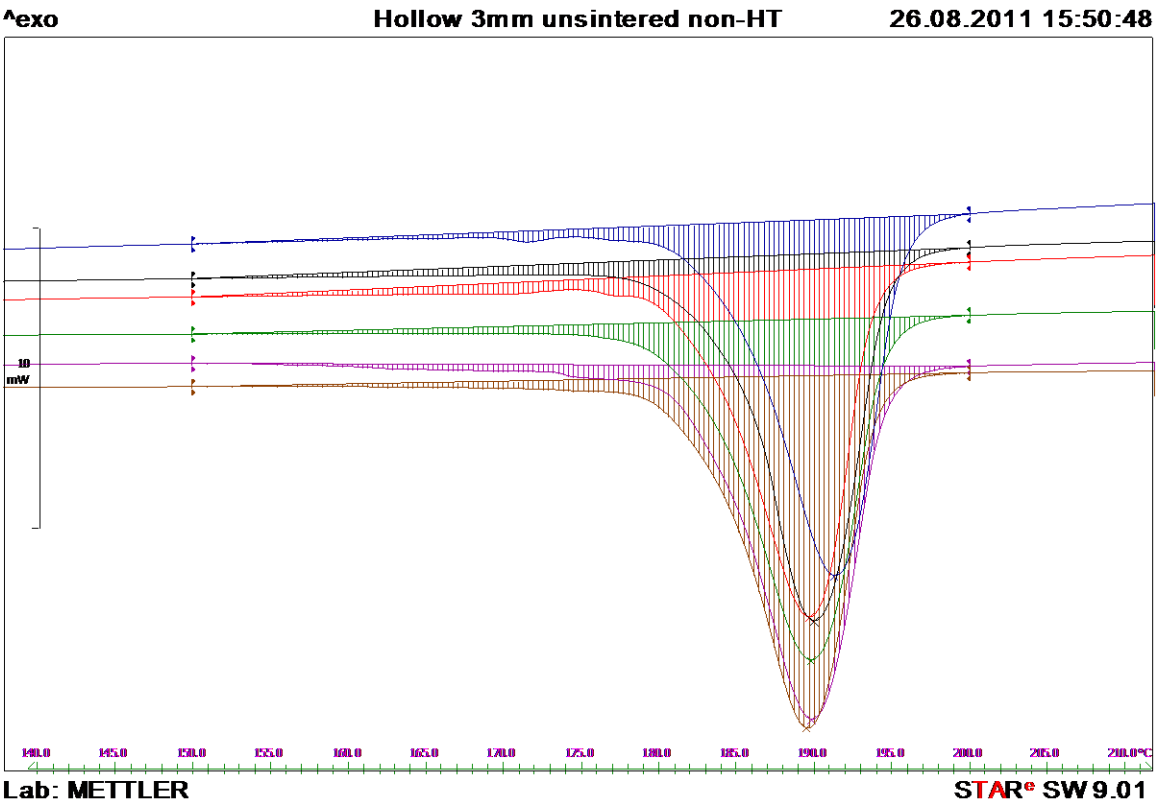
^exo
Hollow 3mm unsintered non-HT
26.08.2011 15:50:48
10
mW
Lab: METTLER
STARe SW 9.01

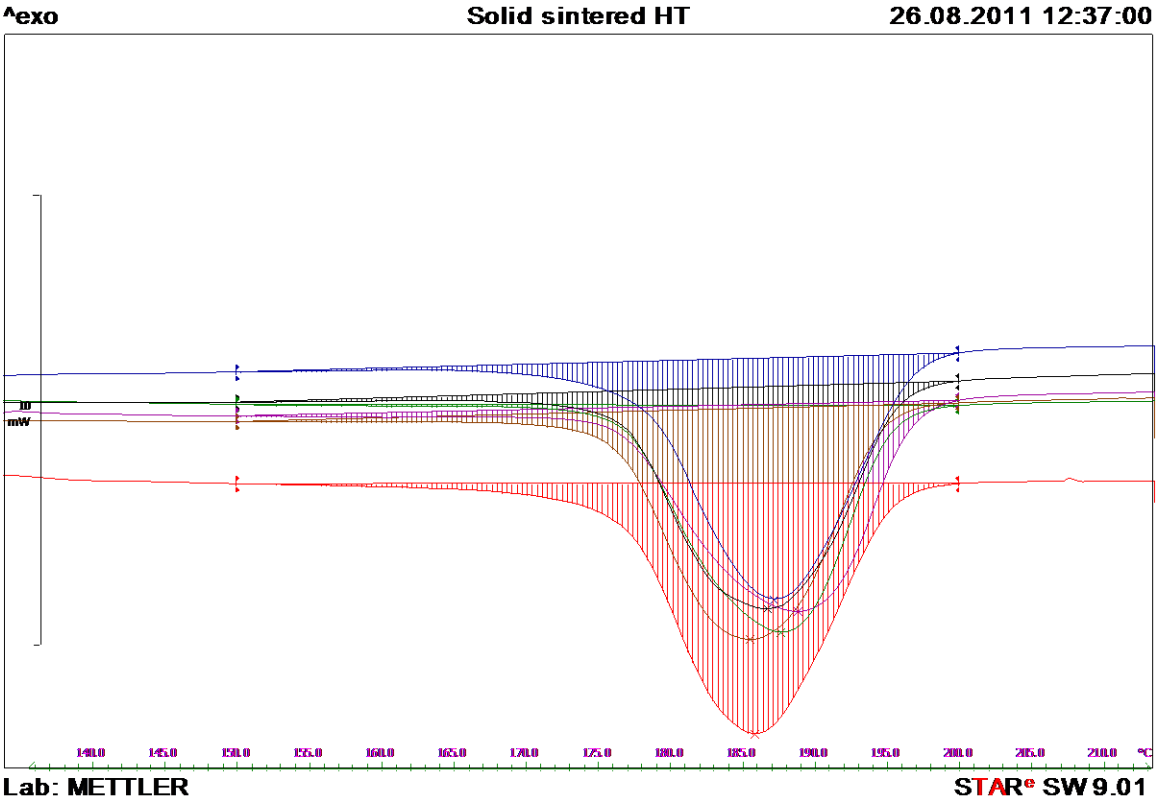
^exo
Solid sintered HT
26.08.2011 12:37:00
10
mW
140.0 145.0 150.0 155.0 160.0 165.0 170.0 175.0 180.0 185.0 190.0 195.0 200.0 205.0 210.0 °C
Lab: METTLER
STARe SW 9.01

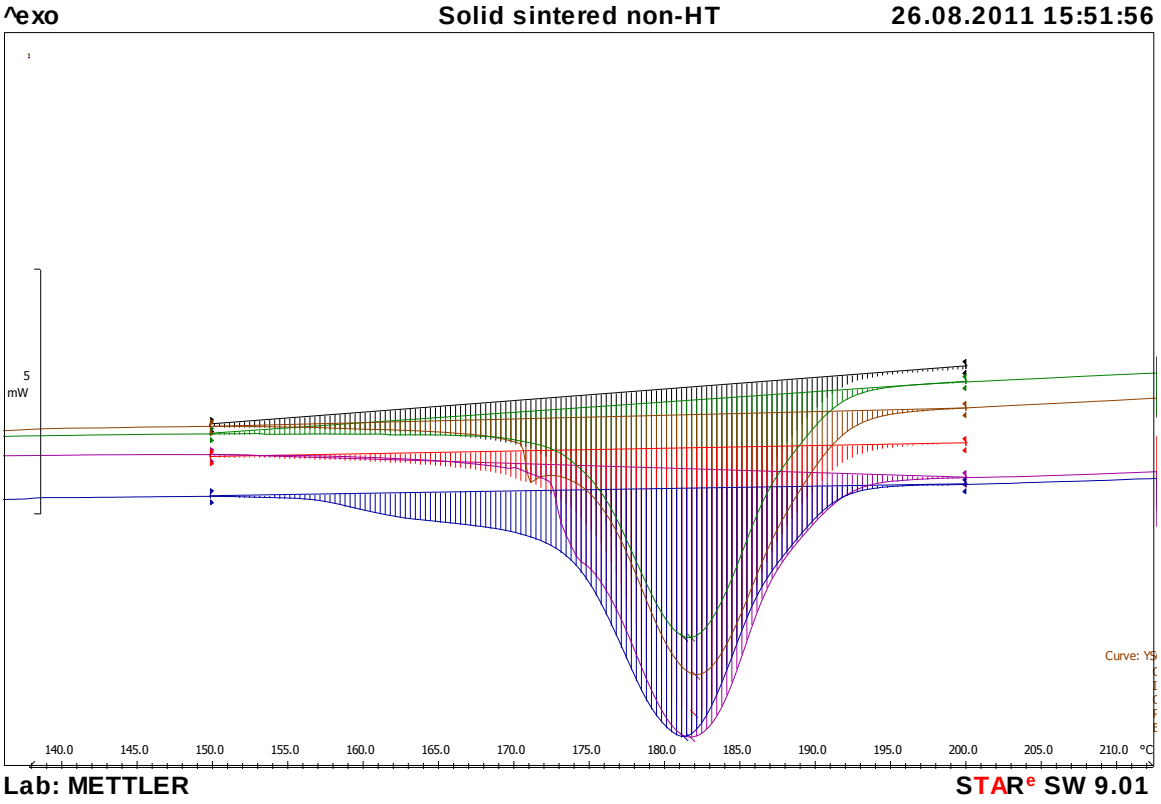
^exo
Solid sintered non-HT
26.08.2011 15:51:56
5
mW
Curve: YS
140.0 145.0 150.0 155.0 160.0 165.0 170.0 175.0 180.0 185.0 190.0 195.0 200.0 205.0 210.0 °C
Lab: METTLER
STARe SW 9.01

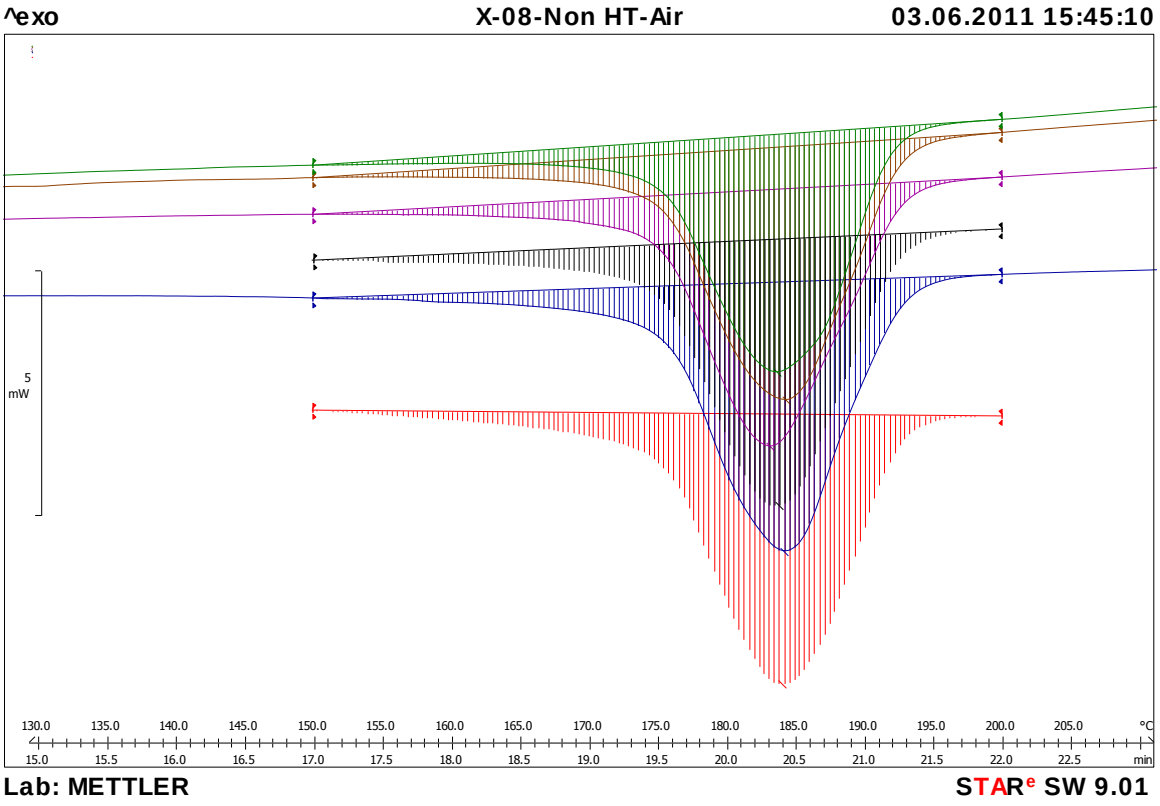
^exo
X-08-Non HT-Air
03.06.2011 15:45:10
5
mW
130.0 135.0 140.0 145.0 150.0 155.0 160.0 165.0 170.0 175.0 180.0 185.0 190.0 195.0 200.0 205.0 °C
15.0 15.5 16.0 16.5 17.0 17.5 18.0 18.5 19.0 19.5 20.0 20.5 21.0 21.5 22.0 22.5 min
Lab: METTLER
STARe SW 9.01

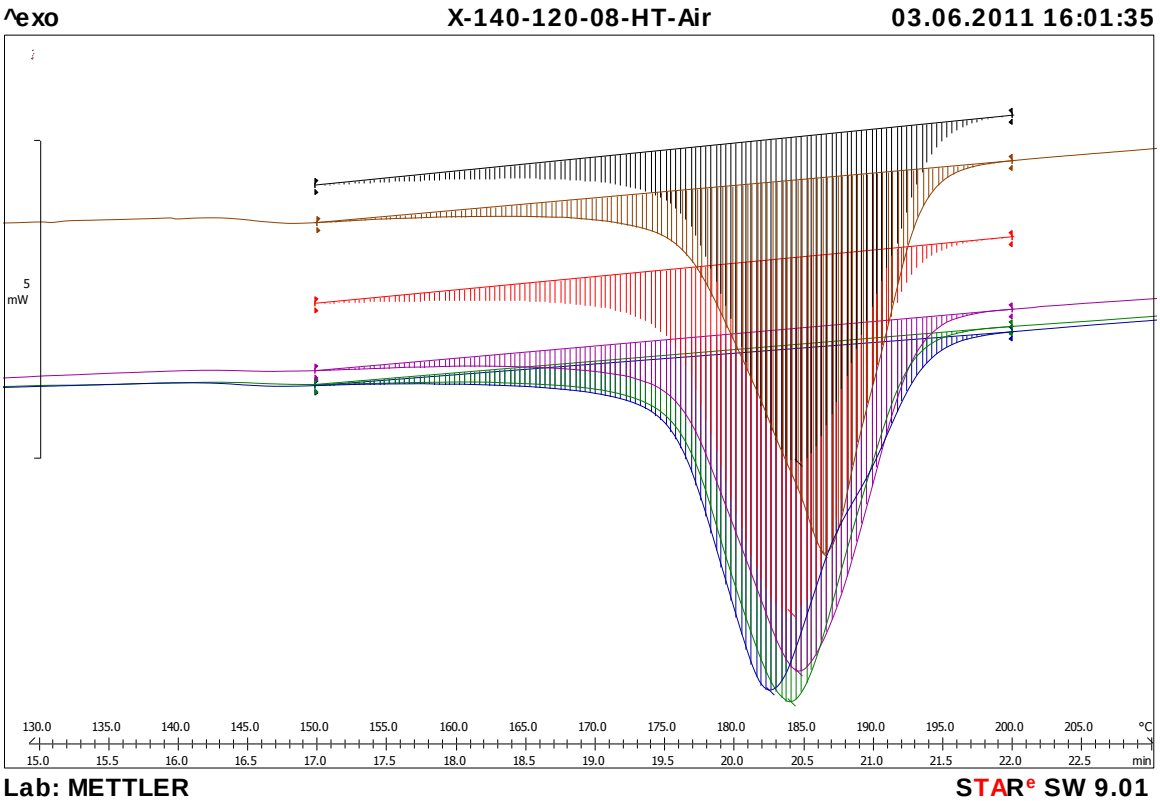
^exo
X-140-120-08-HT-Air
03.06.2011 16:01:35
5
mW
130.0 135.0 140.0 145.0 150.0 155.0 160.0 165.0 170.0 175.0 180.0 185.0 190.0 195.0 200.0 205.0 °C
15.0 15.5 16.0 16.5 17.0 17.5 18.0 18.5 19.0 19.5 20.0 20.5 21.0 21.5 22.0 22.5 min
Lab: METTLER
STARe SW 9.01

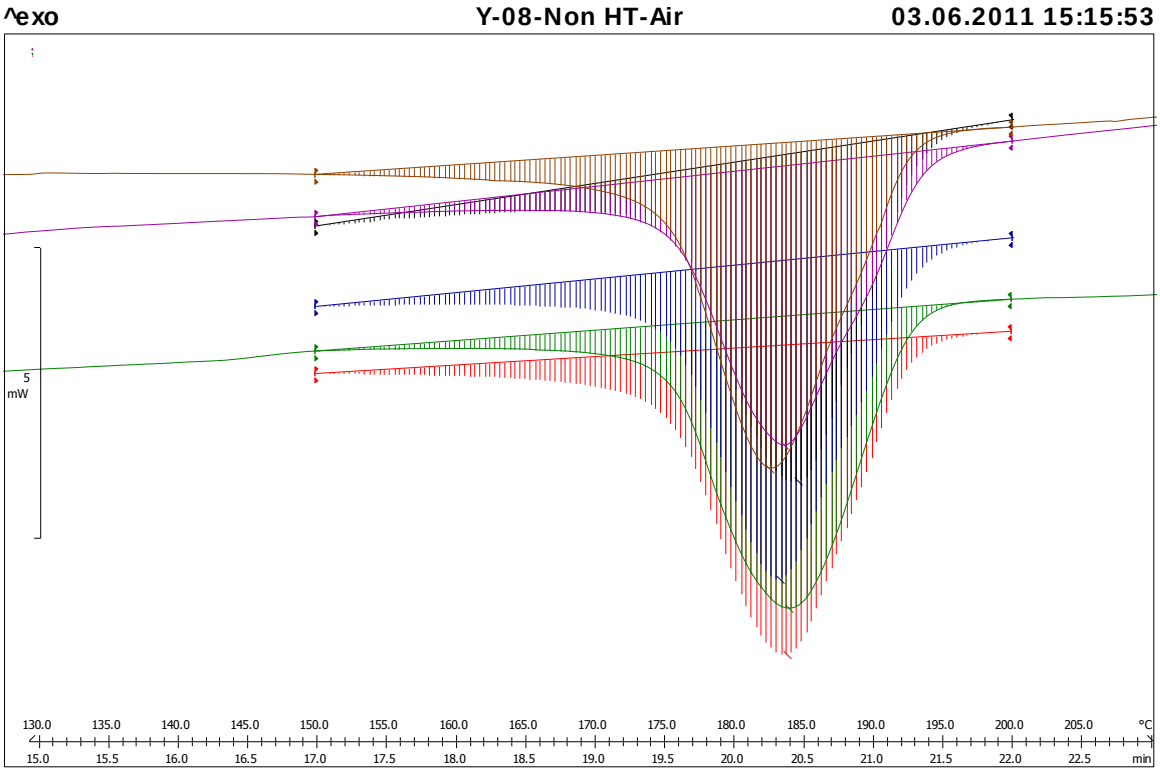
^exo
Y-08-Non HT-Air
03.06.2011 15:15:53
5
mW
130.0 135.0 140.0 145.0 150.0 155.0 160.0 165.0 170.0 175.0 180.0 185.0 190.0 195.0 200.0 205.0 °C
15.0 15.5 16.0 16.5 17.0 17.5 18.0 18.5 19.0 19.5 20.0 20.5 21.0 21.5 22.0 22.5 min
Lab: METTLER
STARe SW 9.01

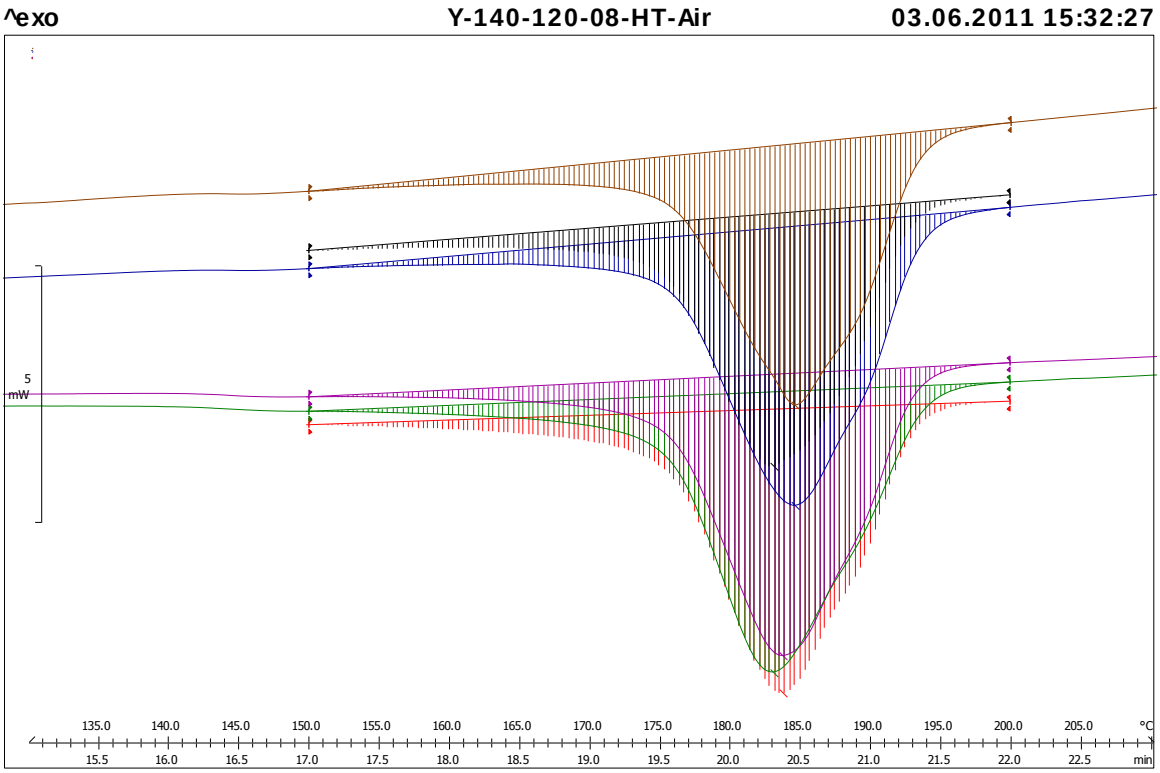
^exo
Y-140-120-08-HT-Air
03.06.2011 15:32:27
5
mW
135.0 140.0 145.0 150.0 155.0 160.0 165.0 170.0 175.0 180.0 185.0 190.0 195.0 200.0 205.0 °C
15.5 16.0 16.5 17.0 17.5 18.0 18.5 19.0 19.5 20.0 20.5 21.0 21.5 22.0 22.5 min
Lab: METTLER
STARe SW 9.01

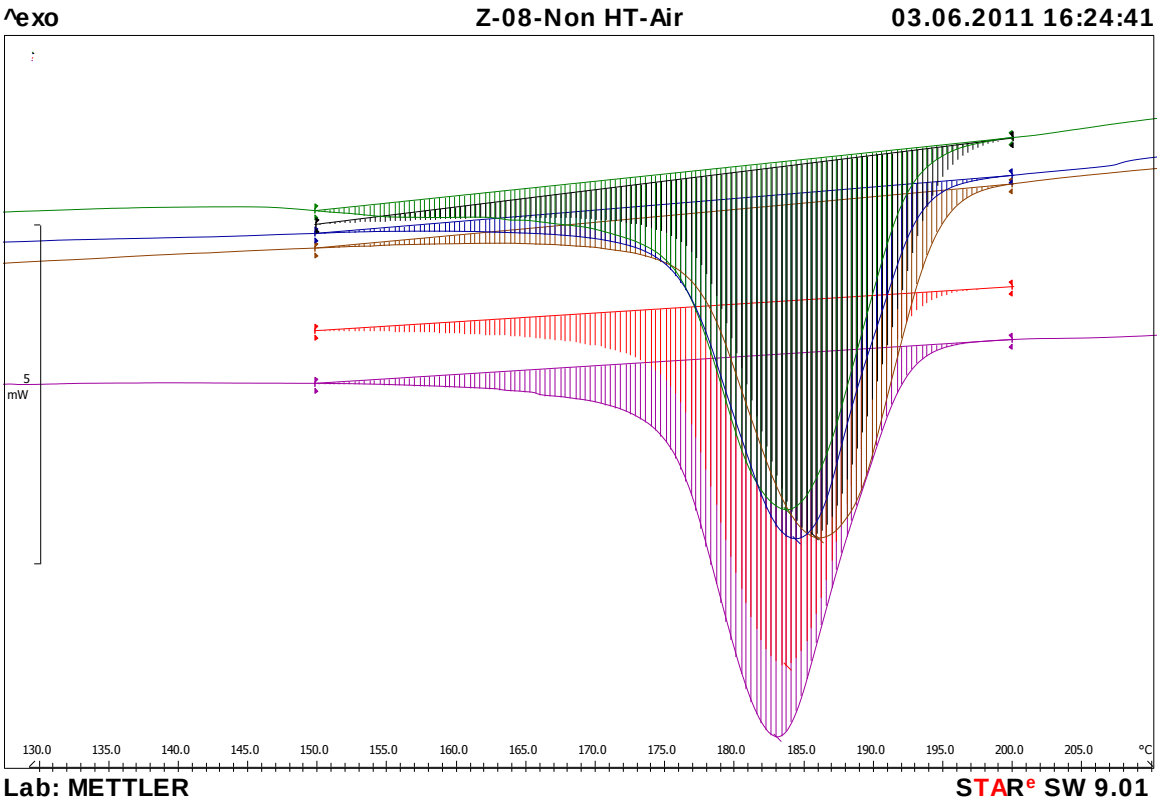
^exo
Z-08-Non HT-Air
03.06.2011 16:24:41
5
mW
130.0 135.0 140.0 145.0 150.0 155.0 160.0 165.0 170.0 175.0 180.0 185.0 190.0 195.0 200.0 205.0 °C
Lab: METTLER
STARe SW 9.01

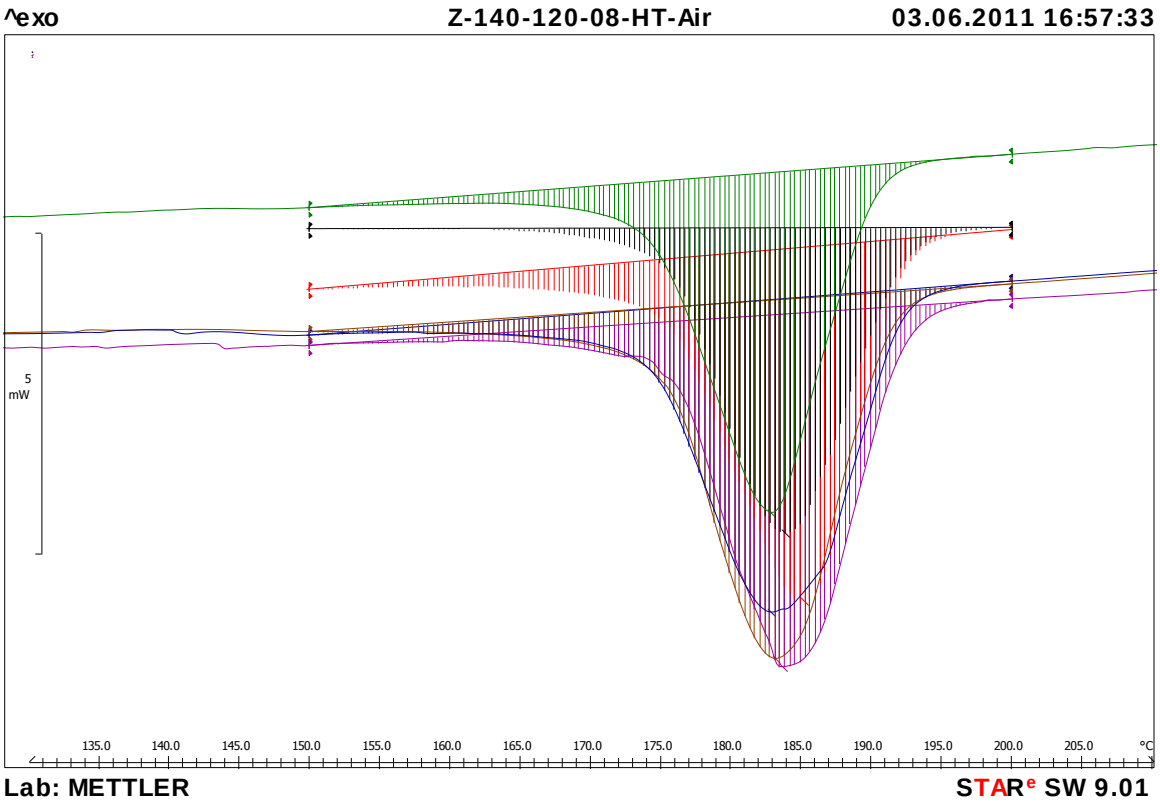
^exo
Z-140-120-08-HT-Air
03.06.2011 16:57:33
5
mW
135.0 140.0 145.0 150.0 155.0 160.0 165.0 170.0 175.0 180.0 185.0 190.0 195.0 200.0 205.0 °C
Lab: METTLER
STARe SW 9.01

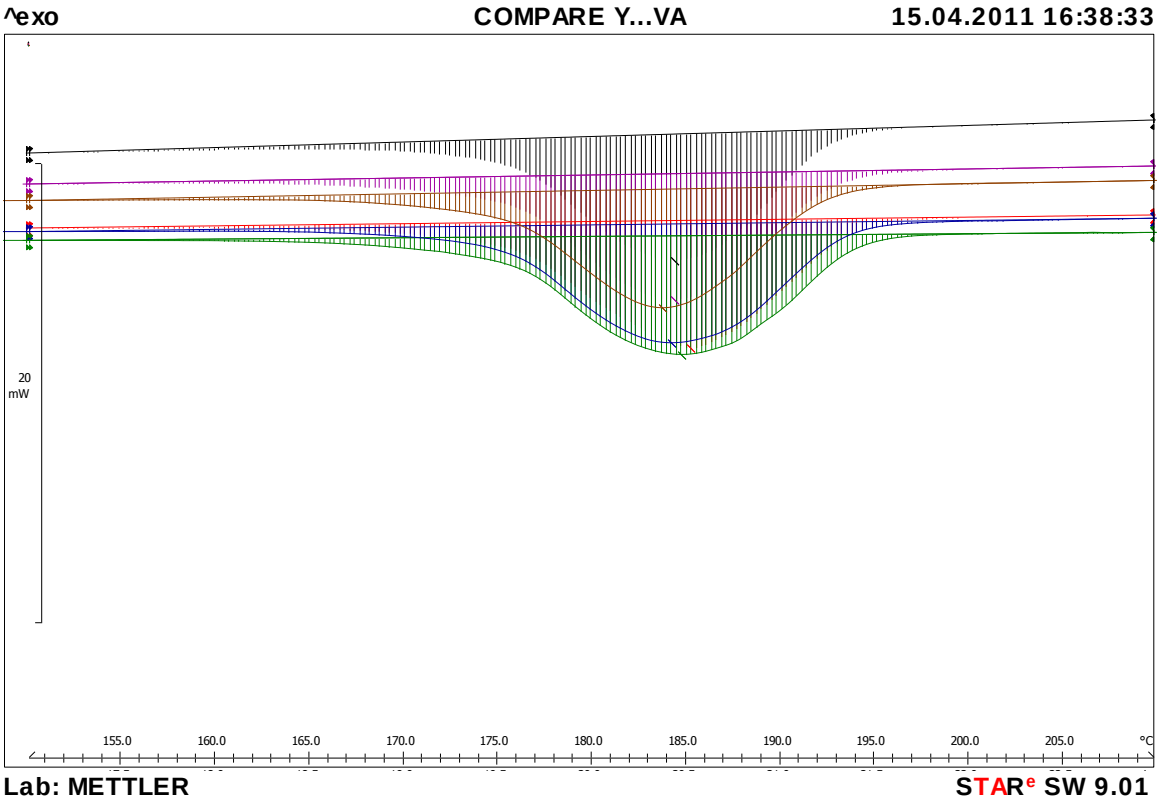
^exo
COMPARE Y...VA
15.04.2011 16:38:33
20
mW
155.0
160.0
165.0
170.0
175.0
180.0
185.0
190.0
195.0
200.0
205.0
°C
Lab: METTLER
STARe SW 9.01

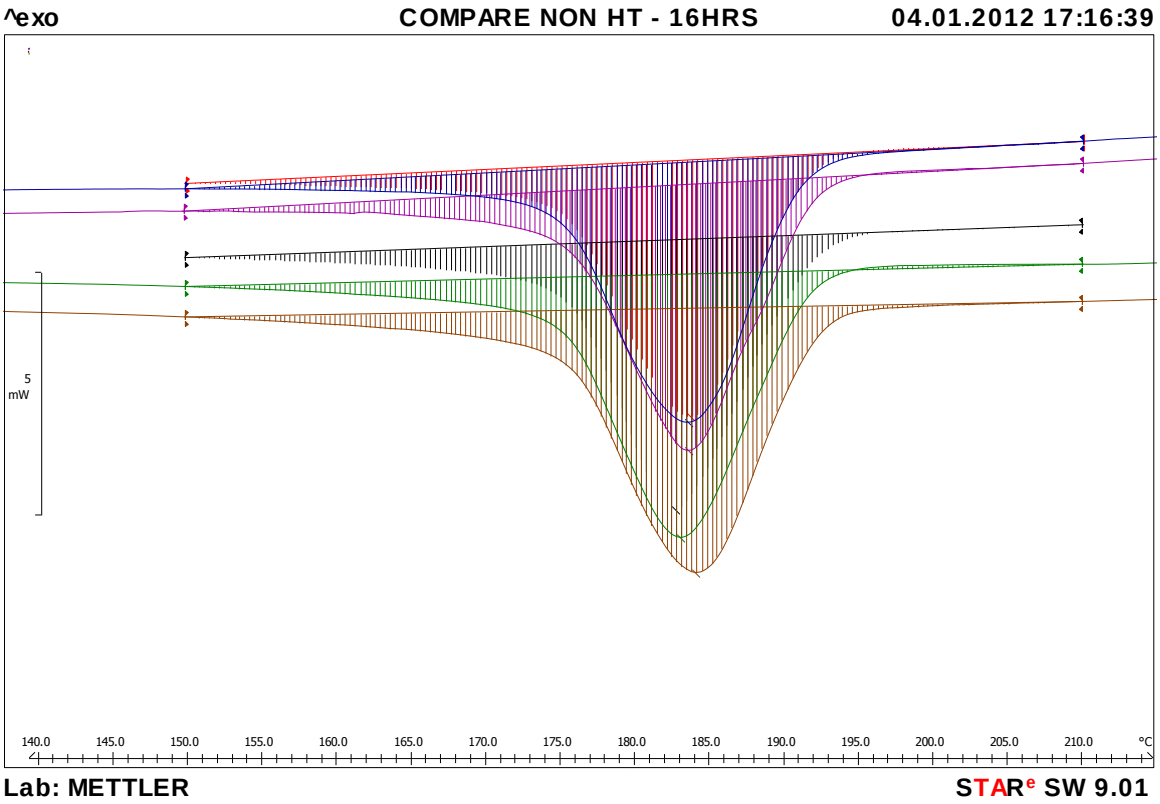
^exo
COMPARE NON HT - 16HRS
04.01.2012 17:16:39
5
mW
140.0
145.0
150.0
155.0
160.0
165.0
170.0
175.0
180.0
185.0
190.0
195.0
200.0
205.0
210.0
°C
Lab: METTLER
STARe SW 9.01

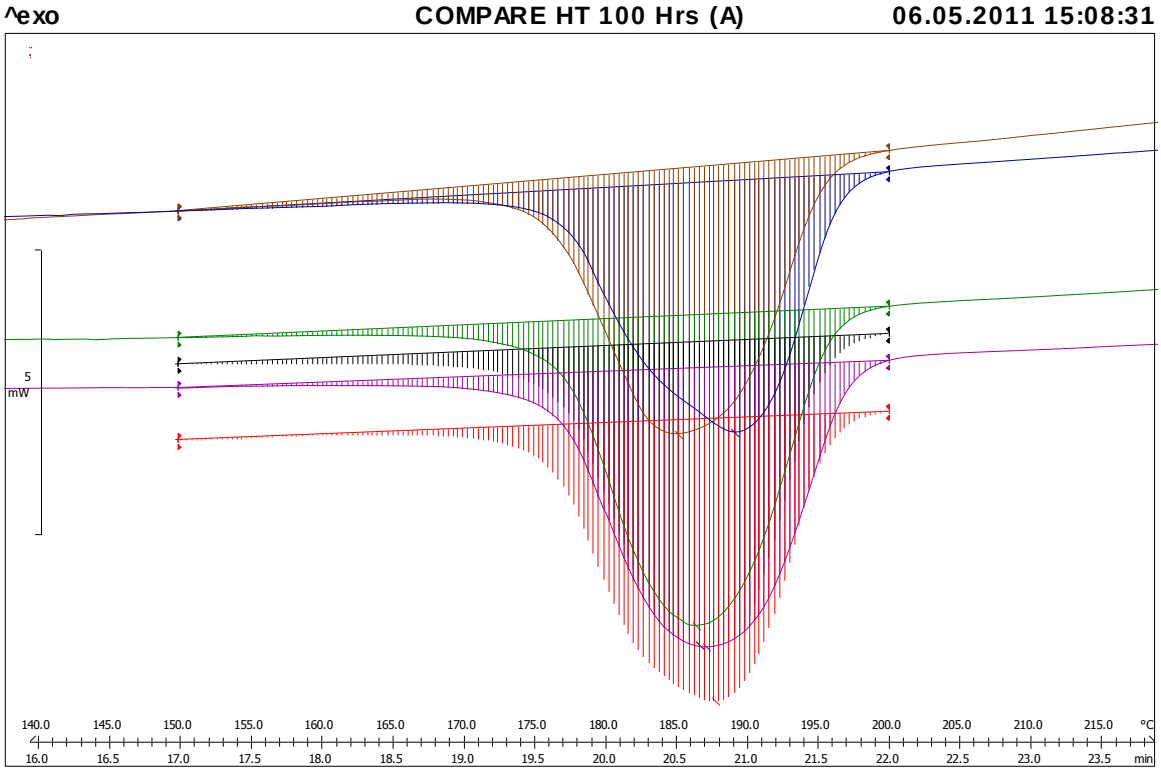
^exo
COMPARE HT 100 Hrs (A)
06.05.2011 15:08:31
5
mW
140.0 145.0 150.0 155.0 160.0 165.0 170.0 175.0 180.0 185.0 190.0 195.0 200.0 205.0 210.0 215.0 °C
16.0 16.5 17.0 17.5 18.0 18.5 19.0 19.5 20.0 20.5 21.0 21.5 22.0 22.5 23.0 23.5 min
Lab: METTLER
STARe SW 9.01

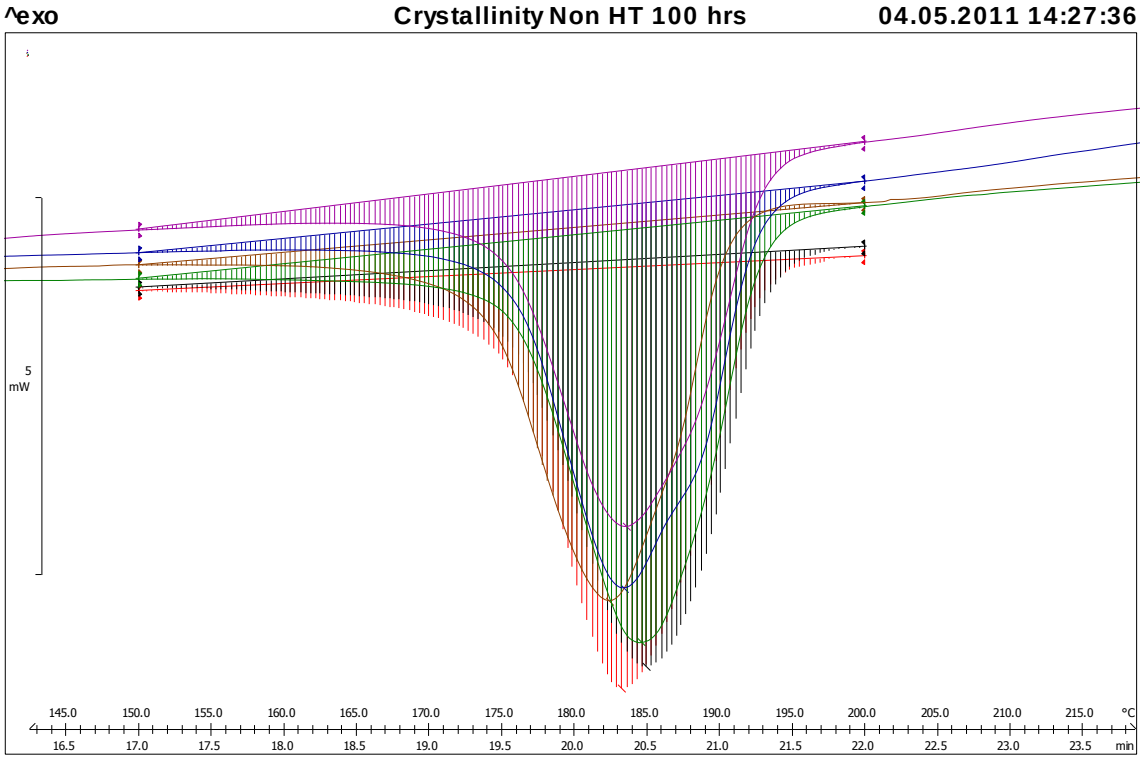
^exo
Crystallinity Non HT 100 hrs
04.05.2011 14:27:36
5
mW
145.0 150.0 155.0 160.0 165.0 170.0 175.0 180.0 185.0 190.0 195.0 200.0 205.0 210.0 215.0 °C
16.5 17.0 17.5 18.0 18.5 19.0 19.5 20.0 20.5 21.0 21.5 22.0 22.5 23.0 23.5 min
Lab: METTLER
STARe SW 9.01

D: DATA RESULTS FOR CH. 6

Non-heat treated with filling scanning:

Table 6-1. Tensile Strength Results of all Non-heat treated Specimens (MPa)
(Noted: *closed hollow and ** open hollow Structure)

Specimen	Sample						Average	95 % Confidence Interval
	1	2	3	4	5	6		
Section 1mm*	19.21	21.18	18.65	17.40	-	21.43	**19.57**	±1.50
Section 2mm*	33.97	29.62	32.48	33.87	33.64	35.18	**33.13**	±1.54
Section 3mm*	39.12	44.05	42.23	41.50	39.61	43.25	**41.63**	±1.57
Solid	46.15	46.33	47.16	47.60	47.17	43.65	**46.34**	±1.14
Section 2mm**	28.40	34.13	28.20	31.57	31.46	31.56	**30.89**	±1.66

Table 6-2. Tensile Modulus Results of All Non-heat treated Specimens (MPa)
(Noted: *Closed hollow and **Open hollow Structure)

Specimen	Sample						Average	95 % C.I.
	1	2	3	4	5	6		
Section 1mm*	1061.20	1059.50	1065.20	1025.60	-	1036.60	1049.62	±15.31
Section 2mm*	1507.80	1327.50	1485.50	1561.10	1542.50	1542.90	1494.55	±69.04
Section 3mm*	1666.00	1700.70	1736.60	1721.50	1692.70	1795.80	1718.88	±35.87
Solid	1770.60	1721.20	1783.70	1857.10	1801.90	1787.30	1786.97	±35.33
Section 2mm**	1315.00	1489.50	1358.00	1380.80	1340.90	1389.40	1378.93	±44.83

Table 6-3. Elongation at break of all Non-heat treated Specimens (%)
(Noted: *Closed hollow and **Open hollow Structure)

Specimen	Sample						Average	95 % Confidence Interval
	1	2	3	4	5	6		
Section 1mm*	3.14	4.15	3.21	2.89	-	5.28	**3.73**	±0.87
Section 2mm*	4.88	4.73	4.29	4.02	4.21	5.28	**4.57**	±0.38
Section 3mm*	5.17	7.54	6.20	6.38	5.44	6.54	**6.21**	±0.68
Solid	16.13	11.55	14.76	13.30	13.61	7.28	**12.77**	±2.48
Section 2mm**	3.84	5.48	3.67	4.79	5.79	4.78	**4.73**	±0.68

Table 6-6. Melting Peak Temperature Sintered Material of Non-heat treated Specimens (^{o}C)

Specimen	Sample						Average	95 % Confidence Interval
	1	2	3	4	5	6		
Section 1mm	185.00	185.46	184.97	183.18	184.19	184.26	**184.51**	±0.65
Section 2mm	185.42	185.83	186.52	185.11	187.92	186.06	**186.14**	±0.80
Section 3mm	183.74	182.25	183.23	183.07	184.03	184.95	**183.55**	±0.74
Solid	181.22	181.81	181.62	181.72	181.12	182.02	**181.59**	±0.28

Table 6-7. Melting Peak Temperature Un-sintered Material of Non-heat treated Specimens (^{o}C)

Specimen	Sample						Average	95 % Confidence Interval
	1	2	3	4	5	6		
Section 1mm	189.82	189.41	189.41	189.46	189.34	189.03	**189.41**	±0.20
Section 2mm	189.35	189.66	189.40	189.70	189.83	189.40	**189.57**	±0.17
Section 3mm	189.58	189.25	190.99	189.35	188.90	189.25	**189.55**	±0.59

Heat treated with filling scanning:

Table 6-8. Tensile Strength Results of Heat Treated Specimens (MPa)

Specimen	Sample						Average	95 % Confidence Interval
	1	2	3	4	5	6		
Section 1mm	25.84	26.54	25.26	25.95	25.96	25.91	**25.91**	±0.33
Section 2mm	-	40.06	39.34	35.31	38.90	39.25	**38.57**	±1.64
Section 3mm	45.21	42.90	43.40	44.74	44.21	43.55	**44.00**	±0.70
Solid	51.50	51.24	51.75	51.22	51.52	50.61	**51.31**	±0.32

Table 6-9. Tensile Modulus Results of Heat Treated Specimens (MPa)

Specimen	Sample						Average	95 % C.I.
	1	2	3	4	5	6		
Section 1mm	1197.60	1240.30	1432.80	1353.70	1323.40	1412.20	**1326.67**	±74.58
Section 2mm	-	1776.50	1690.40	1618.90	1707.30	1752.20	**1709.06**	±53.48
Section 3mm	1983.30	1970.70	1898.20	1930.30	1917.40	1898.70	**1933.10**	±29.05
Solid	1894.40	1945.30	2023.90	1902.40	1962.20	1963.40	**1948.60**	±37.80

Table 6-10. Elongation at break of Heat Treated Specimens (%)

Specimen	Sample						Average	95 % Confidence Interval
	1	2	3	4	5	6		
Section 1mm	3.81	4.25	3.29	3.22	4.09	3.79	**3.74**	±0.33
Section 2mm	-	4.31	4.08	3.81	4.38	4.92	**4.30**	±0.36
Section 3mm	4.04	3.62	4.55	4.50	4.87	4.82	**4.40**	±0.39
Solid	10.58	11.15	9.79	13.05	13.02	12.19	**11.68**	±1.10

Table 6-11. Crystallinity Results Sintered Material of Heat Treated Specimens (%)

Specimen	Sample						Average	95 % Confidence Interval
	1	2	3	4	5	6		
Section 1mm	31.98	29.09	29.72	28.55	28.85	28.76	**29.49**	±1.03
Section 2mm	30.07	30.31	28.19	27.49	28.24	27.30	**28.60**	±0.96
Section 3mm	33.79	29.88	30.22	29.13	28.43	28.47	**29.99**	±1.60
Solid	27.83	28.85	27.36	27.52	25.37	26.87	**27.30**	±0.92

Table 6-12. Crystallinity Results Un-sintered Material of Heat Treated Specimens (%)

Specimen	Sample						Average	95 % Confidence Interval
	1	2	3	4	5	6		
Section 1mm	37.99	40.02	39.51	37.99	38.97	40.56	**39.17**	±0.85
Section 2mm	42.25	41.90	39.57	38.82	36.73	40.86	**40.02**	±1.59
Section 3mm	42.69	41.61	-	41.86	40.60	36.90	**40.73**	±1.99

Table 6-13. Melting Peak Temperature of Heat Treated Sintered Material (^{o}C)

Specimen	Sample						Avera-ge	95 % Confi-dence Interval
	1	2	3	4	5	6		
Section 1mm	191.48	191.74	192.85	194.29	192.66	196.43	**193.24**	±1.48
Section 2mm	189.57	187.39	189.51	191.26	191.61	192.47	**190.30**	±1.47
Section 3mm	191.21	192.83	191.09	193.37	193.55	192.57	**192.44**	±0.85
Solid	186.95	185.47	186.44	185.24	187.42	188.61	**186.69**	±1.01

Table 6-14. Melting Peak Temperature of Heat Treated Un-sintered Material (^{o}C)

Specimen	Sample						Avera-ge	95 % Confi-dence Interval
	1	2	3	4	5	6		
Section 1mm	193.09	196.84	194.05	194.72	194.40	194.55	**194.61**	±0.99
Section 2mm	191.42	191.94	192.37	193.49	192.66	192.99	**192.48**	±0.59
Section 3mm	191.20	191.81	-	192.74	192.84	194.69	**192.66**	±1.16

Non-heat treated with filling and outline scanning

Table 6-15. Tensile Strength Results (MPa) – With Fill and Outline Scanning

Specimen	Sample						Average	95 % Confidence Interval
	1	2	3	4	5	6		
Section 1mm	31.68	30.08	32.79	32.70	33.21	32.01	**32.08**	±0.90
Section 2mm	37.97	38.14	37.55	37.11	36.05	37.13	**37.33**	±0.60
Section 3mm	42.75	45.68	44.86	43.39	44.95	45.86	**44.58**	±1.00
Solid	-	49.40	49.82	48.75	49.45	49.23	**49.33**	±0.34

Table 6-16. Tensile Modulus Results (MPa) – With Fill and Outline Scanning

Specimen	Sample						Averag e	95 % C.I.
	1	2	3	4	5	6		
Section 1mm	1528.10	1554.90	1595.00	1529.80	1585.50	1554.20	**1557.92**	±22.17
Section 2mm	1809.70	1853.90	1770.90	1731.90	1654.30	1695.10	**1752.63**	±64.71
Section 3mm	1831.20	1834.10	1891.50	1830.20	1907.50	1972.90	**1877.90**	±45.91
Solid	-	1970.30	1923.20	1879.60	1946.30	2025.70	**1949.02**	±47.66

Table 6-17. Elongation at break (%) – With Fill and Outline Scanning

Specimen	Sample						Average	95 % Confidence Interval
	1	2	3	4	5	6		
Section 1mm	3.58	3.20	4.12	4.04	3.73	3.58	**3.71**	±0.27
Section 2mm	5.28	4.98	4.37	4.67	4.43	4.87	**4.77**	±0.28
Section 3mm	5.13	6.79	5.63	4.76	5.41	5.87	**5.60**	±0.56
Solid	-	8.73	10.21	8.82	10.20	10.55	**9.70**	±0.75

Table 6-18. Energy Density (J/mm^2)– With Fill Scanning

Specimen	Sample						Average	95 % C.I.
	1	2	3	4	5	6		
Section 1mm	5004.00	5009.80	5010.77	5395.54	-	4988.92	**5081.80**	±153.92
Section 2mm	10355.80	10383.31	10404.44	10389.90	10412.47	10416.90	**76052.2**	±18.12
Section 3mm	14348.61	14323.67	14305.17	14285.84	14307.94	14302.41	**104723.9**	±17.22
Solid	17645.98	17604.99	17693.32	17650.97	17686.47	17632.32	**17652.34**	±26.61

Table 6-19. Energy Density (J/mm^2)– With Fill and Outline Scanning

Specimen	Sample						Average	95 % C.I.
	1	2	3	4	5	6		
Section 1mm	8055.42	7881.59	8116.09	7826.61	7982.49	8184.64	**8007.81**	±110.10
Section 2mm	13068.88	13160.88	13197.30	13179.43	13120.17	13161.69	**13148.06**	±37.20
Section 3mm	16332.60	16427.16	16401.42	16366.99	16395.89	16304.38	**16371.41**	±36.89
Solid	-	18913.11	18995.50	18916.79	18984.41	18964.40	**18954.84**	±33.40

APPENDIX

Jig Fixture for shear test

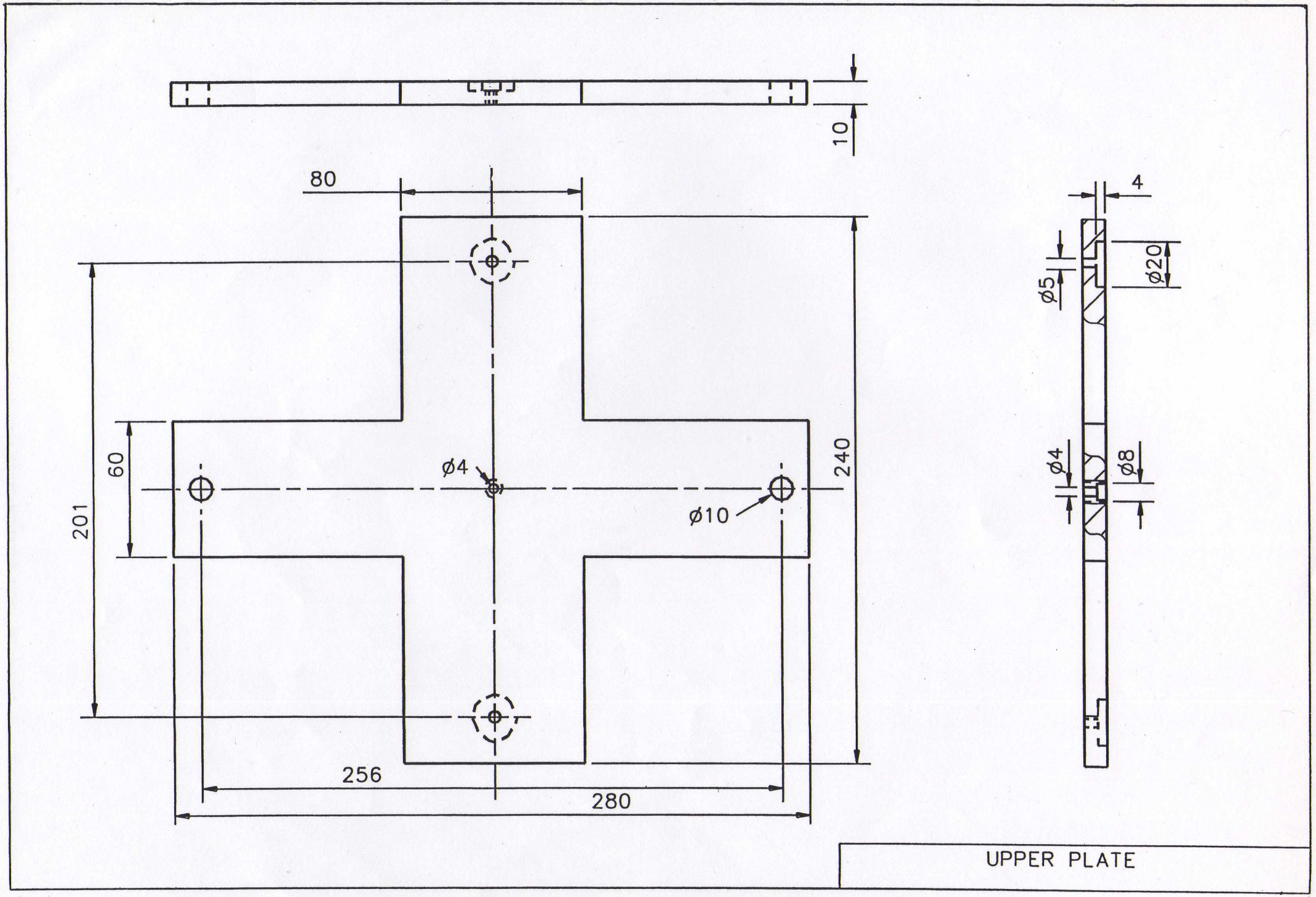

UPPER PLATE

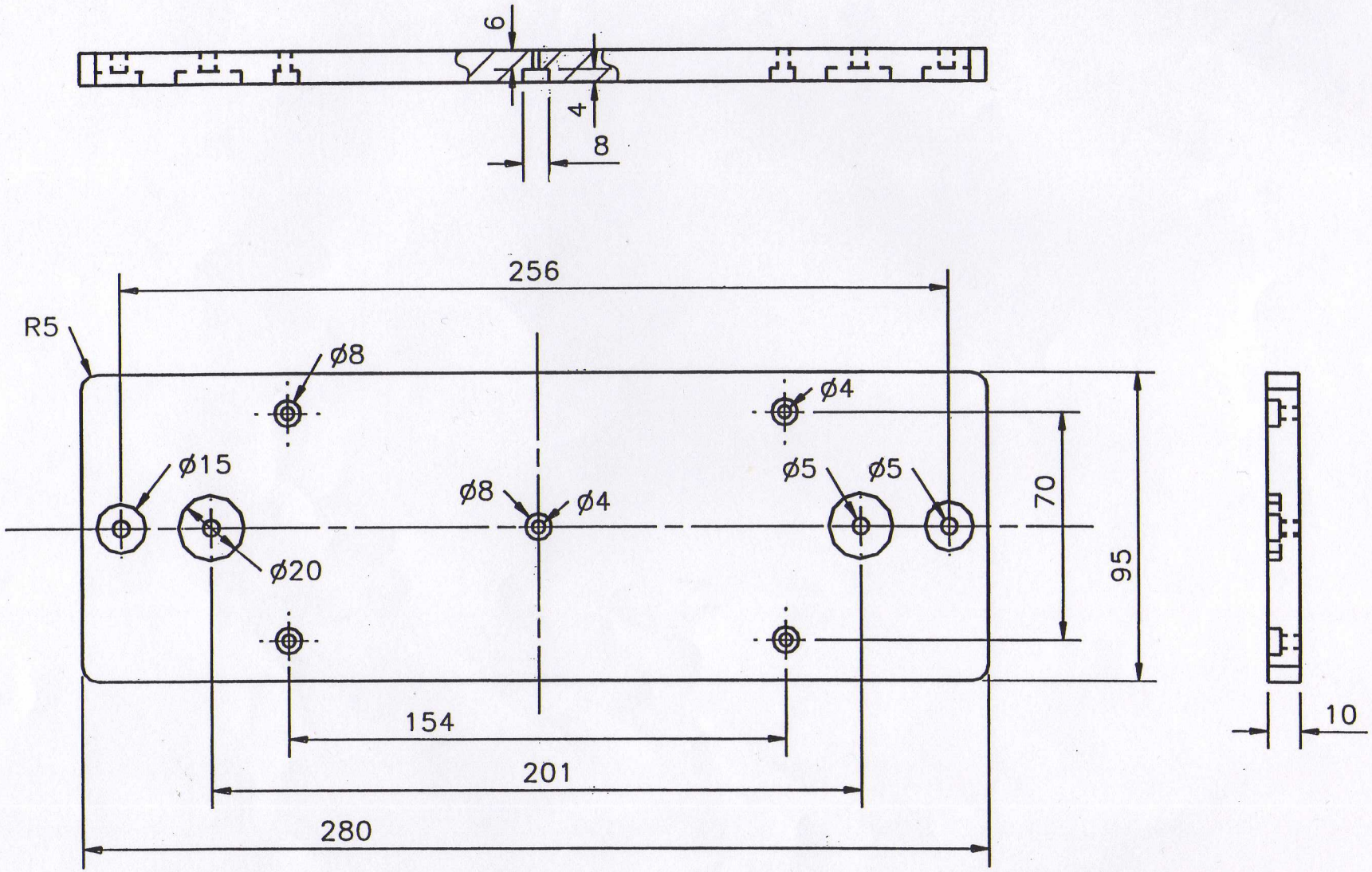

LOWER PLATE

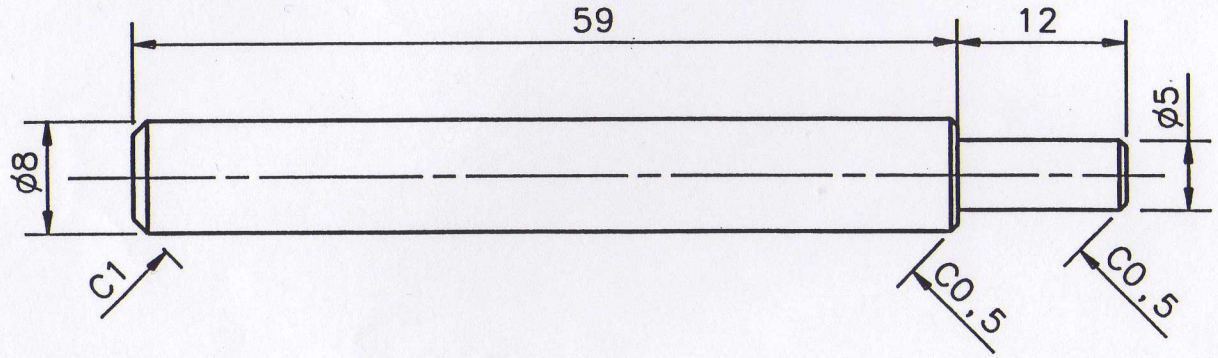

FIXTURE GUIDE

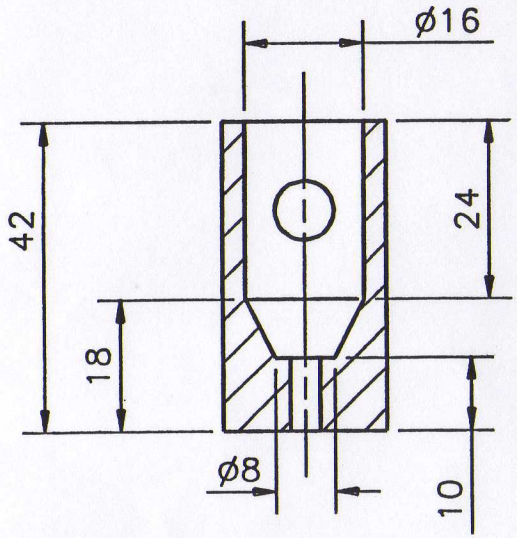

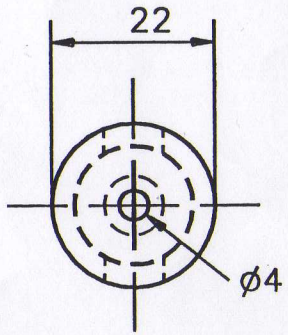

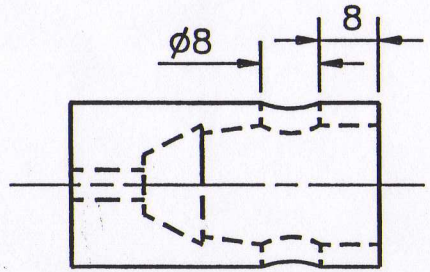

LOADING COULUMN

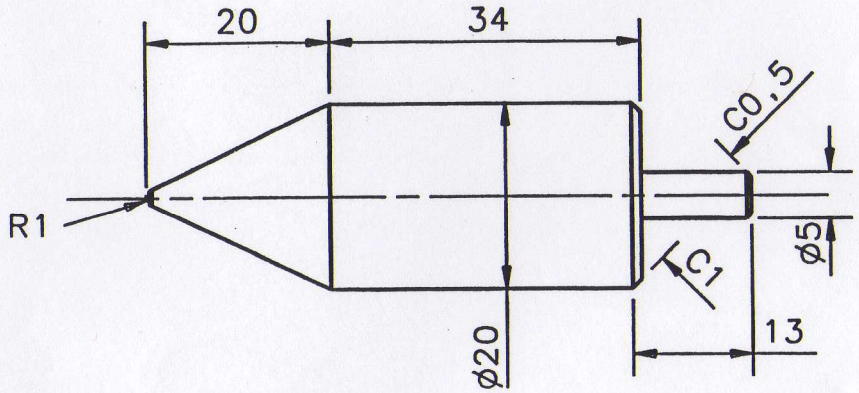

SUPPORT AND LOADING POINT

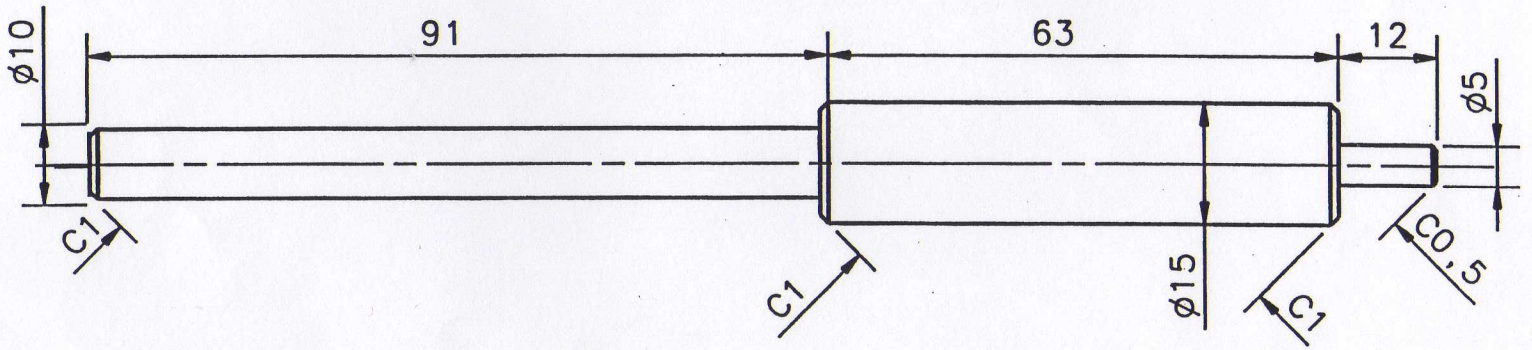

DISPLACEMENT GUIDE